THE BIOLOGY OF IMMUNOGLOBULIN FREE LIGHT CHAINS IN KIDNEY DISEASE:

A STUDY OF MONOCLONAL AND POLYCLONAL LIGHT CHAINS

BY

KOLITHA INDIKA BASNAYAKE

A thesis submitted to
The University of Birmingham
For the degree of
DOCTOR OF PHILOSOPHY

School of Immunity and Infection
College of Medical and Dental Sciences
The University of Birmingham
January 2011

ABSTRACT

Monoclonal immunoglobulin free light chains (FLCs) cause a range of disorders in the kidney. In multiple myeloma, FLCs can activate the proximal tubule to release MCP-1, an important cytokine in renal fibrosis. Distal tubular cast formation can also occur when FLCs co-precipitate with uromodulin. However a pathogenic role for the elevated polyclonal FLC concentrations seen in chronic kidney disease has not been assessed to date. This thesis explores the biology of monoclonal FLCs as well as polyclonal FLCs. Detailed histological analyses demonstrated that in multiple myeloma, interstitial fibrosis can progress rapidly *in situ* and indicated that intratubular cast numbers might be linked to potential for renal recovery. The functional basis of this fibrosis was explored by *in vitro* studies, which showed that upon endocytosis of FLCs, oxidative stress activated redox signalling, resulting in MCP-1 production. Further *in situ* analyses showed that in chronic kidney disease, polyclonal FLCs co-localised with uromodulin in distal tubular casts. Relationships between these casts and markers of progression of chronic kidney disease were demonstrated. *In vitro* analyses then showed that polyclonal FLCs bind to uromodulin and promote aggregation. These findings: (i) further delineate the pathways for proximal tubular injury in myeloma and (ii) indicate a potential pathogenic role for polyclonal FLCs in the distal nephron.

DEDICATION

To Ammi, Thathi & Kathryn.

ACKNOWLEDGMENTS

The work presented in this thesis would not have been possible without the contributions of many people. First and foremost, I must thank Dr Paul Cockwell, who invested a huge amount of time and effort, in the roles of supervisor, colleague and friend. I thank Prof Arthur Bradwell for all the encouragement and the tremendous support he has given. I thank Prof Mark Drayson for his help. Prof Paul Sanders deserves special mention – thank you for all your support, I will always remember Alabama fondly. I thank Dr Gregg Wallis for his expert guidance. A special thank you to Miss for her assistance. I would also like to thank Ltd, the National Institutes for Health and the Department of Veterans Affairs. In addition, the individuals listed below have all helped me at various stages, for which I am very grateful.

Miss Kristal Aaron
Mr Peterson Anand
Mr Richard Barber
Mr Simon Blackmore
Dr Alastair Ferraro
Dr Tarek Ghonemy
Mr John Gregory
Dr Richard Hampton
Miss Lisa Hasty
Dr Colin Hutchison
Dr Laura Ismail
Dr Graham Mead
Dr Matthew Morgan
Dr Timothy Plant
Dr Paul Showell
Dr Helen Smith
Mrs Norma Stewart
Dr Stephanie Stringer
Dr Phillip Stubbs
Mr Phillip Walsh
Dr Betsy Wang
Mrs Ellie White
Dr Wei Zhong Ying
Miss Alice Zhou

CONTENTS

FIGURES

TABLES

ABBREVIATIONS

AA	amino acid
AAFS	Adult Acquired Fanconi Syndrome
ACR	Albumin/Creatinine Ratio
AKI	Acute Kidney Injury
BCA	Bicinchoninic Acid assay
BIAM	N-(biotinoyl)-N'-(iodoacetyl)ethylenediamide
CDR	Complementary Determining Region
CKD	Chronic Kidney Disease
CLSM	Confocal Laser Scanning Microscope
DMTU	Dimethyl Thiourea
ECM	Extracellular Matrix
EMT	Epithelial-to-Mesenchymal Transition
FLC	Free Light Chain
GAPDH	Glyceraldehyde 3-phosphate dehydrogenase
GFR	Glomerular Filtration Rate
H_2O_2	Hydrogen Peroxide
HSA	Human Serum Albumin
HC	Heavy Chain
Ig	Immunoglobulin
LCDD	Light Chain Deposition Disease
LDH	Lactate Dehydrogenase
LMWP	Low Molecular Weight Protein

MAPK	Mitogen Activated Protein Kinase
MC	Mesangial Cell
MCP-1	Monocyte Chemoattractant Protein-1
MGUS	Monoclonal Gammopathy of Uncertain Significance
MMP	Matrix Metalloproteinase
MW	Molecular Weight
NF-κB	Nuclear Factor kappa- light-chain-enhancer of activated B cells
PACAP38	Pituitary Adenylate Cyclase Activating Polypeptide with 38 residues
PAMS	Periodic Acid-Methenamine Silver
PCD	Plasma cell dyscrasia
PDGF-β	Platelet-Derived Growth Factor Beta
PP2	4-amino-5-(4-chlorophenyl)-7-(t-butyl)pyrazolo[3,4-d]pyramidine
PTEC	Proximal Tubule Epithelial Cell
RAP	Receptor Associate Protein
ROS	Reactive Oxygen Species
SAP	Serum Amyloid Protein
SEC	Size-Exclusion Chromatography
siRNA	Small Interfering RNA
TGF-β	Transforming Growth Factor-Beta
TLR4	Toll-Like Receptor-4
TNF-α	Tumour Necrosis Factor-Alpha
TSP	Total Soluble Protein

1. BACKGROUND AND LITERATURE REVIEW

1.1 Introduction

Plasma cell dyscrasias (PCD) are relatively common disorders, the prevalence of monoclonal gammopathy of undetermined significance (MGUS) in the over-50's is around 3.2%, and multiple myeloma accounting for 10% of all haematological malignancies.(Kyle and Rajkumar 2004; Kyle *et al.* 2006) Plasma cell dyscrasias are characterised by the proliferation of a clone of B-cell lineage. There is associated production of clonal immunoglobulin (Ig) which frequently includes a variable quantity of clonal immunoglobulin free light chain (FLC). Each clone of FLC has distinct physico-chemical properties which may lead to differential injury at tissue sites. As FLCs are primarily cleared from the circulation by the kidneys,(Abraham and Waterhouse 1974; Wochner *et al.* 1967; Maack *et al.* 1979) this organ is often damaged in the setting of PCD (Table 1.1). The clinical features of this are wide, ranging from slowly progressive chronic kidney disease (CKD) often associated with heavy proteinuria, to life-threatening acute kidney injury (AKI). In multiple myeloma alone, up to 50% of patients can have renal impairment at diagnosis, 20% may have AKI and up to 10% require dialysis.(Kyle *et al.* 2003; Knudsen *et al.* 2000; Gertz 2005; Blade *et al.* 1998)

Monoclonal FLCs can damage both the glomerular and tubulo-interstitial compartments in disease-dependent patterns.(Sanders *et al.* 1991) For example: primary (AL) amyloidosis can affect all compartments of the kidney, but predominantly involves the glomeruli; in myeloma kidney (cast nephropathy), there is proximal tubular

Table 1.1 Renal manifestations of plasma cell dyscrasias.

Plasma Cell Dyscrasia	**Renal Manifestation**
MGUS	None
Multiple myeloma Smouldering myeloma Plasmacytoma Plasma cell leukaemia	Amyloidosis LCDD HCDD LHCDD Cast nephropathy (myeloma kidney) Cryoglobulinaemic fibrillary glomerulopathy
AL-amyloidosis	Amyloidosis
Waldenstrom's macroglobulinaemia	Hyperviscosity Glomerular endocapillary IgM deposits Casts in distal tubules Amyloidosis
B-cell lymphoproliferative disorders	GOMMID
Other	Proliferative glomerulonephritis with monoclonal Ig deposits

MGUS, monoclonal gammopathy of uncertain significance; LCDD, light chain deposition disease; HCDD, heavy chain deposition disease; LHCDD, light and heavy chain deposition disease; GOMMID, glomerulonephritis with organised microtubular monoclonal immunoglobulin deposits.

inflammation, and in the distal tubules, precipitation of light chain casts, with secondary interstitial involvement; light chain deposition disease (LCDD) can affect the mesangium, the glomerular and tubular basement membranes and blood vessels. The clinical and histological features of the different disease states are summarised in Table 1.2.

Whilst the clinical phenotypes of monoclonal diseases are well recognised and a large body of evidence exists defining the pathogenic effects of monoclonal FLCs, little is known about the pathogenic potential of polyclonal FLCs. The advent of highly sensitive immunoassays has enabled the measurement of the concentrations of these proteins down to even small quantities.(Bradwell *et al.* 2001) These assays have enabled accurate assessments of the concentrations of these proteins in patients with CKD.(Hutchison *et al.* 2008c) These studies have shown that as glomerular filtration rate (GFR) declines, there is a corresponding increase in serum polyclonal FLC concentration, an observation which has led to increasing interest in the potential contribution of these low molecular weight proteins (LMWPs) towards the development of kidney injury, in particular, inflammation and fibrosis.

In this introductory chapter, I explore the current understanding of mechanisms of renal injury due to monoclonal FLCs. I describe how the structure of FLCs facilitates pathological effects that are dependent on both the extracellular deposition of proteins and the activation of intra-cellular signalling pathways, to produce distinct patterns of injury. This will form a basis for understanding the relevance of the experimental work that I performed and is presented in this thesis. In addition I summarise the current

knowledge of the role of polyclonal light chains in inflammation and injury. A significant part of the work that is presented in this thesis describes experiments that were performed to start to ascertain if polyclonal FLCs contribute to the development of CKD.

1.2 Light Chain Structure, Production and Distribution

A basic immunoglobulin molecule consists of four subunits; two identical heavy chains and two identical light chains, linked by disulphide bonds to give a Y-shaped configuration (figure 1.1).(Edelman *et al.* 1968; Porter 1973) There are five known heavy chain isotypes. Two light chain isotypes exist (κ and λ); each containing a variable and a constant region. The variable region of each light chain and each heavy chain pair combine to produce antigen binding sites (Fab) at the two prongs of the "Y".

Each light chain is made up of around 220 amino acids (AAs) and has a molecular weight (MW) of 25 kDa.(Day 1990) The genes coding for κ and λ light chains are situated on chromosomes 2 and 22 respectively.(McBride *et al.* 1982; Malcolm *et al.* 1982; Solomon 1986) There is very little variation within the constant (C_L) region of κ light chain and λ light chain; κ C_L is coded for by a single gene and λ C_L by one of several gene segments.(Solomon 1986; Kawasaki *et al.* 1995) In contrast, the variable (V_L) region of a light chain comprises four framework regions which form a hydrophobic core, (Bruccoleri *et al.* 1988; Chothia and Lesk 1987; Chothia *et al.* 1989; Glockshuber *et al.* 1990; Rocca *et al.* 1993) and within which are scattered three segments of hypervariable AA sequences called complementary determining regions (CDR1, CDR2 and CDR3).(Bruccoleri *et al.* 1988; Chothia and Lesk 1987; Chothia *et*

al. 1989) The diversity of CDRs is attributable to the large number of V_L and joining (J) gene segments which encode them. κ light chain is constructed from 40 Vκ and five Jκ segments and λ light chain from 30 Vλ segments and eight Jλ segments respectively, giving rise to a vast number of possible combinations.(Solomon 1986) Amino Acid substitutions in the V_L region can result in alterations of primary and tertiary structure.(Nyquist *et al.* 1993; Preud'homme *et al.* 1994; Stevens *et al.* 1995; Wetzel 1997) Structural variations due to disparities and mutations in gene segment combinations are important in determining the toxicity of an individual FLC.

The frequent presence of the amphipathic AAs tyrosine and tryptophan in light chain CDRs may enable intact Ig to cross-react with structurally similar ligands.(Mian *et al.* 1991) These AAs: (i) are not affected by the change from a hydrophilic to a hydrophobic environment that occurs on antigen binding; (ii) take part in a wide variety of electrostatic interactions and; (iii) have flexible side chains which can generate a structurally plastic region. Although these factors may improve antigen binding and broaden the repertoire of an antibody, they may also predispose to undesirable effects such as the interaction of FLCs with uromodulin.

Intact Ig production begins in developing B cells. Normally, there is a 40% overproduction of light chain compared to heavy chain.(Bradwell 2010) Around 500 mg/day of polyclonal FLCs are released into the circulation from bone marrow and lymph nodes.(Solomon 1985; Waldmann *et al.* 1972) The biology of polyclonal FLCs are discussed in section 1.12 and in experimental Chapters Six and Seven. If there is

Figure 1.1. Structure of immunoglobulin and light chain.

(Legend on following page)

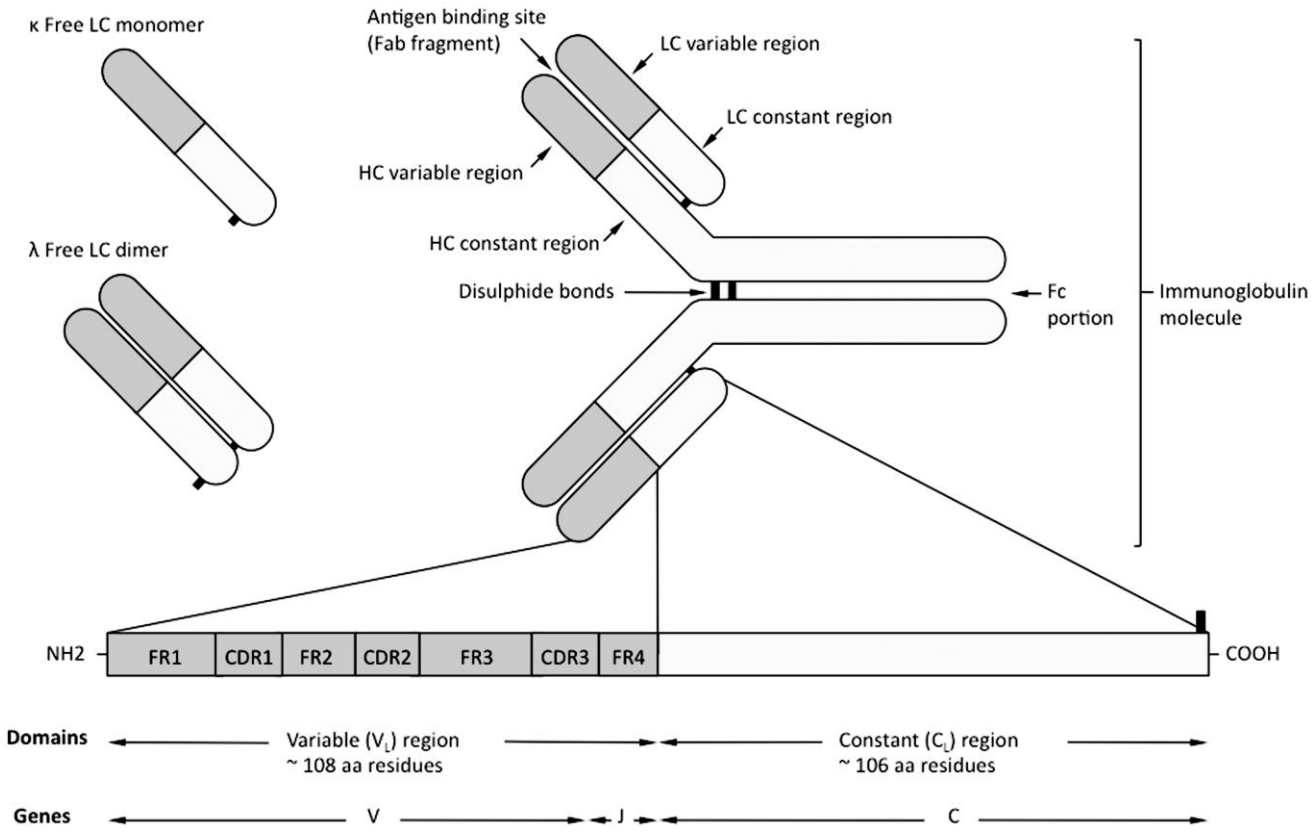

Figure 1.1 Above: An immunoglobulin molecule (e.g. IgG), indicating its modular construction from light chains and heavy chains, held together by disulphide bonds. Antigen binding sites are formed from the variable regions of light and heavy chains, whereas the Fc portion is formed from the constant region of heavy chains. FLCs can exist as monomers, dimers or higher oligomeric and polymeric forms. Below: Light chain domains, showing variable and constant regions. Interspersed between framework regions (FR) within the variable region are the three complimentary determining regions (CDR). CDRs form part of the antigen binding site. It is the variable region which is implicated in the renal manifestations of FLC mediated conditions seen in plasma cell dyscrasias. The reaction site for generation of hydrogen peroxide is located within the V_L region. Domains and their corresponding gene segments are also indicated. The variable region is constructed from a combination of two gene segments, V (variable) and J (joining), while the constant region is constructed from a single C (constant) gene. The J segment comprises the terminal residues of CDR3 and all residues in FR4.

proliferation of an aberrant clone of B cell lineage, it may then secrete clonal FLC, which is detectable in the serum and urine.

Kappa FLC is monomeric and λ FLC dimeric, although higher oligomeric and polymeric forms of both FLCs also occur.(Bradwell 2010; Berggard and Peterson 1969; Myatt *et al.* 1994) Free light chains rapidly disperse such that they are present in roughly equal concentrations throughout extracellular compartments. For an individual with 2.5 L of intravascular fluid and 12 L of extravascular fluid almost 80% of FLC is extravascular.(Hutchison *et al.* 2007) Around two-thirds of light chain production is κ and this is reflected in a serum ratio of κ isotype to λ isotype of 1.8:1.(Katzmann *et al.* 2002)

1.3 Renal Handling of FLCs

The kidney is the major site of FLC removal, primarily by catabolism in proximal tubular epithelial cells (PTEC).(Wochner *et al.* 1967; Miettinen and Kekki 1967; Solomon *et al.* 1964) The precise glomerular clearance is not known but from the size and cationic charge of FLCs,(Maack *et al.* 1979; Camargo *et al.* 1984) and from studies in humans and mice, κ FLCs are cleared at up to 40% per hour and λ FLCs at up to 20% per hour with a serum half-life of 2-4 hours.(Wochner *et al.* 1967; Solomon *et al.* 1964) Consequently the relative serum ratio of FLC isotypes in people with normal renal function is not a true representation of production but a function of differential clearance, with a κ:λ FLC ratio of 0.26-1.65 across all age groups.(Katzmann *et al.* 2002) In established renal failure the reticuloendothelial system becomes the main route

of removal and the serum half-life of FLCs increase to 32 hours or more,(Miettinen and Kekki 1967) and the FLC ratio increases such that it moves closer to that of intact Ig.

There is avid uptake and catabolism of FLCs and other proteins from glomerular ultrafiltrate by PTEC.(Pesce *et al.* 1980; Sanders *et al.* 1987) Up to 30 g/day of low MW protein can be processed by this pathway. Consequently, only 1-10 mg/day of FLC appears in the urine of individuals with normal kidney function.(Wochner *et al.* 1967; Maack *et al.* 1979; Clyne and Pollak 1981) If the FLC load presented to the proximal tubule exceeds reabsorptive capacity, then FLCs will pass into the distal nephron and can ultimately be detected in the urine, where, in PCD, it is also referred to as Bence Jones protein.

The internalisation of FLCs by PTEC is a constant process and not influenced by the isoelectric point (pI) of an individual light chain.(Smolens and Miller 1987) Uptake occurs through rapid and saturable megalin-cubilin receptor-mediated endocytosis that utilises the clathrin-coated pit pathway, and results in vesicular trafficking, where the receptors are returned to the cell surface, and the endocytic vesicles containing their cargo enter the endosomal-lysosomal pathway and are acidified.(Batuman *et al.* 1990; Batuman and Guan 1997; Batuman *et al.* 1998; Klassen *et al.* 2005) This pathway is also dependent on receptor associated protein (RAP), which has a chaperone-like function to megalin.(Verroust *et al.* 2002) Megalin and cubilin also bind a wide range of other ligands, including albumin and provide a highly efficient physiological mechanism for conserving AAs and essential protein-bound molecules.(Christensen and Birn 2001; Kozyraki *et al.* 2001; Birn *et al.* 2005)

1.4 Why do Some Clonal FLCs Cause Kidney Injury?

FLCs isolated from patients with PCD and kidney injury have a higher ability to self-associate and form higher MW aggregates under physiological conditions than FLCs purified from patients with PCD but without kidney injury. This is irrespective of the underlying type of renal injury.(Myatt *et al.* 1994) Furthermore, mice injected with FLCs from patients with a range of renal lesions developed similar lesions in the animal indicating that specific clones of FLCs cause a distinct pattern of injury.(Solomon *et al.* 1991) This supports the principle that the primary structure of the molecule is an important determinant of the pattern of injury seen.

1.5 Resident Renal Cells are Differentially Predisposed to Injury by FLC

FLCs filtered from glomerular capillary blood are transported into the mesangium or pass into tubular ultrafiltrate. The responses of mesangial and tubular epithelial cells to the individual clone of FLC determine the specific patterns of injury that are seen at both sites.

Mesangial Cells (MCs) support and maintain the glomerulus by secreting both extracellular matrix (ECM) and mediators and enzymes such as matrix metalloproteinases (MMPs), which regulate the composition and structure of ECM and the biological activity of MCs and other glomerular cells.(Schlondorff 1996; Vu and Werb 2000; Parks 1999; Mott and Werb 2004; Massova *et al.* 1998; Van Wart and Birkedal-Hansen 1990; Steffensen *et al.* 2001; Visse and Nagase 2003) Clonal FLC may disrupt these processes and cause glomerular injury by: (i) upon uptake promoting phenotypic changes in MCs, (ii) secretion into the ECM by MCs as amyloidosis fibrils

or LCDD deposits; (iii) direct deposition into the mesangium without cell processing. Interactions of mesangial cells with FLCs that cause glomerular injury are summarised in Figure 1.2.

1.6 Disease Specific Considerations for Mesangial Cells and Glomerular Pathology

1.6.1 AL Amyloidosis

FLCs are the commonest cause of amyloidosis of at least 25 structurally unrelated proteins.(Westermark 2005) They are the most structurally diverse group of proteins implicated in this disease. The disease is recognised on histology by Congo red staining and apple-green birefringence under polarised light.(Divry and Florkin 1927) AL-amyloidosis is associated primarily with PCD but can be associated with clonal proliferation of any cell of B-cell lineage.(Simmonds *et al.* 1997; Morel-Maroger *et al.* 1970) Approximately 10% of patients with multiple myeloma also have detectable tissue deposits of AL-amyloid.(Kapadia 1980)

AL-amyloidosis is defined *in situ* by immunostaining and electron microscopy. The presence of hypervariable regions may account for variable detection by specific antisera in conventional immunohistochemistry. Gold immunoelectron microscopy is a more sensitive and reliable method for identifying AL amyloidois *in situ*,(Toyoda *et al.* 1991) however this is not always available in routine clinical practice.(Veeramachaneni *et al.* 2004) Biochemical typing of amyloid from formalin-fixed, paraffin-embedded

Figure 1.2.Interactions of FLCs with mesangial cells.

(Legend on following page)

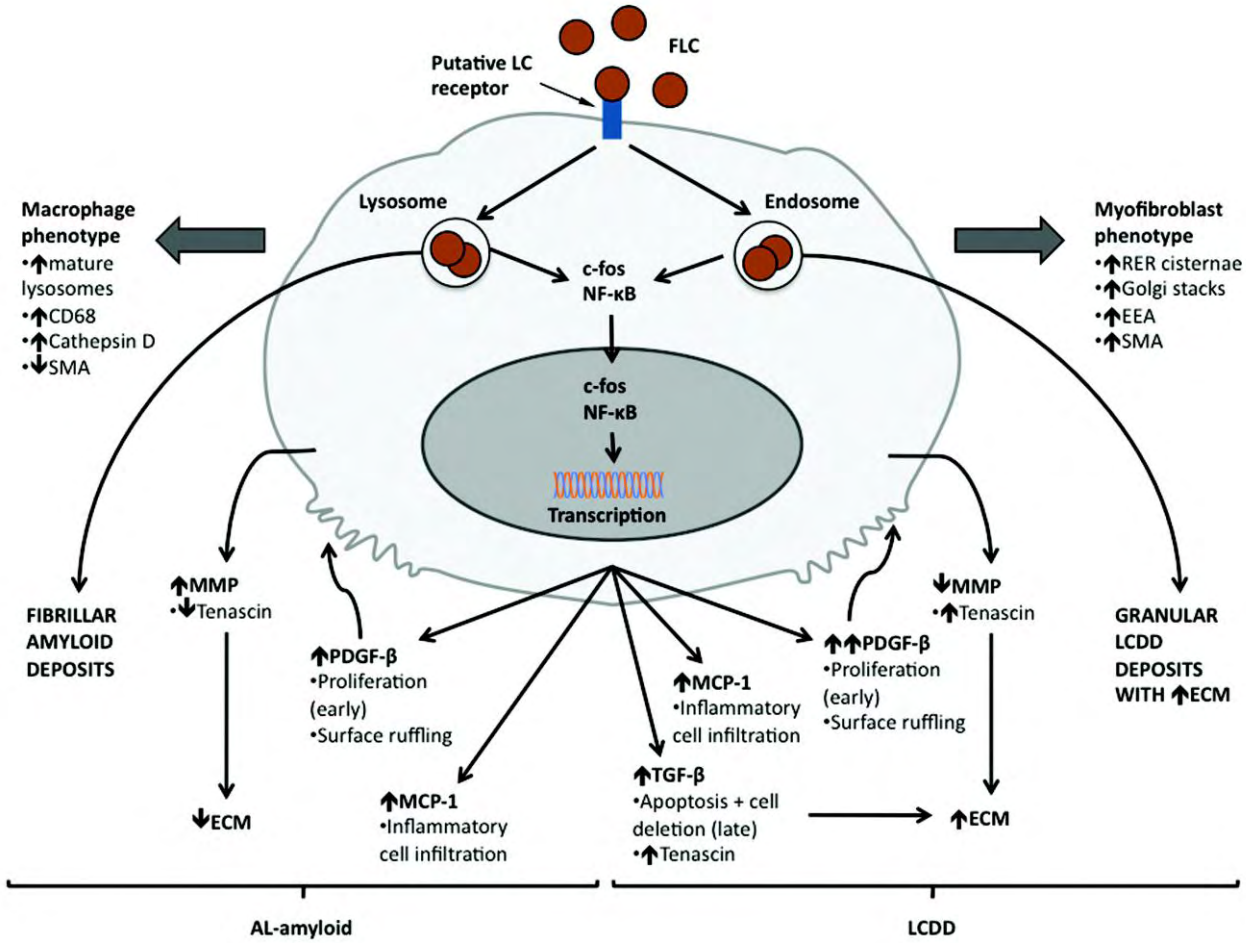

Figure 1.2 AL-amyloidosis (left) and LCDD (right). Both AL-amyloid and LCDD FLCs share a common route of entry into mesangial cells via a putative receptor. However, they are channelled into different intracellular trafficking pathways and exhibit different effects on the cell. AL-amyloid FLCs are catabolised within lysosomes, whereas LCDD FLCs are processed in endosomes. Processed FLCs are deposited in the mesangium as fibrils in the case of AL-amyloidosis, or as granular deposits with increased ECM in the case of LCDD. Both types of FLC initiate intracellular signalling, with migration of c-fos and NF-κB to the nucleus resulting in transcription of MCP-1 and PDGF-β. The release of PDGF-β is more pronounced with LCDD FLCs compared to AL-amyloid FLCs. MCP-1 recruits inflammatory cells. PDGF-β i) causes cell surface ruffling, resulting in increased cell surface area, and ii) promotes early mesangial cell proliferation, which is more pronounced in LCDD than AL-amyloidosis. TGF-β production is increased in LCDD, which i) causes cell deletion later in the disease and, ii) increases production of ECM proteins. Expression of MMP-7, which degrades tenascin, is reduced in LCDD. The result is increased ECM. In AL-amyloidosis, production of TGF-β is not increased and there is increased expression of MMPs, resulting in destruction of ECM, which is then replaced by amyloid fibrils. *In vitro*, mesangial cells undergo phenotypic changes in response to these FLCs: AL-amyloid FLCs induce a macrophage-like phenotype, in keeping with a more catabolic role. LCDD FLCs induce a myofibroblast-like phenotype, in keeping with a more synthetic role.
LC, light chain; SMA, smooth muscle actin; EEA, early endosomal antigen; MMP, matrix metalloproteinases; ECM, extracellular matrix.

specimens, as well as proteomic techniques have been reported, but these are not widely available.(Goni and Gallo 2005; Murphy *et al.* 2001)

In AL amyloidosis FLCs aggregate into fibrillary, non-branching, beta-pleated sheet structures between 7 and 12 nm thick. As the disease develops there is a progressive replacement of normal matrix by amyloid fibrils, leading to destruction of glomerular architecture.(von Gise *et al.* 1981; Herrera *et al.* 1999; Herrera 2000) It has been shown that B cells from patients with AL-amyloidosis produced both intact FLCs and fragments of FLC, and these can then be extracted from amyloid deposits within the patient's kidneys, suggesting that abnormal synthesis and/or ineffective proteolysis are important for the development of the disease.(Picken *et al.* 1986) The role of abnormal synthesis is emphasised by the ability of human amyloidogenic FLCs to cause amyloidosis in a murine model.(Solomon *et al.* 1992) A crucial co-factor in the development of the disease is the presence of serum amyloid protein (SAP) which binds to and protects fibrils from proteolytic degradation.(Gallo *et al.* 1988; Tennent *et al.* 1995) SAP is a member of the pentraxin family of proteins, which are manufactured in the liver and also include C-reactive protein.

1.6.2 Light Chain Variants and Amyloidosis

AL-amyloidosis is more frequently associated with λ FLCs than κ FLCs.(Abraham *et al.* 2003; Bellotti *et al.* 2000; Dember 2006) FLCs containing the V λ VI subgroup have been demonstrated to be differentially deposited in the glomerulus compared to other sites.(Solomon *et al.* 1982; Comenzo *et al.* 2001)

It is the structural heterogeneity of the V_L region that determines the organ specificity of the individual FLC.(Nyquist *et al.* 1993; Preud'homme *et al.* 1994; Abraham *et al.* 2003; Bellotti *et al.* 2000) In one study, two recombinant V_L domains derived from amyloidogenic FLCs were compared to a V_L domain derived from FLC which was not amyloidogenic.(Raffen *et al.* 1999) *In vitro,* amyloidogenic V_L was significantly less stable in thermodynamic studies and tended to form fibrils. Site-directed mutagenesis showed that only destabilising AA substitutions induced fibril formation. Denaturing the non-amyloidogenic V_L with guanidine hydrochloride conferred fibril forming ability, further indicating that the stability of FLCs may determine amyloidogenic properties. Indeed, sequencing of AL-amyloid fibrils have demonstrated that the constituent FLCs can have different primary structures due to AA substitutions.(Dwulet *et al.* 1986; Karimi *et al.* 2003)

Changes in AA sequences lead not only to changes in primary and secondary structure, but also to different post translational modifications, such as glycosylation,(Nyquist *et al.* 1993; Preud'homme *et al.* 1994; Stevens *et al.* 1995; Wetzel 1997) which are strongly correlated with formation of amyloid.(Nyquist *et al.* 1993; Omtvedt *et al.* 2000) Amyloidogenic FLCs may have abnormal glycosylation in the hypervariable CDR or framework regions.(Omtvedt *et al.* 2000) Introduction of glycosylation receptor sites by AA substitutions may also increase the risk of fibril formation.(Stevens 2000)

1.6.3 Differential Tissue Distribution in Amyloid

In some groups of patients, despite the amyloidogenic FLCs being derived from the same gene with subsequent similarities in FLC structure, there can be pronounced

variability in deposition patterns.(Enqvist *et al.*) These observations imply that although the gene has some influence on tissue distribution of amyloid, other factors such as somatic mutations and post-translational modifications are also important determinants of distribution. Additionally, local tissue characteristics at sites of deposition are likely to play a role. This is supported by a recent report of a series of eight patients with cardiac Ig deposition disease, in four of whom there was amyloid deposition at extracardiac sites, while none had cardiac amyloid.(Toor *et al.* 2006) In the kidney, the glomerular basement membrane contains glycosaminoglycans, which are thought to interact with amyloidogenic proteins and promote fibril deposition by: i) inducing conformational changes; ii) stabilizing these proteins and iii) providing protection from proteolysis.(Scholefield *et al.;* Yamaguchi *et al.;* Zhu *et al.;* Ancsin and Kisilevsky; Stevens and Kisilevsky)

1.6.4 Light Chain Deposition Disease

Light chain deposition disease (LCDD) predominantly involves the glomerulus but can also be seen on tubular basement membrane. Kappa FLCs, particularly those containing the VκIV subgroup are over-represented in this disease.(Denoroy *et al.* 1994; Ganeval *et al.* 1984) In patients with PCD, LCDD is present in 5%,(Kyle 1975) and around two-thirds have multiple myeloma.(Pozzi *et al.* 2003) The classical finding by light microscopy is of nodular glomerulosclerosis, similar in appearance to the Kimmelstiel-Wilson nodules of diabetic nephropathy.(Bruneval *et al.* 1985) In early involvement the findings may resemble mesangial or membranoproliferative glomerulonephritis.(Sanders *et al.* 1991; Turbat-Herrera *et al.* 1997) The nodules

consist of extracellular matrix (ECM) proteins and clonal FLC. Free light chains can also be deposited in glomerular capillary walls.

There are unusual hydrophobic AA substitutions in the CDR regions of LCDD associated FLCs.(Deret *et al.* 1997) These may facilitate a one-step precipitation out of solution in tissues, explaining the amorphous nature of LCDD deposits, as opposed to the organised, fibrillary deposition seen in amyloid, where electrostatic interactions may be more important.

1.7 Cell Specific Processing and Activation Leads to the Differential Patterns that are seen in FLC Disease

A direct toxic effect of FLCs on resident renal cells including MCs is supported by the observation that cytoreduction therapy aimed at the FLC-producing B-cell clone can result in the rapid improvement of clinical features such as proteinuria.(Dember *et al.* 2001; Leung *et al.* 2005) These improvements occur too early to be explained purely by regression of disease *in situ*.(Zeier *et al.* 2003; Kyle *et al.* 1982; Merlini and Bellotti 2003)

Light chains affect MC function with expansion of ECM,(Sanders *et al.* 1991; Herrera *et al.* 1999; Turbat-Herrera *et al.* 1997; Johnson 1994; Keeling and Herrera 2005c; Schnaper *et al.* 1996) transformation of MC phenotype,(Johnson 1994; Ronco *et al.* 2001; Darby *et al.* 1990; Watanabe *et al.* 2001; Herrera *et al.* 2001; Striker *et al.* 1989; Keeling *et al.* 2004) and the deposition of FLC derived protein in the mesangium.(Herrera *et al.* 1999; Turbat-Herrera *et al.* 1997) However there are

fundamental differences between different disease states in the handling and therefore the potential clinical manifestations associated with FLC clonality. For example, a central feature of amyloidogenic FLCs *in vitro* is the transformation of MCs to a macrophage phenotype.(Herrera *et al.* 2001; Keeling *et al.* 2004) The cells develop lysosomes within which degradation and remodeling of FLCs into amyloid occurs.(Shirahama and Cohen 1973; Shirahama and Cohen 1975; Bohne *et al.* 2004) Conversely, MC treated with LCDD FLCs are more likely to evolve a myofibroblast phenotype.

Receptor mediated uptake of FLCs by MCs has been proposed.(Russell *et al.* 2001; Teng *et al.* 2004) Although this may be a common receptor, different types of FLCs activate different signalling pathways.(Teng *et al.* 2004; Russell *et al.* 2001) Amyloidogenic FLCs are internalized and transported to mature lysosomes, indicating involvement of the clathrin-coated pit pathway. In contrast, LCDD FLCs are predominantly phagocytosed into the endosomal compartment. Preferential uptake of certain species of FLC by MCs may partly explain favoured deposition in the kidney of light chains derived from specific germ lines such as VλVI.(Comenzo *et al.;* Keeling *et al.;* Teng *et al.*) Further, studies have shown that tubulopathic FLCs are not taken up into MCs, indicating that they do not bind to receptors and *in vivo* would have passed unhindered to the proximal tubule. (Russell *et al.*)

Although MCs are necessary for the formation of amyloid, there is both *in vitro* and *in vivo* evidence to support the hypothesis that amyloid fibrils themselves, once deposited,

can act as niduses for propagation, thus enhancing amyloid deposition.(Tagouri *et al.;* Merlini and Westermark; Lundmark *et al.*)

The signalling pathways that are activated when glomerulopathic FLCs interact with MCs are being defined.(Russell *et al.* 2001; Rovin *et al.* 1995) Free light chains from patients with LCDD and AL-amyloidosis rapidly promote the migration of c-fos and NF-κB to the nucleus.(Russell *et al.* 2001) c-fos promotes cell surface ruffling, which increases cell surface area and interactions with FLC and also promotes secretion of PDGF-β, with cell proliferation.(Russell *et al.* 2001) LCDD FLCs promote more PDGF-β release than Amyloid FLCs; this may account for the early proliferative lesions seen in LCDD, before matrix expansion reaches a stage where cell deletion occurs. NF-κB leads to gene activation and release of CSF-1, RANTES and MCP-1.(Russell *et al.* 2001; Rovin *et al.* 1995; Duque *et al.* 1997) These cytokines promote the recruitment of inflammatory cells to the glomerulus.

1.8 The Differential Role of TGF Beta in Amyloid and LCDD

TGF-β modulates progression of LCDD and AL-amyloid.(Sugiyama *et al.* 1996; Zhu *et al.* 1995; Teng *et al.* 2003) In MC culture, FLCs from patients with LCDD have been shown to alter calcium homeostasis, reduce cell proliferation, and increase extracellular matrix (ECM) secretion, including tenascin, an important protein component of ECM, and these effects are mediated by TGF-β.(Truong *et al.;* Zhu *et al.* 1995; Zhu *et al.* 1997) Blocking vesicular transport between endoplasmic reticulum and the Golgi apparatus in cells exposed to TGF-β normalised production of fibronectin and

tenascin.(Teng *et al.* 2003) PDGF-β and TGF-β act independently. PDGF-β can induce cell proliferation, but does not influence tenascin and fibronectin production, however; these are regulated by TGF-β. TGF-β production has been shown to be increased by LCDD FLCs, but not by AL-amyloidosis FLCs.(Keeling and Herrera 2009) This may explain why in LCDD, there is greatly increased matrix, while in amyloid the matrix is replaced by fibrils. Finally, cell deletion by apoptosis in glomerulosclerosis is in part triggered by TGF-β. *In vitro*, FLCs from LCDD enhance TGF-β mediated apoptosis of MCs.(Sugiyama *et al.* 1996; Negulescu *et al.* 2002; Herrera *et al.* 1994; Tagouri *et al.* 1995)

1.9 Matrix Metalloproteinases

A number of studies have indicated that glomerular pathology may reflect expression patterns of MMPs.(Keeling and Herrera 2005b; Keeling and Herrera 2005c; Keeling and Herrera 2005a; Keeling and Herrera 2009) In one study, the expression of certain MMPs was six times higher in kidney biopsies from patients with AL-amyloidosis compared to LCDD or negative controls.(Keeling and Herrera 2005b) Furthermore, MMP-2 activity is increased in AL-amyloidosis compared to LCDD. These data indicate that activation of MMPs following delivery of amyloidogenic FLCs to the mesangium leads to matrix destruction and replacement with amyloid fibrils.

Conversely, tenascin is present in excess in LCDD, because of decreased levels of MMP-7, which degrades tenascin.(Herrera 2000; Turbat-Herrera *et al.* 1997) There is inhibition of release of MMP-7 from MC by LCDD FLCs (Imai *et al.* 1994); this effect

is not present with AL-amyloidosis FLCs and cast nephropathy FLCs.(Keeling and Herrera 2009)

Finally, MC function may be modulated by extracellular matrix proteins.(Saito *et al.* 1993; Martin *et al.* 2001) So abnormal mesangium produced by MCs activated by FLCs, may itself alter MC function, and further potentiate glomerulosclerosis.

1.10 Tubulointerstitial Disease Associated with Light Chains: The Proximal Tubule

1.10.1 Adult Acquired Fanconi Syndrome

Adult acquired Fanconi syndrome (AAFS) is a unique entity defined by selective reabsorptive dysfunction of the proximal tubule, with glycosuria, aminoaciduria, phosphaturia and hyperuricosuria, as well as bicarbonate loss causing a proximal (type II) renal tubular acidosis.(Lacy and Gertz 1999) The commonest underlying cause is a PCD, which is often low grade.(Maldonado *et al.* 1975) Classically, the histological finding is of crystalline deposits of FLCs within PTEC and which are resistant to proteolysis. However this appearance is not always present. The FLCs responsible are most frequently of the VκI subgroup,(Rocca *et al.* 1995; Messiaen *et al.* 2000) although cases of λ FLCs associated with AAFS have also been reported.(Thorner *et al.* 1983; Bate *et al.* 1998)

In a sequence study of five κ FLCs from patients with AAFS, all three FLCs from patients with crystalline deposits were derived from the same LCO2/O12 gene and had

non-polar AA residues exposed in the CDR1 region and a lack of accessible side chains in CDR3.(Deret *et al.* 1999) Hydrophobic or non-polar AA residues have also been reported elsewhere.(Messiaen *et al.* 2000) Crystallisation may result from these two factors. There has also been a report of a case of a patient with abnormal proximal tubular reabsorption and crystalline inclusions within PTECs.(Decourt *et al.* 2003) Sequencing of this patient's monoclonal protein revealed a FLC of VκI subgroup, with non-polar residue substitutions in CDR1.

In most patients with multiple myeloma, the presence of defects of tubular reabsorption and urine acidification is a consequence of the direct toxicity of FLCs on PTECs in the absence of crystalline deposits.(DeFronzo *et al.* 1978) It has been demonstrated that FLCs from patients with myeloma interfere with uptake of alanine, phosphate and glucose.(Batuman *et al.* 1986; Batuman *et al.* 1994) Finally, there has been one report of case a case of PCD, AAFS (diagnosed without renal biopsy) and nephrogenic diabetes insipidus, suggesting one potential outcome of tubular dysfunction is ADH resistance.(Smithline *et al.* 1976) Interestingly, this patient had distal (type I), not proximal, renal tubular acidosis.

1.10.2 Cast Nephropathy (Myeloma Kidney)

Cast nephropathy, or myeloma kidney, is the commonest renal manifestation in PCDs.(Herrera *et al.* 2004; Ivanyi 1989) This condition is characterised by tubulointerstitial inflammation and fibrosis, associated with hard, often fractured distal tubular protein precipitates (casts), consisting of uromodulin and FLCs (figure 1.3).(Pasquali *et al.* 1987; Pirani *et al.* 1987) There is usually a reaction around the casts

of multinucleated monocyte/macrophage-derived giant cells.(Start *et al.* 1988; Alpers *et al.* 1989) Distal tubular cast formation may also be seen in up to a third of cases of LCDD and AL-amyloid.(Pozzi *et al.* 2003)

1.10.3 Proximal Tubular Toxicity

Proximal tubular epithelial cells (PTEC) are the most abundant cell type in the kidney. They are highly efficient at recovering filtered proteins from the tubular lumen. Excess filtered protein, including FLCs, can overload this process with subsequent tubular injury, inflammation and progressive fibrosis.(Remuzzi and Bertani 1998; Abbate *et al.* 1998; Remuzzi 1999; Zoja *et al.* 1999) In the setting of PCDs, exposure to clonal FLCs can have dramatic pathological effects. Much recent work has elucidated the mechanisms underlying FLC mediated damage to PTECs. Interactions of PTECs with FLCs that cause tubulointerstitial injury are summarised in Figure 1.4.

Studies on the effects of human FLCs on rodent proximal tubule have observed abnormal flux of water, glucose and chloride.(Sanders *et al.* 1987) Histological examination showed desquamation of cells and cytoplasmic vacuolation. Similar findings were reported in renal tissue from human subjects with multiple myeloma but with no tubular cast formation.(Sanders *et al.* 1988b)

A number of studies have contributed significantly to our understanding of the cell signaling events which take place after FLCs are bound by megalin and cubilin and internalised by PTECs. These changes range from functional, such as suppression of Na-K-ATPase gene expression and a decrease in cell metabolism,(Guan *et al.* 1999) to

Figure 1.3. Cast nephropathy and accelerated *in situ* progression of interstitial fibrosis in a patient with multiple myeloma.

A: Renal biopsy at presentation showing typical features of cast nephropathy. There is evidence of proximal tubular damage, with vacuolation of cells and cell debris within the lumina. There is an interstitial cellular infiltrate. Distal tubules contain casts. Note that in this biopsy there is little evidence of fibrosis. B: Renal biopsy from the same patient after 6 weeks. There is extensive interstitial fibrosis, with severe tubular atrophy. Note that some tubules still contain casts. (Both images, periodic acid methanamine silver, x200 magnification) C: High-power view of a light chain cast in a patient with multiple myeloma.The appearance is hard and waxy, with fractures. There is a peritubular inflammatory infiltrate, with invasion of the lumen and adhesion of cells to the cast. A giant cell reaction around the cast is seen. These casts are composed of light chain and uromodulin. (H&E, x400 magnification)

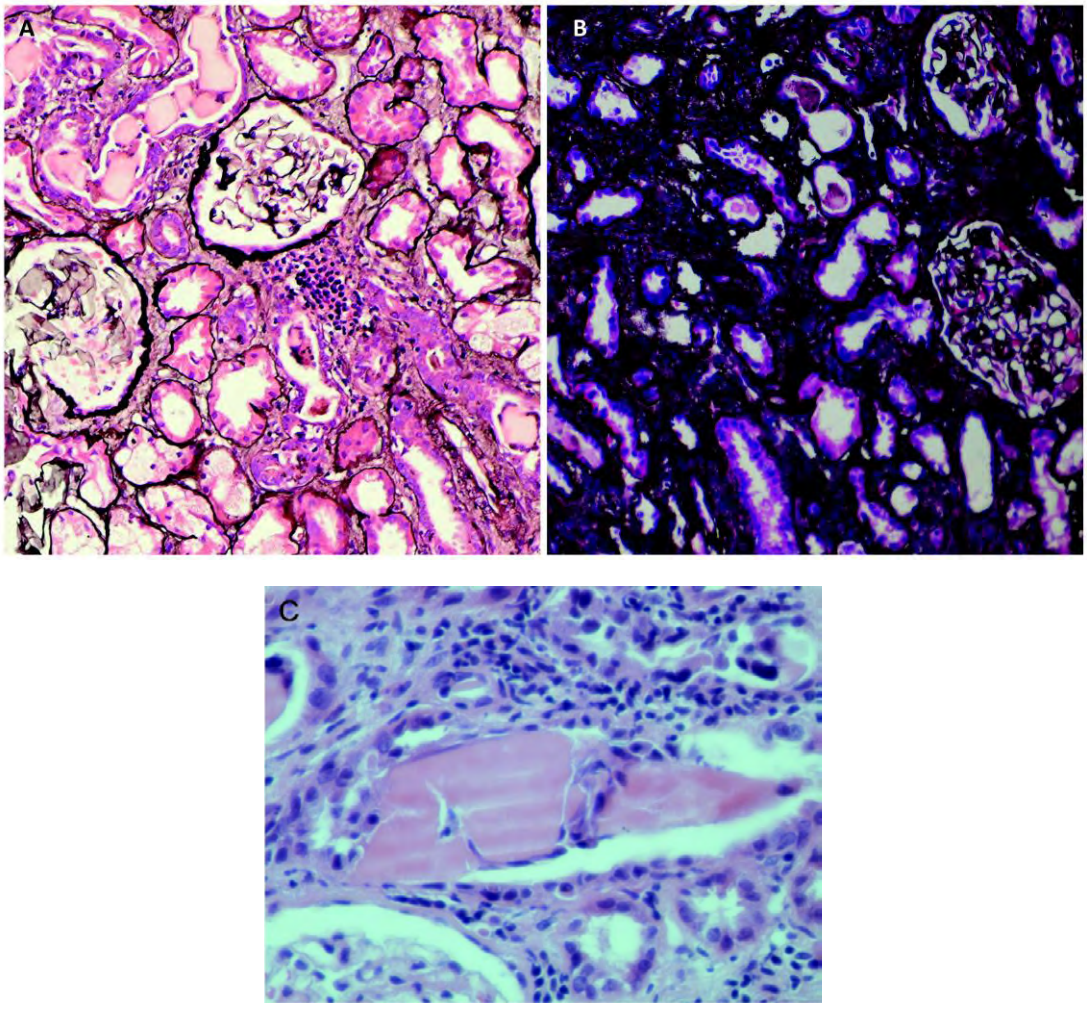

Figure 1.4. Interactions of FLCs with proximal tubule epithelial cells.

(Legend on following page)

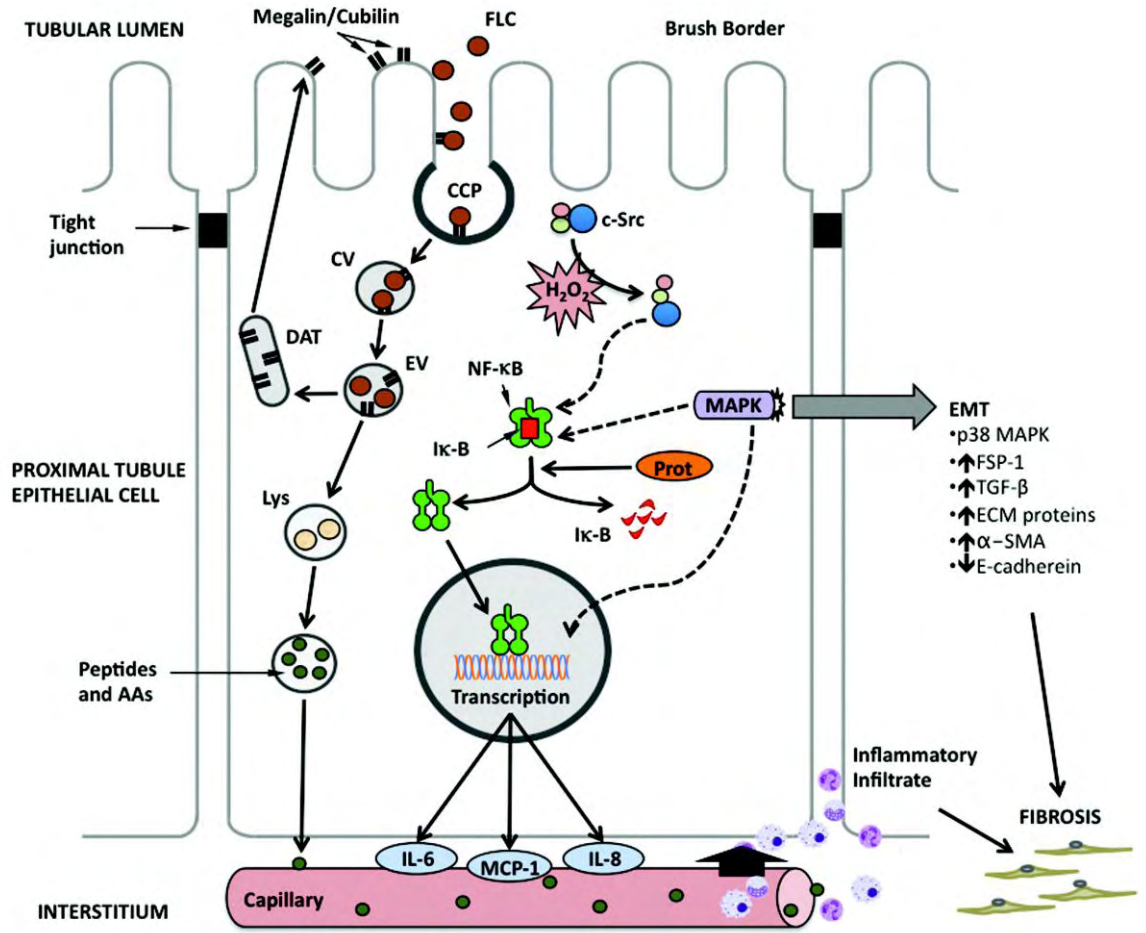

Figure 1.4 Interactions of FLCs with proximal tubule epithelial cells (PTECs). Trafficking events are shown on the left, and signalling events on the right. Filtered FLCs are delivered to the proximal tubule where they engage megalin and cubilin on the brush border. Receptor-ligand complexes are concentrated in clathrin coated pits (CCP) and endocytosed to coated vesicles (CV), which mature into endosomal vesicles (EV), where receptors and ligands are disengaged, following which, receptors are recycled to the luminal cell surface via dense apical tubules (DAT). FLCs undergo proteolysis into their constituent peptides and amino acids within mature lysosomes (Lys), and these products are returned to the circulation. Following endocytosis, an early event is the production of H_2O_2. H_2O_2 oxidises the tyrosine kinase c-Src to its active state. Downstream signalling leads to activation of NF-κB. Proteasome (Prot) mediated degradation of the Iκ-B permits nuclear translocation of NF-κB subunits, leading to transcription of inflammatory cytokines. Recruitment of inflammatory cells to the interstitium ensues, promoting fibrosis. Activation of MAPKs also occurs. These exert additional activating effects on NF-κB, as well as influencing transcription via other pathways. EMT is seen *in vitro* when PTECs are exposed to certain LCs, a phenomenon which may contribute to fibrosis *in vivo*.
FSP-1, fibroblast-specific protein 1; ECM, extracellular matrix.

more dramatic ultrastructural changes. In a study of the differential effects of FLC clones on PTEC, cells underwent changes that included abnormalities in the actin cytoskeleton to DNA degradation, apoptosis and necrosis.(Pote *et al.* 2000) Cytotoxicity of FLCs in this study was also demonstrated by increased levels of lactate dehydrogenase (LDH) in cell culture supernatants, indicating increased cell death.

On endocytosis of clonal FLC there is a dramatic increase in production of the inflammatory cytokines IL-6, IL-8 and MCP-1, events which are dependent on nuclear translocation of NF-κB subunits.(Sengul *et al.* 2002) The release of these cytokines would explain much of the inflammatory cell infiltration and fibrosis seen in myeloma kidney. A subsequent study demonstrated that mitogen activated protein kinases (MAPKs) ERK 1/2, JNK 1/2, and p38 play a role in signaling leading to the production of these cytokines.(Sengul *et al.* 2003) Pituitary adenylate cyclase activating polypeptide with 38 residues (PACAP38) modulates MAPK signaling and activation of NF-κB. It acts via the G-protein-coupled receptors PAC_1, $VPAC_1$ and $VPAC_2$, which are known to initiate several signal transduction pathways.(Harmar *et al.* 1998) In PTECs, PACAP38 acting via PAC_1 and $VPAC_1$, abrogated translocation of NF-κB and cytokine production when exposed to FLCs.(Arimura *et al.* 2006) Cytokine production in rat kidneys after injection of the animal with FLCs was also suppressed by injection of PACAP38. Interestingly, PACAP38 also suppressed growth and proliferation of κ and λ secreting myeloma cells in culture, thereby making PACAP38 a potential therapeutic candidate for treating patients with myeloma kidney through targeting two pathogenic processes.(Li *et al.* 2006) There is a published case report of a patient where

PACAP38 was used and urinary FLC concentrations decreased significantly, however the patient was concomitantly receiving Dexamethasone. (Li *et al.* 2007)

Activation of NF-κB and subsequent nuclear translocation of its subunits is required for transcription of inflammatory mediators in response to FLC. Nuclear translocation and DNA binding is regulated by inhibitors (IκB).(Perkins; Hayden and Ghosh; Sanz *et al.*) Activating stimuli result in engagement of the IκB inhibitor, IκB kinase (IKK). IKK phosphorylates IκB, targeting it for ubiquitination and subsequent degradation by proteasomes, which then permits nuclear translocation of NF-κB.(Sanz *et al.*) Bortezomib, which is used in the treatment of multiple myeloma, specifically inhibits the 26S proteasome.(Richardson *et al.;* Stanford and Zondor; Bonvini *et al.*)

In some forms of renal fibrosis fibroblasts may be derived from epithelial cells, a process referred to as epithelial-to-mesenchymal transition (EMT).(Rastaldi *et al.* 2002; Liu 2004) On exposure of PTECs to FLCs, there is increased expression of cytokines and alpha-SMA and reduced E-cadherin expression, indicating transformation from an epithelial to a myofibroblast phenotype.(Li *et al.* 2008b) There is also increased expression of TGF-ß dependent ECM components. Silencing p38 MAPK suppressed cytokine release and EMT was attenuated by bone morphogenic protein-7 (BMP-7) and PACAP38. Blocking endocytosis of FLCs by silencing megalin and cubilin expression, has been shown to markedly suppress cytokine production and to prevent EMT after exposure of cells to FLCs.(Li *et al.* 2008a)

Antibodies can oxidize water to produce hydrogen peroxide (H_2O_2), a feature that may improve their effectiveness against their targets.(Wentworth *et al.* 2001) The reaction site for this has been localised to a highly conserved segment of the light chain V_L region consisting of β-pleated sheets forming a hydrophobic core. It has now been shown that FLCs in solution can also oxidise water and that H_2O_2 levels are increased in the supernatant of PTEC treated with monoclonal FLCs.(Wang and Sanders 2007) This effect was not seen with non-immunoglobulin-derived proteins. Hydrogen peroxide can act as an intracellular second messenger during signal transduction in response to many stimuli, including protein overload of PTECs.(Rhee 2006; Morigi *et al.* 2002; Nathan 2003) Furthermore, MCP-1 production was markedly reduced when either H_2O_2 or NF-κB activity was blocked. H_2O_2 can diffuse across the cell membrane lipid bilayer and also pass through aquaporin channels, so the specific assessment of the relative contributions of intracellular and extracellular production is difficult;(Bienert *et al.* 2007) however, the addition of catalase to the medium had no effect on MCP-1 production, indicating that sufficient quantities of H_2O_2 were produced intracellularly for signaling. Direct activation of the redox-sensitive tyrosine kinase c-Src by this H_2O_2 has now been established as a key step in the signal transduction cascade.(Basnayake *et al.*) Again, blocking receptor-mediated endocytosis by silencing megalin and cubilin expression was shown to abrogate the MCP-1 response. c-Src has a central role in signal transduction in response to many external stimuli, and may be a potential therapeutic target.(Parsons and Parsons; Kim *et al.*)

In many of these studies, it was repeatedly observed that FLCs have far more powerful proinflammatory effects on PTECs than other filtered proteins commonly implicated in

proximal tubule inflammation, such as albumin.(Sanders *et al.* 1987; Sengul *et al.* 2002; Li *et al.* 2008b; Wang and Sanders 2007) Although this effect may be multifactorial is likely that a significant component is associated with H_2O_2 production.

1.11 Distal Tubular Cast Formation

1.11.1 Tubular Toxicity and Cast Formation

The primary structure of a protein influences the pI; when the pI is close to the ambient pH a protein carries no net charge and tends to precipitate out of solution.(Arakawa and Timasheff 1985) There is no correlation between the pI of a FLC clone and cytotoxicity to PTEC,(Sanders *et al.* 1988a; Norden *et al.* 1989; Smolens *et al.* 1983) despite a wide variation in pI between FLC clones.(Johns *et al.* 1986) This reflects pI independent receptor-mediated uptake of FLCs into PTECs. However, the pI does influence the potential of FLCs to precipitate in the distal nephron.(Sanders *et al.* 1988a) Low MW proteins with pIs of 5.6-7.3 precipitated in the ascending limb of the Loop of Henle and distal tubule, while a protein with a pI of 5.1 precipitated more distally. As tubular fluid travels down the distal nephron acidification occurs through physiological mechanisms, this may then facilitate precipitation of proteins of progressively lower pI. This is supported by the observation that alkalinisation of urine ameliorated the negative effects of FLCs on inulin clearance in rats.(Holland *et al.* 1985) Other factors such as tubular fluid concentration, reduced flow rates, and the presence of uromodulin may also contribute.

Uromodulin is secreted by cells of the thick ascending limb of the Loop of Henle. It is heavily glycosylated, with the carbohydrate moiety accounting for 30% of a molecular weight of 80 kDa. It has a pI of 3.5.(Fletcher *et al.* 1970b; Fletcher *et al.* 1970a; Clyne *et al.* 1979) Uromodulin is tethered to the luminal cell surface membrane by a glycosylphosphatidylinositol (GPI) anchor. This is eventually cleaved, allowing uromodulin to be carried by tubular fluid down the distal nephron and to appear in the urine.(Rindler *et al.* 1990; Weichhart *et al.* 2005) It is the main urinary protein in healthy individuals, excreted at 30-50mg/day.(Hoyer and Seiler 1979; Kumar and Muchmore 1990; Serafini-Cessi *et al.* 2003) Uromodulin can self-aggregate into a gel-like material, a process which is affected by increasing electrolyte concentrations in ambient solution.(Porter and Tamm 1955; Patel *et al.* 1964; Stevenson *et al.* 1971) It has the ability to bind to and co-precipitate with many low molecular weight proteins.(Sanders *et al.* 1988a; Koss *et al.* 1976; Bock 1997; Sanders *et al.* 1990) FLC interactions with uromodulin to promote cast formation in the distal nephron are summarised in figure 1.5.

The specific physiological functions of uromodulin have yet to be elucidated. However there is evidence to support roles in protecting against ascending urinary tract infection and modulating immune responses.(Kumar and Muchmore 1990; Bates *et al.* 2004; Pak *et al.* 2001) Uromodulin has been shown to bind directly to certain fimbriated *Escherichia coli* strains.(Pak *et al.* 2001) It may have a pro-inflammatory role by the induction of inflammatory cytokines such as TNF-α and IL-8 from monocyte/macrophages and neutrophils.(Su *et al.* 1997; Kreft *et al.* 2002; Prajczer *et al.* 2010) Uromodulin has also been shown to encourage neutrophil transmigration across

Figure 1.5. Light chain interactions in the distal nephron.

(Legend on following page)

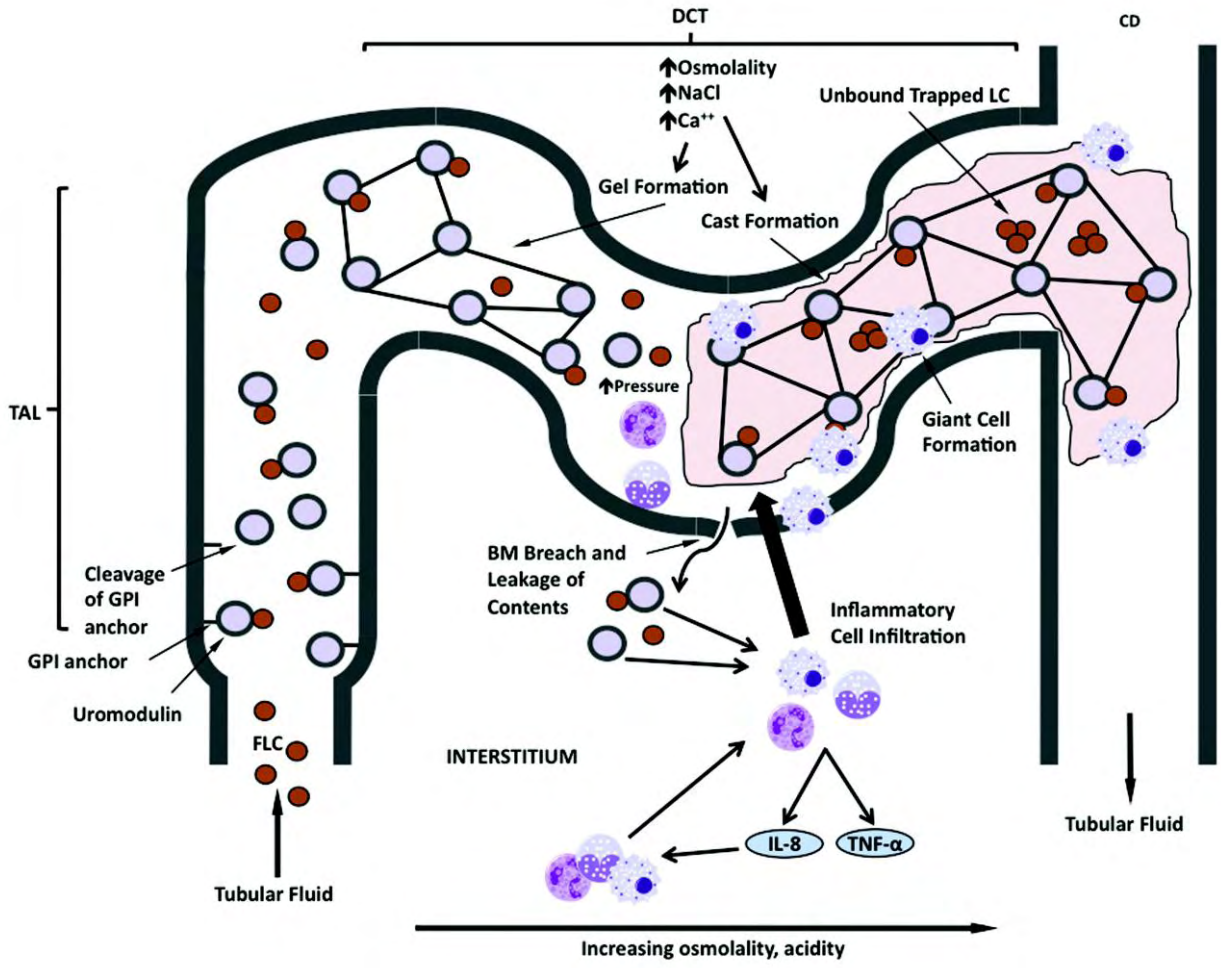

Figure 1.5 Uromodulin is secreted from the thick ascending limb of the loop of Henle. Upon cleavage of its glycosylphosphatidylinositol (GPI) anchor, free uromodulin is released into the tubular lumen. FLCs entering this section of the nephron can bind directly to uromodulin. Uromodulin has the ability to form a gel, influenced by increasing electrolyte content and osmolality. Cast formation is also enhanced by these factors, which in the clinical setting can be caused by dehydration, hypercalcaemia, diuretics, non-steroidal anti-inflammatory agents and radiocontrast media. Cast formation results in increased intratubular pressure. Physiological mechanisms can increase tubular fluid osmolality and acidity, and the latter may affect FLC solubility by virtue of isoelectric point. Cast nephropathy is associated with interstitial inflammatory cell infiltration and invasion of the tubule, with macrophage-derived giant cell reaction around the casts. Uromodulin has been shown to activate dendritic cells and macrophage by direct engagement of toll-like receptor-4, facilitate transmigration of neutrophils across epithelial monolayers *in vitro*, and effect the release of inflammatory mediators from these cells. Inflammation may be exacerbated by damage to tubular basement membrane (BM) with leakage of uromodulin into the interstitium.
Abbreviations: TAL, thick ascending limb; LC, light chain; BM, basement membrane.

renal epithelial monolayers *in vitro*.(Schmid *et al.* 2010) Macrophages and dendritic cells are activated by uromodulin through direct engagement of toll-like receptor 4 (TLR4) and subsequent mobilisation of NF-κB, a phenomenon which may help innate immune cells identify invading pathogens with uromodulin bound to their surfaces.(Saemann *et al.* 2005; Anders *et al.* 2004) Although speculative, it is possible that, through these mechanisms, uromodulin attracts inflammatory cells to sites of cast formation, one consequence of which is the frequently seen giant cell reaction around casts.

Animal studies have elucidated our understanding of myeloma cast formation to a considerable extent. Using an *in vivo* rodent nephron microperfusion model, it has been shown that certain low MW proteins (including FLCs), caused morphological damage to PTECs and interfered with fluid, chloride and glucose transport, while others precipitated in the distal tubule as casts.(Sanders *et al.* 1988a) These data support the concept that some FLC clones are toxic to the proximal tubule, while others FLC clones are cast-forming.

A subsequent microperfusion study demonstrated that cast forming proteins (FLCs and myoglobin) reduced chloride absorption in the proximal tubule. With FLCs, this was observed in a dose-dependent manner. *In vitro*, low MW proteins including all FLCs tested aggregated with uromodulin. Aggregation was dependent on the pI of the protein, as evidenced by albumin (pI 4.8) not binding uromodulin but cationic albumin (pI 9.2) binding very strongly. Aggregation was enhanced by increasing sodium chloride and

calcium ion concentrations in the solution. This may be a result of sodium and calcium ions increasing the viscosity of solutions containing uromodulin.(Stevenson *et al.* 1971)

The rate of cast precipitation in nephrons infused with FLCs is related to the concentration of FLCs in solution, but can occur down to very low concentrations.(Sanders and Booker 1992) Obstruction of individual nephrons can result in tubular atrophy.(Tanner and Knopp 1986; Tanner and Evan 1989) Cast formation is accompanied by a rise in intratubular pressure, confirming the physical obstruction of tubules by casts.(Sanders and Booker 1992) Impairment of tubular fluid flow in other conditions has been associated with backflow and the presence of uromodulin upstream of its site of production, as far as the glomerulus.(McGiven *et al.* 1978) It may be possible that uromodulin also contributes to inflammation at these sites.

Reducing extracellular fluid volume by reducing fluid delivery to the animal, or concentrating tubular fluid by administering furosemide promoted aggregation of FLCs with uromodulin. Colchicine, by reducing uromodulin secretion by the nephron and reducing the carbohydrate composition of uromodulin, prevented cast formation.(Sanders and Booker 1992) An *in vitro* study to investigate the nature of FLC binding to uromodulin was then performed.(Huang *et al.* 1993) Different clones of FLCs bound to uromodulin with varying affinities. A specific region of uromodulin was identified as the binding site of all the FLCs tested. As FLCs bound to glycosylated as well as deglycosylated uromodulin, this region was inferred to be a peptide sequence. This was supported by blockade of FLC binding by a monoclonal antibody against a specific peptide segment of uromodulin. Subsequently a 9 AA sequence on uromodulin

was identified as the FLC binding domain,(Huang and Sanders 1997) with the CDR3 region of FLCs as the site of interaction with uromodulin.(Ying and Sanders 2001)

The presentation of patients with acute cast nephropathy has been associated with dehydration, hypercalcaemia, administration of diuretics and radiological contrast media.(Goranov 1996) The role of some of these co-factors have also been investigated in the binding of FLCs to uromodulin.(Huang and Sanders 1995) Acidic pH, calcium and furosemide increased FLC aggregation with uromodulin obtained from the urine of healthy donors. Treatment of the donors with colchicine resulted in them excreting uromodulin with reduced self-aggregation, but with no difference in the binding potential to FLC clones.

The process of cast formation is likely to reflect multiple factors. The binding of FLCs to uromodulin is not multivalent. However, uromodulin can aggregate to form a gel depending on ambient conditions and it may be that upon FLC engagement, uromodulin undergoes an unknown conformational change, which further promotes aggregation or precipitation out of solution. Influenced by pH and other factors, FLCs in high concentrations entering the distal tubule may also precipitate without interaction with uromodulin, and be trapped within the uromodulin-gel, forming part of a larger cast.(Wangsiripaisan *et al.* 2001)

1.12 Polyclonal Elevations in Light Chain Levels

Polyclonal elevations in FLCs may result from either reduced clearance or increased production. Hutchison *et al* have shown that serum and urine polyclonal FLC

concentrations are raised in patients with CKD.(Hutchison *et al.* 2008c) In this study, the authors demonstrated a stepwise increase in serum polyclonal FLCs with an incremental decline in kidney function, an observation which reflects the fact that clearance of FLCs is GFR dependent. The results of this study raises the hypothesis that as CKD progresses and the number of functioning nephrons declines, the remaining nephrons are exposed to higher concentrations of polyclonal FLCs, leading to potentiation of pro-inflammatory signalling and thus fibrosis. Although the concentrations of polyclonal FLCs in CKD are lower than those of monoclonal FLCs often seen in multiple myeloma, the exposure occurs over a prolonged period.

Polyclonal FLC levels are also elevated (independent of renal function) with generalised B-cell stimulation, in conditions such as systemic lupus erythematosus, rheumatoid arthritis, primary Sjogren's disease and chronic infections.(Hoffman *et al.* 2003; Gottenberg *et al.* 2007; Solling *et al.* 1981) It is worth noting that although renal impairment is not infrequently seen in such conditions, the underlying causes of kidney injury are related to the individual disease or treatment and not related to FLCs.(O'Callaghan 2004)

Investigations into the biological effects of polyclonal FLCs in the literature are few. The paucity of *in vitro* studies is likely to be a reflection of the complexity of purifying these proteins. They are normally present in serum and urine in only small concentrations and form only a small proportion of the total soluble protein. These factors can affect the efficiency of protein extraction processes.

A role for polyclonal FLCs as uraemic toxins which affect neutrophil function has been investigated by Cohen and co-workers.(Cohen *et al.* 1995; Cohen *et al.* 2003) These *in vitro* studies demonstrated that polyclonal FLCs isolated from dialysis effluent were capable of inhibiting essential functions of neutrophils. Neutrophils exposed to these FLCs exhibited a reduced state of activation, as assessed by hexose uptake, as well as reduced chemotaxis towards N-formyl-methionyl-leucyl-phenylalanine methyl-ester (fMLP-M). One consequence of this phenomenon *in vivo* might be an increased susceptibility to bacterial infections. These polyclonal FLCs were also able to prevent neutrophil apoptosis in a concentration-dependent manner *in vitro*. Phagocytic function was unaffected. *In vivo*, neutrophils perform a vital role in attacking and killing invading microorganisms. Timely removal of spent neutrophils, which are senescent and apoptotic, by macrophages is a crucial factor in controlling the balance between inflammation and repair at sites of infection and injury, by preventing excessive collateral damage and prolonged inflammation that may be caused by toxic neutrophil contents spilling into the interstitium.(Savill *et al.* 1989; Heinzelmann *et al.* 1999)

Whilst polyclonal FLCs may have a dysregulatory effect on neutrophil function, there have been no published basic science studies to date on a direct renal effect and there is no demonstrable causative link between polyclonal FLCs and the progression of renal disease.

As CKD progresses and serum polyclonal FLC concentrations rise, the remaining nephrons are exposed to increased levels filtered of FLCs. This would then result in increased uptake of FLCs into PTECs by receptor-mediated endocytosis. It may be

possible that in this setting, polyclonal FLCs exert pro-inflammatory effects on PTECs similar to monoclonal FLCs. If this were to be true, then it would be expected that *in vitro*, H_2O_2 generation might be observed in response to polyclonal FLCs. Such an observation would be highly significant, because this appears to be the initiating event in signal transduction, following endocytosis, resulting in the release of MCP-1 from PTECs, when they are exposed to monoclonal FLCs.(Wang and Sanders 2007)

Another observation that would be expected if polyclonal FLCs contributed to renal disease, is increased release of MCP-1 from PTECs after exposure. Although a number of cytokines have been reported to be released from PTECs in response to monoclonal FLCs, including IL-6 and IL-8, MCP-1 is of particular interest in the development and progression of renal interstitial fibrosis for a number of reasons. First, localised, intra-renal production of MCP-1 plays a major role in inflammation by directing macrophage recruitment to sites of injury in the interstitium.(Grandaliano *et al.* 1996; Tesch *et al.* 1999) Second, urinary, but not serum, MCP-1 levels are elevated in patients with CKD, supporting the importance of intra-renal production.(Wada *et al.* 2000) Third, there are close relationships between urinary MCP-1 and both albumin/creatinine ratio (ACR) and infiltrating macrophage numbers.(Eardley *et al.* 2006) Fourth, PTECs are likely to be the major source of MCP-1 in CKD in the absence of acute proliferative glomerulonephritis.(Grandaliano *et al.* 1996) Fifth, MCP-1 can also stimulate PTECs to secrete additional inflammatory mediators.(Viedt *et al.* 2002) All of these observations point to a central role for MCP-1 in progression of renal fibrosis.

Some monoclonal FLCs have also been shown to have cytotoxic effects on PTECs.(Pote *et al.* 2000) If polyclonal FLCs also had such cytotoxic potential, PTECs exposed to these FLCs would be expected to undergo lysis, releasing LDH into the cell culture supernatants.

One of the most commonly performed tests in the investigation of kidney disease is the microscopic examination of urinary sediment. A common finding in patients with CKD are urinary casts, composed of proteins (hyaline casts) or a mixture of cell types (granular, waxy or broad casts) bound together with uromodulin.(Simerville *et al.*) Since it is known that uromodulin also binds to FLCs with high affinity, and there is an increased filtered load of FLCs in CKD, it may be possible that polyclonal FLCs exert a biological effect in the kidney in CKD. If this hypothesis were true, then it could be expected that polyclonal FLCs could be detected in kidney tissue from patients with CKD by immunohistochemical methods. Quantification of casts *in situ* might also provide useful information on progression of disease.

1.13 Scope of this Thesis and Hypothesis

From reviewing the literature it is clear that monoclonal FLCs cause a broad spectrum of renal diseases. All compartments of the kidney can be affected, and diseases can be broadly classified into those affecting the glomerulus or the tubulo-interstitium. Knowledge of how injury is mediated is growing. Free light chains can: promote functional changes; be processed and deposited; mediate inflammation, apoptosis and fibrosis; and physically obstruct nephrons. Each clone of FLC is unique and the precise type of pathology caused is determined by the primary structure and post-translational

modification of that clone. Treatment of clonal FLC disease is evolving and knowledge of the pathways that promote renal injury should lead to the further development of new treatments that specifically target this component of plasma cell dyscrasias.

In CKD, the clearance of FLCs is dependent on GFR. As CKD progresses and the number of functioning nephrons dwindles, the quantity of polyclonal FLCs delivered to the remaining hyperfiltering nephrons increases. Although there have been a small number of studies on neutrophils, there are no published studies to date on the effects of polyclonal FLCs in the kidney and on progression of renal fibrosis.

The primary hypothesis of this thesis is that in the setting of CKD, polyclonal FLCs exert pro-inflammatory effects, which are similar to those exerted by monoclonal FLCs in myeloma kidney. These effects are achieved by activation of PTECs and cast formation in distal tubules leading to progressive fibrosis and progression of CKD.

The aims of the studies presented in this thesis are: (i) to further assess the pathogenicity of monoclonal immunoglobulin light chains in myeloma kidney; (ii) to explore the hypothesis that increased serum polyclonal FLC levels in the setting of CKD and the resulting increased delivery of polyclonal FLCs to remaining nephrons leads to injury, which then contributes to progression CKD.

To address these aims, firstly I have performed detailed *in situ* morphometric analyses on kidney biopsy specimens obtained from patients with acute kidney injury due to myeloma cast nephropathy, as detailed in Chapter 3. Here, in addition to detailed

examination of the features of myeloma cast nephropathy, a comparison of histological features before and after a period of treatment aimed at reducing FLC concentrations and a comparison of histological features associated with renal outcomes is made. The findings indicated that whilst fibrosis may progress rapidly, a reduction in cast numbers in response to treatment might indicate potential for late renal recovery.

In Chapter 4, I present results from an *in vitro* study of specific signalling events that occur with monoclonal FLCs. Here, it is shown that the link between H_2O_2 generation following FLC endocytosis and pro-inflammatory intracellular signalling, which results in transcription of MCP-1, is oxidation and activation of the redox-sensitive tyrosine kinase c-Src.

Chapter 5 details the development of methodology for the purification of polyclonal κ and λ FLCs from pooled blood donor sera, by applying advanced protein chemistry techniques.

In Chapter 6, I present results from detailed *in situ* studies performed on kidney biopsies from patients with CKD. First, patterns of deposition and co-localisation of polyclonal FLCs were demonstrated. Polyclonal FLCs were seen within PTECs, as well as in distal tubular casts. An assessment of casts in these biopsies is then presented, demonstrating their relationship with established, robust markers of CKD progression.

In Chapter 7, the *in situ* findings of Chapter 6 are complemented by *in vitro* studies, using the polyclonal FLCs purified as described in Chapter 5. Here, an assessment of

the pathogenicity of polyclonal FLCs in the proximal tubule is presented, followed by an assessment of the cast-forming ability of polyclonal FLCs in the distal nephron. The results indicated that whilst there is no detectable pro-inflammatory effect on PTECs, polyclonal FLCs, like monoclonal FLCs, can co-precipitate with uromodulin in distal tubules, to form casts.

Chapter 2 contains details of materials and methods used. Chapter 8 is the discussion and conclusion.

Table 1.2. Renal manifestations of plasma cell dyscrasias, site and composition of deposits and summary of clinical and histological features.

Renal Manifestation	Associated Monoclonal Gammopathies	Sites of Deposits	Composition of Deposits	Clinical Features	Histological Features
Cast nephropathy (myeloma kidney)	Multiple myeloma, plasma cell leukaemia, Waldenström's macroglobulinaemia	PTEC, interstitium, distal tubules	LC + Uromodulin	Renal impairment: 20-40% of patients at diagnosis, >50% during illness. ESRF: up to 10%	PTEC damage, interstitial inflammation and fibrosis. Distal tubular casts with giant cell reaction

Renal Manifestation	**Associated Monoclonal Gammopathies**	**Sites of Deposits**	**Composition of Deposits**	**Clinical Features**	**Histological Features**
Amyloidosis	AL-amyloidosis, AH-amyloidosis, multiple myeloma, plasma cell leukaemia, Waldenstrom's macroglobulinaemia	All compartments of kidney may be affected, but glomeruli predominate.	LC: κ/λ 1:3 HC	Renal impairment: 20% of patients at diagnosis, ESRF in 20% by 1 year Proteinuria common	Deposits stain with Congo red giving apple green birefringence under polarised light. EM: fibrils 7-12nm wide and 30-1000nm long

Renal Manifestation	**Associated Monoclonal Gammopathies**	**Sites of Deposits**	**Composition of Deposits**	**Clinical Features**	**Histological Features**
Monoclonal Ig deposition diseases i)LCDD ii) HCDD iii)LHCDD	Multiple myeloma, plasma cell leukaemia	Mesangium, peritubular areas, vascular and GBM	i) LC: mainly VκI and VκIV ii) HC iii)LC + HC (~10% of LCDD cases)	Renal impairment: 96% of patients over course of illness. ESRF in 60% at 1year. Proteinuria >1g/day: 84%. Nephrotic range proteinuria: 40%	Prominent mesangial nodules, thickening of peripheral basement membrane IF: LC (also HC in HCDD and LHCDD) in mesangial nodules, peritubular regions, vessels, interstitium and GBM. EM: Fine granular deposits

Renal Manifestation	**Associated Monoclonal Gammopathies**	**Sites of Deposits**	**Composition of Deposits**	**Clinical Features**	**Histological Features**
Crystal storing histiocytosis	Multiple myeloma, Waldenström's macroglobulinaemia	Lysosomes in PTEC	κ:λ 9:1	Acquired Fanconi syndrome, type II RTA, chronic renal impairment.	Tubular atrophy and interstitial fibrosis, crystals concentrated in PTEC lysosomes

Renal Manifestation	**Associated Monoclonal Gammopathies**	**Sites of Deposits**	**Composition of Deposits**	**Clinical Features**	**Histological Features**
Cryoglobulinaemic GN	Multiple myeloma, plasma cell leukaemia	Glomeruli	IgG κ or λ IgMκ and polyclonal IgG	Renal disease: 20% of patients at diagnosis and >50% during course of illness. Proteinuria and microscopic haematuria (30%), nephrotic syndrome (20%), CRF (20%), ARF (10%), ESRF in 15%.	Thickened GBM, capillary thrombi containing precipitated cryoglobulins. IF: Diffuse glomerular intracapillary IgM deposits EM: Subendothelial fibrilar deposits

Renal Manifestation	**Associated Monoclonal Gammopathies**	**Sites of Deposits**	**Composition of Deposits**	**Clinical Features**	**Histological Features**
Waldenström's macroglobulinaemia glomerulonephritis	Waldenström's macroglobulinaemia	Glomeruli	IgM κ or λ, LC	Renal involvement rare. Nephrotic syndrome and ARF can occur (the latter due to hyaline thrombi)	Nodular glomerulosclerosis may be seen. most patients have interstitial infiltrates. IF: IgM deposits within capillary lumina

Renal Manifestation	**Associated Monoclonal Gammopathies**	**Sites of Deposits**	**Composition of Deposits**	**Clinical Features**	**Histological Features**
GOMMID	Multiple myeloma	Small vessels and capillaries	IgG κ or λ	Renal impairment, systemic vasculopathy, erosive polyarthropathy	Neutrophil and macrophage infiltration, endocapillary hyperplasia and protein thrombi EM: Subendothelial mixed granular and organised deposits with microtubular organisation.

Renal Manifestation	**Associated Monoclonal Gammopathies**	**Sites of Deposits**	**Composition of Deposits**	**Clinical Features**	**Histological Features**
Proliferative GN with monoclonal Ig deposits	Serum monoclonal IgG detected in 50%	Glomeruli	Monoclonal IgG κ or λ	Proteinuria present in all, nephrotic syndrome in 44%. Renal failure seen in 80%	Endocapillary proliferative or membranoproliferative GN. IF: Monoclonal IgG. EM: Mesangial and subendothelial granular deposits.

PTEC, proximal tubule epithelial cell; LC, light chain; ESRF, end stage renal failure; HC, heavy chain; EM, electron microscopy; LCDD, light chain deposition disease; HCDD, heavy chain deposition disease; LHCDD, light and heavy chain deposition disease; IF, immunofluorescence; GBM, glomerular basement membrane; RTA, renal tubular acidosis; GN, glomerulonephritis; CRF, chronic renal failure; ARF, acute renal failure; GOMMID, glomerulonephritis with organised microtubular monoclonal immunoglobulin deposits.

2. MATERIALS AND METHODS

2.1 Introduction

This chapter presents the methods that were used for the experiments that I performed, the results of which are presented in this thesis. A wide variety of methods were employed. These included: quantitative image analysis techniques for morphometric analyses on kidney biopsy tissue (chapters three and six); *in vitro* cell culture based assays for the assessment of the effects of monoclonal and polyclonal FLCs on human PTECs (chapters four and seven); extensive protein chemistry techniques to produce purified polyclonal FLCs (chapter five). Additionally, immunofluorescence and immunohistochemistry techniques were used to assess the presence of polyclonal FLCs in kidney biopsies (chapter six). Finally, in chapter seven, protein chemistry techniques were used to investigate interactions between proteins that may be relevant to cast formation in chronic kidney disease.

2.2 Immunohistochemistry and Immunofluorescence

2.2.1 Background

Immunohistochemistry (IHC) is a widely used technique in the detection of specific antigens at tissue sites. The pivotal reagent common to all IHC techniques is the antigen-specific antibody (also referred to as the primary antibody). These antibodies are prepared by immunising animals with the target antigen (the immunogen). The result of immunisation is the production of IgG against the immunogen by the host's B-

cells.(Hayat 2002; Onley 2007) The primary antibody is applied to the tissue in conditions determined experimentally to be optimal.

2.2.2 Polyclonal Antibodies

Following immunisation, many B-cells will be stimulated to produce antibodies against more than one epitope on the immunogen; each one will be immunochemically distinct from the others. These are termed polyclonal antibodies. They are most frequently raised in the rabbit, but also in the goat, sheep and donkey, amongst others. Polyclonal antibodies have the advantages of being relatively cost-effective and straightforward to produce. The potential limitations of polyclonal antibodies include cross-reactivity and batch-to-batch variation. Polyclonal antibodies are vended in varying grades, representing different degrees of purity, ranging from total IgG fraction to affinity purified.(Onley 2007)

2.2.3 Monoclonal Antibodies

Following immunisation of a mouse, B-cells may be harvested from spleen or lymph node and then fused with non-secreting murine myeloma cells, to create hybridomas. These are long-lived in culture and secrete immunochemically identical antibodies. These are termed monoclonal antibodies. Hybridomas may be grown in live mice (in ascitic fluid), or by cell culture *in vitro*. The main advantages of monoclonal antibodies over polyclonal antibodies are that they react to a single epitope only, and thus possess better specificity, homogeneity and consistency. However these properties can limit their range of applications and the experimental conditions under which they may be used. If the target epitope is unstable and easily lost upon tissue fixation or antigen retrieval,

monoclonal antibodies are at a disadvantage when compared to polyclonal antibodies.(Onley 2007)

2.2.4 Recombinant Antibody Technology

Recombinant antibodies can be produced *in vitro*. These frequently have applications as therapeutic antibodies, and their usage as laboratory reagents is increasing. The basic unit of a recombinant antibody is usually composed of a V_L and V_H segments, similar to a Fab fragment, joined by a linker. These can be dimerised to improve avidity for antigen, and thereby improve utility.(Onley 2007)

2.2.5 Detection Systems

Antibody bound to an antigen of interest must be visualised in some way. This is achieved by a colour change, which may be seen on ordinary light microscopy, or by the use of fluorescent markers, which emit light, and can be detected by specialised fluorescence microscopes or confocal laser scanning microscope (CLSM).

2.2.6 Chromogenic Detection

Chromogenic detection utilises an enzymatic reaction on a substrate, which results in a colour change at the site where antibody has bound antigen. The enzyme can be conjugated directly to the primary antibody (direct detection), or to secondary antibodies or avidin-biotin complexes (indirect detection). The latter two are incubated with tissue after application of primary antibody. Substrate is applied, which undergoes enzymatic conversion to a stable precipitate of a specific colour, which is then visible on ordinary

light microscopy. The most commonly used label and substrate are horseradish peroxidase (HrP) and 3,3'diaminobenzidine tetrahydrochloride (DAB), which gives a brown-black colour.(Mardle 2007) Secondary antibodies and enzyme can also be attached to a polymer backbone. In this type of system, a single length of polymer may have numerous secondary antibodies and enzyme molecules, thus giving significant signal amplification.(Kumar and Rudbeck 2009)

2.2.7 Fluorescence Detection

Fluorescence detection, or immunofluorescence (IF) utilises fluorochromes conjugated to the primary antibody (direct detection), or to secondary antibodies or avidin-biotin complexes (indirect detection). The latter two are incubated with tissue after application of primary antibody. Fluorochromes absorb energy from light of a specific wavelength (the excitation wavelength) and then emit light at a lower wavelength (the emission wavelength). Different fluorochromes absorb and emit at different wavelengths, which enables detection of multiple antigen targets on the same tissue section.(Mardle 2007)

2.2.8 Labelling of Antibodies with Fluorochromes

An initial immunohistochemical study was planned for the investigation of *in situ* deposition patterns FLC in the kidney. The experiments were designed to detect the presence of κ and λ FLC, and to differentiate between proximal and distal tubules. This required applying antibodies against at least 3 antigens on the same section. Traditional enzyme-based chromogenic detection systems would have been hard to interpret, especially where targets co-localise. Therefore fluorescence detection was chosen.

Antibodies against κ and λ FLC and uromodulin (The Binding Site) were raised in sheep. This made indirect detection difficult, as anti-sheep secondary antibody would have reacted with all three antibodies, so direct detection was chosen, where the primary antibodies were labelled with fluorochrome.

Anti-κ antibody was conjugated to fluorescein isothiocyanate (FITC) by the manufacturer. Anti-λ and anti-uromodulin antibodies were conjugated to DyLight 649 and DyLight 549 fluorochromes, respectively, in the laboratory using a kit (Thermo Scientific Pierce) where the fluorochromes were activated with *N*-hydroxysuccinimide (NHS) esters, which reacts with primary amines on the antibody. These fluorochromes were chosen because (i) of their intense fluorescence output, (ii) their excitation spectra were compatible with instruments in our laboratory, and (iii) their emission spectra were sufficiently separated to minimise fluorescence overlap, thus improving their ability to identify colocalising targets.

Both anti-λ and anti-uromodulin antibodies were shipped in glycine buffered saline, which was incompatible with the selected method of protein labeling, as well as bicinchoninic acid (BCA) assay. Dialysis into phosphate buffered saline (PBS) was carried out by five repeated cycles of diluting 1 ml of antibody 1:10 in PBS followed by centrifugation back down to 1 ml in a spin column with a molecular weight cut-off o 10 kDa (Vivaproducts, Littleton, MA, USA). In the final cycle, centrifugation was continued until the retentate, (containing antibody) volume was approximately 0.5 ml. TSP in the retentate was then measured by BCA assay; if necessary, PBS was added to adjust TSP to between 1-2 mg/ml. The retentate was transferred to a microfuge tube.

The filtrate was tested by A280 to ensure it did not contain significant quantities of protein, and then discarded.

Forty µl of the labeling buffer (0.67 M sodium borate pH 8.5) was added to 0.5 ml of antibody. This solution was pipetted into the vial containing the DyLight reagent, gently vortexed and briefly centrifuged to collect sample at the bottom of the tube. The reaction vial was then incubated in the dark, at room temperature, for 2 hours. The supplied purification resin was centrifuged in a spin column to remove its storage solution. 240-270 µl of the reaction mixture was then added to the resin, and gently mixed by pipetting up and down. The columns were centrifuged for 45 seconds at x1000g to collect the labeled antibody in the filtrate. Bovine serum albumin (BSA) was added to a final concentration of 1% as a stabilising agent, and antibodies were stored in the dark at 4 ˚C.

2.2.9 Tissue Fixation and Embedding

As soon as tissue is removed for histology, it begins to undergo deterioration as a result of hypoxia, autolysis, lysosomal degradation, and putrefaction due to environmental organisms. Fixation and embedding is therefore an essential step in preserving tissue. Formaldehyde is the most commonly used fixative, and acts by reacting with basic amino acids, resulting in protein cross-linking by methylene bridges. Formaldehyde fixing can react with the target antigen however, rendering it non-immune reactive to antibody detection. Antigen retrieval is then required to restore epitopes to an immune-reactive state prior to detection by antibody.(Renshaw 2007)

Paraffin wax is used most commonly as the embedding medium for tissue that has been fixed in formaldehyde, and functions to support the tissue during transport, storage and microtomy. Fixatives are aqueous, whereas paraffin is hydrophobic; thus there is a need for a transition phase, which in practice usually involves passing the tissue through graded alcohols of increasing concentration, then into a solvent that is miscible with paraffin, such as xylene, and then allowing the paraffin to replace the xylene.(Renshaw 2007) Prior to IHC staining, paraffin must be removed, by the reversal of the process described above.

2.2.10 Tissue Sectioning

Sections of tissue for IHC were prepared by John Gregory, Department of Cellular Pathology, University Hospital Birmingham. Formaldehyde-fixed, paraffin-embedded tissue blocks were sectioned to a consistent thickness of 2 µm using a microtome (Leica Microsystems, Milton Keynes, UK), and placed on glass slides (Superfrost Plus, Surgipath Europe, Peterborough, UK) before being oven-dried at 60 °C overnight. These slides were cooled and stored until required.

2.2.11 Dewaxing

The embedding paraffin wax was softened by warming the slides in an oven for 30 minutes, at 60 ˚C. Dewaxing was then carried out by sequentially transferring the slides through baths of xylene and ethanol (Fisher Scientific, Loughborough, UK), for 3 minutes each, as follows: xylene, xylene, ethanol 100%, ethanol 100%, ethanol 95%, ethanol 95%. Transfer from oven to xylene and from one solvent bath to another was

done quickly to prevent the wax setting again or the tissue drying out in air. After the final ethanol bath, sections were rinsed gently with distilled water and then transferred to wash buffer, normally either PBS or tris-buffered saline (TBS). A ring was drawn around each section with a PAP pen to easily identify the location of the tissue, and to retain solutions placed over the tissue.(Kumar and Rudbeck 2009)

2.2.12 Antigen Retrieval

Antigen retrieval is required in formaldehyde-fixed specimens in order to break cross-linking methylene bridges, thus unmasking epitopes and restoring their immune reactivity.

2.2.13 Proteolytic Digestion

Proteolytic enzymes such as trypsin, pronase, and proteinase K can be used to carry out antigen retrieval. Enzymatic antigen retrieval can be problematic due to the temperature-sensitivity of enzymes, as well as the risk of over-digestion of tissues. However, this method has been described as useful in IF studies performed on formaldehyde-fixed, paraffin-embedded tissue, and therefore was of interest to me.(Viegas *et al.* 2007)

2.2.14 Proteinase K

Lyophilised proteinase K (Sigma-Aldrich, Gillingham, UK) was reconstituted in distilled deionised water to make a stock solution of 1 mg/ml. For the working solution, this was diluted 1:50 in PBS, pH 8.0, to make 20 µg/ml. 100 µl of working solution was applied by pipette to each tissue section and incubated in a humidity chamber for 10

minutes at room temperature. Sections were then rinsed gently with PBS with 0.05% Tween-20 (PBS-T) from a wash bottle, and then washed three times in a bath of PBS-T for 5 minutes each.

2.2.15 Heat Induced Epitope Retrieval (HIER)

This may be performed in a variety of appliances, such as a microwave oven, pressure cooker, vegetable steamer or autoclave. A microwave oven set at 800 W was used. Slides with dewaxed sections were placed in a plastic rack and completely immersed in a bath of 0.01 M sodium citrate (Sigma-Aldrich) at room temperature. This was placed in the microwave oven set to 800 W and heated to 95 ˚C for 25 minutes, then allowed to cool for 30 minutes.(Renshaw 2007) Slides were then transferred to wash buffer.

2.2.16 Quenching and Blocking Steps – Prevention of Background Staining

Endogenous biotin can react with detection systems which utilise avidin/biotin. Endogenous enzymes such as peroxidase can react with chromogen. The kidney is rich in both. The presence of Fc receptors in tissue can also cause non-specific binding of antibody. All three factors can give rise to undesirable background staining. Blocking steps are therefore required to prevent these from occurring.

2.2.17 Endogenous Peroxidase Quenching with Hydrogen Peroxide

This step was performed in all IHC experiments using a HrP enzymatic detection system. 0.3% v/v hydrogen peroxide (H_2O_2; Sigma-Aldrich) in methanol (Fisher Scientific) was applied to each slide after antigen retrieval, and incubated in a humidity

chamber for 30 minutes. Sections were then gently rinsed with TBS-T using a wash bottle, and then washed 3 times in a bath of TBS-T for 5 minutes each.

2.2.18 Endogenous Biotin Block with Avidin and Biotin

This step was performed in all IHC experiments using an avidin/biotin complex detection system. 0.1% avidin solution (Dako, Ely, UK) was applied for 10 minutes, and incubated in a humidity chamber. Sections were then washed in TBS-T as above. 0.01 % biotin solution (Dako) was then applied for 10 minutes, followed by TBS-T washes as above.

2.2.19 Fc Receptor Block with Serum

This step was performed in all IHC and IF experiments. Serum from the same species as the secondary antibody (or primary antibody in the case of primary-labelled antibodies) was diluted in wash buffer to 10% v/v. Diluted serum was applied to each tissue section for 20 minutes in a humidity chamber, and the excess serum was then gently tapped off.

2.2.20 Primary Antibody

The primary antibody was applied to the tissue in conditions determined experimentally to be optimal. These variables included antibody dilution and duration of incubation. The dilutions for each antibody are shown in the Appendix. Following application of the primary antibody, slides were rinsed gently with wash buffer from a wash bottle, and then further washed three times in baths of wash buffer, for five minutes each.

2.2.21 Isotype Control

For each immunohistochemical experiment performed, a tissue section should be processed in parallel, in an identical fashion, except with the primary antibody substituted with an isotype control antibody. This isotype control antibody, which is not antigen-specific but in all other respects similar to the primary antibody, ensures that any positive staining observed is due to binding of antibody to the specific antigen of interest, and not just a result of non-specific antibody binding leading to artefact. This is implied if positive staining is seen in the same regions on the isotype control section as the test section.

2.2.22 Autofluorescence

Autofluorescence results from the natural ability of biological tissues to fluoresce. This occurs independently of fluorochromes used in staining, and can be problematic, leading to false-positives, and masking true staining. Autofluorescence is commonly attributable to three causes: (i) elastin and collagen, (ii) lipofuscin, and (iii) aldehyde fixative-induced. Elastin and collagen are present in abundance in the kidney, in blood vessels, and in areas of established chronic damage. Lipofuscin is a product of peroxidation of lipids. It accumulates with age within lysosomes of many cells, including those in the kidney. The use of aldehyde fixatives results in the formation of fluorescent compounds. This phenomenon is most pronounced with the use of glutaraldehyde, but still significant with formaldehyde. It tends to have a more diffuse and more generalised appearance than specific staining. The best approaches to removing autofluorescence are: avoiding it (which is not always possible), filtering it out during image acquisition (which is not always practical as molecules responsible for autofluorescence have broad combined

emission spectra), and chemically removing it (which can result in reduced "real" signal).(Jackson 2007) However, there are numerous studies, which report the successful use of formaldehyde-fixed, paraffin-embedded tissue in immunofluorescence studies.(Mason *et al.* 2000; Baschong *et al.* 2001; Nasr *et al.* 2006; Viegas *et al.* 2007)

Pontamine blue dye has been described as an effective means of quenching elastin and collagen derived autofluorescence, but because the dye works by shifting the fluorescent emission of elastin and collagen from green to red, it is only of use in reducing autofluorescent interference with FITC staining.(Cowen *et al.* 1985) It has been reported that lipofuscin autofluorescence can be effectively quenched using Sudan black, including in studies using CLSM techniques, and that improved results were obtained when short-burst UV-irradiation was also carried out (253-400 nm, at 30 W for 2 hours).(Baschong *et al.* 2001; Viegas *et al.* 2007) Sodium borohydrate treatment is used to quench aldehyde-induced autofluorescence. However sodium borohydrate is a highly dangerous explosive.(Jackson 2007)

2.2.23 Protocol for Quenching of Autofluorescence

A combination of photobleaching and Sudan black, reported as effective in minimising autofluorescence was tested in early experiments.(Viegas *et al.* 2007) Slides with sections of tissue were first photobleached prior to dewaxing under a high-intensity (30 W) UV lamp with a discreet emission spectrum of 253-400 nm (Philips, Guilford, UK) for 2 hours at room temperature. Dewaxing and antigen retrieval was carried out in the usual way. Immediately prior to the serum block, sections were incubated with 0.1% Sudan black in 70% ethanol for 20 minutes at room temperature, and then washed with

PBS-T 5 times. A final jet of PBS-T was applied to remove any excess completely. Serum block was then applied and the staining procedure proceeded according to the standard method. This method resulted in satisfactory quenching of autofluorescence, but also caused excessive interference with staining, to the point where very little staining was visible. This method was therefore abandoned.

2.2.24 Protocol for Multiple Immunofluorescent Staining of FLC in Kidneys

Slides with sections of formaldehyde-fixed, paraffin-embedded tissue were dewaxed in xylene and graded ethanol and transferred to PBS. A ring was drawn around each section with a PAP pen. HIER was performed in a microwave oven, and slides were allowed to cool for 30 minutes, and then transferred to PBS-T wash buffer. A serum block was performed using 10% sheep serum for 20 minutes. Antibodies were prepared by mixing together as a cocktail in PBS-T: anti-κ, 1:100; anti-λ, 1:50; anti-uromodulin, 1:100. After gently tapping off excess serum, antibody cocktail was pipetted over the sections. From this point onwards slides were protected from light. Slides were then placed in a humidity chamber and incubated overnight at 4˚C. Slides were then washed in PBS-T three times. Nuclear counterstaining was performed with 300 nM 4',6-diamidino-2-phenylindole, dilactate (DAPI) for 10 minutes, followed by washing three times in PBS-T. Slides were incubated with equilibration buffer provided with the anti-fade mounting medium (ProLong Gold; Invitrogen, Paisley, UK) for 10 minutes. After tapping off equilibration buffer, one drop of anti-fade mounting medium was placed over each section and a glass coverslip was lowered into place. The mountant cures, thus negating the need to seal edges with nail polish. Slides were stored at -20 ˚C.

2.2.25 Protocol for multiple IF staining - controls

Polyclonal IgG from non-immunised sheep () was used as isotype control. One possible source of false-positive staining was the reactivity of anti-FLC antibodies with intact immunoglobulin, which may have been present in the kidneys. Although these antibodies are specifically raised against light chain epitopes normally hidden in intact immunoglobulin, fixation or antigen retrieval may have resulted in these epitopes being exposed. To assess this, additional controls were performed in parallel to each experiment using a cocktail of FITC-labelled anti-IgG, anti-IgA and anti-IgM antibodies (). Each antibody was present at a final dilution of 1:100. Positive staining in these sections was interpreted as indicating potential false-positive staining in the test sections stained with anti-FLC antibodies. A third control section was also included in each experiment, to give an indication of the degree of background autofluorescence. This section was processed in an identical fashion to the others, except that primary antibody was substituted with PBS-T.

In initial experiments calbindin D28K was chosen as a marker for distal tubules, using a mouse monoclonal antibody (Sigma-Aldrich), which was detected by an anti-mouse antibody labelled with DyLight 549.(Kumar *et al.* 1994; Loffing *et al.* 2004) However, staining with this antibody was suboptimal, and this method was abandoned, in favour of the anti-uromodulin antibody, as described above.

2.2.26 Visualisation of Immunofluorescent Staining and Image Acquisition

Initial attempts to visualise antibody binding using a standard fluorescence microscope were unsuccessful due to high levels of autofluorescence. Attempts to quench

autofluorescence resulted in significant interference with staining. Therefore a confocal laser scanning microscope (Axiovert 100M; Carl Zeiss,) was employed. This method had the advantage of being able to adjust the settings of the microscope digitally to minimise autofluorescence. A control section was processed with each experiment, which was processed in an identical fashion, except that antibody was substituted with wash buffer. This section was examined first under the CLSM and gain settings adjusted to cut out autofluorescence. These settings were used for the parallel test slide in the experiment.

Images were visualised with the microscope and lasers set up with four collection windows as follows: 351, 364 nm laser (14.9%), window 385-470 nm; 488 nm laser (5%), window 505-550 nm; 543 nm laser (100%), window 560-615 nm; 633 nm laser (20%), window 650 nm. Images were routinely acquired using the x10, x20 and x40 water immersion objective lenses, with microscope in sequential mode, with a line average of 4 and a resolution of 1024 x 1024 pixels. Images were viewed using proprietary software (LSM Image Browser; Carl Zeiss)

2.2.27 Protocol for Immunohistochemical Staining of Macrophages and Interstitial Capillaries

Initial experiments using a polymer-backboned system to detect primary antibodies (EnVision; Dako) resulted in extensive background staining, and was therefore abandoned in favour of an established avidin-biotin detection method.(Eardley *et al.* 2006; Eardley *et al.* 2008) Formalin-fixed, paraffin-embedded sections were dewaxed and rehydrated, then HIER was carried out in 0.01M citrate buffer. Slides were then

transferred to TBS-T. Endogenous peroxidase was blocked with 0.3% H_2O_2 in 70% methanol for 30 minutes, Endogenous biotin was blocked by sequential application of first 0.1% avidin, then 0.01% biotin. Sections were then blocked with 10% rabbit serum for 20 minutes, and excess gently tapped off. This serum block was not washed off prior to application of primary antibody. Three-stage indirect immunohistochemical staining was then performed. Primary antibody (either anti-C68 or anti-CD34) were applied as follows: anti- CD68, pan-macrophage antigen (clone KP1; Dako) at 1:200 dilution; anti-CD34, endothelial marker (Clone QBEnd 10; Dako) at 1:25 dilution for 30 minutes at room temperature. Biotinylated anti-mouse secondary antibody (Dako) at 1:100 dilution was applied or 30 minutes, followed by a HrP-conjugated streptavidin-biotin complex (StreptABComplex; Dako) for 30 minutes. Antibody binding was visualised by the addition of DAB for 1-10 minutes. Sections were counterstained with Mayer's haematoxylin (Sigma-Aldrich), except those sections for quantitative analysis, which were left uncounterstained. Slides were washed thrice for 10 minutes each time in TBS-T between each of the above steps unless otherwise stated. They were then dehydrated with graded alcohol as follows: ethanol 100%, 10 minutes; xylene, 10 minutes. One drop of synthetic resin mountant (DPX; Sigma-Aldrich) was placed on a coverslip, and the coverslip was then lowered onto the tissue section, and allowed to dry in a fume cupboard. Mouse monoclonal IgG1 (Dako) was used as an isotype control for both anti-CD68 and anti-CD34 antibodies, at 1:200 and 1:25 dilutions respectively. Tissue sections were grouped into batches of 20 to help maintain consistency in the technique used between samples.

2.3 Image Analysis of Kidney Biopsies

2.3.1 Patients

Approval was sought from and granted by the local ethics committee to use kidney tissue taken from patients undergoing renal biopsy at University Hospital Birmingham (South Staffordshire Research Ethics Committee, project reference 07/Q2602/42). The scope of the ethics application was to investigate the deposition patterns of free light chains (FLC) in kidneys of patients with chronic kidney disease (CKD) and other factors related to inflammation and fibrosis. The tissue used for experiments represented archived tissue that was surplus to diagnosis. The study population included any patient who had undergone a renal biopsy at this institution, who fulfilled the criteria for this study.

2.3.2 Quantification of Interstitial Macrophage Infiltration and Interstitial Capillary Density

Coded sections stained for CD68 and CD34 were observed under a microscope (Eclipse E400; Nikon Instruments, Amstelveen, The Netherlands) at x200 magnification, and images acquired using proprietary software. The entire length of each biopsy section was imaged in this way.

The Aequitas interactive image analysis system was used for blinded assessment of interstitial macrophage numbers. This technique has previously been found to be a reliable method in the analysis of human and animal renal sections.(Furness *et al.* 1997; Thomas *et al.* 2002) For analysis, each image was converted to a two-colour scale image. By altering the threshold the image was processed so that positive staining was

represented by yellow pixels measured as a percentage of the area of total image analysed. Sections where background staining made it impossible to digitally differentiate specific staining were excluded from analysis. For each patient a mean measurement of 5 randomly selected non-confluent microscopic fields was determined. Glomerular staining was excluded from the analysis by the computer software.

2.3.3 Quantification of Interstitial Fibrosis/Chronic Damage

Chronic damage, representative of areas of fibrosis within kidney biopsies, was measured using a previously validated image analysis technique. This index of chronic damage has previously been demonstrated to be a rigorous predictor of renal outcome.(Howie *et al.* 2001) Briefly, one routinely prepared, periodic acid-methenamine silver (PAMS) stained section from each patient was examined under a microscope (Nikon) at x100 magnification and images were captured. Using image analysis software (Aequitas IA; Dynamic Data Links, Cambridge, UK), the cortical area was outlined, selected and the area quantified. The cortex was defined as that part of the biopsy core beneath the capsule extending to the medullary aspect of the deepest glomeruli, or the cortical aspect of arcuate vessels. Areas of established chronic damage were defined as glomeruli which were globally (but not partially) sclerosed; areas of interstitial fibrosis, which appeared more solid and deeply stained than normal; or areas of interstitial oedema, atrophic tubules, defined as those smaller than normal, with thinned epithelium, including those which were cystic, and any arteries that were completely occluded. Within this, areas of chronic damage were outlined. After outlining areas of chronic damage, the image was then exported as a screen-grab, using computer software (Grab, , Cupertino CA, USA) for the purposes of cast counting (see below). The index of chronic

damage was then quantified as the percentage of total cortical area occupied by areas of chronic damage.

2.3.4 Cast Counting

Screen-grab images taken from the Aequitas IA program (see above) were opened in a second image analysis program (ImageJ, National Institutes of Health, USA). The number of proteinaceous precipitates (casts) in distal tubules were counted using ImageJ as follows. A grid was applied to the image using ImageJ. Using the cell counting function in ImageJ and the computer mouse as a button counter, all tubules were counted, and subdivided firstly into those located inside or outside areas of chronic damage and secondly into those containing or not containing casts. The cast burden could then be calculated as the percentage of the total tubules counted which contained casts, rounded to the nearest integer.

2.4 Cell Culture: HK-2 Cells

2.4.1 Culture and Propagation of HK-2 Cells

HK-2 Cells (American Type Culture Collection, Manassas, VA, USA) are a proximal tubule epithelial cell (PTEC) line derived from transfection with HPV 16 E6/E7 genes. (Ryan *et al.* 1994) Grown as a monolayer, they exhibit brush-border enzymes, cell surface receptors and biochemical and morphological characteristics similar to other widely used PTECs in stable culture. HK-2 cells have been used in numerous studies on the effects of monoclonal FLC on kidney cells, and have exhibit similar responses to monoclonal FLCs exposure as other proximal tubule cell lines, and therefore are a good

model in this setting.(Basnayake *et al.* 2010) See Appendix for an image of normal HK-2 cells.

2.4.2 Containers

Culture flasks, plates and dishes (Nunc, Rochester, NY, USA) were coated with 5 μg/cm^2 rat tail collagen type 1 (Invitrogen, Carlsbad, CA, USA) for 1 hour at room temperature. Thin-coating with type 1 collagen was used to facilitate anchorage and proliferation of HK-2 cells to containers. This type of collagen has been used in the past in studies investigating the effects of myeloma FLCs on PTECs, at independent laboratories.(Pote *et al.* 2000; Wang and Sanders 2007). Type 4 collagen is found in basement membranes in the kidney and therefore may be a more physiological anchorage agent with fewer pro-inflammatory effects than type 1 collagen. However, as previous studies using the same myeloma FLCs successfully utilised type 1 collagen coated containers, this type of collagen was selected for my own studies for consistency. In addition, as control proteins did not elicit significant responses from PTECs in culture, it was felt that any pro-inflammatory effects of type 1 collagen were negligible. Immediately prior to use, the collagen was aspirated, and the containers rinsed twice with PBS (Invitrogen).

2.4.3 Growth Medium

Complete growth medium (hereafter referred to as K-SFM) was prepared as follows: keratinocyte serum-free medium, supplemented with 5 ng/ml recombinant human

epidermal growth factor and 0.05 mg/ml bovine pituitary extract, 100 µg/ml penicillin, 100 µg/ml streptomycin and 250 ng/ml amphotericin B (Invitrogen).

2.4.4 Initiation of Culture

Cells were shipped frozen on dry ice, and stored in liquid nitrogen vapour phase. After rapid thawing to 37 ˚C (≤1 minute) in a bead bath, each vial of cells was diluted in 5-7 ml of K-SFM and transferred to a T-25 flask. The cells were routinely cultured at 37°C in a humidified atmosphere of 95% air-5% CO_2. Medium was exchanged at 48-hour intervals. Cells were never allowed to become overcrowded, and were passaged when they reached 80% confluence.

2.4.5 Passaging of Cells

Medium was aspirated and cells were washed briefly in PBS. Cells were detached by incubating with typsin 0.05% and ethylenediaminetetraacetic acid (EDTA) 0.2 g/L (Invitrogen) for 1-5 minutes at 37 ˚C, diluted in K-SFM and centrifuged at x 125 g for 10 minutes to collect a soft pellet. Supernatant medium was poured off and the pellet gently resuspended in fresh K-SFM. Cell counting was done at this stage, if required for estimating seeding density into plates or dishes for experiments (see below). For the purposes of propagation, each flask was split 1:2 or 1:3, transferred to the incubator. Cells were not passaged beyond 25 to 30 times.

2.4.6 Enumeration of Cells using a Haemocytometer

Cells were counted using a Neubauer haemocytometer. This instrument facilitates the quantification of cells in a determined volume of fluid, thus enabling the quantification of the total number of cells in a suspension. A standard haemocytometer is made of glass, scored to form a grid of nine large squares, which are further subdivided by scoring. A coverslip is placed over the grid. When a suspension of cells is infused, capillary action draws the fluid under the coverslip. Each square represents a volume of 10^{-4} cm^3. See Appendix for a figure of a haemocytometer.

To be able to count cells accurately, it is important that they are not so concentrated that they overlap on the grid; serial dilutions may be required. Prior to transferring to the haemocytometer, the cell suspension is mixed 1:2 with trypan blue. This dye is taken up into dead cells, thus helping differentiate viable ones from those that are dead or dying.

10 µl of prepared cell suspension is pipetted into each groove-shaped sample introduction point. Using a button-counter, the total number of cells in several squares is counted. For cells at the boundaries of the squares, those touching the left and top boundaries are counted, while those touching the right and bottom boundaries are disregarded. The number of cells per ml can then be calculated as follows:

$$\text{Cells/ml} = \frac{\text{Total no cells in } n \text{ squares}}{n} \times 10^4 \times \text{dilution factor}$$

Where *n* is the number of large squares in which cells were counted.

2.4.7 Cryopreservation

Cells were detached from the flask with trypsin as above, diluted in K-SFM and centrifuged at x 125 g for 10 minutes to form a soft pellet. The supernatant was discarded and cells were gently resuspended in freezing medium (K-SFM supplemented with 7.5% v/v dimethyl sulfoxide; Sigma-Aldrich). Roughly, 8 x 10^6 cells (approximately equivalent to one T-75 flask or half of one T-160 flask) were suspended in 1.5 ml freezing medium, and stored in a single cryogenic vial, in liquid nitrogen vapour phase.

2.4.8 Preparation of Polyclonal FLC Stock Solution for *In Vitro* use

Lyophilised polyclonal κ and λ FLCs were made into stock solutions, which were diluted as required for experiments. FLCs were weighed and dissolved in the relevant medium for the cell type used at 10 mg/ml. This solution was filter sterilised by passing through a 0.22 μm filter (Millipore, Billerica, MA, USA). Stock solution was aliquoted and stored at -20 ˚C until required.

2.4.9 Protocol for Incubation of HK-2 Cells with FLC

HK-2 cells were grown on collagen coated 6-well plates until they reached 80% confluence, the medium was removed, and cells washed briefly in PBS. Each well was then overlaid with 1 ml of medium containing protein at the desired concentration and the plates returned to the incubator. After incubating for the designated amount of time,

medium was collected, placed on ice, centrifuged at 4 ˚C to pellet any debris, and assayed. Where cell lysates were required, lysis was carried out (see below)

2.4.10 Protocol for Cell Lysis

Plates were placed on ice. After removal of medium, cells were washed briefly in cold PBS. Cells were lysed in radioimmunoprecipitation (RIPA) buffer, supplemented with protease inhibitor cocktail (cOmplete; Roche Applied Science, Indianapolis, IN, USA) was applied (roughly 200 µl per well in a 6-well plate), and placed on a rocking platform at 4 ˚C for 15 minutes. Wells were then scraped and the lysate was transferred to microfuge tubes, centrifuged at x 15,000 g for 15 minutes, at 4 ˚C to pellet cellular debris. The supernatants were transferred to fresh microfuge tubes on ice, and then promptly either assayed or placed in a freezer at -70 ˚C.

2.4.11 Hydrogen Peroxide Assay

A critical event following endocytosis of tubulo-toxic monoclonal FLCs by PTECs is the generation of H_2O_2.(Wang and Sanders 2007) This phenomenon was investigated with polyclonal FLCs. Cells were incubated with FLCs as above, overnight. Supernatants were collected, centrifuged and promptly assayed. H_2O_2 concentration was measured using one-step assay a kit (Amplex Red Hydrogen Peroxide/Peroxidase Assay Kit; Invitrogen) and was carried out according to manufacturer's instructions. The assay utilises the reaction of Amplex Red (10-acetyl-3,7-dihydroxyphenoxazine) in the presence of peroxidase, to form a red-fluorescent oxidation product, resorufin. 50 µl per well of samples and H_2O_2 standards were pipetted in duplicate into a black, 96-well

fluorescence plate (Nunc). 50 µl of Amplex Red working solution was then added to each well, and the plate was incubated at room temperature for 30 minutes, shielded from light. Fluorescence emission was measured using a plate reader, at an excitation frequency of 535 nm and emission at 560 nm.

2.4.12 MCP-1 Assay

Human MCP-1 in cell culture supernatants was measured by an enzyme-linked immunosorbent assay (ELISA). A capture assay was performed according to manufacturer's instructions (Human CCL2/MCP-1 Immunoassay; R&D Systems, Minneapolis, MN, USA). All reagents were brought to room temperature. Cell culture supernatants were centrifuged at 4 ˚C at x 10,000 g for 5 minutes to pellet any debris, and were subsequently kept on ice. Standards, wash buffer, calibrator diluent and substrate solution were prepared according to instructions. 200 µl of each standard and sample were added in duplicate to wells in the provided microplate, and incubated for 2 hours. The wells are provided pre-coated with an anti-MCP-1 capture antibody. Wells were then aspirated and washed 3 times using a plate washer. After the third wash, the plate was inverted and blotted against paper towels to ensure all liquid was removed from the wells. 200 µl of HrP-conjugated detection antibody was then added to each well, and incubated for 1 hour, followed by washing as above, before 200 µl per well of substrate solution was added, and the plate incubated, protected from light, for 20 minutes, after which 50 µl of stop solution was added to each well. Absorbance was measured using a plate reader at 450 nm. Sample readings were measured against the standard curve generated by a four-parameter logistic curve-fit using plate reader software. Where necessary, results were expressed by multiplying concentration (in

pg/ml) by the volume of medium per well (in ml) and expressed as pg/day.

2.4.13 Lactate Dehyrogenase Assay

Monoclonal FLCs have cytotoxic effects on proximal tubular cells, resulting in increased lactate dehydrogenase (LDH) release due to cell death.(Pote *et al.* 2000) The cytotoxic effects of polyclonal FLC on HK-2 cells were studied using a colorimetric assay kit, which quantitatively measures LDH by the conversion of tetrazolium salt into a red formazan product (CytoTox 96; Promega, Madison, WI, USA). After incubation of cells with K-SFM containing protein or controls as above, medium was harvested, and centrifuged to pellet debris. A control plate, to measure the maximum LDH release from the cells, was incubated with K-SFM alone, and lysed by 3 freeze-thaw cycles in liquid nitrogen. 50 µl of supernatant from each well was transferred in duplicate to a 96-well plate. K-SFM alone was also loaded onto the plate as a control for background absorbance, which could be subtracted from the sample readings. The substrate mix was prepared and 50 µl added to each well, the plate covered and incubated for 30 minutes at room temperature, shielded from light. Stop solution was added, and absorbance measured at 490 nm using a plate reader.

When it was required, cytotoxicity could then be expressed as the experimental release of LDH as a percentage of the maximum LDH release:

$$\% \text{ Cytotocity} = \frac{\text{Experimental LDH release}}{\text{Maximum LDH release}} \times 100$$

2.4.14 Silencing of Gene Expression with siRNA

Small interfering RNA (siRNA) are short (20-25 nucleotide) double-stranded RNAs, which prevent gene expression at a post-transcriptional level, by preventing translation of mRNA into polypeptide.(Elbashir *et al.* 2001) They are highly specific. In practice, a lipid-based transfection reagent is used to deliver double-stranded siRNA cytoplasm, where it engages RNA-induced silencing complex (RISC). RISC has an RNAse component, which then destroys one siRNA strand. The remaining strand acts as a guide, by binding to its complementary target sequence in the cell's mRNA, results in the mRNA being cleaved by RISC. siRNA mode of action is summarised in the Appendix. All reagents for silencing of gene expression were obtained from Santa Cruz Biotechnology, Santa Cruz, CA, USA, unless otherwise stated, and protocols carried out according to manufacturer's instructions. siRNAs specifically targeting mRNA for human c-Src, megalin, and cubilin and a non-targeting scramble-sequence siRNA as a negative control were used. c-Src expression was silenced by transfecting HK-2 cells with a pool of four target-specific 20- to 25-nucleotide siRNAs (50 pmol). Targeted knockdown of megalin and cubilin was achieved using pools of three target-specific 20- to 25-nucleotide siRNAs (50 pmol). HK-2 cells in log phase were enumerated and seeded onto 6-well plates at a density of 4×10^5 per well in antibiotic-free growth medium. At 60-80% confluence, cells were washed with transfection medium, then overlaid with siRNA-transfection reagent complexes, and returned to the incubator. After 6 hours, fresh medium was added to minimize toxicity. Cells were incubated for a further 48 hours, before protein expression was assessed by Western blotting.

2.4.15 Immunoblotting of Cell Culture Lysates

2.4.15.1 Western Blotting - c-Src Phosphorylation

In the inactive state, c-Src is phosphorylated at Y527. Upon oxidation at C245 and C487, it becomes dephosphorylated at Y527, phosphorylated at Y416, undergoes conformational change, and becomes active. This was detected by Western blot analysis of cell lysates using a primary antibody that specifically detects phosphorylation at Y416.

SDS-PAGE gels were cast in the laboratory according to instructions (see Appendix). Cell lysates (20-60 µg) were boiled for 3 minutes in Laemmli buffer and separated by 12% SDS-PAGE (BioRad), before undergoing electrophoretic wet-tank transfer onto polyvinylidene difluoride (PVDF) membranes at 4 ˚C. These were blocked in 5% skim milk for and then incubated at 4°C overnight with one of the following primary antibodies: rabbit-anti-human phospho-c-Src Y416 (1:1000 dilution) or rabbit-anti-human total c-Src (1:1000; Cell Signaling Technology, Danvers, MA). Blots were incubated for 1 hour at room temperature with horseradish peroxidase (HrP)-conjugated goat-anti-rabbit secondary antibody (1:2000 dilution; Thermo Scientific Pierce). Visualization was by enhanced chemiluminescence (ECL, SuperSignal West Dura, Thermo Scientific Pierce) on film (BioMax MR; Carestream Health, Rochester, NY).

GAPDH served as a loading normalisation control and was determined by stripping the blots (Restore; Thermo Scientific Pierce) and reprobing with mouse-anti-human GAPDH (1:10,000; Abcam, Cambridge, MA), detected with a HrP-conjugated goat-anti-mouse (1:2000 dilution) secondary antibody.

For experiments investigating the effect of DMTU on c-Src phosphorylation, total c-Src was used as a normalisation control.

2.4.15.2 Western Blotting - Megalin and Cubilin

Cell lysates (20- 60 µg) were boiled for 3 minutes in Laemmli buffer and separated by 7-12% gradient SDS-PAGE (purchased pre-cast gels from BioRad), transferred onto PVDF membranes, and blocked in skim milk as above. Blots were then incubated at 4°C overnight with one of the following primary anti-bodies: goat-anti-human megalin (C19) or cubilin (Y20) (1:250 dilution; Santa Cruz). GAPDH served as a loading normalization control as above. Blots were incubated for 1 hour at room temperature with horseradish peroxidase (HrP)-conjugated donkey-anti-goat (1:10,000 dilution; BioRad) secondary antibodies. GAPDH was used as a normalisation control. Visualisation and densitometry was performed as above.

2.4.15.3 Densitometry

Films were scanned (Microtek Int., Taiwan) and band densitometry was performed using Quantity One software (BioRad).

2.4.15.4 Detection of c-Src Oxidation by Carboxymethylation

To determine whether oxidation of c-Src occurs in response to exposure to FLC in HK-2 cells, *N*-(biotinoyl)-*N'*-(iodoacetyl)ethylenediamide (BIAM, Invitrogen), a thiol-reactive biotinylating reagent for proteins, was used. BIAM specifically identifies the thiolate

form of cysteine residues when they are in the reduced state, making it a very useful tool to detect redox-regulation of proteins, including c-Src.(Dominici *et al.* 1999; Kim *et al.* 2000; Giannoni *et al.* 2005) Using this method, I measured reduced c-Src levels in HK-2 cells after exposure to FLC.

Cells were grown on 100 mm dishes and allowed to reach 80-90% confluence. Medium was then removed, the cells were rinsed briefly with PBS, and then medium containing FLC (1 mg/ml) was added. At 2, 6, 12, and 24 hours, medium was removed and cells were snap-frozen in liquid nitrogen. RIPA buffer containing 100 µM BIAM was rendered free of oxygen by bubbling with nitrogen gas at a low flow rate for 20 minutes. Frozen cells were then exposed to 0.5 ml of this RIPA buffer, followed by sonication for three periods of 1 minute each separated by 30-second intervals, and then incubated for 15 minutes at room temperature. Lysates were then clarified by centrifugation and immunoprecipitated with anti-human total c-Src antibody (Cell Signaling Technology, Danvers, MA, USA) using Protein G PLUS-Agarose immunoprecipitation reagent (Santa Cruz Biotechnology). Total soluble protein concentration was determined by BCA assay, before separation by SDS-PAGE and transferred to polyvinylidene difluoride membranes as above. Each sample was divided into two equal parts: one half was used for detection of c-Src labeled with BIAM by HrP-conjugated streptavidin and the other half was probed for total c-Src for normalisation, as above. Visualisation was by ECL onto film as above.

2.4.16 Inhibition of c-Src Activity

4-Amino-5-(4-chlorophenyl)-7-(tert-butyl)pyrazolo[3,4-d]pyramidine (PP2; EMD Biosciences, Gibbstown, NJ) is a potent selective chemical inhibitor of c-Src activity.(Hanke *et al.* 1996) To suppress c-Src activity in HK-2 cells during experiments, PP2 was added to the medium to a final concentration of 10 µM at the same time FLC was added.

2.4.17 Removal of Extracellular and Intracellular H_2O_2

To investigate whether H_2O_2 involved in signaling was produced intracellularly or extracellularly, catalase was added to the medium. As a powerful extracellular scavenger of H_2O_2, exogenously applied catalase would quickly destroy any H_2O_2 in the supernatant. For experiments where the effect of extracellular H_2O_2 was to be abolished, catalase from bovine liver (Sigma-Aldrich) was added to the medium to a final concentration of 500 U/ml before addition to wells containing HK-2 cells.

The effect of inhibition of intracellular reactive oxygen species (ROS) on FLC–induced MCP-1 production was examined by overnight co-incubation of HK-2 cells exposed to FLC with DMTU, 30 mM, a cell-permeable chemical trap for H_2O_2.(Parker *et al.* 1985)

2.5 Purification of Polyclonal FLCs and Protein Chemistry

2.5.1 Total Soluble Protein (TSP) Quantification

2.5.1.1 Ultraviolet Absorbance at 280 nm (A280)

Proteins absorb UV light due to the presence of tyrosine and tryptophan residues. The quantities of these amino acids vary considerably between proteins, and so the molar extinction coefficient (a measure of how strongly a chemical absorbs light at a given wavelength, per unit mass) varies from protein to protein (Appendix). For crude solutions and extracts, nucleic acids and nucleotides can interfere with absorbance and requires correction. However, as protein purification progresses and such interfering compounds are removed this effect becomes negligible. (Scopes 1994)

A280 was measured using a spectrophotometer (Ultrospec II; Pharmacia-LKB, Uppsala, Sweden). After setting the absorbance wavelength to 280 nm. 1,000 µl of buffer was placed in a clean glass cuvette, placed in the chamber, and the reading was set to 0. This was then exchanged for a cuvette containing 1,000 µl of sample, and the reading taken. If the readout was above 1.0, the solution would be diluted 1:2 in buffer and retested. TSP was calculated using the following equation:

$$\text{TSP (mg/ml or g/L)} = \frac{\text{OD} \times \text{Path Length*} \text{ of Cuvette (mm)} \times \text{Dilution Factor}}{\text{Extinction Coefficient}}$$

*Path length of most cuvettes is 10 mm.

2.5.1.2 Bicinchoninic Acid (BCA) Assay

This method utilises the biuret reaction (reduction of Cu^{+2} to Cu^{+1} by amino acid residues in an alkaline environment), and the highly sensitive and selective colorimetric detection of Cu^{+1} using bicinchoninic acid. (Smith *et al.* 1985) The assay is robust, easily reproducible, detergent-compatible and the intensity of colour change is nearly linear across a broad concentration range of protein (20 – 2,000 µg/ml). A BCA assay kit was obtained (Thermo Scientific Pierce, Rockford, IL, USA) and assays carried out according to the manufacturer's protocol. BSA standards were prepared to dilutions between 0 – 2,000 µg/ml. Serial dilutions of sample were made in buffer. In a 96-well plate, 25 µl per well of standards and samples were loaded using a pipette. The BCA working reagent was prepared by mixing BCA Reagent A from the kit with BCA reagent B in a 50:1 ratio. Using a multi-channel pipette, 200 µl per well of the working reagent was loaded and the plate was covered and mixed on a plate shaker for 30 seconds. The microplate was then incubated at 37 ˚C for 30 minutes. Absorbance was read at 562 nm on a plate reader (Spectramax M2e; Molecular Devices, Sunnyvale, CA, USA). Results were viewed with plate reader software, which compared standard curve to results from samples (SoftMax Pro; Molecular Devices).

2.5.2 Free Light Chain Quantification

The FLC concentration in samples during the protein purification process was measured at Ltd, using a particle-enhanced nephelometric assay (Freelite; , Birmingham, UK).(Bradwell *et al.* 2001)

2.5.3 Sodium Dodecyl Sulphate-Polyacrylamide Gel Electrophoresis

Sodium dodecyl sulphate-polyacrylamide gel electrophoresis (SDS-PAGE) was performed for Coomassie staining, silver staining and Western blotting.

2.5.3.1 Coomassie Brilliant Blue

Samples were mixed with Laemmli buffer (Bio-Rad, Hercules, CA). Where analysis was to be performed under reducing conditions, dithiothreitol or β-mercaptoethanol was added to the Laemmli buffer and samples boiled for 3 minutes. Proteins were resolved on 4-12% gels (NUPAGE, Invitrogen) and placed in fixative, before being stained with Coomassie Brilliant Blue (Bio-Rad) and then washed in destaining solution until bands were clearly visible.

2.5.3.2 Silver Stain

Proteins were separated by SDS-PAGE and treated with fixative as above. The gel was placed in 50 ml of sensitisation reagent overnight. After washing, silver solution was added and incubated for 45 minutes protected from light, and washed again. Developer solution was added, and stop solution added when bands were adequately visible.

2.5.4 Immunoblotting

2.5.4.1 Western Blotting - Protein Purity Testing

During polyclonal FLC purification, western blotting was used to identify bands on SDS-PAGE. Proteins were resolved as above. Proteins were electrophoretically transferred to nitrocellulose membranes in a wet tank. Membranes were blocked in 5% skim milk and then incubated with primary antibody for 2 hours at room temperature. Blots were washed, incubated with HrP conjugated secondary antibody for 1 hour and then bands were visualised by incubating with AEC staining reagent until bands were developed adequately.

2.5.4.2 Dot Blotting

Dot blotting was used to probe for the presence of a particular protein of interest in chromatography fractions. It involves loading sample of interest directly onto a membrane without the need for resolving on a gel and transferring.

A nitrocellulose membrane was marked to form a grid with a pencil. Samples were spotted in1-2 µl volumes onto the membrane using a 10 µl pipette tip pressed firmly against the membrane, taking care not to rupture the membrane, and allowed to air-dry. The membrane was then rehydrated in water, blocked in 5% skim milk and then incubated with primary antibody for 2 hours, followed by HrP-conjugated secondary antibody for 1 hour, and developed with AEC as above.

2.5.5 Endotoxin Assays

2.5.5.1 Colorimetric Assay

A quantitative, chromogenic Limulus amoebocyte lysate (LAL) assay kit was used, according to manufacturer's instructions, to test for the presence of endotoxin in monoclonal FLC (QCL-1000, Lonza, Walkersville, MD, USA). This assay utilises the reaction of endotoxin with LAL to activate an enzyme, which in turn acts on a synthetic substrate to produce a yellow colour. A 96-well microplate was warmed to 37 ˚C. At T = 0 minutes, in duplicate, 50 µl per well of endotoxin standards and samples were pipetted into the wells. 50 µl of LAL was then added to each well and incubated until T = 10 minutes. 100 µl of substrate solution per well was then added. At T = 16 minutes, 100 µl per well of stop solution was added. Absorbance was measured using a plate reader at 405-410 nm.

2.5.5.2 Gel Clot Assay

Endotoxin in polyclonal FLC was measured using a LAL gel-clot assay (E-TOXATE; Sigma-Aldrich). The assay utilises the formation of a gel when LAL interacts with even minute quantities of endotoxin.(Bang 1956) Sterile, plugged pipettes and autoclaved, new, 10 x 75 mm glass tubes were used. The pH of the FLC solution was measured and confirmed to be within the working range of the assay. The LAL reagent and endotoxin standards were prepared as instructed. Samples (undiluted) and standards were added to tubes, followed by LAL reagent, and incubated at 37 ˚C in a water bath. After 1 hour, tubes were gently inverted while observing for evidence of gel formation. A hard gel that permits complete inversion without disruption of the gel was taken as a positive

result; all other results, including soft gels or turbid solutions were taken as negative (Appendix).

2.5.6 Endotoxin Removal

Endotoxin removal from polyclonal FLC was carried out using polymixin B, immobilised onto cross-linked 6% agarose resin (Detoxi-Gel; Thermo Scientific). Polymixin B binds to the lipid A portion of endotoxin.(Issekutz 1983) Endotoxin-free water (Sigma Aldrich) was used at all times. Resin was degassed by placing slurry in a suction filter flask, stirring with a magnetic stirrer, and applying suction for 15 minutes. Slurry was then packed into disposable 10 ml centrifuge columns (Thermo Scientific). The resin was regenerated by running through 5 bed volumes of 1 % sodium deoxycholate (Sigma Aldrich), then washed with 5 bed volumes of water. Columns were centrifuged at 100 x g for 30 seconds to remove liquid from resin, and the resin was immediately resuspended in the sample (polyclonal FLC). Columns were then incubated at room temperature for 2 hours on a roller, centrifuged again and the filtrate collected, and the resin resuspended in water. The resin was then washed with deoxycholate and water as above to regenerate and elute off bound endotoxin. Samples were then tested by E-TOXATE as above, and, if necessary, endotoxin removal repeated.

2.5.7 Monoclonal FLC Preparation

Monoclonal FLCs used in experiments were previously prepared by Dr Paul W. Sanders at the University of Alabama at Birmingham from the urines of patients with multiple myeloma.(Sanders *et al.* 1987)

2.5.8 Polyclonal FLC Preparation

Polyclonal FLCs were extracted from pooled blood donor sera. These were obtained from a vendor (Bio Products Laboratories, Elstree, UK) following removal of albumin by ethanol precipitation. The final production process for polyclonal FLCs is summarised in Chapter Five.

2.5.8.1 Initial Steps

These initial steps were performed at Ltd, by Simon Blackmore. Precipitate was resuspended in PBS and remaining particulate matter allowed to settle. Using a peristaltic pump, the supernatant was dialysed using a membrane with increased permeability to molecules up to 60 kDa (HCO-1100, Gambro, Stockholm, Sweden). The filtrate was analysed for soluble protein, and found to contain significant quantities of IgG and albumin. A significant proportion of this IgG was removed by protein A immobilised on agarose (3 loops). The unbound fraction from this step was passed onto me for further processing.

2.5.8.2 Coupling of Antibody to Matrix

An anti-κ FLC affinity column was manufactured by coupling antibody to Sepharose matrix. 500 mg of anti-κ FLC antibody, raised in sheep, was obtained from Ltd, along with CNBr activated Sepharose matrix (GE Healthcare). The ligand (antibody) was dialysed for 24 hours into coupling buffer, and transferred to a temporary column. Sepharose matrix was washed under suction in 1 mM HCl, and allowed to pack down

under suction to a cake. This was transferred to the temporary column, and gently resuspended by shaking, and left to couple through the day and overnight on a roller. The outlet was then opened, and the coupling buffer was drained out. The matrix was washed with 1 bed volume of acetate buffer, alternating with Tris-HCl, three times, then with one bed volume of elution buffer (glycine), then finally with running buffer (PBS).

Protein content of the drained coupling buffer was determined by A280, and discarded after confirmation of adequate ligand binding.

2.5.8.3 Affinity Chromatography

Column chromatography was used extensively during the process of purifying polyclonal FLC. The principal methods applied were affinity chromatography and size-exclusion chromatography.

Affinity chromatography relies on the binding of a molecule of interest in solution (the liquid phase) to a molecule immobilised on a matrix (the solid phase) under designated conditions (e.g. a given pH), thus removing that molecule of interest from the solution.(Scopes 1994) These can be disassociated, by altering conditions (e.g. a different pH) with subsequent elution. Matrix conjugated with relevant antibody was packed into a column, and connected to an automated pumped liquid chromatography system (AKTAprime plus; GE Healthcare, Uppsala, Sweden). This system enables loading of samples and passage of buffers at a range of designated speeds, monitoring of solute content of column eluent by an UV light absorption detector, and collection of eluent in fractions (Appendix). The buffer volumes, process running time, solution

conductivity, collected fractions and UV absorption was depicted graphically in real-time using proprietary software installed on a computer connected to the AKTAprime plus.

All samples and buffers were passed through a 0.45 µm filter prior to application to the column. The column was washed in three bed volumes of running buffer (usually PBS, pH 7.2), elution buffer (usually glycine, pH 3) and then running buffer again. Sample was then loaded onto the column, and run through. The unbound fraction was collected for further analysis. The bound fraction was then eluted in glycine, and neutralisation buffer promptly added (Appendix).

2.5.8.4 Size-Exclusion Chromatography

Size-exclusion chromatography (SEC) is a process that enables separation of molecules according to their size. It relies on the differential speeds at which molecules of different sizes in solution (the liquid phase) travel through a porous matrix (the solid phase). Smaller molecules will be able to enter every corner of the matrix's intra-particle pore system, and thus its progress will be retarded, causing it to be eluted late. (Lathe and Ruthven 1956; Scopes 1994) A larger molecule will permeate the pore system to a lesser extent, thus mostly passing through the inter-particle spaces, and will be eluted earlier.

Columns were packed with matrix (GE Healthcare), connected to an AKTAprime system as above, and equilibrated with PBS running buffer which had been filtered to 0.22 µm. Samples were injected via a loop, the buffer was run at 0.5 ml/min and fractions collected in 4 ml aliquots. Fractions of interest were then analysed as required.

2.5.9 Lyophilisation of Polyclonal FLC for Storage and Transportation

After confirmation of the absence of endotoxin, polyclonal FLC was dialysed extensively for 72 hours into cell culture grade water, and transferred to 10 ml glass vials. Proteins were then lyophilised at Ltd. Following lyophilisation, an aliquot was redissolved in buffer to confirm that solubility of protein was retained.

2.6 Uromodulin

2.6.1 Purification of Uromodulin

Uromodulin was purified from the urines of healthy volunteers, according to the original method of Tamm and Horsfall.(Tamm and Horsfall 1952) Urine from healthy volunteers was collected and divided into 40-45 ml aliquots and placed on ice. Sodium chloride was added to a final concentration of 0.58 M, and allowed to dissolve on a roller at 4 ˚C. Once dissolved, the tubes were left upright, overnight at 4 ˚C. Samples were then centrifuged at 10,000 x g at 4 ˚C for 1 hour. The supernatant was discarded, the gel-like flocculent pellet redissolved in 10 ml of water, sodium chloride added again to a concentration of 0.58 M, and left overnight again. The solution was centrifuged as above, and the pellet redissolved in 2 ml of water. This was then dialysed into water for 24 hours and protein concentration assessed by BCA assay. Protein was concentrated until it reached a TSP value of 2 mg/ml. For storage, the proteins could be frozen to -70˚C.

When making dilutions of uromodulin in buffer, stock solutions were made by combining the uromodulin solution in water, with equivalent volumes of x 2 strength buffer (prepared by diluting x 10 buffer 1:5 in distilled, deionised water) and serially diluting this stock solution with x 1 buffer.

2.6.2 Binding of Uromodulin to Polyclonal FLC

The binding of uromodulin to polyclonal FLC was assessed by ELISA, immunoblotting and nephelometry.

2.6.2.1 Indirect ELISA

Plates were coated with polyclonal FLCs and control proteins (monoclonal FLCs purchased from a vendor; κ FLC and λ FLC, both from Sigma Aldrich; and HSA in PBS-T overnight at 4 ˚C. After washing, the wells were blocked with 1% BSA for 30 min, and incubated with uromodulin for 2 hours, washed, incubated with HrP-conjugated anti-sheep antibody (The Binding Site) for 1 hour, and developed with TMB substrate, and stopped with sulphuric acid, as above. Absorbance was measured at 450 nm. For background measurement, wells were loaded with buffer only instead of protein and probed with primary and secondary antibodies as normal; absorbance values from these wells were subtracted from the results from the rest of the plate. No standard curve was generated, as the aim of the experiment was a comparison between polyclonal FLC and other proteins.

Plates were also coated with uromodulin, and then incubated with different dilutions of polyclonal FLC, probed with anti-κ FLC or anti-λ FLC primary antibodies, followed by HrP-conjugated secondary antibody.

2.6.2.2 Sandwich ELISA

A sandwich ELISA approach was attempted to reduce background signal from indirect ELISA. Plates were coated with anti-uromodulin antibody. Uromodulin was then applied at fixed concentration and incubated for 2 hours at room temperature. After washing, dilutions of polyclonal FLC were added to the wells, and incubated for 2 hours. Plates were then washed again, and incubated with HrP-conjugated anti-κ FLC or anti-λ FLC antibody for 1 hour at room temperature, and developed with TMB substrate as above. Background absorbance was measured and subtracted from the results as above.

2.6.2.3 Dot Blot

Dilutions of polyclonal FLC were made, spotted onto a nitrocellulose membrane, air-dried, rehydrated with water, and blocked in 5% milk, before being incubated with uromodulin. Blots were then incubated with anti-uromodulin primary antibody, followed by HrP-conjugated secondary antibody, and developed with AEC.

In other experiments, dilutions of uromodulin were spotted onto membranes, incubated with polyclonal FLC, and probed with anti-κ FLC and anti-λ FLC antibodies.

2.6.2.4 Nephelometry

The formation of aggregates between polyclonal FLC in free and uromodulin in free solution was also investigated by measuring dynamic light scattering.(Sanders *et al.* 1990) The instrument (MiniNeph;) was a bench-top nephelometer with a 670 nm laser, using a 1 cm constant path length cuvette, with a reaction volume of 400 µl, and detected light scatter at an angle of 18˚ to the incident beam. Results were expressed as arbitrary Scatter Units against the reading from a blank cuvette containing buffer only, as zero.

Uromodulin was added to the cuvette, and the reaction started by addition of polyclonal FLC or control protein, prepared in buffer with different salt concentrations. The open end of the cuvette was then promptly covered with plastic film to prevent excess evaporation. Scatter readings were taken at intervals and plotted against time.

2.7 Statistical Analyses

Statistical analysis was carried out using software packages Prism, GraphPad Software, La Jolla, CA, USA) and PASW Statistics (SPSS Inc, Chicago, IL, USA). A p-value of < 0.05 was assigned statistical significance.

2.7.1 Assessment of Normality of Data

Data was analysed to assess whether they were from a Gaussian distribution, by applying both a Kolmogorov-Smirnov test (with Dallal-Wilkinson-Lilliefor p-value) and a d'Agostino and Pearson omnibus normality test.

2.7.2 Normalisation of Data

Where required, data, which was not normally distributed was normalised by log-transformation.

2.7.3 Correlations

Linear regression analyses were performed to determine correlations between normally distributed data variables. Correlations between data were assessed by Pearson's test (after log-transformation, if required) and Spearman's calculations, with 2-tailed p-values. Linear regression stepwise multivariate analysis of these correlations with a dependent variable was also performed.

2.7.4 ANOVA

Where measurements involved the use of ELISA, H_2O_2 measurement, LDH release, and nephelometry, each experiment was performed with at least 3 replicates and results were expressed as mean, with standard error of the mean (SEM). Statistical differences between results were assessed by one-way and two-way analysis of variance (ANOVA) with Bonferroni *post hoc* testing.

2.7.5 Test of Intra- and Inter-observer Variability of Image Analysis Data

To test the validity of data obtained from quantitative image analysis for chronic damage, capillary density and macrophage infiltration, intra- and inter-observer

variability was tested. Inter-observer variation was assessed by having two observers measure 20 specimens independently. One observer was an independent research associate, and the other was myself. These 20 specimens were also measured twice, at intervals, by myself. This was to test for intra-observer variability. Concurrence was tested by the method described by Bland and Altman.(Bland and Altman 1986) This method gives the bias, or mean difference between measurements and limits of agreement, or 2 SDs either side of the mean, with 95% confidence intervals (CIs) for the bias and limits of agreement.

2.7.6 Assessment of Distribution of Casts

Statistical comparison of distribution of casts between areas with or without chronic damage was made with the two-tailed unpaired non-parametric Mann-Whitney test.

3. RENAL INFLAMMATION AND FIBROSIS IN MONOCLONAL DISEASE: IN SITU STUDIES

3.1 Introduction

Renal failure is a common finding in multiple myeloma, and is associated with significantly increased morbidity and mortality.(Kyle *et al.* 2003) The predominant histological lesion is myeloma kidney, or cast nephropathy, which is seen in up to 70% of cases at biopsy.(Ivanyi 1989; Herrera *et al.* 2004) Cast nephropathy is characterised by the presence of proximal tubular cell injury, interstitial inflammation, and hard, waxy casts in the distal tubules. Associated interstitial fibrosis is frequently seen. Currently there is no specific treatment for myeloma cast nephropathy, beyond treatment of the underlying plasma cell clone with chemotherapy.

Excess circulating FLCs produced by the aberrant plasma cell clone are freely filtered at the glomerulus and presented to PTECs where they are taken up via the multi-ligand receptors megalin and cubilin and undergo lysosomal degradation.(Batuman *et al.* 1998; Klassen *et al.* 2005) During this process, signalling events lead to release of inflammatory mediators (including MCP-1) from PTECs, resulting in inflammatory cell recruitment and progressive interstitial fibrosis.(Sengul *et al.* 2002; Wang and Sanders 2007) When the resorptive capacity of the proximal tubule is exceeded, FLCs then travel to the distal nephron, where they co-precipitate with uromodulin to form casts.(Sanders *et al.* 1990; Huang *et al.* 1993) These casts have a hard, waxy appearance and are frequently associated with a cellular reaction consisting of macrophage-derived giant cells.(Alpers *et al.* 1985)

Despite a wealth of information from *in vitro* and *in vivo* studies, little data exists on the *in situ* evolution of renal injury in humans. There has been one previous report of a follow-up renal biopsy after the initial diagnostic biopsy showing cast nephropathy.(Rose *et al.* 1987). This patient was treated with chemotherapy and initially received haemodialysis, converting to continuous ambulatory peritoneal dialysis. The patient became dialysis-independent after 3 months (although renal function did not normalize), with an associated reduction in serum paraprotein concentration and urinary light chain excretion. A repeat renal biopsy at 8 months showed an improvement in the adverse histological features present in the index biopsy.

At our centre, a recent study has analysed treatment for patients presenting with AKI secondary to cast nephropathy with the combination of chemotherapy and high cut-off haemodialysis.(Hutchison *et al.* 2009) A number of patients who received this treatment and did not achieve independence from dialysis were assessed by a repeat renal biopsy.

The aims of the work reported in this chapter were to: (i) perform a detailed histological examination of kidney tissue in these patients; (ii) compare the features seen before and after a period of treatment; and (iii) compare histological features which might be associated with renal outcomes.

3.2 Results

3.2.1 Patients

Patients treated by chemotherapy and high-cut off dialysis who remained dialysis dependent at six weeks were offered a repeat renal biopsy to assess the potential for recovery of independent renal function. Four patients (referred to as A, B, C and D) consented to undergo the second renal biopsy. The four patients, who comprised two male and two female adult Caucasians, presented with AKI requiring dialysis. None of the patients were known to have pre-existing renal disease, or any other significant medical history. After a paraprotein was detected in their sera, the patients underwent bone marrow biopsies to confirm the diagnosis of multiple myeloma. Serum FLCs were measured using the Freelite assay. A renal biopsy was also performed, which in each case showed myeloma cast nephropathy.

All four patients received standard chemotherapy according to the local protocol. Patients A, B and C received thalidomide and dexamethasone, whilst patient D received cyclophosphamide, thalidomide and dexamethasone. Patients A, B and C were treated at our centre, while patient D was treated at another centre. As an adjunct, they also received high cut-off haemodialysis to maximise extracorporeal removal of light chains and minimise renal toxicity. After six weeks of treatment, for the purpose of further assessment, including quantification of chronic damage and the potential for recovery of independent renal function, each patient underwent a second renal biopsy.

Table 3.1 summarises patient demographics, histological findings and biochemical data. All biopsies contained adequate cortical tissue to enable morphometric analysis.

Significant reductions in light chain concentrations were achieved in all patients (median 76.5%, range 63.9-92.9%). Three patients (A, B and C) eventually achieved independence from dialysis at 51, 67 and 105 days, respectively. The six-week biopsies showed differential changes in the degree of chronic damage and cast numbers.

3.2.2 Histological Diagnosis of Cast Nephropathy

The initial biopsies fulfilled diagnostic criteria for cast nephropathy. In all four there was evidence of vacuolation and desquamation of PTECs, interstitial inflammation and fibrosis, and distal tubular casts. There was no evidence of amyloid or light chain deposition disease in any of the biopsies. In addition to standard diagnostic assessments, renal biopsy specimens were also assessed in detail for chronic damage and light chain cast formation. Figure 3.1 shows the initial diagnostic and six-week biopsies for the patients.

Table 3.1. Summary of patient demographics, histological findings and biochemical data.

Patient	Age	Sex	Medication Prior to Presentation	FLC Isotype	Treatment Regimen	Serum FLC at Treatment Initiation (mg/L)	Serum FLC at 6 Weeks (mg/L)	Reduction in Serum FLC by 6 Weeks (%)	Index of Chronic Damage (%)		Number of Tubules with Casts (%)		Interstitial Infiltrate		Time to Independence from Dialysis (Days)
									0 Weeks	6 Weeks	0 Weeks	6 Weeks	0 Weeks	6 Weeks	
A	61	F	None	Free κ	TD	1,990	334	83.2 %	28.1	40.3	37.5	5.7	Heavy	Moderate	51
B	56	M	None	IgA λ	TD	9,918	704	92.9 %	10.7	42.2	37.3	10.0	Moderate	Moderate	67
C	55	F	None	Free κ	TD	7,675	2,318	69.8 %	35.7	37.3	21.9	8.3	Moderate	Moderate	105
D	55	M	None	IgG κ	CTD	5,870	2,119	63.9 %	28.3	31.7	24.6	24.0	Heavy	Light	No Recovery

TD, thalidomide and dexamethasone; CTD, cyclophosphamide, thalidomide and dexamethasone.

3.2.3 Index of Chronic Damage

Figure 3.2A shows changes in the index of chronic damage over six weeks. At initiation of treatment, the index of chronic damage for patients A-D was 28.1%, 10.7%, 35.7% and 28.3%, respectively. At six weeks, patient A had sustained a moderate increase in chronic damage, up to 40.3%. Patients C and D showed minimal increases in chronic damage, up to 37.3% and 31.7%, respectively. In contrast, patient B sustained a fourfold increase in the degree of renal scarring, from 10.7% up to 42.4%, despite a rapid and sustained reduction in serum light chain levels to lower than 10% of starting level at six weeks.

3.2.4 Number of Tubules with Casts

Figure 3.2B shows changes in cast numbers over six weeks. The median number of tubules counted per biopsy was 368.5 (range 145-1302). Three patients, A, B and C, showed major reductions in intratubular cast numbers at six weeks, from 37.5% to 5.7%, 27.3% to 10.0% and 21.9% to 8.3%, respectively. Patient D continued to have high cast formation at six weeks, and there was no renal recovery in this case.

Figure 3.1. Renal biopsies from patients A-D.

Renal biopsies at initiation of treatement (i) and after six weeks (ii), showing observed changes in interstitial inflammation, degree of interstitial scarring and cast numbers. (H&E, original magnification x200)

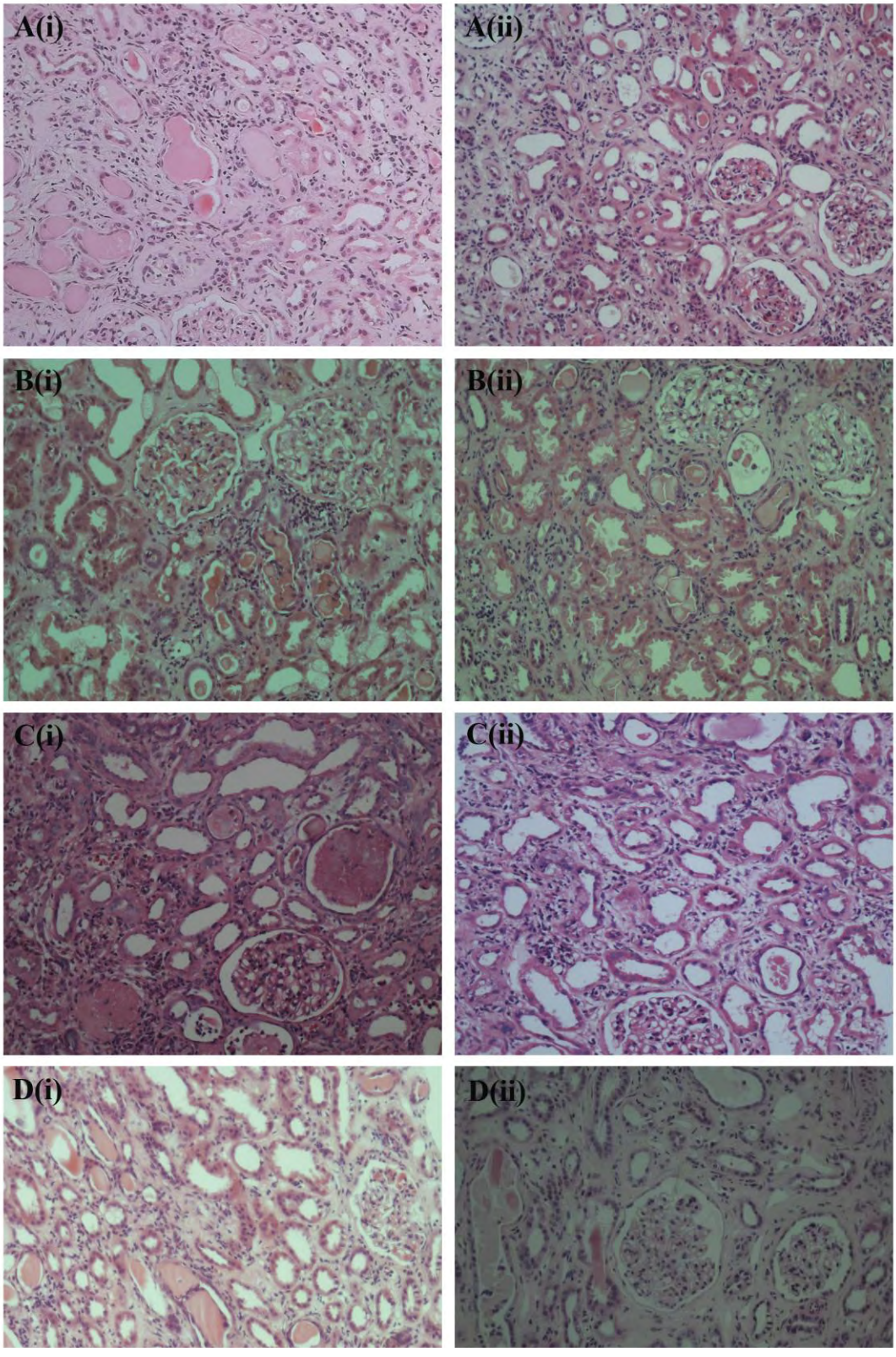

Figure 3.2. Changes in the index of chronic damage and cast numbers over six weeks.

Changes in the index of chronic damage (A), and cast numbers (B) at initiation of treatment and after six weeks. Patient A sustained a moderate increase in chronic damage, while Patients C and D showed minimal increases. Patient B sustained a fourfold increase in chronic damage. Patients A, B and C showed major reductions in the numbers of intratubular casts seen on biopsy, while patient D continued to have high numbers of casts after six weeks.

A

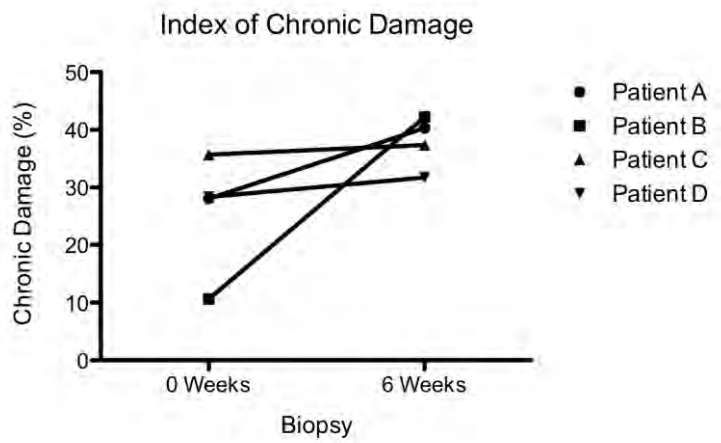

B

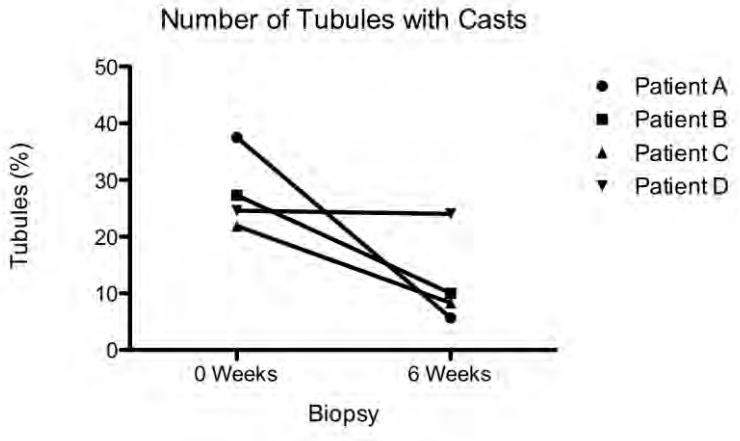

3.2.5 Interstitial Infiltrate

For the purpose of scoring the degree of interstitial infiltrate, sections were anonymised and blinded assessment was carried out by two observers independently (Dr and Dr Dia Kamel). The degree of interstitial infiltrate was determined by eye, and graded as heavy, moderate or light.

The degree of interstitial infiltrate at six weeks was reduced in patient A from heavy to moderate, and markedly reduced in patient D from heavy to light. In patients B and C there were moderate interstitial infiltrates on the first biopsy, which had not changed at six weeks.

3.3 Discussion

This is the first series detailing the *in situ* changes with time in patients with myeloma cast nephropathy. The patients who are reported remained dialysis dependent after six weeks, which prompted further assessment by a repeat biopsy. The purpose of repeat biopsy included assessment of chronic damage and estimation of potential for the recovery of renal function. Despite significant reductions in serum FLC levels in all cases, chronic damage *in situ* on repeat biopsy ranged from no change from baseline to progression to severe chronic damage. Despite these observations, it was the patient who had no progression of chronic damage, but no decrease in cast numbers, who failed to recover independent renal function. Those patients who had reductions in cast numbers at six weeks did subsequently recover independent renal function.

In patients with multiple myeloma and cast nephropathy, failure to become independent of dialysis is associated with a worse outcome. A previous histological study indicated that the degree of interstitial fibrosis seen in the diagnostic biopsy correlated well with the prospect of renal recovery.(Pasquali *et al.* 1987) Another study has indicated that early renal recovery correlated with the severity of chronic damage and cast numbers seen in the biopsy.(Pozzi *et al.* 1987) In this study, some patients with severe tubular atrophy and interstitial fibrosis still recovered independent renal function. However, there are no other reliable predictors of renal recovery in this setting. In patients who are receiving disease-specific treatment for multiple myeloma in the setting of dialysis-dependent AKI and who have not achieved independent renal function after significant reductions in serum FLC levels, a repeat biopsy to assess in situ chronic damage and cast numbers may be useful as a guide to further treatment. Reduction in cast numbers may also indicate the potential for a late recovery.

Cast formation can also be promoted by increasing the salt concentration, acidification or slowing the flow rate of distal tubular fluid, as well as a high load of light chain delivered to the distal tubule. These conditions are potentiated by dehydration, administration of drugs such as furosemide or non-steroidal anti-inflammatory agents, and a higher serum FLC load. Therefore appropriate management of the patient can potentially reverse all these factors. Irrespective of any clinical changes, the reduction in cast numbers seen in patients A, B and C could reflect the fall in serum FLCs seen in these patients. The reason for the persistence of casts in patient D is hypothetical, but may be a reflection of the affinity of the clone of light chain in that patient for

uromodulin. Also in patient D, an improvement in the degree of interstitial infiltrate was not associated with subsequent renal recovery.

In these four patients, serum FLC measurements were taken into account at initiation of treatment, and at six weeks. Because the patients described in this study were treated at different centres, there were local variations in treatment strategies and serum FLC measurement intervals during treatment. As a result it was not known if there were differences between patients in serum FLC reductions during this six week period. In patients C and D, the reductions in serum FLC levels were less pronounced than in patients A and B. Patient C took longer to achieve independence from dialysis than patients A or B, while patient D did not recover independent renal function despite receiving more intensive chemotherapy than the other three patients. It is therefore also possible that better responsiveness to treatment (i.e. earlier, more pronounced reductions in serum FLC levels) might account for the differences in clinical outcomes.(Hutchison *et al.* 2009)

The findings presented in this chapter are based on the study of patients who underwent a repeat renal biopsy due to their failure to respond adequately to treatment. Patients who rapidly recover independent renal function are rarely offered a repeat biopsy. Therefore the data are gathered from a biased cohort, and may not necessarily be representative of *in situ* histological changes in all patients with myeloma kidney.

Studies using myeloma light chains purified from the urine of different patients have demonstrated that different species of light chains have differing degrees and patterns of

toxicity in the kidney, in both the proximal tubule and the distal tubule. Some light chains tend to cause more proximal tubular damage, while others have a strong tendency to co-precipitate in the distal nephron with uromodulin, to form casts.(Sanders *et al.* 1988a; Sanders *et al.* 1990; Sanders and Booker 1992) Sanders and co-workers have shown that it is the CDR3 region of both κ and λ FLCs that interacts with a single, 9 amino acid binding domain on uromodulin.(Huang *et al.* 1993; Huang and Sanders 1997; Ying and Sanders 2001) Both the degree of proximal tubular inflammation and avidity for binding to uromodulin varies from light chain to light chain.(Sanders *et al.* 1988a) In addition, although a link to progression of renal fibrosis has not been established, uromodulin is capable of activating macrophages through TLR4,(Saemann *et al.* 2005) a phenomenon which may in part account for the giant cell reaction frequently seen around myeloma casts.

The development of interstitial fibrosis leading to established chronic damage is associated with and dependent on the release of cytokines from PTECs in response to light chain endocytosis and the subsequent recruitment of inflammatory cells. One explanation for these differing degrees of toxicity may derive from the fact that light chains are coded for multiple gene segments which have a huge number of possible combinations, thus giving rise to extreme primary structure heterogeneity.(Bradwell 2006) These differences in primary structure and subsequent post-translational modifications can give an individual light chain unique physicochemical properties.

A recent, elegant study from the laboratory of Sanders showed that different monoclonal FLCs are capable of generating varying quantities of H_2O_2 in solution, a

property not exhibited by non-immunoglobulin derived proteins.(Wang and Sanders 2007) H_2O_2 was also detected in PTEC culture supernatants after exposure to FLCs, and subsequent release of cytokines was dependent on this H_2O_2. H_2O_2 acts as a second messenger in many signaling pathways, and so this finding had significant implications in terms of potential downstream inflammatory signaling following FLC endocytosis. It was possible that the inflammatory potential of FLCs was related to their ability to generate H_2O_2.

4. RENAL INFLAMMATION AND FIBROSIS IN MONOCLONAL DISEASE: IN VITRO STUDIES

4.1 Introduction

In the previous chapter, a detailed histological examination of renal biopsies was presented. In one of the patients, the degree of interstitial fibrosis was noted to have advanced rapidly, compared to the other three patients. The development of fibrosis is dependent on the activation of PTECs following FLC exposure, resulting in activation of MAPKs and NF-κB and downstream release of inflammatory cytokines such as MCP-1.(Sengul *et al.* 2002) One possible contributory factor is the differential toxicity of each clone of FLC. Two consistent findings in studies performed *in vitro* have been that (i) FLCs are more potent inducers of cytokines than other proteins commonly implicated in renal inflammation and (ii) the quantity of cytokines produced varies from one FLC to another.

A possible explanation for this phenomenon may lie in the ability of light chains to generate H_2O_2 in a catalytic fashion.(Wentworth *et al.* 2000; Wentworth *et al.* 2001) Recently, it was shown that myeloma FLCs also possess this ability, and that the release of MCP-1 from PTECs in response to FLC was dependent upon this.(Wang and Sanders 2007) These data pointed to a key role played by H_2O_2 in the signal transduction cascades that are set in motion after internalisation of excess light chain. The single initiating event for signal transduction, however, has remained elusive. H_2O_2 is known to act as a second messenger in signalling pathways.(Rhee 2006) If H_2O_2 were to

activate a molecule acting as a central signalling hub, the potential effects of H_2O_2 generation in monoclonal FLC related kidney disease might be far-reaching.

One potential candidate early signalling molecule was c-Src. c-Src is a member of the Src tyrosine kinase family, which plays a role in signal transduction in response to many external stimuli and its activity is under tight redox control (figure 4.1).(Parsons and Parsons 2004) When reduced by phosphorylation at Y527, it is inactive.(Cooper and Howell 1993) However, when oxidised at cysteine residues C245 & C487, it is dephosphorylated at Y527, undergoes conformational change, is autophosphorylated at Y416, and becomes active.(Brown and Cooper 1996; Xu *et al.* 1997) This process of activation has been shown to be dependent on ROS.(Cooper and Howell 1993; Giannoni *et al.* 2005) This chapter presents results from investigations into the relationship between H_2O_2, c-Src and the release of MCP-1 from PTECs in response to two monoclonal FLCs, referred to here as κ2 and λ2. These two monoclonal FLCs were purified from the urines of two patients with multiple myeloma.(Wang and Sanders 2007) Both patients had clinical evidence of significant renal damage, which was presumed to be cast nephropathy. However renal biopsy was not routinely performed in these patients. Endotoxin levels in both FLCs were shown to be below the detection limit of the QCL-1000 colourimetric assay (see Chapter 2). Both these FLCs had previously been shown to cause generation of H_2O_2 in HK-2 cell culture, and the production of this H_2O_2 was an integral step in the release of MCP-1 from cells.(Wang and Sanders 2007) The methods that were used to perform these experiments are presented in Chapter 2.

Figure 4.1. The c-Src molecule, and its activation.

In the inactive, reduced state, c-Src is phosphorylated at Y527. Oxidation at C245 & C487 results in dephosphorylation at Y527, subsequent conformational change, and autophosphorylation at Y416, causing the molecule to becomes active. This process has been shown to be dependent on ROS. SH, Src homology domains.

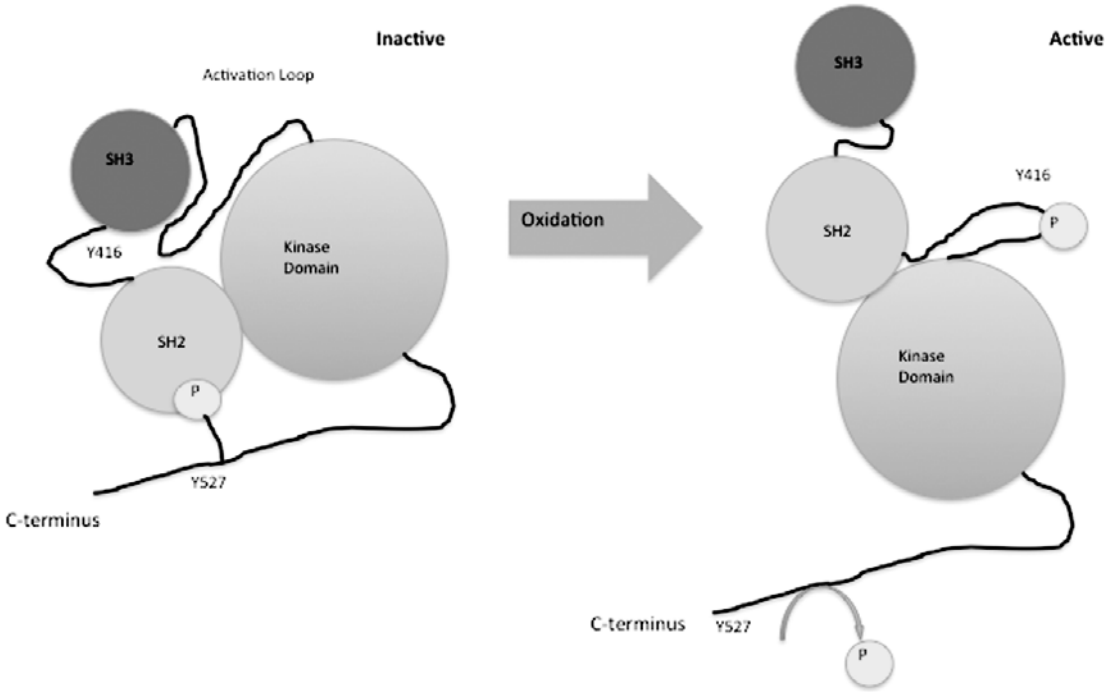

4.2 Results

4.2.1 Immunoglobulin Light Chains Activate c-Src

c-Src activation by phosphorylation (phospho-c-Src) was detected by Western blot analysis of cell lysates using a primary antibody that specifically detects phosphorylation at Y416. The amount of active c-Src in cells exposed to light chain (1 mg/ml) relative to the amount of GAPDH in the lysate were determined by densitometry (figure 4.2). After exposure to both κ2 and λ2 light chains, phospho-c-Src levels increased rapidly, representing activation of this enzyme, in a time-dependent manner, with a peak being observed at 12 h and declining thereafter. At this point they were up to 8-fold to 9-fold higher than the amounts seen in cells treated with vehicle alone. No time-dependent change in phospho-c-Src levels were seen in cells exposed to vehicle alone. After 12 h, phospho-c-Src concentrations declined, reducing to less than 50% of the peak levels by 24 h. There were no significant differences in the relative increase of phospho-c-Src between the two species of light chains at each time point.

4.2.2 DMTU Inhibits c-Src Activation

Co-incubation of HK-2 cells with either light chain and 1,3-dimethyl-2-thiourea (DMTU, 30 mM) a cell permeable chemical trap for H_2O_2, prevented activation of c-Src, as determined by the ratio of phospho- c-Src to total c-Src in the lysate obtained (Figure 4.3). Compared with κ2 alone, the increase in the relative amount of phospho-c-Src induced by the κ2 light chain was inhibited ($P < 0.05$) by DMTU (0.28 +-/- 0.04 for vehicle alone; 0.96 +/- 0.07 for light chain alone; 0.28 +/- 0.04 for light chain plus DMTU). Compared with λ2 light chain alone, the increase in phospho-c-Src induced by

the λ2 light chain was inhibited (P < 0.05) by DMTU (0.46 +/- 0.04 for vehicle alone;

0.80 +/- 0.12 for light chain alone; 0.41 +/- 0.02 for light chain plus DMTU).

Figure 4.2. Immunoglobulin free light chains activate c-Src.

Time dependent activation of c-Src by light chains. Exposure to both κ2 and λ2 light chain resulted in an increase in phosphorylation at Y416, representing activation of this enzyme, when compared with lysates of cells exposed to vehicle alone. Densitometric analysis of bands shows the increase was similar for both light chains and occurred in a time-dependent manner, reaching a peak at 12 hours, and declining thereafter. N = 3 experiments in each group.

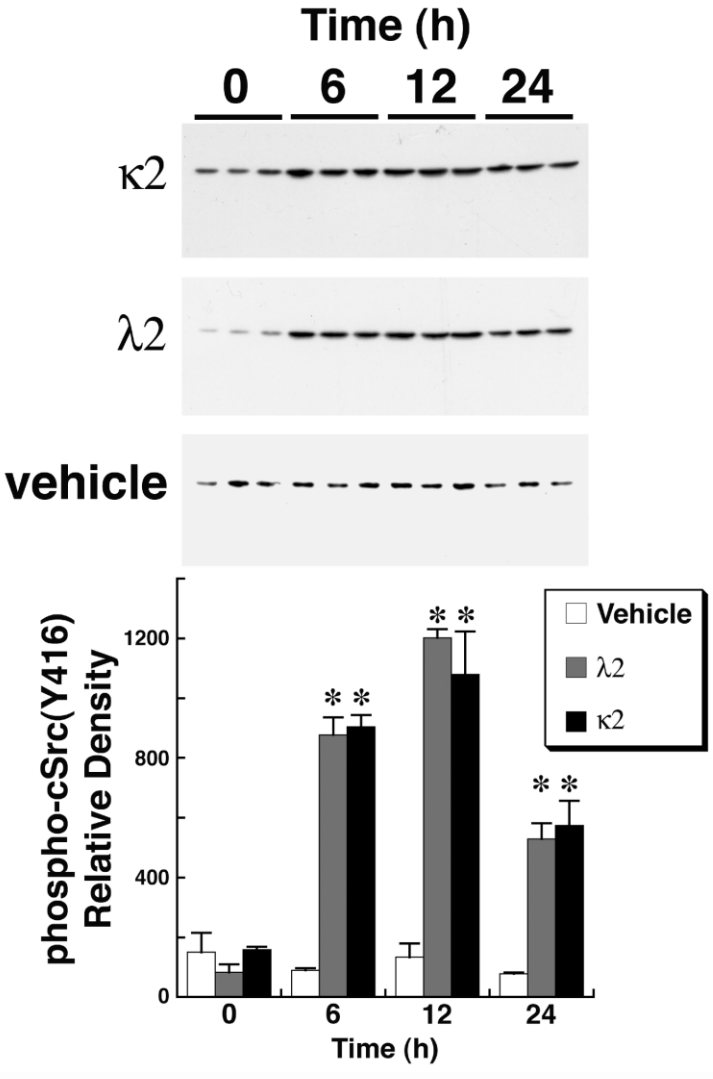

Figure 4.3. DMTU inhibits c-Src activation.

Addition of DMTU inhibits light chain-induced activation of c-Src in HK-2 cells, as determined by the ratio of phospho-c-Src to total c-Src in the lysate obtained following overnight incubation. Compared with K2 alone, the increase in the relative amount of phospho-c-Src induced by the K2 light chain was inhibited ($P < 0.05$) by DMTU (0.28 +-/- 0.04 for vehicle alone; 0.96 +/- 0.07 for light chain alone; 0.28 +/- 0.04 for light chain plus DMTU). Compared with L2 light chain alone, the increase in phospho-c-Src induced by the L2 light chain was inhibited ($P < 0.05$) by DMTU (0.46 +/- 0.04 for vehicle alone; 0.80 +/- 0.12 for light chain alone; 0.41 +/- 0.02 for light chain plus DMTU). N = 4 experiments in each group.

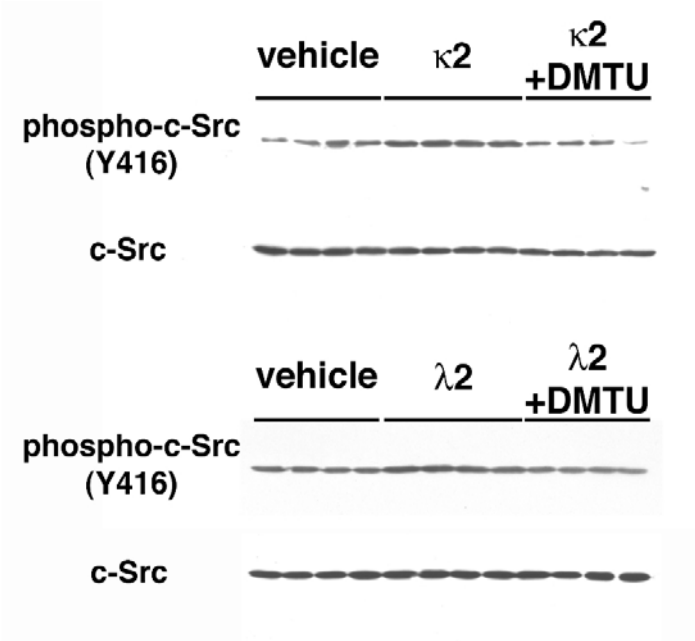

4.2.3 Inhibition of c-Src Suppresses MCP-1 Production but does not Suppress H_2O_2 Production

Overnight incubation of HK-2 cells with both κ2 and λ2 light chains (1 mg/ml) increased production of MCP-1 and H_2O_2 in the cell culture supernatant, when compared to medium alone, as measured by sandwich ELISA and Amplex Red, respectively (figure 4.4). When 10 μM 4-amino-5-(4-chlorophenyl)-7-(*t*-butyl)pyrazolo[3,4-*d*]pyramidine (PP2), an inhibitor of c-Src activity, was added to the

culture medium, MCP-1 concentrations in the supernatant remained at baseline levels.

However PP2 did not have such an effect on H_2O_2 in the supernatant.

Figure 4.4. Inhibition of c-Src suppresses MCP-1 production but not H_2O_2 production.

Inhibition of c-Src prevents light chain-induced production of MCP-1, but not H2O2. There is a rise in H_2O_2 after exposure of HK-2 cells to both κ2 (top) and λ2 (bottom) light chains. This is unaffected by the addition of 10 μM PP2, an inhibitor of c-Src activity, indicating that the production of H_2O_2 takes place upstream of c-Src. There is also an increase in MCP-1 release into the supernatant. Inhibition of c-Src activity by PP2 returns MCP-1 levels to baseline, indicating that c-Src activation is necessary for the release of MCP-1. n = 6 experiments in each group.

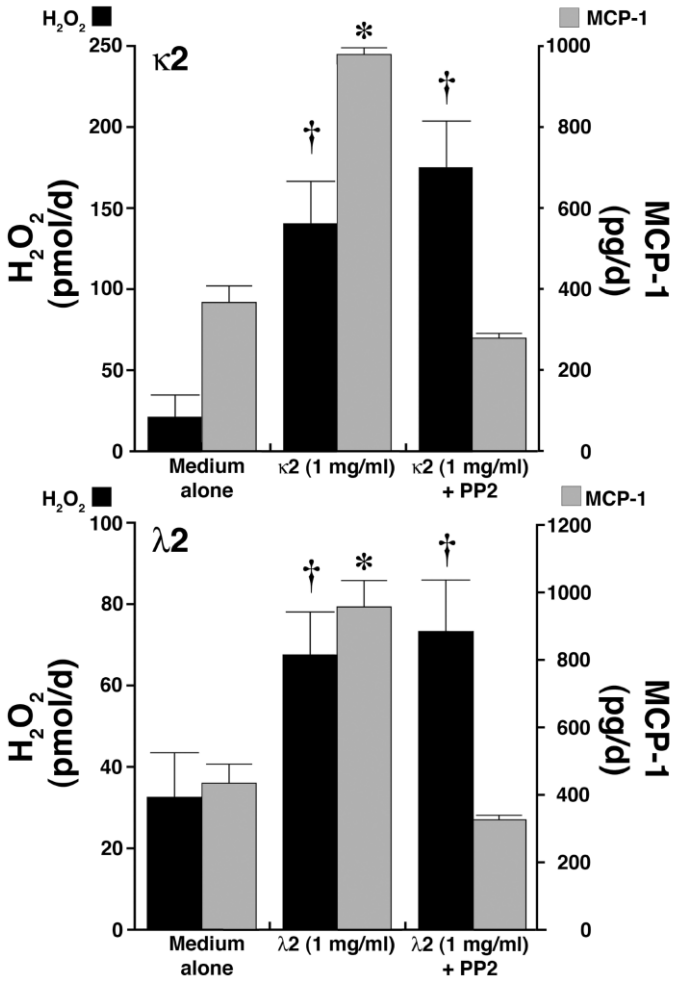

4.2.4 Removal of Extracellular H_2O_2 by Catalase has no Impact on MCP-1 Production

To investigate whether H_2O_2 involved in signaling was produced intracellularly or extracellularly, catalase was added to the medium. As a powerful extracellular scavenger of H_2O_2, exogenously applied catalase would quickly destroy any H_2O_2 in the supernatant. Cells exposed to medium containing catalase produced MCP-1 at a rate of 302.8±10.3 pg/day. Addition of catalase to the medium along with κ2 and λ2 light chains did not prevent the increase in MCP-1 (672.5±37.3 and 1018.3±28.7 pg/day, respectively; $P < 0.05$ compared to control).

4.2.5 Silencing of c-Src Expression Suppresses MCP-1 Production in Response to Light Chain Exposure

c-Src expression was silenced by transfecting HK-2 cells with siRNA specifically targeted to c-Src. Western blot analysis of cell lysates confirmed successful silencing of total-c-Src production (figure 4.5A). Densitometry relative to GAPDH expression showed an approximate 80% reduction in c-Src expression when compared to lysates from cells exposed to the non-targeting siRNA. When HK-2 cells were incubated with κ2 and λ2 light chains, cells in which c-Src expression was reduced did not release MCP-1 into the supernatant above baseline levels (figure 4.5B).

4.2.6 c-Src is Oxidised Following Light Chain Treatment

To determine whether oxidation of c-Src occurs in response to exposure to light chain in HK-2 cells, N-(biotinoyl)-N'-(iodoacetyl)ethylenediamide (BIAM), a thiol-reactive

Figure 4.5. Silencing of c-Src expression suppresses MCP-1 production in response to light chain exposure.

Silencing c-Src expression in HK-2 cells abrogates the MCP-1 response that follows exposure to either κ2 or λ2 light chains. Cells were transfected with siRNA specific for c-Src. (A) Successful knockdown of c-Src expression was confirmed by Western blot analysis, normalized to a GAPDH loading control. Densitometric analysis shows an approximate 80% reduction compared with negative control. Bars represent means of four individual experiments. (B) MCP-1 release from transfected cells after light chain challenge. Knockdown of c-Src expression abrogates the MCP-1 response, indicating that the presence of c-Src is necessary for signal transduction, leading to MCP-1 release. N = 8 experiments in each group.

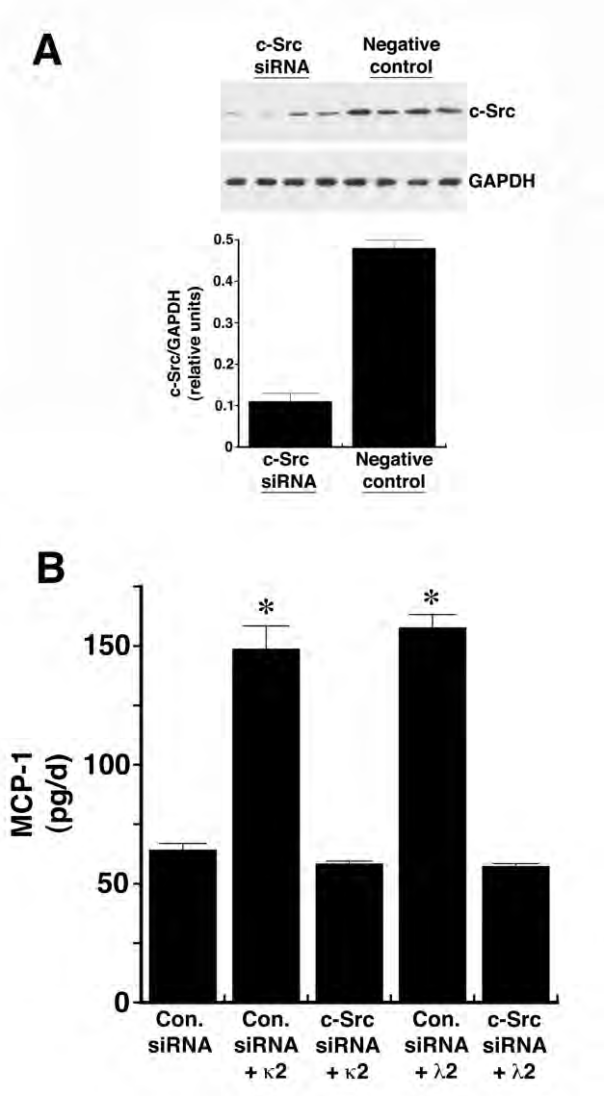

biotinylating reagent for proteins, was used. BIAM specifically identifies the thiolate form of cysteine residues when they are in the reduced state, making it a very useful tool to detect redox-regulation of proteins.(Dominici *et al.* 1999; Kim *et al.* 2000) Using this method, we measured reduced-c-Src levels in HK-2 cells after exposure to κ2 and λ2 light chains (figure 4.6). There was a time-dependent reduction in reduced-c-Src levels, when compared to those treated with vehicle alone. Data in the bottom panels show that total c-Src levels in the samples did not differ among the groups. These data confirm that c-Src is directly oxidised when cells are treated with light chains.

4.2.7 Silencing of Megalin and Cubilin Suppresses MCP-1 Production

To confirm that MCP-1 production was dependent on cellular uptake of light chain through interaction with megalin and cubilin, expression of these two proteins was silenced by transfecting HK-2 cells with specific siRNAs. Successful knockdown was confirmed by Western blot analysis for both proteins (figure 4.7A). Silencing of megalin and cubilin significantly reduced MCP-1 release by HK-2 cells in response to exposure to κ2 and λ2 light chains (figure 4.7B). MCP-1 production between controls, where cells were transfected with non-targeting sequence siRNA or exposed to vehicle alone, did not differ. MCP-1 production increased when cells were exposed to light chains, the response being stronger with λ2 compared with κ2. After megalin and cubilin knockdown, this response was markedly reduced, by approximately 60% with κ2 and 63% with λ2, but remained slightly above production levels seen in the control samples.

Figure 4.6. c-Src in oxidised following light chain treatment.

Incubation of HK-2 cells with the two light chains oxidizes c-Src. Cells were exposed to either κ2 or λ2 light chain, and c-Src oxidation was assessed at 2-, 6-, 12-, and 24-hour time points. Cells were lysed and reduced c-Src was labelled with BIAM and immunoprecipitated before detection by immunoblotting. Half of each sample was probed with an anti-total-c-Src antibody for the purpose of normalization. Reduced-c-Src levels declined during the time course of the experiment, indicating that direct oxidation and activation of c-Src was taking place.

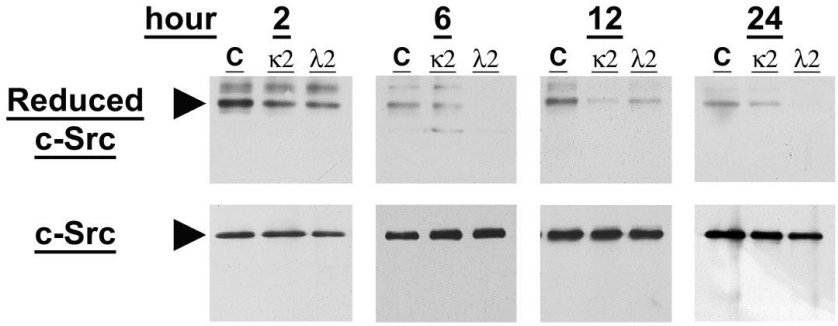

4.3 Discussion

In the setting of renal disease attributable to monoclonal FLCs, renal fibrosis can progress rapidly despite treatment in this condition, as indicated in the previous chapter. Understanding pathways to inflammation driven by cytokine release from the proximal tubule becomes important from a translational point of view, if ways of preventing the resulting irreversible renal fibrosis are to be found.

The purpose of the studies reported here was to investigate the links between light chains, oxidative stress, c-Src activation and production of MCP-1, a key chemokine in inflammation. The data from this series of experiments show that two unique light chains, in concentrations relevant to levels exposed to proximal tubule cells *in vivo*,

Figure 4.7. Silencing of megalin and cubilin suppress MCP-1 production.

Silencing megalin and cubilin expression inhibits light chain-induced MCP-1 production by HK-2 cells. Megalin and cubilin expression was silenced by specific siRNAs. (A) Successful knockdown was confirmed by Western blot analysis, normalized to a GAPDH loading control. Lane 1, control; lane 2, vehicle; lane 3, addition of nontargeting siRNA; lane 4, addition of siRNA targeted for megalin; lane 5, addition of siRNA targeted for cubilin; and lane 6, addition of siRNA targeted for both megalin and cubilin. Densitometric analyses showed a greater than 85% reduction in megalin and an approximate 95% reduction in cubilin. (B) MCP-1 release is significantly reduced after knockdown, compared with nontargeting scramble sequence siRNA. However, the response was not completely abrogated, indicating ongoing signal transduction likely due to incomplete knockdown of the machinery involved in transport of the light chains into the cell. N = 6 experiments in each group.

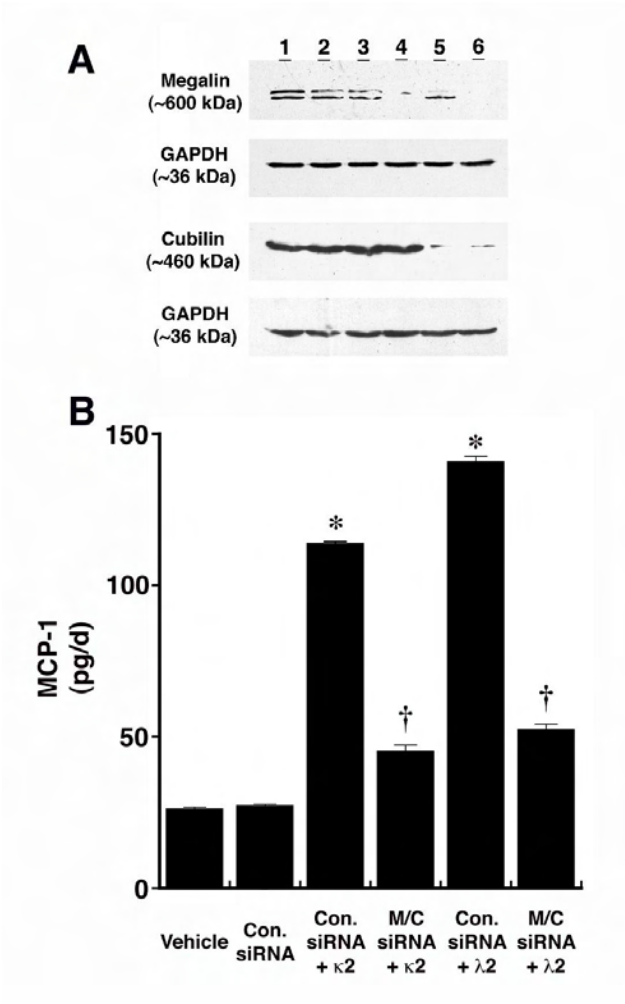

induce activation of c-Src, a tyrosine kinase known to be involved in several signal transduction pathways. Sengul *et al*. demonstrated that NF-κB is activated in HK-2 cells

when they are exposed to and internalise light chains, resulting in the release of MCP-1.(Sengul *et al.* 2002) Findings in the present study agree with these data and complement the previous findings that production of MCP-1 was also dependent on H_2O_2 and NF-κB, because inhibition of ROS with 1,3-dimethyl-2-thiourea (DMTU) and inhibition NF-κB with pyrrolidine dithiocarbamate (PDTC) suppressed MCP-1 release.(Wang and Sanders 2007) The present data further demonstrate that c-Src is integrally involved in production of MCP-1 by proximal tubule cells following exposure to light chains.

Because of the observed capability of FLC to generate H_2O_2,(Wang and Sanders 2007) the present study therefore focused on activation of c-Src as an intermediate in the signal transduction process that produced MCP-1 by FLC. The addition of PP2 abrogated the MCP-1 response quite effectively, indicating that activation of c-Src plays a key role in MCP-1 production. To reaffirm that c-Src was necessary for the production of MCP-1 after light chain exposure, c-Src synthesis was silenced with the use of siRNA. After successful knockdown, the release of MCP-1 into the supernatant in response to light chains was abolished. This was further evidence that as well as H_2O_2 and NF-κB, c-Src served as a vital link in the chain of events leading to MCP-1 release. Experiments then investigated whether the H_2O_2 generated after light chain challenge led to oxidation of c-Src. The data show that c-Src in the reduced state (as detected by BIAM labeling) is depleted in a time-dependent fashion temporally associated with c-

Src activation. These observations are consistent with previous results demonstrating the presence of intracellular oxidative stress within HK-2 cells.(Wang and Sanders 2007) The data are also supported by the results published by Giannoni *et al*.(Giannoni *et al.* 2005) showing that intracellular oxidative stress causes direct oxidation of c-Src at Cys245 and Cys487, thereby facilitating c-Src activation.

Inhibition of c-Src by PP2 however had no effect on H_2O_2 levels in the supernatant. This would suggest that H_2O_2 generation occurs independently of c-Src activation. Although the major source of H_2O_2 is likely from the light chain itself,(Wang and Sanders 2007) the precise intracellular location where H_2O_2 was produced in these experiments remains unclear. However, an elegant series of experiments by DeYulia *et al*. has revealed that the interaction of receptor and its ligand can generate H_2O_2, independent of subsequent signal transduction.(DeYulia *et al.* 2005) This ability was conserved even when cells were fixed, or purified receptor and ligand interacted in the absence of cells. Although this phenomenon has not been shown when megalin-cubilin receptors interact with light chains, it is yet another possible source of H_2O_2.

In a fashion similar to immunoglobulins,(Wentworth *et al.* 2001) Sanders *et al* have previously shown that light chains alone in solution are capable of catalysing the production H_2O_2.(Wang and Sanders 2007) Although all proteins have the intrinsic ability to do this, the effect is usually quickly saturable, resulting in low levels of production of ROS. In contrast, light chains are much more efficient and have a much higher capacity for catalysing this reaction when compared to non-immunoglobulin-derived proteins. While the ability of immunoglobulins to generate H_2O_2 may improve

the ability of the antibody to destroy pathogens, the present series of experiments show that the generation of H_2O_2 by light chains may have deleterious effects on the kidney proximal tubule by initiating inflammatory signaling pathways.

A recent study by Li *et al*. from the laboratory of Batuman has shown that by silencing the expression of megalin and cubilin with siRNAs, endocytosis of light chains could be blocked, resulting in the amelioration of toxic effects, cytokine release such as that of MCP-1, and epithelial-to-mesenchymal transition (EMT).(Li *et al.* 2008a) The findings from the current study were in agreement with the role of megalin and cubilin in these processes. Along with the lack of efficacy of extracellular catalase, these data indicate that endocytosis of light chains is an important step in signal transduction leading to cytokine release.

The inhibitory agents PP2 and siRNAs are highly specific inhibitors of their respective targets. In addition to H_2O_2, other intracellular ROS such as peroxynitrite may activate c-Src in response to pro-inflammatory stimuli.(Mallozzi *et al.* 1999) Although the role of peroxynitrite in the pathogenesis of myeloma cast nephropathy has not been described, it is conceivable that this form of ROS also plays a role. The inhibitory agent for ROS used in the studies presented in this chapter, DMTU, is capable of blocking the activity of peroxynitrite as well as H_2O_2, thus dissecting any individual contributions of each of these ROS is not possible by this approach alone.(Whiteman and Halliwell 1997) Wentworth *et al* have shown that immunoglobulins can generate H_2O_2, and Sanders *et al* have demonstrated that myeloma FLCs also possess this ability.(Wentworth *et al.* 2000; Wang and Sanders 2007) In the studies presented in this

chapter, the Amplex Red assay which is highly specific for H_2O_2 was used.(Zhou *et al.* 1997; Mohanty *et al.* 1997) It is therefore clear from the studies presented in this chapter, and previous studies from the laboratory of Sanders, that H_2O_2 is indeed generated in response endocytosis of FLCs by PTECs, leading to the inference that this is the primary ROS involved in signaling. Additional studies in the future would be required to distinguish between the contributions of H_2O_2 and peroxynitrite in the setting of myeloma cast nephropathy. The peroxynitrite decomposition catalyst 5,10,15,20-tetrakis-[4-sulfonatophenyl]-porphyrinato-iron[III] (FeTPPS) would be a suitable inhibitory agent is this setting.(Misko *et al.* 1998)

Other proteins such as albumin have been shown to stimulate MCP-1 production in PTECs.(Wang *et al.* 1999; Morigi *et al.* 2002) However, it has been repeatedly observed that the ability of light chains to induce cytokine production in PTECs far exceeds that of other such filtered proteins implicated in proximal tubule inflammation.(Sengul *et al.* 2002; Wang and Sanders 2007) These proteins share a common route of entry into PTECs via megalin and cubilin, suggesting that there is another mechanism for generation of oxidative stress aside from ligand-receptor interaction. In the context of inflammation in the proximal tubule, the intrinsic ability of light chains to generate H_2O_2 and the highly efficient manner in which they do this puts them in a class of proteins quite separate from non-immunoglobulin-derived proteins. The data presented here show that in order for PTECs to reach an inflammatory state in response to light chains, the activation of the tyrosine kinase c-Src is necessary. The generation of H_2O_2 occurs upstream of c-Src activation, which in turn is dependent on H_2O_2. Indeed, this event appears to be mediated by H_2O_2 directly oxidising this enzyme.

Because the rate of clearance of FLCs is linked to GFR, in CKD, where there is gradual loss of functioning nephrons, the serum concentrations of polyclonal FLCs rise, presenting the remaining nephrons with increased levels of filtered FLC.(Hutchison *et al.* 2008c) Given the findings with monoclonal FLCs, I hypothesised that the polyclonal FLCs in CKD might exert a pro-inflammatory biological effect on PTECs, as well as in distal tubules with uromodulin.

5. PURIFICATION OF POLYCLONAL FREE LIGHT CHAINS

5.1 Introduction

In the setting of plasma cell dyscrasias (PCDs), free light chains (FLCs) have been shown to activate PTECs and effect the release of cytokines such as MCP-1, IL-6 and IL-8, resulting in inflammatory cell infiltration and established interstitial fibrosis.(Sengul *et al.* 2002; Wang and Sanders 2007) In distal tubules, FLCs co-precipitate with uromodulin to form casts, which are also associated with inflammatory cell invasion of the interstitium and tubules.(Sanders and Booker 1992) Because FLCs are cleared from the circulation by the kidneys, serum FLC levels are dependent upon glomerular filtration rate (GFR). Consequently, both serum κ and λ FLCs are present at concentrations in patients with CKD, that are several orders of magnitude higher than in healthy controls.(Hutchison *et al.* 2008c) I set out to purify polyclonal FLCs, to perform experiment to assess if they exert similar biological effects in chronic kidney disease, as monoclonal FLCs do in PCDs. This chapter presents the development and optimisation of methodology for the purification of polyclonal κ and λ FLCs.

5.2 Choice of Source of Polyclonal Free Light Chains

Broadly speaking, previous studies of FLCs have utilised proteins derived from two sources: urine from patients with PCDs or dialysis effluent. Urine has several advantages. The glomerular filtration barrier acts as a natural sieve, preventing the passage of larger proteins like whole immunoglobulin. In myeloma, where the serum concentration of monoclonal FLC can be very high, FLC is often the main protein in the urine, which helps simplify the purification process. However in CKD, urinary FLC

levels are elevated to a lesser extent, and there are often other proteins such as albumin present. Due to the effect of receptor-mediated endocytosis reclaiming proteins in the proximal tubule, urinary FLCs from patients with CKD might not have been entirely representative of the serum FLC population. In addition, patients with CKD have elevated levels of cytokines in their urine, which might affect downstream *in vitro* assays.(Morii *et al.* 2003; Eardley *et al.* 2006) These factors mean that large quantities of urine from patients with CKD, and rigorous screening for and removal of cytokines, would have been needed to produce an adequate yield of FLC.

In the published literature, polyclonal FLCs have been extracted from dialysis effluent for experimental use by one group.(Cohen *et al.* 1995) FLCs were successfully purified from both haemodialysis and peritoneal dialysis effluent. In this case, as with urine, the dialyser and peritoneal membranes would act as filters. One major disadvantage of using dialysis effluent is the presence of cytokines, found both in peritoneal dialysis and haemodialysis.(Wong *et al.* 2003; Catalan *et al.* 2003; Goldfarb and Golper 1994) Again, as with urine from patients with CKD, the use of dialysis fluid would have required large volumes of fluid to be processed, along with detection and, if necessary, removal of cytokines.

Therefore, for the purpose of purifying polyclonal FLCs for *in vitro* studies, pooled, precipitated sera from blood donors was chosen. These originated from the national blood transfusion service, and had undergone large scale fractionation during which the majority of albumin had been removed for therapeutic applications. This source had a number of advantages: (i) it represented a large cohort of healthy donors, translating

into increased diversity of FLCs and thus a true polyclonal pool; (ii) it was a good bulk product to work with as a large quantity was available; (iii) it was obtained after a significant quantity of the albumin had been removed, which was the contaminating protein present in the highest concentration.

5.3 Analysis of Resuspended Sera

Initial steps in purification were performed by Simon Blackmore, in the Subclass Antisera department at . Precipitated sera were resuspended, filtered through a membrane with an effective MW cut-off of 60 kDa (HCO-1100; Gambro), the filtrate subjected to immunoglobulin removal by repeated loops through a protein A column, and the unbound fraction was then provided to me for further processing. This will be referred to as the starting sample. Table 5.1 summarises the quantities of TSP and FLC, as well as the final quantities of FLCs recovered from the batches.

For an indication of the different types and sizes of proteins which required removal in order to obtain pure FLC, an initial assessment of the protein content was made by separating 5-20 µl of protein A affinity unbound fractions and pre-protein A treated samples, on 4-12% SDS-PAGE (Figure 5.1). The results showed a broad range of proteins in solution, of differing MWs, representing contaminants, which would need to be removed. Bands representing IgM, IgA and IgG were observed. A band just above the 66 kDa standard indicated significant albumin levels. A large, broad band, likely to represent multiple overlapping bands was seen between the 55 kDa and 42 kDa standards. Multiple overlapping bands were also seen at the level of the 42 kDa standard, in the region where dimeric FLCs would be expected, indicating that there

Table 5.1. Batches of resuspended sera received after filtration and passage through protein A column.

Batch	Volume	Total Soluble Protein		FLC (Freelite)				FLC Final Yield (Freelite)		FLC Final Yield (BCA)	
	(ml)	Conc (mg/ml)	Total (mg)	Conc (mg/ml)		Total (mg)				(mg)	
				κ	λ	κ	λ	κ	λ	κ	λ
1	1350	27.6	37260	0.244	0.393	33	53	-	-	7	23.7
2	1330	-	-	0.266	0.359	353.3	477	92.5	117.7	50.5	82.2
3	1726	-	-	0.479	0.134	827.2	231.9	16.5	72.2	2.1	28.4

Figure 5.1. Electrophoretic (SDS-PAGE) analysis of the FLC extract after passage through the protein A column.

There are a broad range of contaminant proteins in solution of differing MWs, including immunoglobulins and albumin. FLCs are present, among other proteins, at the level of the 42 kDa and 27 kDa standards. Coomassie Brilliant Blue. Lanes L-R, and volume loaded: 1: standard; 2: post protein-A, 20µL; 3: post protein-A, 10µL; 4: post protein-A, 5µL; 5: blank; 6: pre protein-A, 20µL; 7: pre protein-A, 10µL; 8: pre protein-A, 5µL.

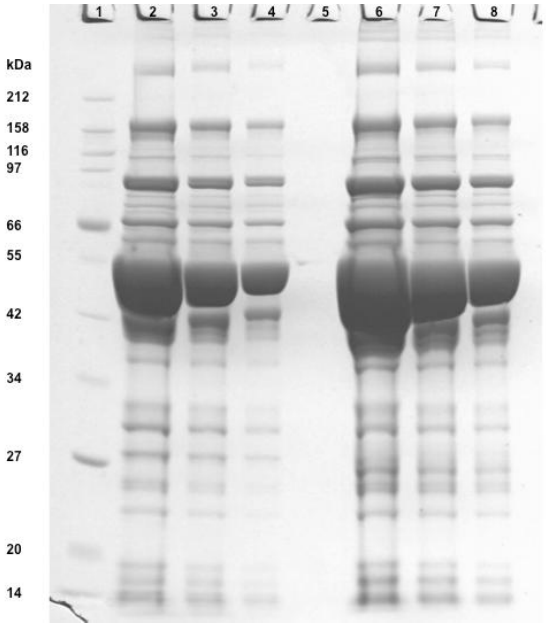

were multiple other protein contaminants of similar MW. Two discreet bands were seen just below the level of the 27 kDa standard, where monomeric FLC would be expected. Bands were noted to be weaker in samples after passage through the protein A column. However, this could have been a result of dilution in buffer after repeated passages through the column; TSP was not measured in the sample prior to protein A. The presence of contaminants of similar size to FLC meant that a combination of affinity and size-exclusion techniques would be necessary to purify FLC.

5.4 Extraction of Proteins Containing Light Chains from Starting Sample

Proteins containing light chains (Immunoglobulins as well as FLCs) were extracted from the starting sample using affinity chromatography, with antibodies which recognise both free and bound light chains () immobilised on a Sepharose bead matrix, packed into columns. Matrix for both columns had been previously coupled to antibody at . Figure 5.2 summarises the polyclonal FLC purification process.

5.4.1 Anti-κ Light Chain Matrix – Assessment of Suitability

In order to assess the suitability of the anti-κ light chain matrix, a small volume of matrix (10 ml) was assessed initially. 200 ml of start sample was run through the column. Fractions were collected during the loading phase and elution phase. The chromatogram summarising this process is shown in figure 5.3. These fractions were then assessed for presence of light chain by dot blot (figure 5.4) and SDS-PAGE (figure 5.5). The chromatogram showed an increase in UV absorbance after around 90 ml, due to an abrupt rise in protein concentration, indicating that the capacity of the column had been exceeded at that point. The dot blot showed no detectable light chain in the unbound fractions 1-8. From fraction 9 onwards, there is a detectable signal, indicating the "breakthrough" of light chain containing proteins. This coincides with the rise in UV absorbance seen on the chromatogram. The Elution fractions show strong signals. Coomassie brilliant blue staining after SDS-PAGE shows that this affinity step has successfully removed a large quantity of contaminants, particularly the non-immunoglobulin derived proteins. However there are still significant quantities of higher MW contaminants. Upon reduction, these resolve to bands corresponding to the

Figure 5.2. Polyclonal FLC purification protocol.

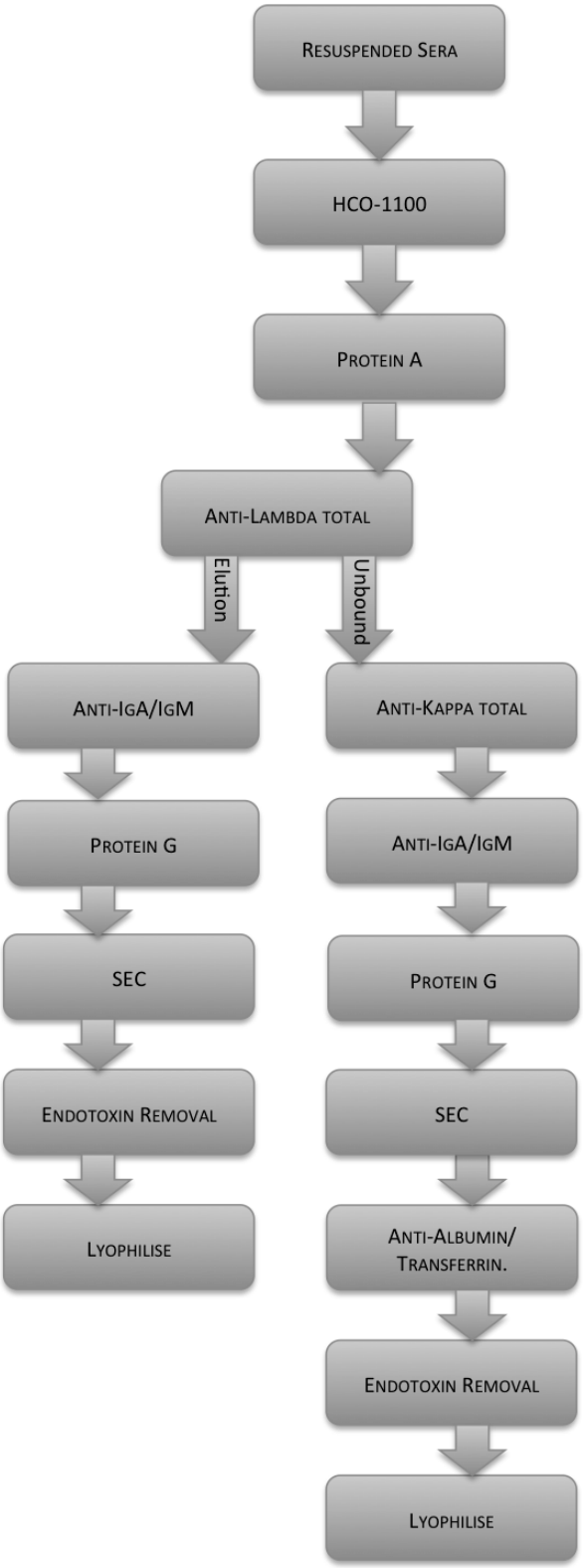

Figure 5.3. Chromatogram of assessment of suitability of anti-κ light chain matrix.

Two hundred millilitres of start sample was run through the column. An increase in UV absorbance after 90 ml (arrowed) indicates a rise in protein concentration, indicating the limit of the column's capacity. Red line, conductivity; blue line, UV absorbance; green line, % elution buffer. U, unbound; E, elution.

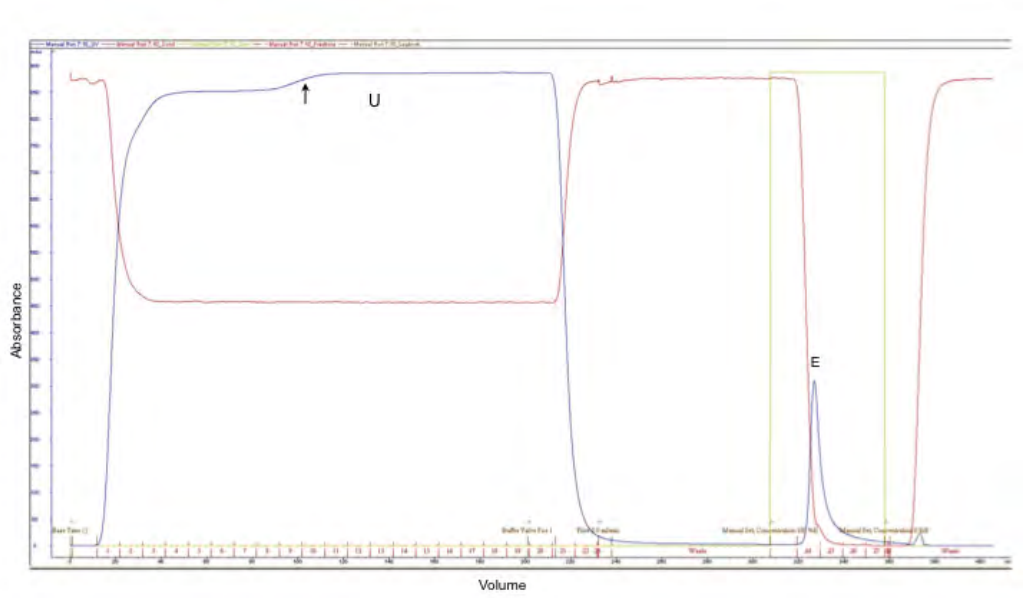

MWs of light chain and heavy chain, indicating that these contaminants are immunoglobulin. A faint band is also seen in the reduced samples just above the 66 kDa standard, which may represent incomplete separation of light chain and heavy chain.

This experiment showed that the anti-κ matrix has adequate capacity to separate κ light chain containing proteins from the starting sample. The eluate from the column consisted mostly of immunoglobulin and free light chain. 10 ml of matrix would remove all the κ light chain containing proteins from around 80-90 mls of starting

sample. A decision was therefore made to manufacture additional anti-κ matrix and increase the column size to 100 ml.

Figure 5.4. Dot blot demonstrating anti-κ light chain matrix capacity.

Numbers represent fractions. The blot has been probed with anti-κ light chain antibody. No detectable κ light chains are present in unbound fractions 1 – 8. From fraction 9 onwards, there is detectable signal, showing "breakthrough" of κ light chain containing proteins, indicating the capacity of the column had been exceeded. This coincides with the rise in UV absorbance seen in the chromatogram (Figure 5.3).

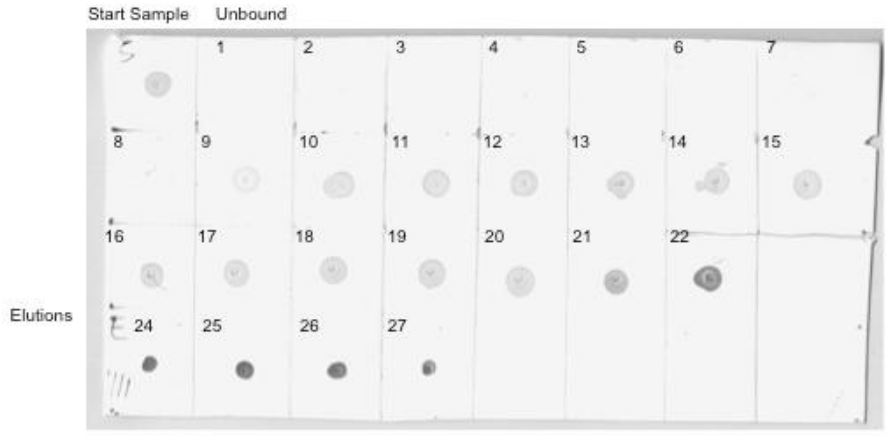

5.4.2 Anti-λ Light Chain Matrix – Assessment of Suitability

An initial assessment of the anti-λ light chain matrix was carried out with 65 ml of matrix. Five hundred mls of starting sample was run through the column, and fractions collected during the loading and elution phases. The chromatogram for this process is shown in figure 5.6. This chromatogram shows a rise in UV absorbance at around 200 ml, indicating when the capacity of the column had been exceeded. Dot-blotting was performed on unbound and elution samples (figure 5.7). This shows breakthrough of light chain containing proteins at fraction 6, at around 210 ml, coinciding with the rise in UV absorbance seen on the chromatogram. Strong signals are seen in the elution

fractions. Coomassie brilliant blue staining after SDS-PAGE (figure 5.8) showed the

Figure 5.5. SDS-PAGE analysis of pooled elutions from the anti-κ column.

A large proportion of contaminants have been removed, compared with starting sample (lanes 2 and 5). Many of the bands representing non-immunoglobulin derived proteins are no longer present in the elutions. Significant quantities of higher MW contaminants persist. These resolve upon reduction to molecular weights which correspond to heavy chain and light chain, indicating the contaminants are immunoglobulins. Lanes L-R and volumes loaded: 1, standard; 2, starting sample (non-reduced); 3 elution (non-reduced) 20 µl; 4, elution (non-reduced) 10 µl; 5 starting sample (reduced); 6, elution (reduced) 20 µl; 7, elution (reduced) 10 µl.

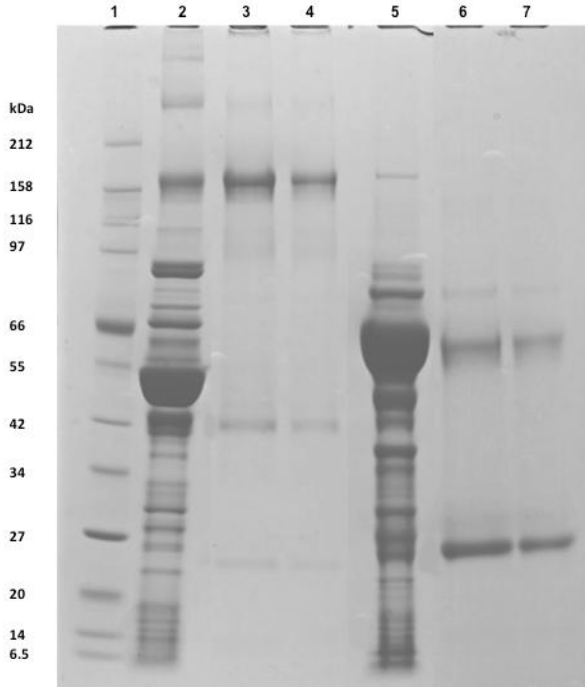

presence of higher MW contaminants likely to represent IgG. A double-band at the level of the 42 kDa standard representing dimeric λ FLC was seen, while no band was seen at the level of the 27 kDa standard. Upon reduction, these bands resolve to just above 55 kDa and around 27 kDa, corresponding to the MWs of heavy chain and monomeric FLC. An additional unidentified faint band was seen in the reduced lane between the 66 and 97 kDa standards.

This experiment showed that the anti-λ light chain matrix has adequate capacity to separate light chain containing proteins from the starting sample. The eluate consisted mostly of intact immunoglobulin and free light chain. 65 ml of matrix will remove all of the light-chain containing proteins from around 200 ml of starting sample. The remaining matrix was incorporated into the column, increasing the column size to 80 ml.

Figure 5.6. Chromatogram of assessment of suitability of anti-λ light chain matrix.

Five hundred millilitres of starting sample was run through the column. There is a rise in UV absorbance at 200 ml (arrowed), indicating the limit of the column's capacity. Red line, conductivity; blue line, UV absorbance; green line, % elution buffer. U, unbound; E, elution. .

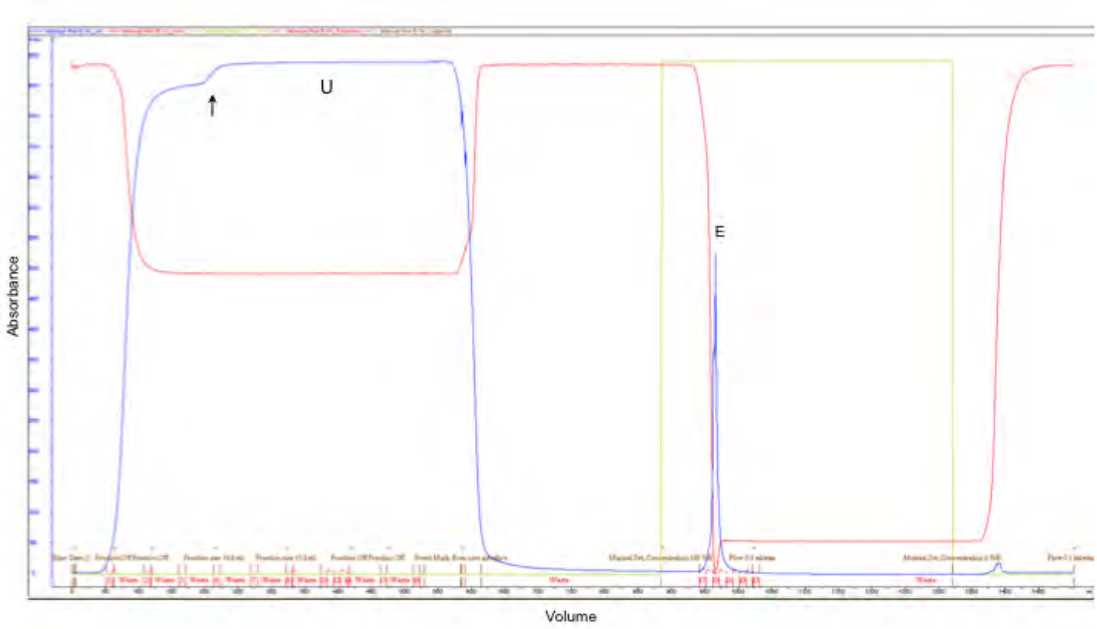

Figure 5.7. Dot blot demonstrating anti-λ light chain matrix capacity.

Numbers represent fractions. The blot has been probed with anti-λ light chain antibody. No detectable λ light chain containing proteins are seen in unbound fractions 1 – 5. From fraction 6 onwards, there is detectable signal, indicating "breakthrough" of λ light chain containing proteins. This coincides with the rise in UV absorbance seen in the chromatogram (Figure 5.6).

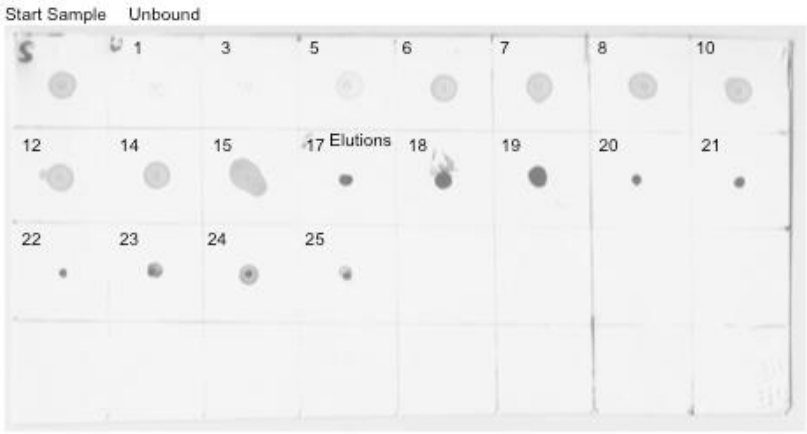

Figure 5.8. SDS-PAGE analysis of pooled elutions from the anti-λ column.

There are persistent higher molecular weight contaminants, which resolve to bands corresponding to the MWs of heavy chain and light chain upon reduction, indicating that these represent IgG. Lanes L-R and volumes loaded: 1, standard; 2, elution (non-reduced); 3 blank; 4, elution (reduced)

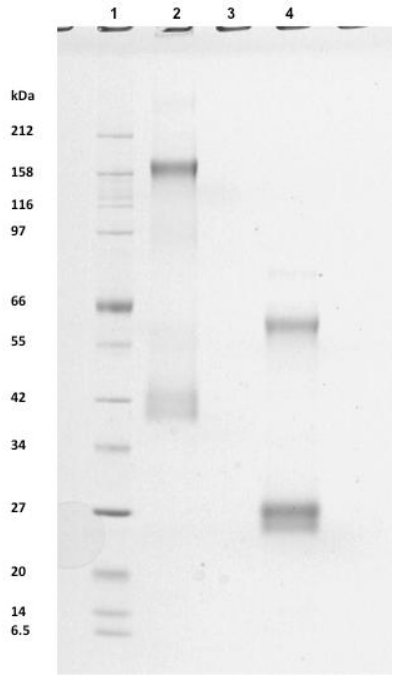

5.4.3 Extraction of λ-Light Chain Containing Proteins From Starting Sample

Following the initial assessment of the capacity of the matrix, the entire starting sample was applied to the anti-λ column by loading in five 200 ml aliquots, and two 150 ml aliquots. This process is summarised in the chromatograms in figure 5.9. Elutions were collected in fractions, which were pooled, dialysed into PBS and concentrated down to a volume of 130 ml in spin columns (Vivaproducts). TSP concentration in the eluate was measured by BCA assay to be 0.73 mg/ml, giving a total of 94.9 mg of TSP.

Figure 5.9. Chromatograms showing extraction of λ-light chain containing proteins from the starting sample.

Starting sample was loaded onto the anti-λ column in five 200 ml aliquots (A) and two 150 ml aliquots (B). Each loading step was followed by an elution, to regenerate the column before the next loading step. Elutions were collected in fractions, which were pooled. Red line, conductivity; blue line, UV absorbance; green line, % elution buffer. U, unbound; E, elution.

A

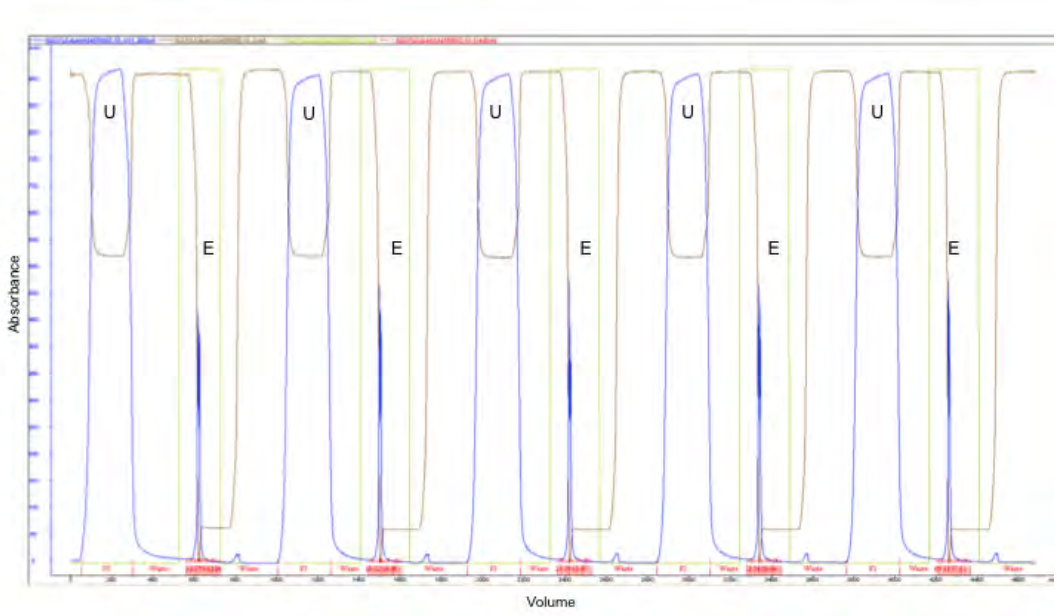

B

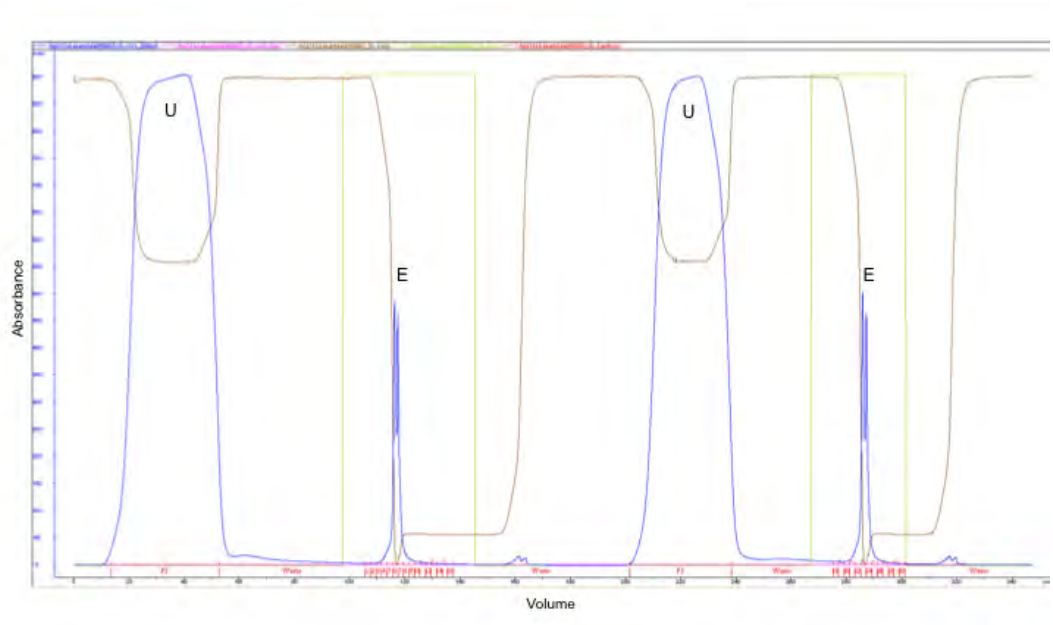

Western blotting was then performed on the elution pool, probing for light chain as well as intact immunoglobulin (figure 5.10). The anti-λ and anti-κ light chain blots showed a signal at the bases of the wells in the stacking region and these corresponded to the presence of IgM. λ and κ signals above the 225 kDa standard corresponded to the presence of IgA. A κ and a λ signal just above the 150 kDa standard corresponded to the presence of IgG as well as IgA, possibly in the form of fragments or monomer. A λ signal was seen at the level of the 102 kDa standard, which was not seen in the whole immunoglobulin blots, indicating that this might be oligomeric FLC. Signals were seen in both the κ and the λ blots between the 38 and 52 kDa standards, representing dimeric FLC. A faint λ signal was seen at the level of the 24 kDa standard, representing monomeric FLC. Very little signal was seen at this level in the κ FLC blot.

5.4.4 Anti-κ Light Chain Matrix Manufacture

Additional anti-κ matrix for affinity extraction of κ light chain containing proteins was manufactured by coupling 500 mg of anti-κ light chain antibody (AU015; The Binding Site) to 100 ml of CNBr activated Sepharose beads. The antibody was supplied at 4.5 mg/ml. After dialysis into coupling buffer, A280 analysis measurement showed the protein concentration to be 4.6 mg/ml, meaning that antibody concentration was maintained during dialysis. Following coupling, BCA assay showed that only 3 mg of protein had not bound to the matrix. This represented 0.6% of the total protein, meaning that 99.4% of antibody had bound to the beads. The matrix was washed in PBS and packed into a column for use.

Figure 5.10. Western blots of anti-λ elution pool.

Western blotting, probing for κ and λ light chains in lanes 1 and 3 show high MW signals at the base of the wells, corresponding to the presence of IgM. There are also high MW κ and λ signals, corresponding to the presence of IgA and IgG. A signal in the λ FLC blot (lane 1) at the level of 102 kDa is present, which is not seen in the whole immunogloblulin blots (lanes 5, 7 and 9) indicating the possible presence of oligomeric FLCs. A signal in both the κ and λ blots (lanes 1 and 3) between the 38 – 52 kDa represents dimeric FLC. Lanes L-R (2 µg per lane): 1, anti-λ light chain; 2, standard; 3, anti-κ light chain; 4, standard; 5, anti-IgM; 6, standard; 7, anti-IgA; 8, standard; 9, anti IgG. Arrow shows the protein of interest, lambda FLC (nearly all dimer here)

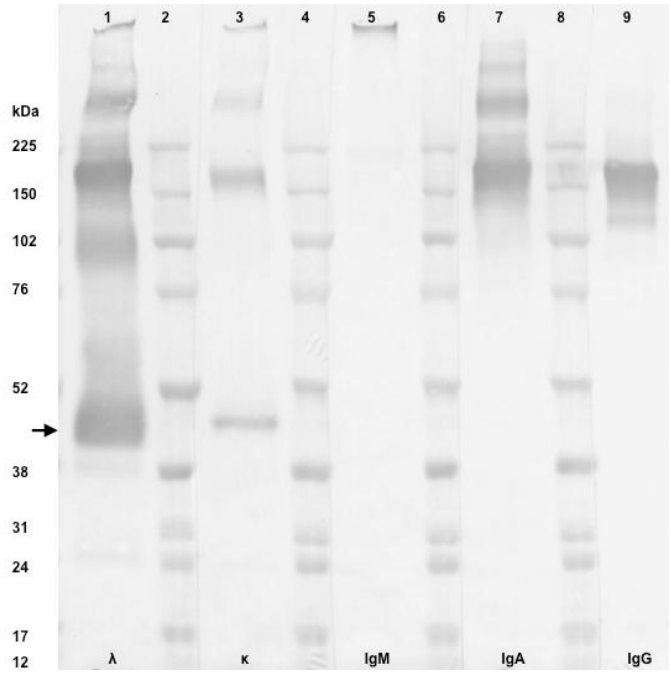

5.4.5 Anti-κ Light Chain Column – Assessment of Capacity

The capacity of the new anti-κ column was tested by loading 500 ml of the unbound fraction from the anti-λ column. Fractions of unbound and elutions were collected during the loading and elution phases, respectively, as shown in the chromatogram in figure 5.11. These fractions were assessed for the presence of κ light chain by dot

blotting (figure 5.12). This showed that no κ light chain was detectable in any of the unbound fractions up to 500 ml, indicating that the capacity of the column had not been exceeded. The elutions were pooled and stored for further downstream processing.

Figure 5.11. Chromatogram of assessment of suitability of manufactured anti-κ matrix.

Five hundred millilitres of the unbound fraction from the anti-λ column was passed through the new anti-κ column. The UV absorbance during the running phase remained unchanged, indicating that the capacity of the column was not exceeded. Both unbound and elution phases were collected in fractions. Red line, conductivity, blue line, UV absorbance, green line, % elution buffer. U, unbound; E, elution.

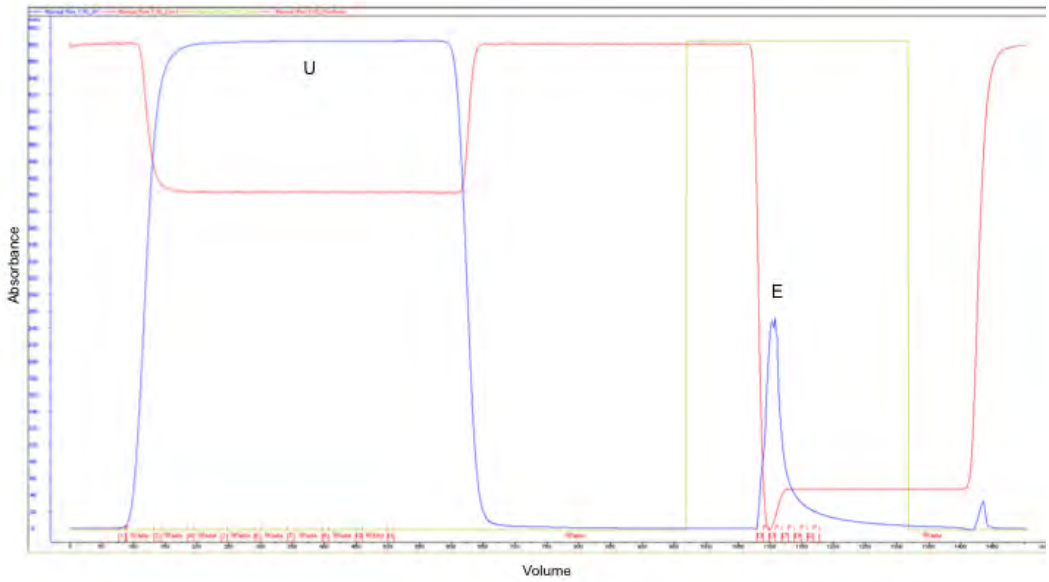

Figure 5.12, Dot blot demonstrating capacity of the manufactured anti-κ light chain matrix.

Numbers represent fractions. The blot has been probed with anti-κ light chain antibody. No κ light chain containing proteins were detected in any of the elutions (1 – 12), confirming that the capacity of the column was not exceeded. Strong signals were detected in the elution fractions.

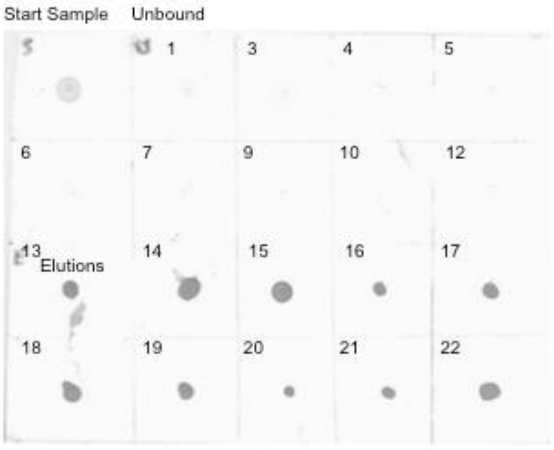

5.4.6 Extraction of κ-Light Chain Containing Proteins From the Anti-λ Unbound Fraction

After the starting sample had been processed through the anti-λ column, the entire unbound fraction was then applied to the new anti-κ column by loading in three 450 ml aliquots and one 530 ml aliquot. Chromatograms for this process are shown in figure 5.13. Elution fractions were pooled, dialysed into PBS, and concentrated in spin columns down to a volume of 130 ml. TSP concentration in the eluate was measured by BCA assay and found to be 1.2 mg/ml, giving a total of 156 mg of TSP.

Western blotting was performed on the elution pool, probing for light chain as well as intact immunoglobulin (figure 5.14). This Western blot shows the enrichment of κ light

chain containing proteins including FLC and intact immunoglobulins, while the amounts of λ light chain containing proteins was significantly reduced. The anti-κ and anti- λ blots showed multiple signals at the base of the wells in the stacking region, above the 225 kDa standard, and at the level of the 150 kDa marker. These corresponded to the presence of IgM, IgA and IgG respectively. In addition, an unidentified signal was detected at the level of the 102 kDa standard in the anti-κ blot, with a much weaker signal in the anti-λ blot. A signal between the 52 and 38 kDa standards represented dimeric κ FLC. No monomer signal was detected. There was no detectable contamination with λ FLC.

Figure 5.13. Chromatograms showing extraction of κ-light chain containing proteins from the anti-λ unbound fraction.

The unbound portion from the anti-λ column was onto the anti-κ column in three 450 ml aliquots (A) and one 530 ml aliquot (B). Each loading step was followed by an elution, to regenerate the column before the next loading step. Elutions were collected in fractions, which were pooled. Red line, conductivity; blue line, UV absorbance; green line, % elution buffer. U, unbound; E, elution.

A

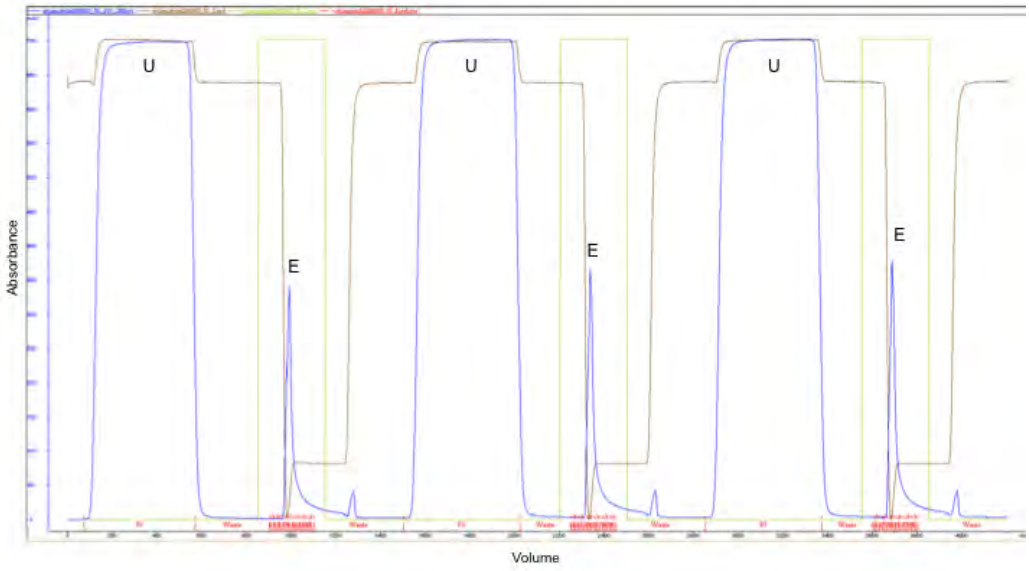

B

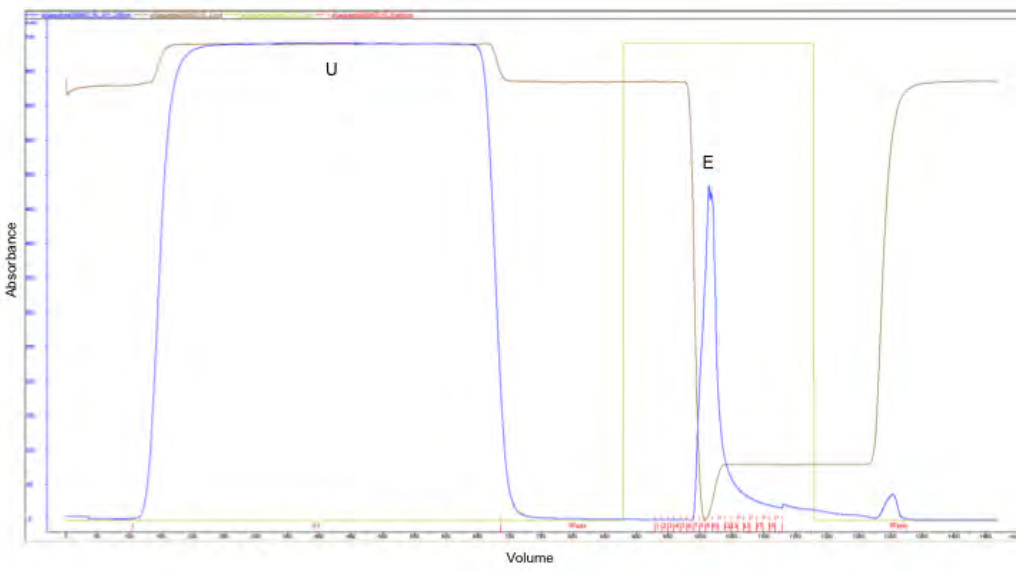

Figure 5.14. Western blot showing enrichment of κ-light chain containing proteins in the anti-total κ elutions.

Western blot of elutions from anti-total kappa column, showing enrichment of κ-light chain containing proteins, including FLC and intact immunoglobulin. There is a reduction in the quantity of λ light chain containing proteins. Significant quantities of immunoglobulin contaminants persist. Arrow shows the protein of interest, κ-FLC, nearly all dimer here. Lanes L-R: 1, anti-IgG; 2, standard; 3, anti-IgA; 4, standard; 5, anti-IgM; 6, standard; 7, anti-κ LC; 8, standard; 9, anti-λ light chain; 10, standard.

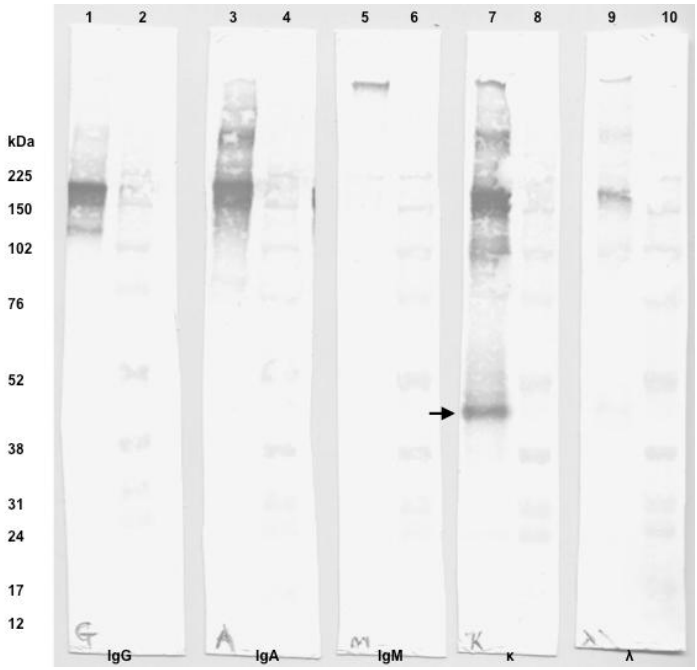

5.5 Removal of Intact Immunoglobulin and Higher Molecular Weight Contaminants

5.5.1 Protein G

Protein G was used to remove IgG from the samples. Five ml of protein G immobilised on Sepharose beads (Calbiochem, Merck, Darmstadt, Germany) was packed into a column. This volume of matrix was known to have a capacity to bind around 50 mg of

IgG. Quantification of IgG by nephelometric assay performed at The Binding Site showed that the elution fractions from the anti-κ and anti-λ columns contained 21.87 mg and 10.73 mg of IgG respectively. The anti-κ elution was applied to this column by loading in two 45 ml aliquots and one 40 ml aliquot, while the anti-λ elution was applied in two equal aliquots of 65 ml, as shown in figure 5.15. The unbound fraction volumes were 180 ml for the κ sample and 230 ml for the λ sample.

Repeat analysis of the unbound fractions for immunoglobulin was performed at The Binding Site. The results are summarised in table 5.2, showing that the samples still contained significant quantities of immunoglobulin. A decision was made to proceed to removal of IgA and IgM by affinity chromatography. This step was to be followed up with size exclusion chromatography (SEC).

5.5.2 Removal of IgA and IgM

Two columns, one containing 10 ml of anti-IgA matrix, and the other containing 20 ml of anti-IgM matrix (both previously manufactured at The Binding Site), were connected in series. These columns were known to have capacities for binding of around 10 mg of IgA and 20 mg of IgM respectively. The κ FLC containing sample was applied to these columns by loading in three 60 ml aliquots (figure 5.16), while the λ FLC containing sample was applied to the columns by loading in two 115 ml aliquots as shown in the chromatograms in figure 5.17.

Protein concentration in the unbound fractions (κ, 233 ml; λ, 270 ml) was measured by BCA assay to be 0.11 mg/ml and 0.09 mg/ml, giving TSP values of 25.63 mg and 24.30 mg respectively. Samples were concentrated down to 7.5 ml, to maintain protein stability and in preparation for size-exclusion chromatography (SEC).

Figure 5.15. Chromatograms showing anti-κ and anti-λ elutions applied to protein G column.

Protein G was used to remove IgG from the elutions from the anti-κ and anti-λ columns. The anti-κ elution was applied to the protein G column in two 45 ml aliquots and one 40 ml aliquot (A). The anti-λ elution was applied to the protein G column in two 65 ml aliquots (B). Each loading step was followed by an elution, to regenerate the column before the next loading step. Red line, conductivity; blue line, UV absorbance; green line, % elution buffer. U, unbound; E, elution.

A

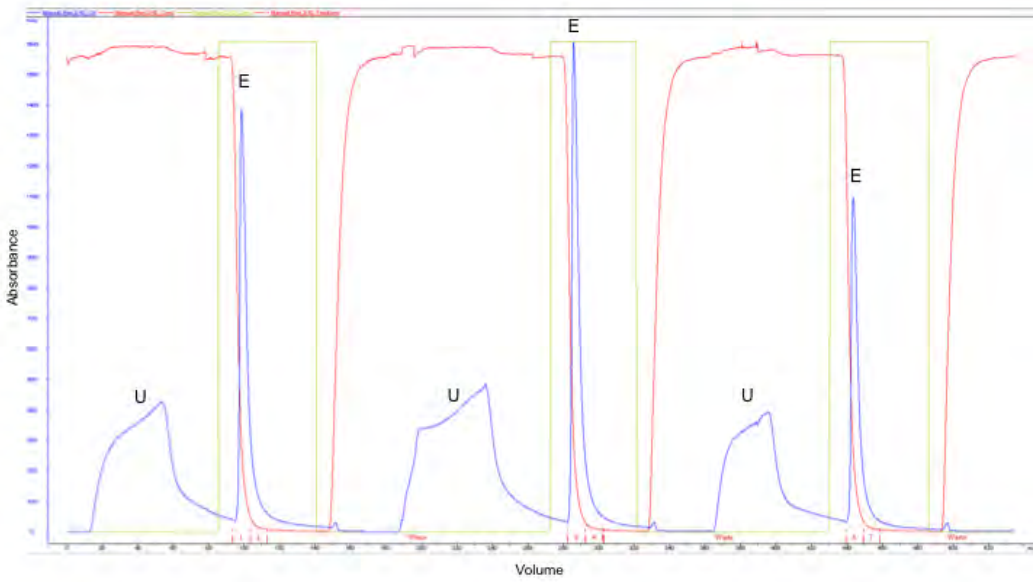

B

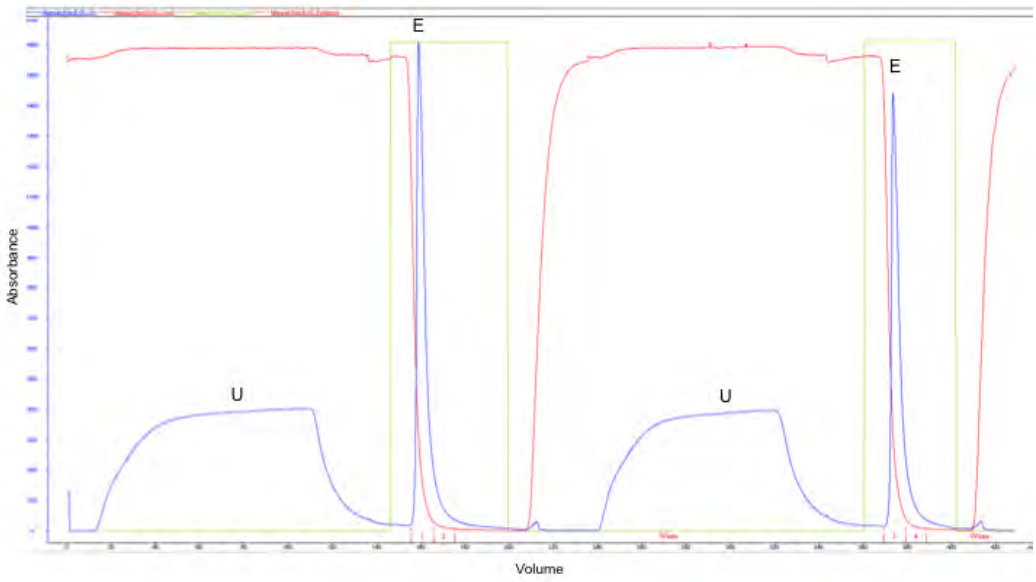

Table 5.2. Nephelometric analysis of immunoglobulin content of fraction unbound to protein G.

	κ Sample (180 ml)		λ Sample (230 ml)	
	Conc (mg/ml)	Total (mg)	Conc (mg/ml)	Total (mg)
IgG	0.012	2.16	<0.011	-
IgA	0.13	23.4	0.065	14.95
IgM	<0.024	-	0.034	7.82

Figure 5.16. Chromatogram showing the κ-FLC sample applied to anti-IgA and anti-IgM columns.

The κ-FLC containing sample was applied to anti-IgA and anti-IgM columns in series, in three 60 ml aliquots. Each loading step was followed by an elution, to regenerate the columns. Red line, conductivity; blue line, UV absorbance; green line, % elution buffer. U, unbound; E, elution.

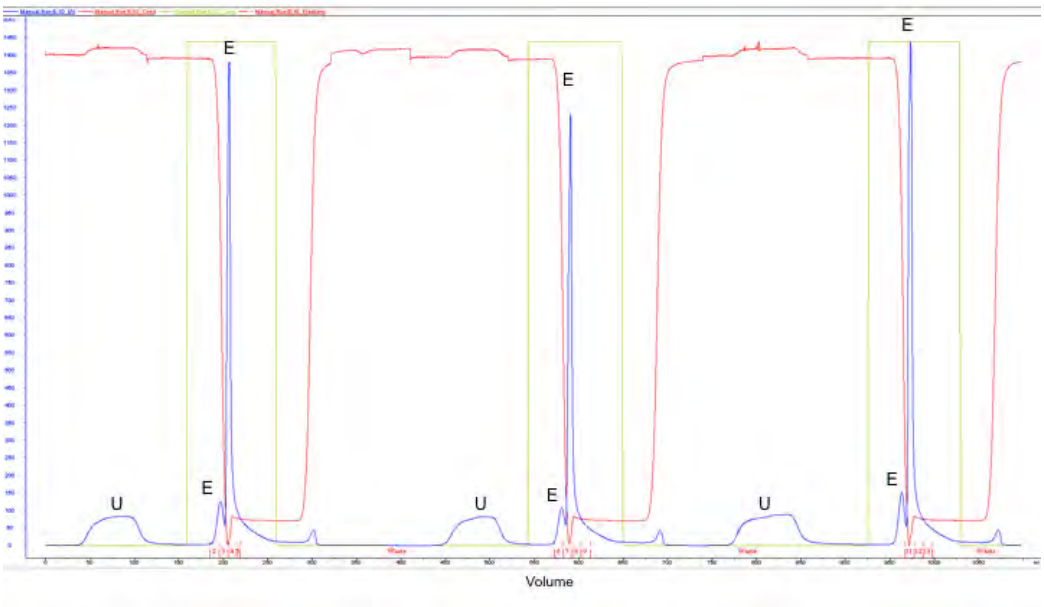

Figure 5.17. Chromatograms showing the λ-FLC sample applied to anti-IgA and anti-IgM columns.

The λ-FLC containing sample was applied to anti-IgA and anti-IgM columns in series, in two 115 ml aliquots. Each loading step was followed by an elution, to regenerate the columns. Red line, conductivity; blue line, UV absorbance; green line, % elution buffer. U, unbound; E, elution.

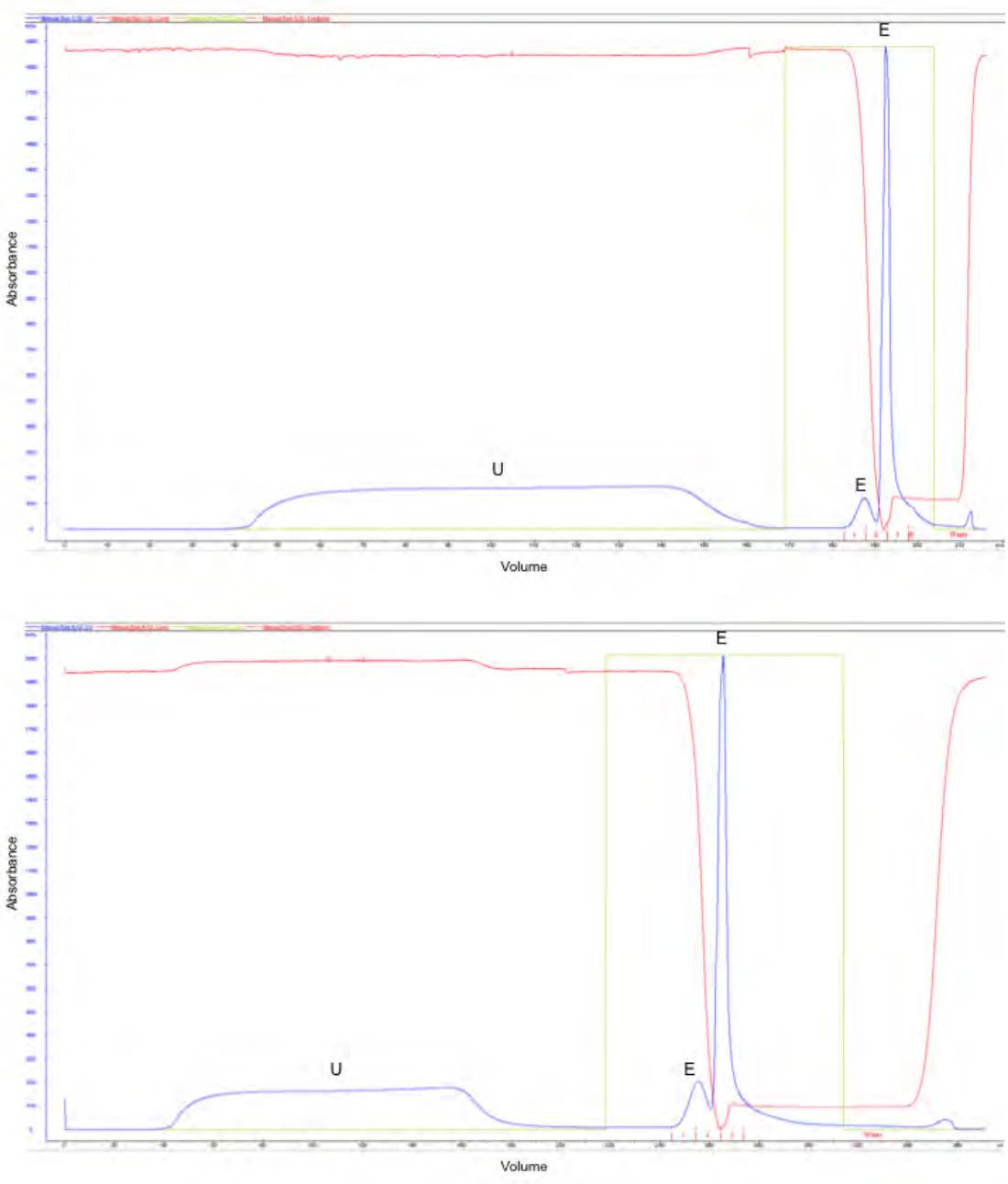

5.5.3 Size Exclusion Chromatography

Concentrated κ and λ samples were loaded separately onto a 300 ml Superdex S200 SEC column and run overnight at 0.5 ml/min. Chromatograms for these processes are shown in figure 5.18. Fractions corresponding to the peaks on the chromatograms were collected for analysis. In the κ sample, peaks B and C, and E and F were pooled as they were overlapping significantly. In the λ sample, peaks B and C were pooled. To ascertain which peaks contained FLC, aliquots were sent to The Binding Site quantification using the Freelite assay (table 5.3).

TSP was measured separately by BCA assay, which showed the protein concentrations to be 0.32 mg/ml in the κ sample and 0.85 mg/ml in the λ sample. The κ sample was concentrated to a volume of 25 ml, while the λ sample was concentrated to 36 ml in order to preserve protein stability.

5.6 Assessment of Polyclonal FLC Purity

Purity of polyclonal FLC was measured at this point by SDS-PAGE and Western blotting. Coomassie blue staining (figure 5.19A) revealed a strong band in the κ FLC lane, corresponding to dimer and a weaker monomer band. In addition, there was a broad, smudge-like band at the level of the 55 kDa standard. Higher MW bands were

Figure 5.18. Chromatograms showing removal of impurities from κ and λ FLC samples by size-exclusion chromatography.

Removal of residual impurities from the κ-FLC sample (A) and the λ-FLC sample (B) by size-exclusion chromatography. Samples were loaded onto a 300 ml Superdex S200 SEC column and run overnight at 0.5 ml/min. Peaks are labelled alphabetically on the chormatograms. Fractions corresponding to these peaks were collected. Red line, conductivity; blue line, UV absorbance; green line, % elution buffer. U, unbound; E, elution.

A

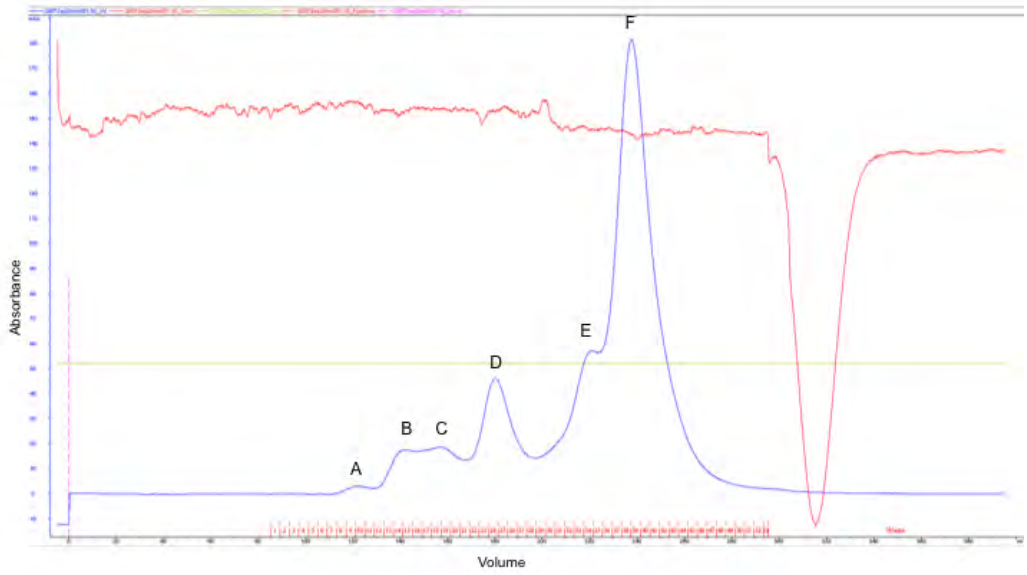

B

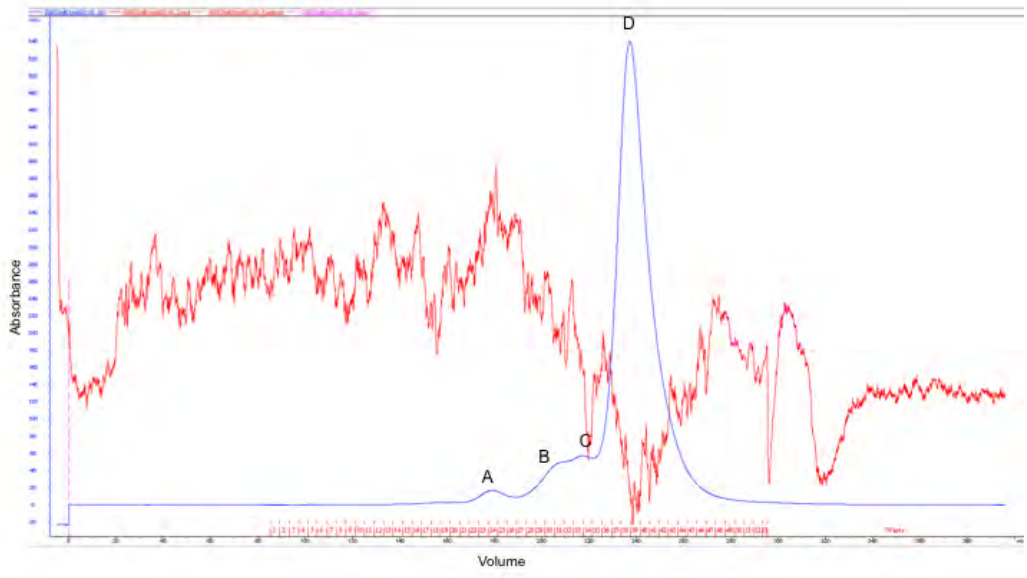

seen at the level of the 158 kDa standard. Upon reduction, the bands resolve to two main bands, just below the 55 kDa standard and the 27 kDa standard, representing heavy chain and light chain, respectively. This indicated that the attempts to remove all the IgG from the κ sample had been unsuccessful. The λ FLC lane showed the presence of a strong dimer band and a weaker monomer band, which resolved upon reduction to a double band just below 27 kDa standard, indicating that the λ sample is relatively pure.

Table 5.3. Nephelometric analysis of FLC content of κ and λ samples after SEC.

Peak	Volume (ml)	κ FLC		λ FLC	
		Conc (mg/ml)	Total (mg)	Conc (mg/ml)	Total (mg)
κ A	20	0.00012	0.0024		
κ B+C	40	0.0021	0.08		
κ D	28	0.00278	0.08		
κ E+F	100	0.0777	7.77	0.00114	0.11
λ A	24			0.00263	0.06
λ B+C	36			0.0568	2.04
λ D	72	0.0078	0.56	0.202	14.54

Performed using a commercial nephelometric assay (Freelite) using a Dade-Behring BNII analyser at The Binding Site. Peaks containing FLC of interest have been highlighted.

Silver staining was carried out for a more sensitive assessment of the bands seen on Coomassie staining (Figure 5.19B). This confirmed the presence of a significant band in the κ FLC lane at the 158 kDa level, most likely to be IgG. Other, faint bands were also seen, including one just above the 66 kDa standard, which could be albumin. The presence of small quantities of transferrin could not be excluded. Upon reduction, these bands resolved to mainly heavy chain and light chain, with three other very faint bands. The λ lane showed two very faint bands just above and below the dimer band. Upon reduction, there appeared a very faint band just below the 55 kDa standard, and another band at the 14 kDa level, which were unidentified. This indicated that the λ FLC sample contained only very small quantities of unidentified contaminants.

Western blotting was then performed (figure 5.19C). The λ FLC sample showed that the bands seen on silver staining were immune reactive with anti-λ antibody, confirming that λ FLC sample was highly pure. No further purification steps would be necessary for the λ sample. Higher MW signals were seen in the κ sample, confirming the presence of significant contamination, most likely due to the presence of IgG.

Further Western blots were performed on the κ sample, probing for the presence of two other possible contaminants: albumin and transferrin (figure 5.20). These blots identified both albumin and transferrin as contaminants of the κ sample. These would need to be removed, in addition to the excess IgG present.

5.7 κ FLC – Removal of IgG, Human Serum Albumin and Transferrin

An initial assessment was undertaken to determine whether it was feasible to remove IgG, albumin and transferrin from the κ FLC sample. Small aliquots of sample were incubated in spin columns containing (i) Sepharose matrix with immobilised anti-human albumin antibody, (ii) a mixture of immobilised anti-human albumin and anti-human transferrin antibodies, or (iii) protein G immobilised of a glass matrix (Prosep G, Millipore). The unbound fractions were evaluated by silver staining (figure 5.21). This showed that both albumin and IgG could effectively be removed using these methods. There was some loss of intensity of the FLC bands after incubation with protein G, however it was decided to sacrifice some FLC in order to remove most of the IgG. The entire κ sample was incubated first with anti-human albumin and transferring matrix, and the unbound then incubated with protein G for three hours at room temperature. As the incubations were performed in spin columns, which were loaded manually, no chromatograms were generated.

The unbound fraction was re-assessed for purity by silver staining (figure 5.22A). This showed that the IgG band had been greatly attenuated. A very weak band at 14 kDa was noted, which intensified on reduction. This band was noted to be immune reactive to anti-κ light chain antibody on western blotting (figure 5.22B), showing that it represented FLC or FLC fragment.

TSP was measured by BCA assay showed a total of 7 mg of κ FLC and 23.7 mg of λ FLC.

Figure 5.19. SDS-PAGE analysis of the purity of κ and λ FLC samples.

SDS-PAGE analysis of κ and λ FLC samples. Coomassie staining (A) and silver staining (B) revealed a strong band in the κ-FLC lane at 42 kDa, corresponding to dimer, and a weaker monomer band below 27 kDa. There is a broad band at 55 kDa in the κ sample which resolves on reduction. There is also a higher MW band 158 kDa, which resolves upon reduction indicating it is IgG. The λ-FLC lane showed the presence of a strong dimer band and a weaker monomer band, which resolved upon reduction to a double band just below 27 kDa. Other faint bands were also seen, including one above 66 kDa, which could be albumin. Lane L-R: 1, standard; 2, κ-FLC (non-reduced); 3, κ-FLC (reduced); 4, λ-FLC (non-reduced); 5, λ-FLC (reduced). Western blotting (C) showed that in the λ sample, bands seen on silver staining were immune reactive to anti-λ antibody, confirming that the λ-FLC sample was highly pure. The presence of IgG was also confirmed in the κ sample, as well as a band above 97 kDa, which may represent oligomeric FLC.

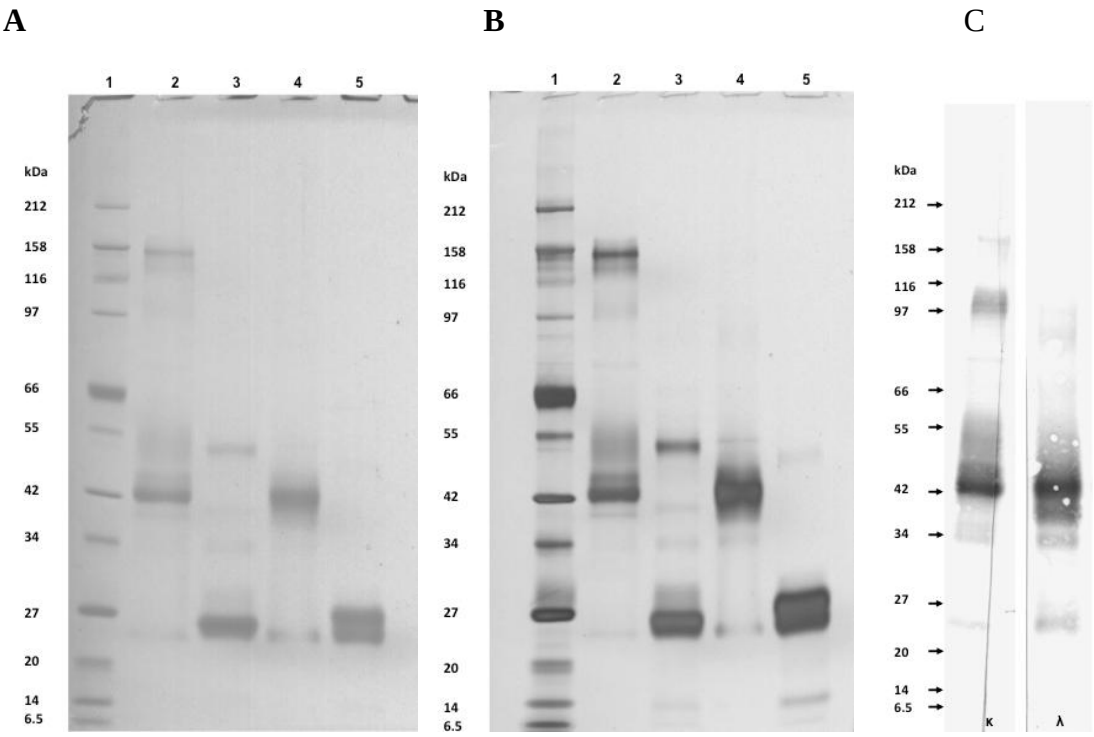

Figure 5.20. Western blots showing the presence of albumin and transferrin contaminants in the κ-FLC sample.

Western blotting for albumin (A) and transferrin in the κ-FLC sample shows the presence of contamination by these proteins (arrowed). HSA, human serum albumin; TF, transferrin. Lanes L-R: 1, standard; 2, HSA positive control; 3, κ-FLC, anti-HSA probe; 4, standard; 5, transferrin positive control; 6, κ-FLC, a-TF probe.

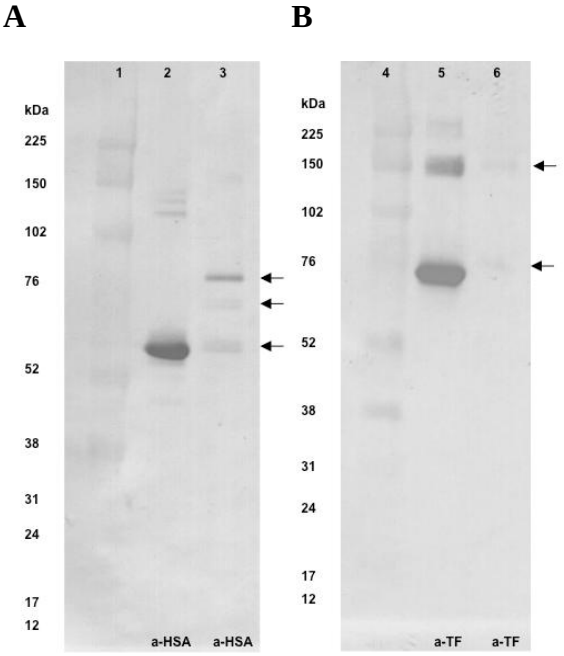

5.8 Detection and Removal of Endotoxin

As the proteins were to be used in an experimental setting it was critical that the proteins would be free of bacterial endotoxin. Samples were filtered through 0.22 μm filters and testing for endotoxin was then performed using the E-TOXATE gel-clot assay. Both κ and λ samples tested positive. The samples were therefore treated by incubating with immobilised polymixin B (Detoxi-Gel). Repeat testing with E-TOXATE showed that the samples had successfully been cleared of endotoxin to levels below the detection limit of the assay.

Figure 5.21. SDS_PAGE analysis of unbound fractions after incubation with anti-HSA, anti-HSA+anti-TF and protein G.

Silver staining showed that albumin and transferrin could be effectively removed by incubating the sample with anti-HSA (lane 4) and anti HSA+anti-TF matrices (lane 5). IgG could be removed by incubation with protein G matrix, although this method leads to loss of some protein (lane 6). Lanes L-R: 1, standard; 2, κ-FLC (non-reduced); 3, κ-FLC (reduced); 4, post anti-HSA (non-reduced); 5, post anti-HSA+anti-TF (non-reduced); 6, post protein G (non-reduced).

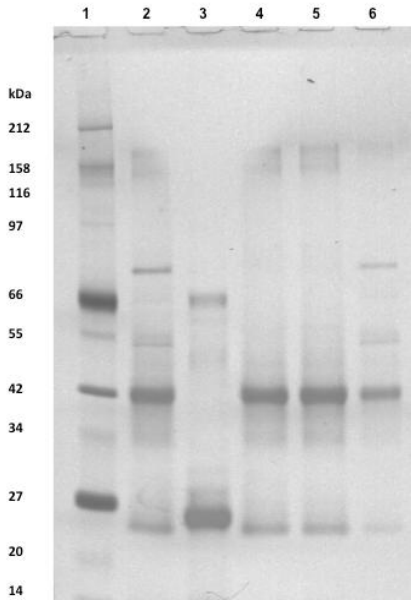

5.9 Assessment of Solubility After Lyophilisation

Three aliquots of κ FLC (0.4 mg) were dialysed into water and sent to The Binding Site for lyophilisation. Each lyophilised sample was dissolved in 1 ml of PBS, and TSP measured by BCA (table 5.4). Recovery rate was between 100% and 85%. The samples were also analysed by SDS-PAGE with Coomassie staining (figure 5.23), which showed that the proteins appeared identical before and after lyophilisation. The remainder of the samples were then dialysed extensively (48 h) into water, and sent to The Binding Site for lyophilisation.

Figure 5.22. SDS-PAGE analysis of κ-FLC sample, after incubation with anti-HSA+anti-TF and protein G.

Silver stain (A) sowing that the IgG band in the κ-FLC sample has been greatly attenuated, indicating effective removal. Lanes L-R: 1, standard; 2, κ-FLC (non-reduced); 3, κ-FLC (reduced). Western blot (B) confirms effective removal of IgG, with only a very weak band appearing after prolonged development of the blot (arrowed "IgG"). The weak band at 17 kDa is immune reactive to anti-κ FLC antibody, indicating it is FLC or FLC fragment. Lanes L-R: 1, standard; 2, κFLC.

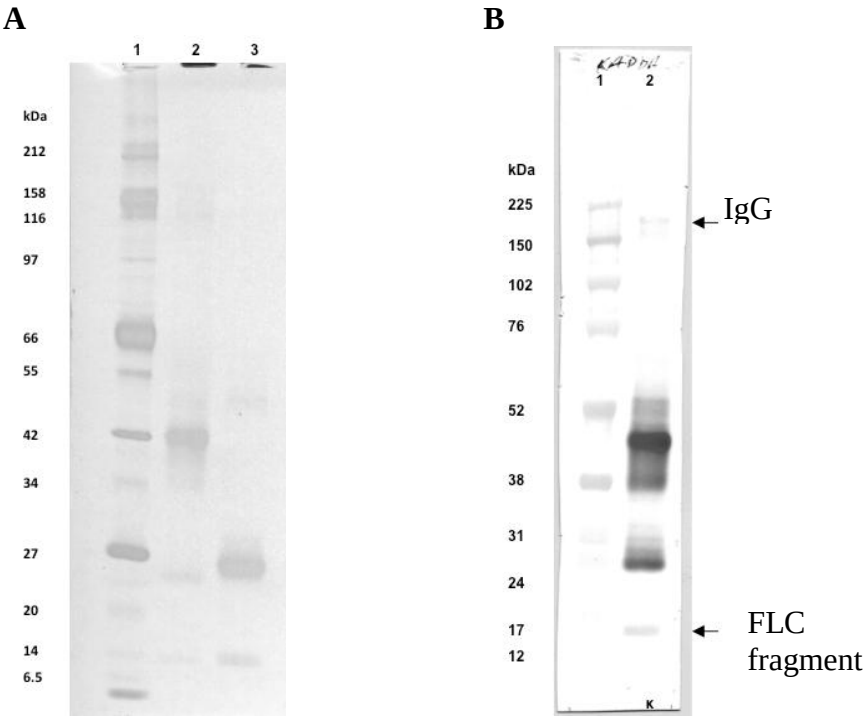

Table 5.4. FLC κ recovery after lyophilisation.

Sample	TSP Before Lyophilising (mg)	TSP After Lyophilising (mg)	% Recovery
A	0.4	0.4	100
B	0.4	0.34	85
C	0.4	0.39	98

Figure 5.23. SDS-PAGE analysis of κ FLC recovery after lyophilisation.

Comparison of κ-FLC pre and post lyophilisation, showing that proteins appear identical before and after lyophilisation on SDS-PAGE analysis. Coomassie brilliant blue, lanes L-R: 1, standard; 2, pre-lyophilisation (non-reduced); 3, post-lyophilisation, sample A (non-reduced); 4, post-lyophylisation, sample B (non-reduced); 5, post-lyophilisation, sample C (non-reduced); 6, pre-lyophilisation (reduced); 7, post-lyophilisation, sample A (reduced); 8, post-lyophilisation, sample B (reduced); 9, post-lyophilisation, sample C (reduced).

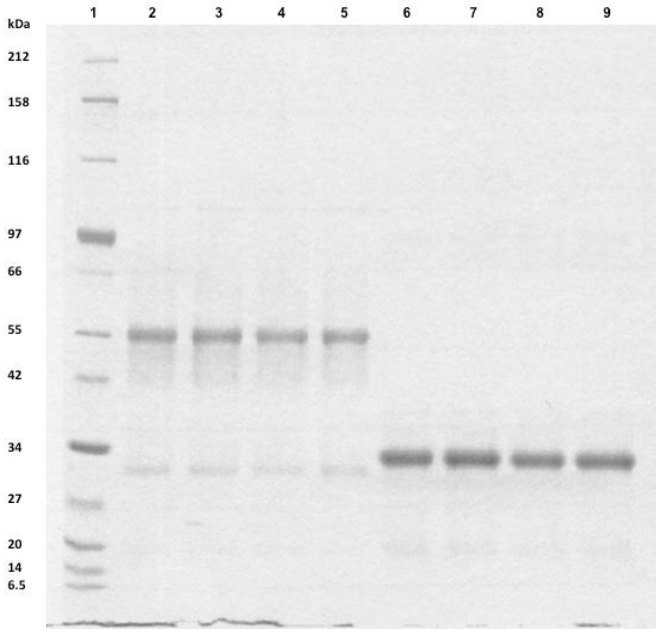

5.10 Discussion

The polyclonal FLCs obtained as a result of the above processes were shown to be highly pure. The FLCs were shown to exist as monomers and dimers mainly, but higher oligomeric forms were also seen. The ability of FLCs to aggregate into higher MW forms has previously been described with myeloma FLCs.(Sanders *et al.* 1987)

An initial assessment of the starting sample revealed that it contained a very large number of different proteins. The FLC content of the starting sample represented only a very small proportion of the TSP. In batch 1, for example, FLC constituted just 0.23 % of TSP. The starting sample contained significant quantities of immunoglobulin, as well as albumin. These were the main contaminants that needed to be removed. The efficiency of affinity chromatography declines as the concentration of the protein of interest relative to the concentration of other proteins in the solution is reduced. (Scopes 1994) The initial approach of choice was to apply affinity chromatography to the starting sample, thus extracting those proteins that contained light chain – FLC and immunoglobulin. Dot-blotting confirmed that the anti-κ and anti-λ columns extracted all detectable light chain containing proteins. From here, immunoglobulin could be removed by further affinity chromatography.

The polyclonal λ FLC sample was much more readily purified than the κ sample. All the bands seen on SDS-PAGE in the non-reduced lanes were immune reactive to anti-light chain antibody, indicating that these were FLC. On the silver stained gel, on reduction, two faint bands appeared in the λ sample, one between the 42 and 55 kDa standards, and one at 14 kDa. These were not seen on Coomassie staining, however, and remained unidentified.

The polyclonal κ sample had persistent IgG and albumin impurities, despite multiple further attempts to remove them. The major disadvantage of repeated chromatography processes is the loss of protein at each step.(Scopes 1994) The requirement to process the κ sample in this way was reflected in the very poor recovery rates. The incubation of

the κ sample with protein G resulted in additional protein loss, suggesting protein G binding of κ FLC, as demonstrated by the weakening of the band seen on silver stained SDS-PAGE. In the final analysis of the κ sample, there was still a faint band seen on silver staining and Western blotting which represents IgG contamination. Similar to the λ sample, a faint band was seen in the κ sample at around 14 kDa. This is shown to be FLC on the corresponding Western blot.

As the degree of contamination was small, a decision was made not to pursue any further removal of contaminants from the FLC samples in the interests of preserving protein.

There was some disagreement between FLC readings measured using the Freelite assay and the TSP measured in the final purified samples by BCA assay. Despite the final products being near-pure FLC, in solution at around 1 mg/ml, the Freelite readings were consistently higher than TSP measured by BCA. However, in early steps, Freelite was used to provide an indication of how much FLC was present in the start samples. In the final stages, BCA assay was used to determine volumes to which samples needed to be concentrated. In the downstream application of polyclonal FLC *in vitro*, protein concentration was ascertained by weighing lyophilised protein and adding to cell culture medium to make a stock, this being more robust than the above measurements.

In conclusion, the proteins obtained from the processes described in this chapter were were highly purified FLCs. The endotoxin-free lyophilised final product was suitable for application *in vitro*, as described in the next chapter.

6. TISSUE DISTRIBUTION OF POLYCLONAL FREE LIGHT CHAINS IN CHRONIC KIDNEY DISEASE: IN SITU STUDIES

6.1 Introduction

Results from the investigations presented in the preceding chapters have shown that in the setting of myeloma, monoclonal FLCs are responsible for the development of tubulointerstitial inflammation and fibrosis. These effects are mediated by the release of inflammatory cytokines, especially MCP-1, from PTECs in response to endocytosis of FLCs, via mechanisms which are unique to FLCs. In addition, there is a contributory effect from cast formation with uromodulin in the distal nephron, resulting in tubular obstruction, stasis and leakage of tubular contents into the interstitium. Tubular casts are a common finding in acute kidney injury (AKI) that has not been caused by cast nephropathy. (Patel *et al.* 1964; Abuelo 2007) The presence of tubular casts is also recognised in chronic kidney disease (CKD), a phenomenon sometimes referred to as "thyroidisation", and has been considered non-specific (figure 6.1).(Walker 2003) Because the clearance of FLCs from serum is dependent on GFR, elevated polyclonal FLC levels are observed in the setting of CKD, even in the absence of plasma cell dyscrasia.(Hutchison *et al.* 2008c) This raises the question of whether polyclonal FLCs exert a direct biological effect at tissue sites. However there is little data on the pathogenicity of polyclonal FLCs in CKD. This may be an important deficit in the literature: in CKD, as the functioning nephron mass declines, the remaining hyperfiltering nephrons will be exposed to higher concentrations of FLCs and other low molecular weight proteins over prolonged periods. Furthermore nephrons may

Figure 6.1. A proteinaceous cast in a renal biopsy from a patient with CKD.

Intratubular proteinaceous precipitates in a renal biopsy specimen (arrowed), taken from a patient with chronic kidney disease. PAMS, original magnification x 400.

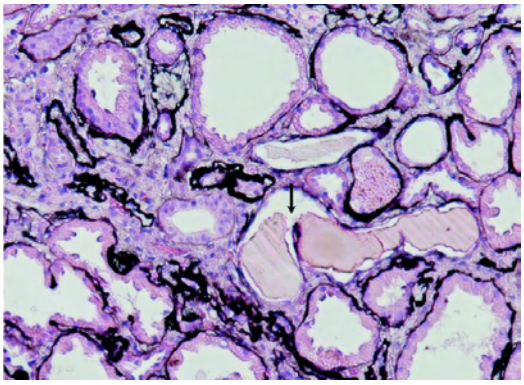

experience reduced tubular fluid flow and dysregulation of concentrating and acidification processes, thus favouring cast formation.

The distribution of FLCs within renal tissues in the setting of CKD may provide an indication of the targets for potential injury. This chapter presents data from a detailed investigation into the distribution of FLCs in the kidney, in the setting of CKD, followed by a study of *in situ* distribution of casts in CKD, and their relationship to known markers of progression for CKD.

Figure 6.2. Uromodulin is produced in the distal nephron and is present in casts.

Uromodulin is expressed on apical surfaces of cells of the distal tubules (A) and seen in proteinaceous precipitates (B). Confocal laser scanning microscope, original magnification x 400.

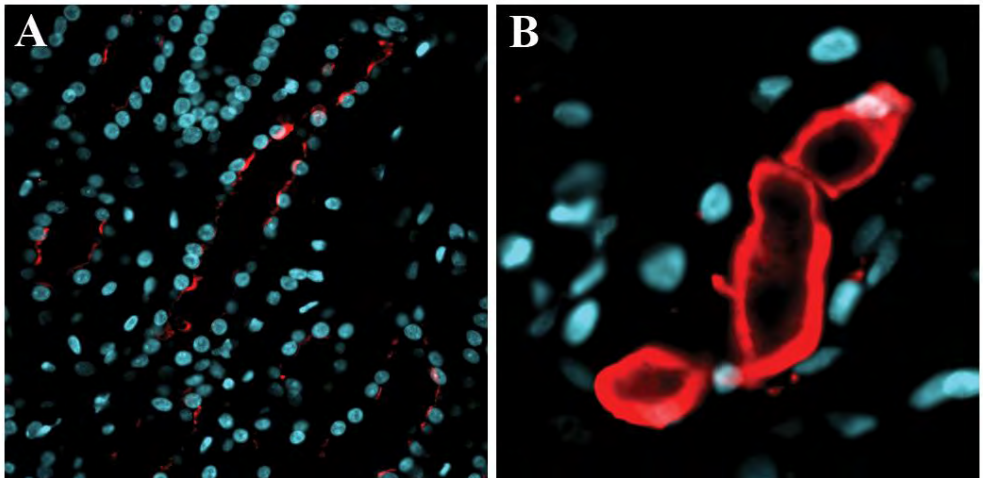

6.2 Patients

Following approval from the local Ethics Committee, all patients who had undergone a renal biopsy at University Hospital Birmingham between 2005 and 2008 were screened. Patients with a histological diagnosis of "ischaemic/hypertensive nephropathy" were chosen for this study, the aim of which was to investigate the relationship between tubulointerstitial fibrosis in CKD and increased serum polyclonal FLCs as a result of decreased GFR.

The disease group of ischaemic/hypertensive nephropathy was chosen and other diagnostic groups were excluded, to control for other mechanisms that may contribute to progressive CKD, such as diabetes, and selective proteinuria in the

glomerulonephritides. Furthermore I excluded conditions such as systemic lupus erythematosus and vasculitides, where serum FLCs might be elevated as a result of increased B-cell activity, independent of GFR. After exclusion criteria were applied, tissue was available for study from 102 patients.

6.3 Results

6.3.1 Immunofluorescence

An immunofluorescence study was initially undertaken on renal biopsies from 20 patients, to assess the overall pattern of polyclonal FLC distribution at tissue sites. Tissue sections were probed with fluorochrome-labelled polyclonal antibodies against κ and λ FLC. Images were acquired using a confocal laser scanning microscope. Uromodulin, which is transcribed exclusively by the cells of the thick ascending limb of the loop of Henle, expressed apically and subsequently present in tubular filtrate distal to this point, was used both as a marker for casts, as well as to help differentiate between proximal and distal tubules (figure 6.2).

No staining was seen in control sections for isotype antibody, immunoglobulin controls, and intra-species cross-reactivity controls. Thus, no non-specific binding of sheep IgG to human kidney tissue, to other sheep IgG, and to human immunoglobulins was demonstrable, and any staining seen truly represented polyclonal FLC.

6.3.2 Polyclonal FLCs are Present in PTECs

Positive staining for both κ and λ FLCs were seen co-localising within the cytoplasm of cells of many tubules (figure 6.3). These tubular cells did not stain positively for uromodulin, thus identifying them as PTECs. Strong staining was demonstrated near the apical surfaces of these cells, indicating where FLCs were concentrated by binding to the cell-surface receptors megalin and cubilin, prior to endocytosis. Staining near the basal surfaces of these cells was weaker, which may be explained by proteolytic breakdown of FLCs after endocytosis within lysosomes, which would result in diminished reactivity to the antibodies.

Tubules where cells stained positively for uromodulin were taken to represent the thick ascending limb of the Loop of Henle and distal tubule. Both κ and λ FLC staining was seen to co-localise with uromodulin in these tubules, but the distribution was noted to be almost exclusively apical (figure 6.4). This supports the conclusion that polyclonal FLCs interact with and bind to uromodulin in the distal nephron, but endocytosis and subsequent proteolytic digestion does not take place.

6.3.3 Polyclonal FLC Co-localise with Uromodulin in Distal Tubules

As described above, the presence of uromodulin was used as a marker to identify tubules of the distal nephron. Uromodulin staining was also used to identify the presence of casts. Both κ and λ polyclonal FLC staining was seen co-localising with uromodulin in distal tubules, supporting the hypothesis that polyclonal FLC do indeed interact with and bind to uromodulin in CKD (figure 6.5). Where casts were identified,

Figure 6.3. Free light chains in the proximal tubule in CKD.

Positive staining for κ, in green, (A) and λ, in blue, (D) FLCs was seen co-localising within epithelial cell cytoplasms. The absence of uromodulin (B) confirms that this is a proximal tubule. C, nuclei; E, combined image. Confocal laser scanning microscope, original magnification x 400.

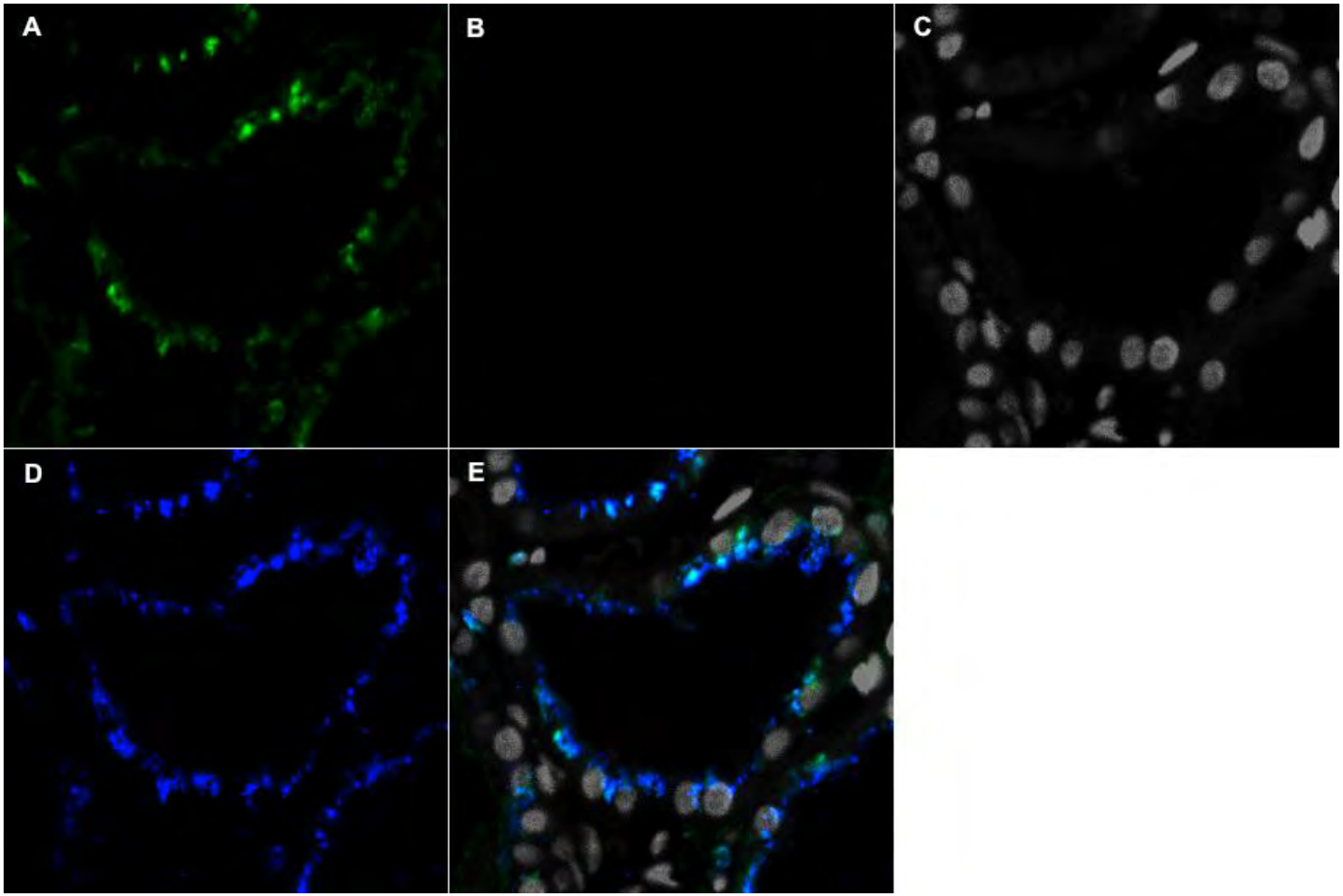

Figure 6.4. Confocal image of proximal and distal tubules showing distribution of κ-FLC, λ-FLC and uromodulin.

In proximal tubules, κ, in green, (A) and λ, in blue, (D) FLCs were seen colocalising in proximal tubule epithelial cell cytoplasms. The absence of co-localising uromodulin staining confirms that these were proximal tubule cells. Distal tubules are indicated by uromodulin staining, in red (B). C, nuclei; E, combined image. Confocal laser scanning microscope, original magnification x 200.

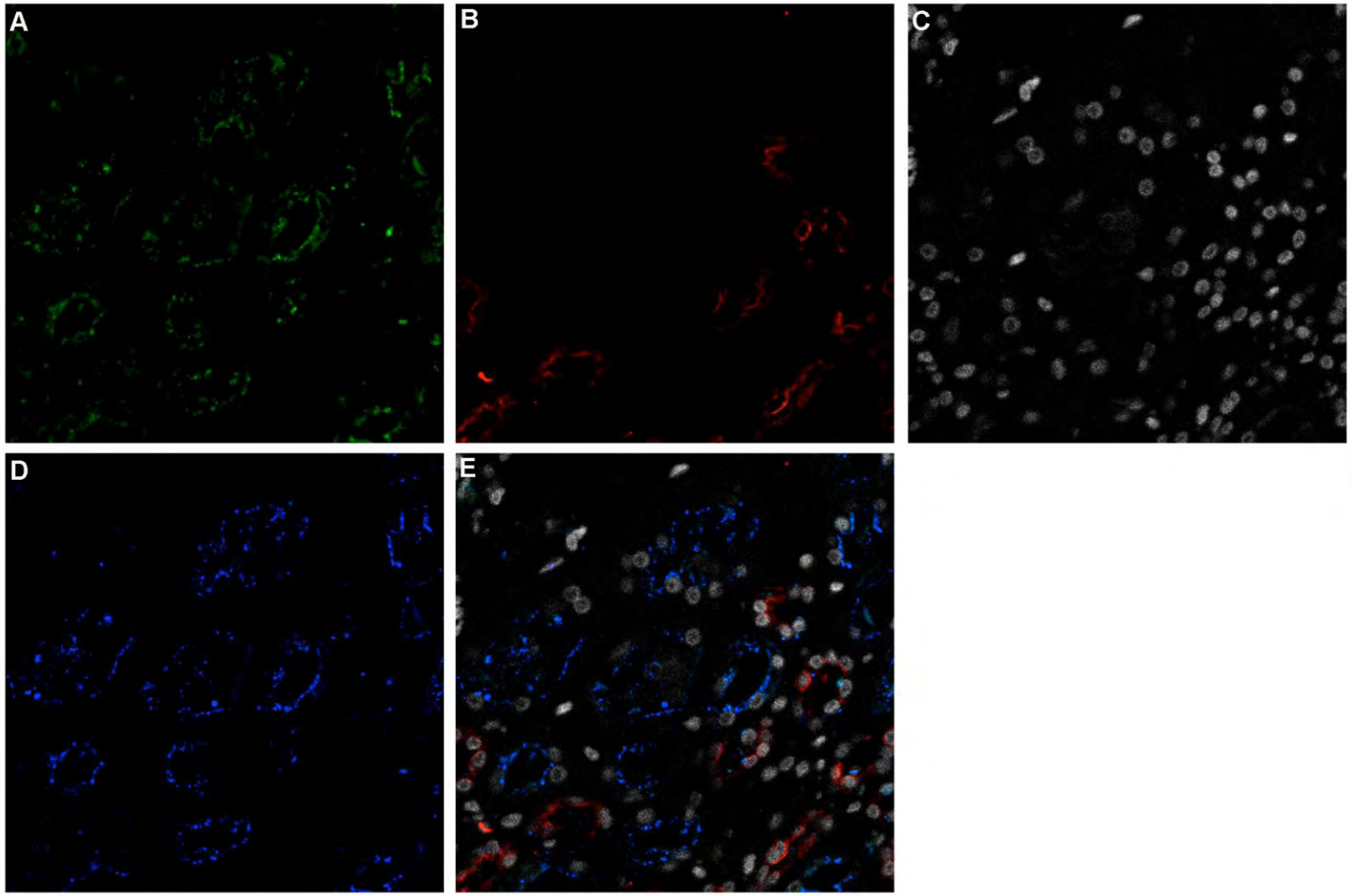

Figure 6.5. Confocal image of casts in a renal biopsy from a patient with CKD.

Intratubular casts in a biopsy from a patient with chronic kidney disease. Both κ, in green, (A) and λ, in blue, (D) FLCs are seen co-localising with uromodulin, in red (B). C, nuclei; D, λ FLC; E, combined image. Confocal laser scanning microscope, original magnification x 100.

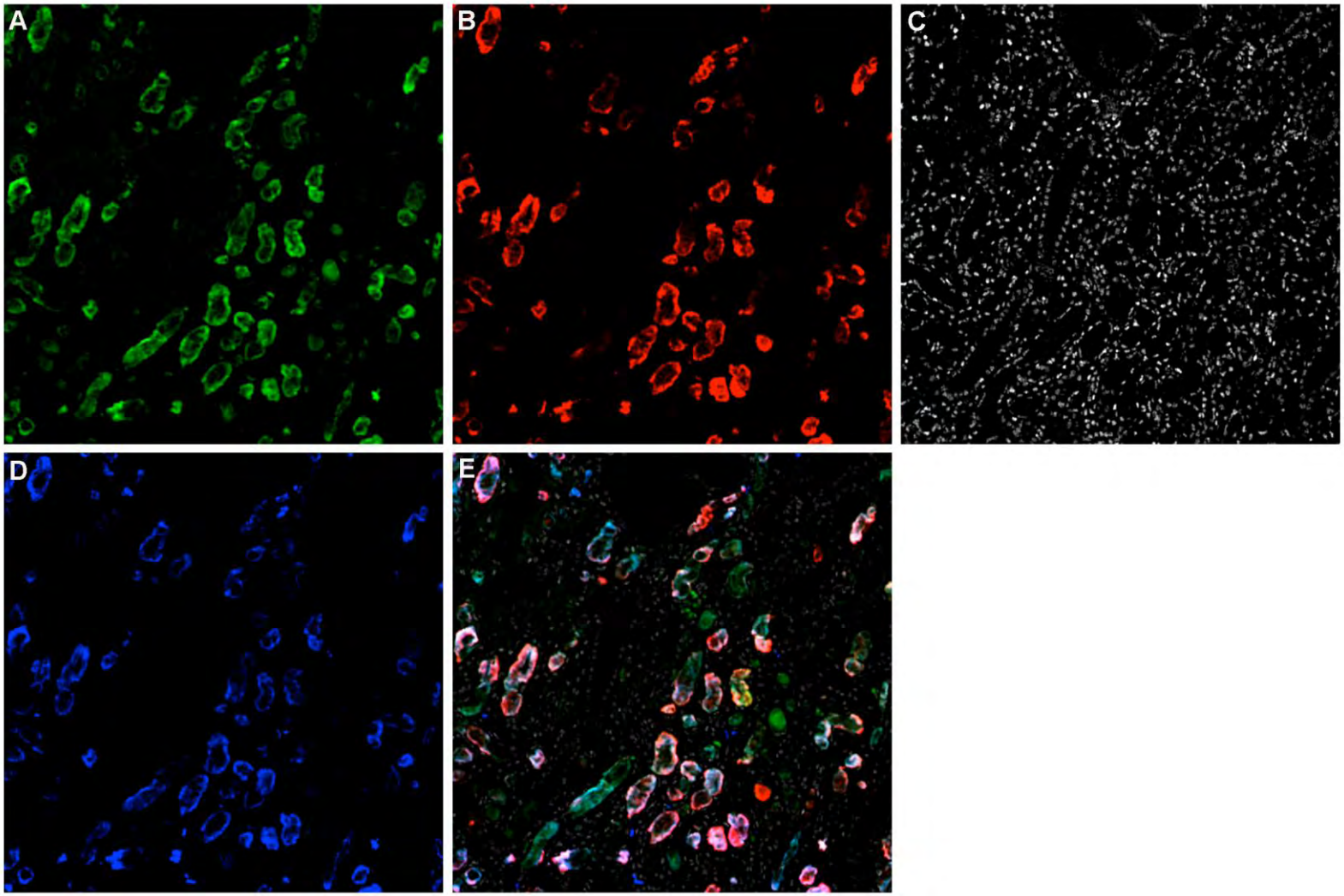

Figure 6.6. High-power confocal image of a cast in a renal biopsy from a patient with CKD.

High-power image of a cast in CKD, showing that staining for κ-FLC, in green, λ-FLC, in blue, and uromodulin, in red appears stronger in the periphery, compared to the central area. A, κ FLC; B, uromodulin; C, nuclei; D, λ FLC; E, combined image. Confocal laser scanning microscope, original magnification x 400.

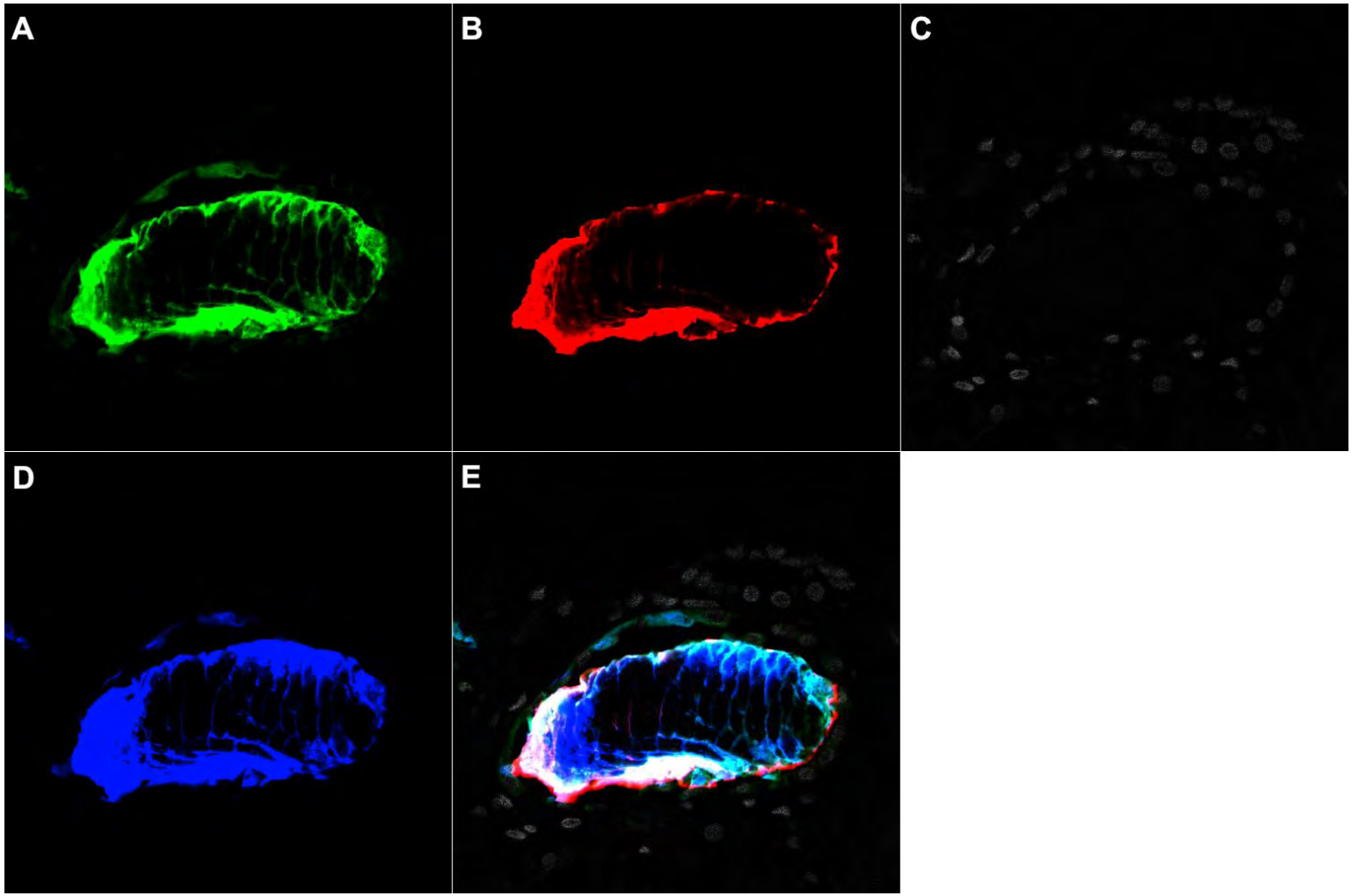

the intensity of staining was usually more intense peripherally than centrally (figure 6.6). These appearances might suggest that FLCs are not present in these casts in the same relative quantities that they are in myeloma cast nephropathy.

6.4 Measurement of Cast Numbers, Index of Chronic Damage, Interstitial Capillary Density and Macrophage Numbers

Following the finding of polyclonal κ and λ FLCs within renal tubular casts, a formal quantification of cast numbers, as well as other markers of progression of CKD, was undertaken for the 102 patients in the cohort. For the purpose of quantifying the index of chronic damage, sections routinely stained with PAMS were retrieved from the pathology archive at University Hospital Birmingham. The method is summarised in figure 6.7. Cast numbers were quantified using the same sections, and the process is summarised in figure 6.8. For capillary density and macrophage numbers, separate sections were stained for CD34 and CD68. Data was collected using Aequitas image analysis software, as described in the Chapter 2. The methods are summarised in figures 6.9 and 6.10 respectively.

6.4.1 Test of Normality of Data

The data failed to pass normality testing for skewness, as determined by applying the D'Agostino and Pearson omnibus normality test. The data variables were therefore normalised by log transformation. In the case of cast numbers, because some values were equal to 0, 1 was added to each data value in the set, prior to log transformation.

Figure 6.7. Quantification of the index of chronic damage.

The cortex is outlined and selected using Aequitas image analysis software (A). Areas of chronic damage are then encircled by freehand drawing (B). This image is then exported as a screen-grab for cast counting using ImageJ software. In Aequitas, areas of chronic damage are quantified and expressed as a percentage of the total cortical area (C). Original magnification x 100.

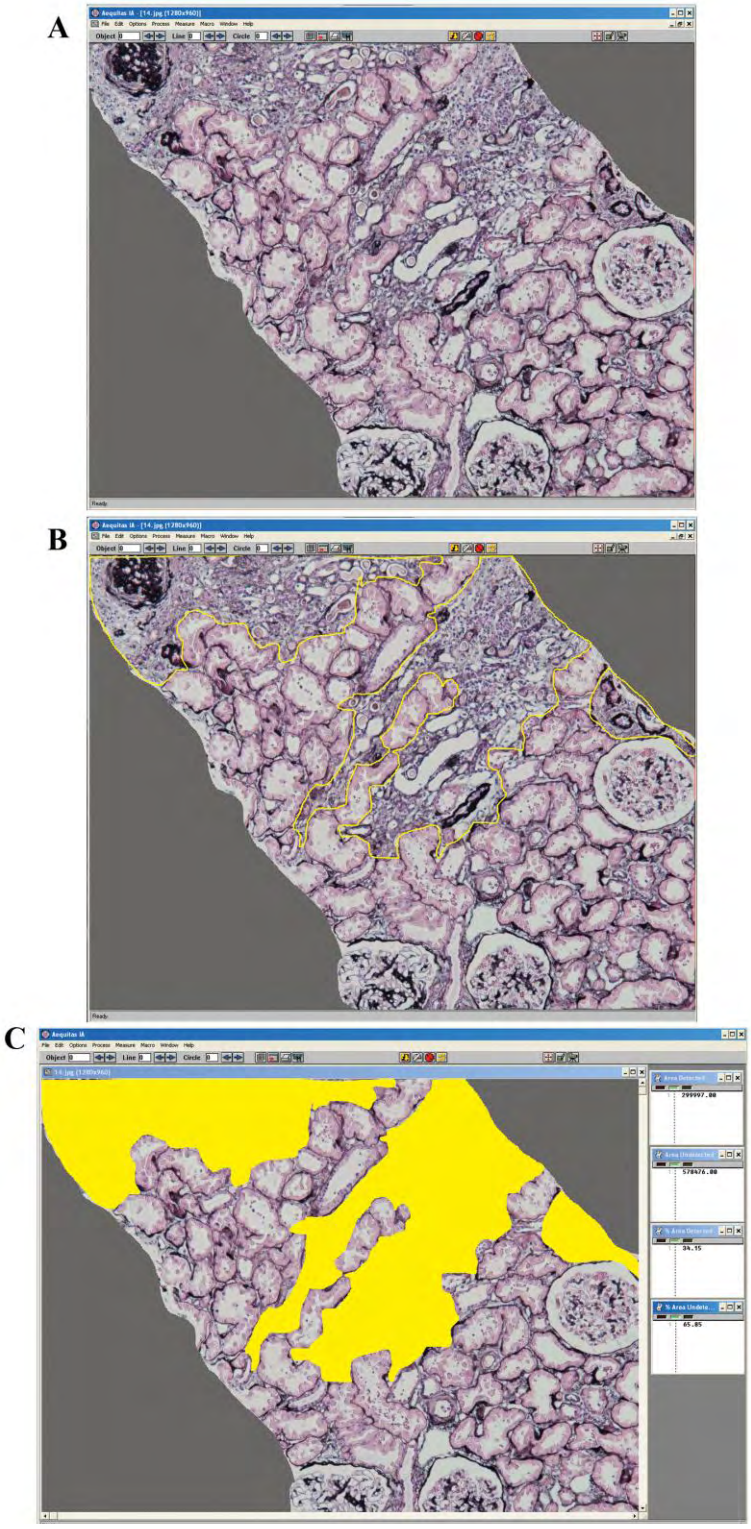

Figure 6.8. Quantification of cast numbers.

After marking out areas of chronic damage using the Aequitas software, the image is exported to ImageJ software. Using the cell counting function in ImageJ, casts were counted in areas with and without chronic damage. Original magnification x 100.

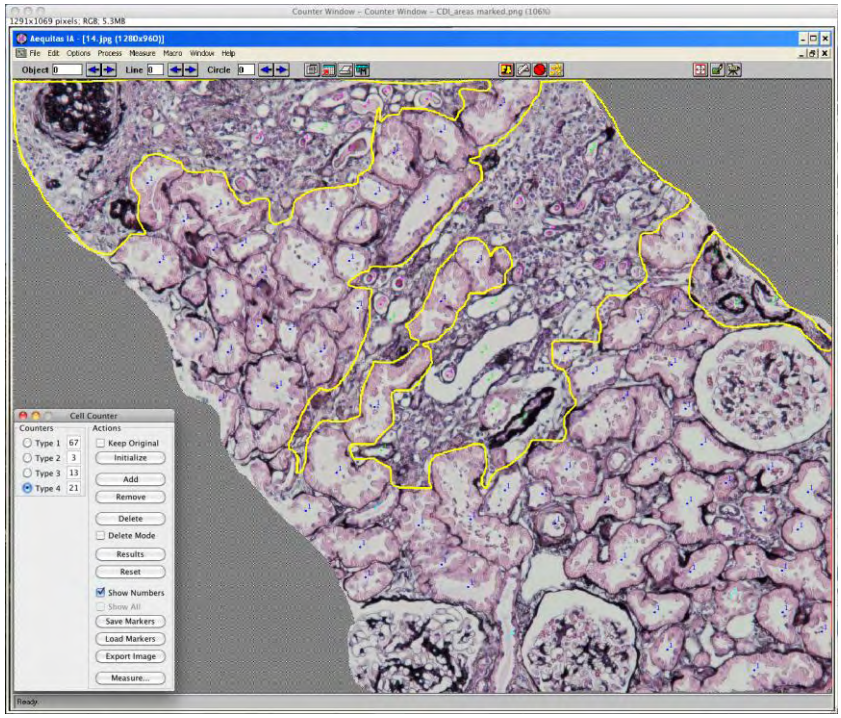

Figure 6.9. Quantification of interstitial capillary density.

The image has been converted to a two-colour scale image using Aequitas software. A threshold was then applied so that the areas of staining were detected (A). Using Aequitas software, areas of staining were then quantified and expressed as a percentage of total area (B). Note that the glomerulus has been ignored in the measurement. Original magnification x 200.

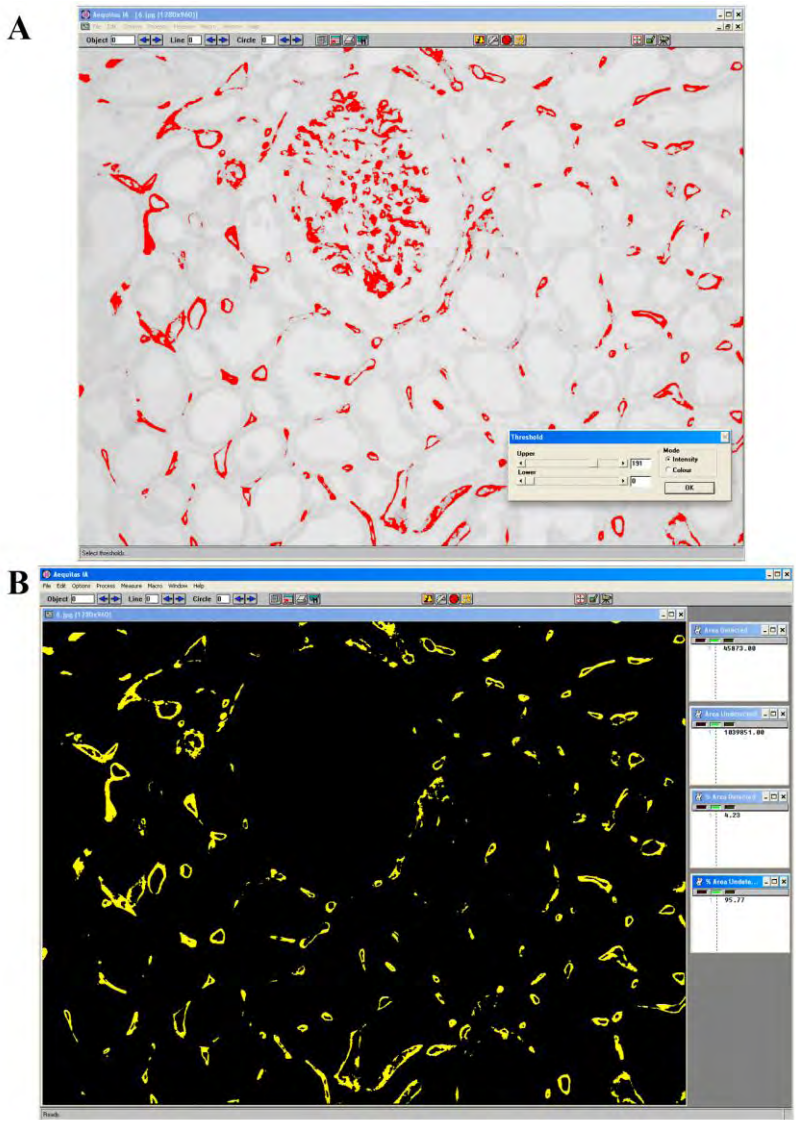

Figure 6.10. Quantification of macrophage numbers.

The image has been converted to a two-colour scale image using Aequitas software. A threshold was then applied so that the areas of staining were detected (A). Using Aequitas software, area of staining were then quantified and expressed as a percentage of total area (B). Original magnification x 200.

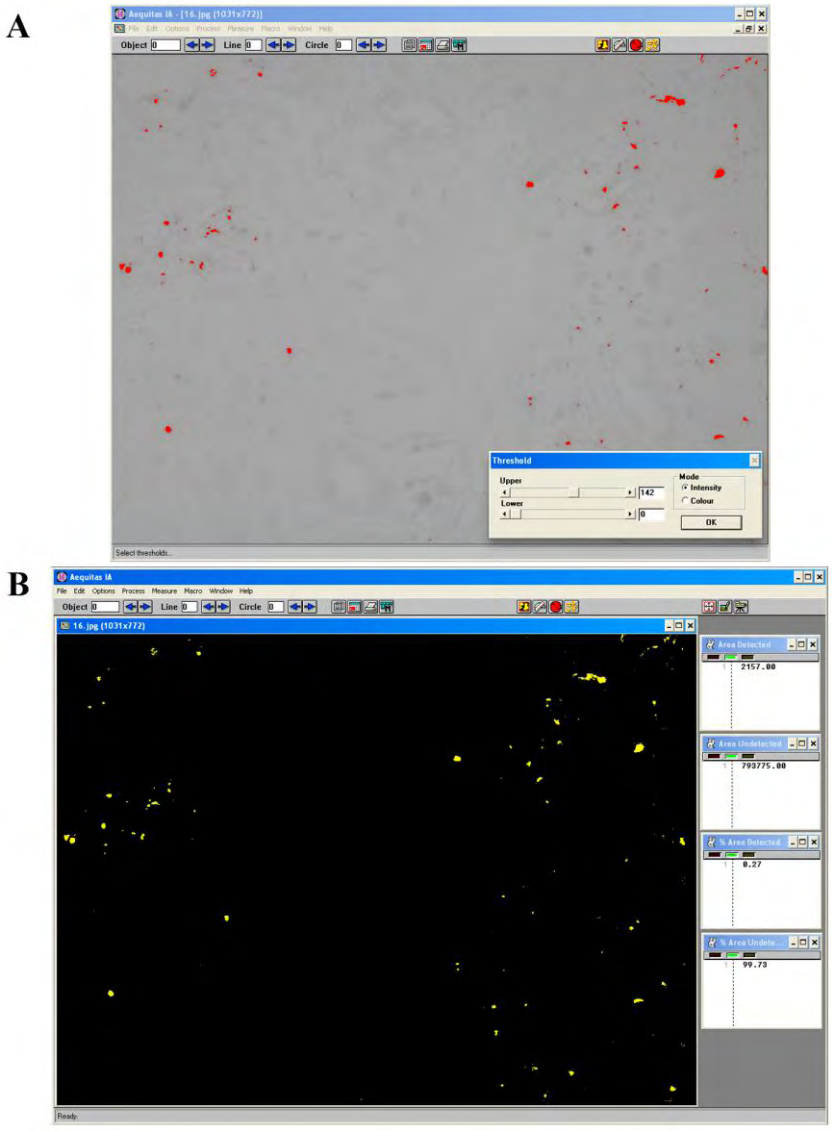

6.4.2 Assessment of Validity of Quantification Methods

To assess the validity of the methods used in quantifying the data, variability between intra-observer results and inter-observer results were determined. All the specimens were measured by myself first. For inter-observer variation, 20 specimens were measured again by a second observer independently. This observer was a research associate who had assisted in developing the method. For the purpose of testing intra-observer variability, the same 20 specimens were measured again, after an interval, by myself.

Agreement between the different measurements was assessed using the method described by Bland and Altman.(Bland and Altman 1986) Because the difference in measurements was proportional to the mean, log transformation was carried out prior to testing, as described above. The Bland-Altman method calculates the bias (the mean difference between measurements) and limits of agreement (2 SDs two-tailed) with 95% CIs for the bias, which are expressed as ratios when back-transformed. The results are shown in table 6.1. There was no significant bias detected between inter- and intra-observer results obtained for cast numbers, capillary density, index of chronic damage or macrophage numbers.

6.4.3 Casts in CKD are Situated in Areas of Established Chronic Damage

By light microscopy, most of the casts were distributed within areas of established fibrosis. Cast numbers were counted within areas of chronic damage, and areas deemed to be normal. There was a significant difference between the median percentages of

Table 6.1. Assessment of agreement between two observers by the Bland-Altman method.

	Index of Chronic Damage		Capillary Density		Macrophages		% Casts	
	Obsv 1 vs Obsv 1	**Obsv 1 vs Obsv 2**	**Obsv 1 vs Obsv 1**	**Obsv 1 vs Obsv 2**	**Obsv 1 vs Obsv 1**	**Obsv 1 vs Obsv 2**	**Obsv 1 vs Obsv 1**	**Obsv 1 vs Obsv 2**
Bias (SD)	1.023 (1.083)	1.014 (1.116)	1.040 (1.097)	0.994 (1.078)	0.983 (1.090)	0.980 (1.070)	0.992 (1.074)	0.992 (1.059)
95% CI of Bias	0.986-1.061	0.963-1.067	0.996-1.086	0.960-1.030	0.945-1.024	0.950-1.012	0.960-1.026	0.965-1.019
95% LoA	0.876-1.195	0.818-1.256	0.867-1.248	0.858-1.152	0.831-1.164	0.860-1.118	0.863-1.141	0.886-1.111

tubules containing casts in normal areas compared to the median in areas of established chronic damage (0 and 35, n=98, p <0.0001), as shown in figure 6.11.

6.4.4 Capillary Density Correlates with the Index of Chronic Damage and Macrophage Numbers

By univariate analysis, interstitial capillary density showed a negative correlation with the index of chronic damage (r = -0.539; p <0.0001; n = 98) and a negative correlation with interstitial macrophage numbers (r = -0.444; p <0.0001; n = 100). These data are summarised in table 6.2 and linear regression is shown in figure 6.12.

Figure 6.11. Comparison of cast numbers between areas with or without chronic damage.

Most of the casts counted were present in areas of established chronic damage. The median percentage of tubules containing casts in areas without chronic damage was 0, while in areas of established chronic damage, the median percentage of tubules containing casts was 35. ***p = < 0.0001

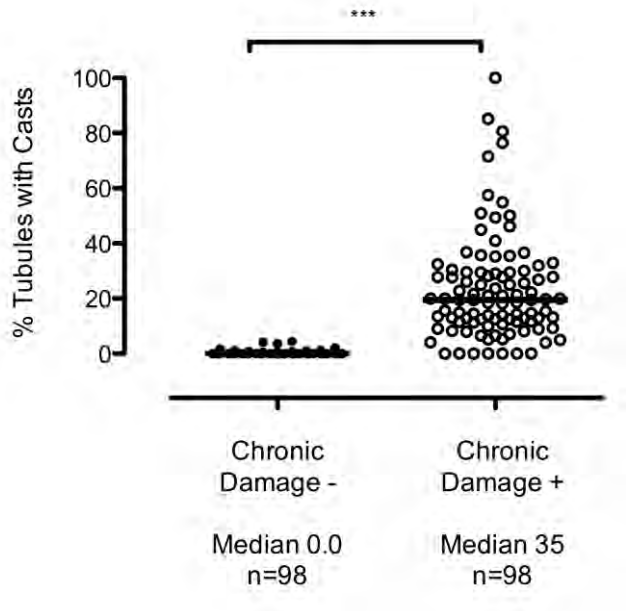

Table 6.2. Univariate analyses of cast numbers, index of chronic damage, capillary density and macrophage numbers.

	Cast No			
Cast No	1.000 (Correlation; p value) <0.0001; n = 98	**Index of Chronic Damage**		
Index of Chronic Damage	0.736; <0.0001 98	1.000; <0.0001 98	**Capillary Density**	
Capillary Density	-0.471; <0.0001 98	-0.539; <0.0001 98	1.000; <0.0001 102	**Macrophage Infiltration**
Macrophage Infiltration	0.515; <0.0001 96	0.695; <0.0001 96	-0.444; <0.0001 100	1.000; <0.0001 100

Figure 6.12. Correlations of capillary density with index of chronic damage and macrophage numbers.

Linear regression analysis of capillary density with index of chronic damage (A) and macrophage numbers (B), indicated inverse relationships, which were confirmed by univariate analyses. Negative correlations of capillary density were were shown with chronic damage ($r = -0.539$; $p < 0.0001$, $n = 98$) and macrophages ($r = -0.444$; $p < 0.0001$; $n = 100$).

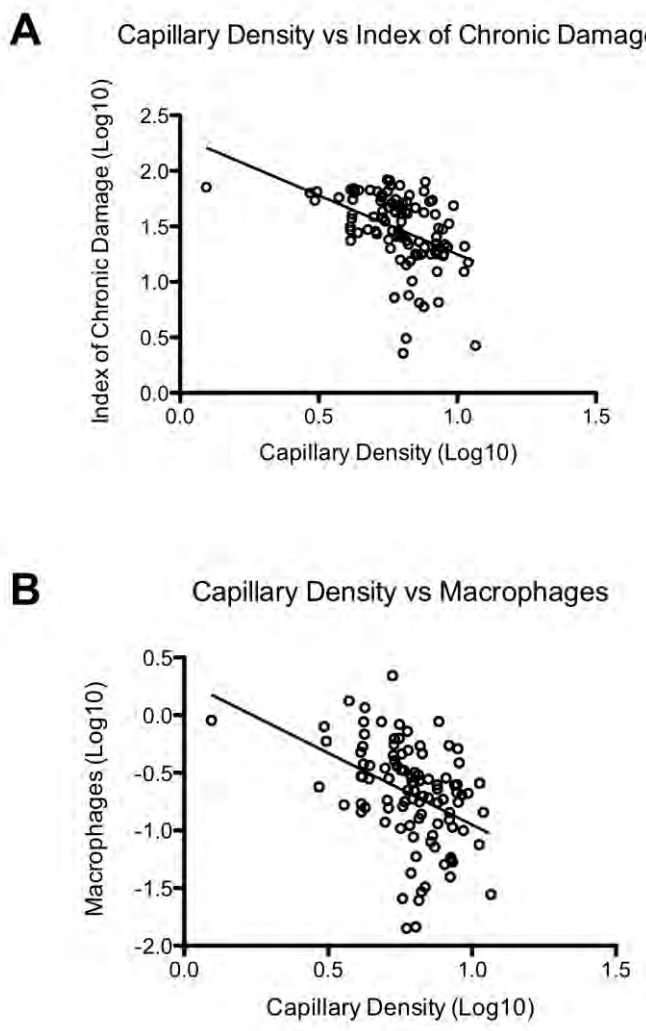

6.4.5 Macrophage Numbers Correlate with Index of Chronic Damage

Macrophage numbers, as quantified by image analysis, correlated positively with the index of chronic damage ($r = 0.695$; $p < 0.0001$; $n = 96$). These data are summarised in table 6.2 and linear regression is shown in figure 6.13.

6.4.6 Cast Numbers Correlate with Index of Chronic Damage, Capillary Density and Macrophage Numbers

The percentage of tubules counted in each biopsy that contained casts showed a positive correlation with the index of chronic damage ($r = 0.736$; $p < 0.0001$; $n = 98$), a negative correlation with interstitial capillary density ($r = -0.471$; $p < 0.0001$; $n = 98$), and a positive correlation with infiltrating interstitial macrophage numbers ($r = 0.515$; $p < 0.0001$; $n = 96$). These data are summarised in table 6.2 and linear regression is shown in figure 6.14.

Figure 6.13. Correlation of macrophage numbers with index of chronic damage.

Linear regression analysis of macrophages with chronic damage indicated a positive relationship, confirmed by univariate analysis, which showed a positive correlation ($r = 0.695$; $p < 0.0001$, $n = 96$).

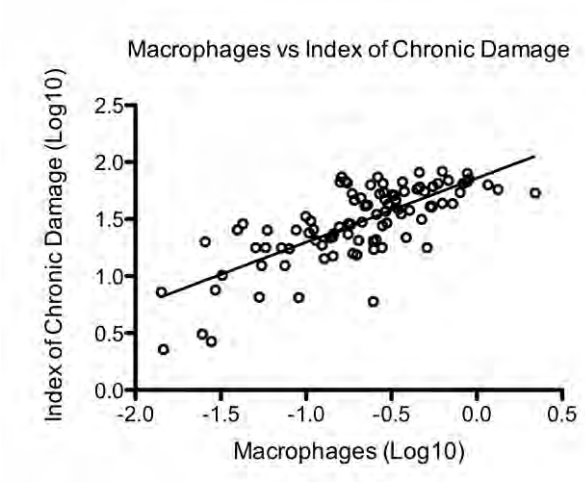

Figure 6.14. Correlations of cast numbers with index of chronic damage, capillary density and macrophage numbers.

Linear regression analyses of cast numbers with index of chronic damage (A), capillary density (B) and macrophage numbers (C). Univariate analyses showed a positive correlation with chronic damage ($r = 0.736$; $p < 0.0001$; $n = 98$), a negative correlation with interstitial capillary density ($r = -0.471$; $p < 0.0001$; $n = 98$) and a positive relationship with macrophage numbers ($r = 0.515$; $p < 0.0001$; $n = 96$).

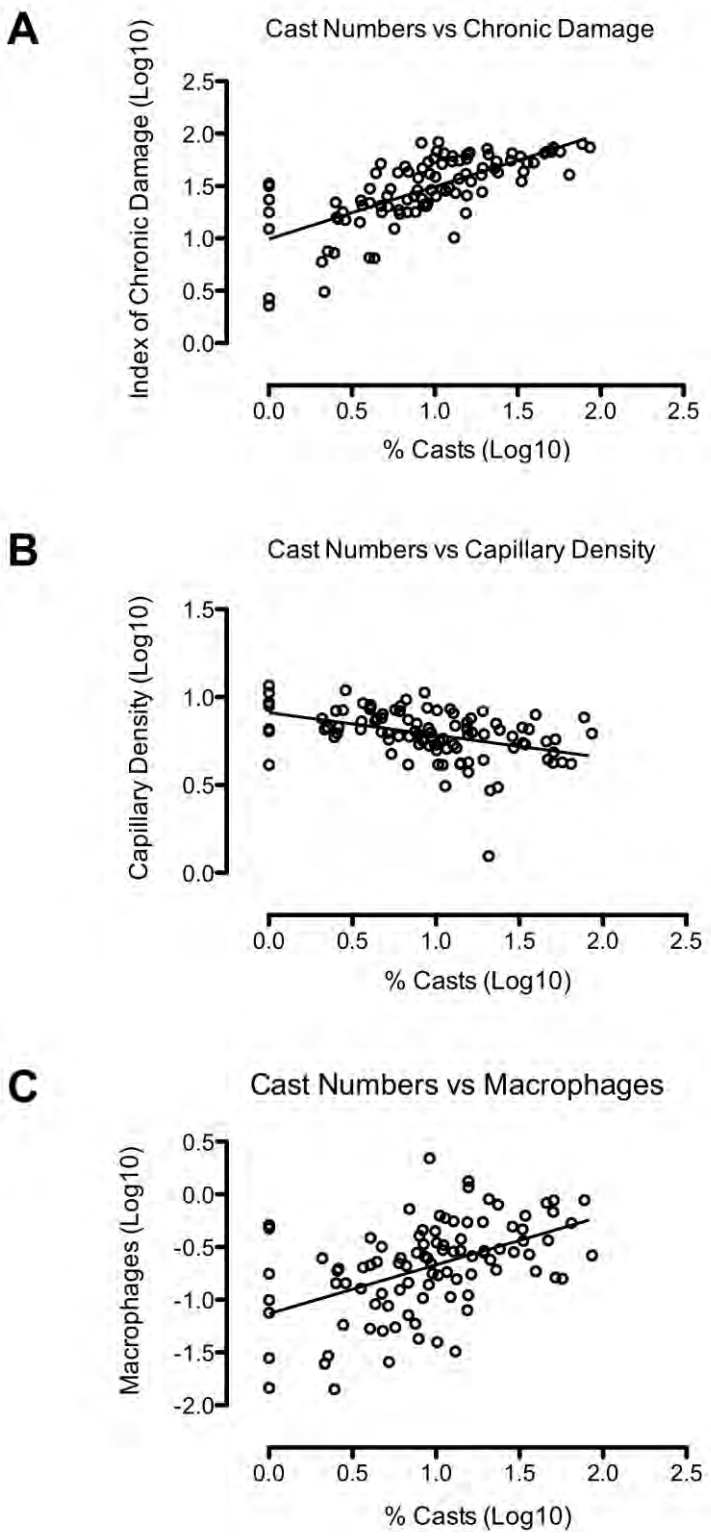

Table 6.3. Multivariate analysis of correlations between index of chronic damage, capillary density, macrophage numbers and cast numbers.

		Dependent Variable			
		Index of Chronic Damage	**Capillary Density**	**Macrophages**	**% Casts**
Index of Chronic Damage	Correlation; p value	n.a.	n.s.	0.741; < 0.0001	0.703 < 0.0001
Capillary Density		n.s.	n.a.	n.s.	n.s.
Macrophages		0.522; < 0.0001	n.s.	n.a.	n.s.
% Casts		0.446; < 0.0001	n.s.	n.s.	n.a.

n.a., not applicable; n.s., not statistically significant

6.4.7 Multivariate Analysis of Correlations

Linear regression stepwise multivariate analysis of these correlations with a dependent variable was performed for correlations between cast numbers, interstitial capillary density, macrophages and the index of chronic damage (table 6.3) In this analysis, the index of chronic damage and macrophage numbers were independent predictors of each

other. The index of chronic damage and the percentage of tubules containing casts were also independent predictors of each other. However no other significant relationships were shown.

6.5 Discussion

In this chapter, results are presented outlining the *in situ* tissue distribution of polyclonal FLCs seen in chronic kidney disease. The presence of positive staining for FLCs in proximal tubules confirmed that in CKD, polyclonal FLCs that are filtered at the glomerulus are indeed processed by PTECs. The presence of these polyclonal FLCs in increased concentrations in the serum would translate to increased exposure of PTECs to these proteins. Because of the nature of recovery of filtered proteins from the tubular lumen by the multi-ligand, tandem endocytic receptors, megalin and cubilin, PTECs are a preferential target for injury by filtered proteins.(Birn and Christensen 2006) Although in this study, co-localisation with megalin and cubilin was not investigated, the increased intensity of staining at the apical surfaces of cells indicated that there may be concentration of polyclonal FLCs at these sites as a result of engagement with these receptors. Staining within the cytoplasm weakened towards the basal aspect of PTECs, possibly due to lysosomal degradation of endocytosed FLCs rendering them less immune reactive.

Uromodulin was chosen as the marker not only because of its utility in differentiating proximal tubules from those of the distal nephron, but also because it is an important component of casts. The co-localisation of both κ and λ polyclonal FLC with

uromodulin in distal tubular casts confirms that in CKD, polyclonal FLCs do indeed interact with and bind to uromodulin. In myeloma cast nephropathy, the casts have a characteristic hard appearance, often fractured. Invasion of the tubule by macrophages and giant cells is seen. In the casts associated with CKD, the appearance is different. The intensity of immunofluorescence staining was stronger at the periphery, indicating that the cast might be denser at the periphery than the centre, and indeed may be patent centrally. These appearances may be the result of different mechanisms of formation. In myeloma, cast formation is often precipitated rapidly by high concentrations of FLC delivered to the tubule, in conjunction with other factors such as dehydration or drugs. In CKD the formation of casts is likely to be a slower process, which occurs as tubules are surrounded by fibrotic tissue, lose their capillary blood supply and become senescent, tubular fluid flow decreases, stasis occurs, with dysregulation of electrolyte control and acidification. Proximal tubular dysfunction may also play a role, with reduced reabsorption of filtered proteins having the effect of increasing FLCs delivered to the distal nephron, thus promoting cast formation.

Along with quantification of cast numbers in the patient group described, other histological parameters associated with progression of CKD were studied. The index of chronic damage has been established as a rigorous predictor of renal outcome in CKD.(Howie *et al.* 2001) Eardley *et al* have shown that in addition, infiltrating macrophage numbers and interstitial capillary density are also predictors of renal outcomes, and that these parameters are inter-related.(Eardley *et al.* 2006; Eardley *et al.* 2008) I hypothesised that, if polyclonal FLCs did indeed have a biological effect in the progression of CKD, histological features associated with polyclonal FLCs would be

correlated with the index of chronic damage, interstitial capillary density and infiltrating macrophage numbers. The identification of polyclonal FLCs within PTECs, although a good qualitative measure, is not a robust quantitative measure, due to variances in staining intensity, and the fact that all PTECs would be exposed to at least some FLC. Casts, however, were easily identifiable and could be easily counted. It was therefore chosen as the parameter of interest. In the studies reported by Eardley *et al*, quantification methods for capillary density and macrophage numbers were shown to be robust and reproducible, a feature seen in my own studies presented here.

In order to validate results obtained from morphometric analyses of renal biopsy material, the results were analysed for intra-observer as well as inter-observer variability with an independent, blinded second observer. In order for the results to be valid, high levels of agreement needed to be demonstrated. One suitable method for testing inter-observer agreement is the Cohen's kappa calculation.(Cohen 1960) However, in my studies, an additional aspect was the intra-observer variability. Kappa can qualitatively test whether there is inter-observer variability or not. However, as a quantitative tool, there are limitations to kappa, in that it is not a true chance-corrected measurement, and that its value can often be low, despite high levels of agreement.(Feinstein and Cicchetti 1990; Cicchetti and Feinstein 1990) The Bland-Altman method, although primarily designed to measure agreement between different methods, is able to give the bias, or mean difference between measurements, and limits of agreement, or 2 standard deviations either side of the mean, with 95% CIs for the bias and limits of agreement. This methods has been successfully used to quantitatively

demonstrate high levels of both inter-observer and intra-observer variability by Eardley *et al*, and therefore was chosen for my own studies.(Eardley *et al.* 2006)

Despite CD68 being a consistent macrophage marker, accurate histological characterisation of macrophages in the kidney is complex and the precise identity of cells staining positively for CD68 has been questioned. A recent study by Segerer *et al* has indicated that in certain forms of kidney disease, a proportion of interstitial CD68 positive cells in renal biopsies from patients with a range of glomerulonephritides were in fact dendritic cells, rather than macrophages.(Segerer *et al.* 2008) In order to distinguish true macrophages, it would be necessary to demonstrate either the absence of dendritic cell markers or to show co-localisation with a macrophage marker, usually using immunofluorescence. In my studies, this approach was not taken. First, the study by Segerer *et al* focussed on a population of patients with glomerulonephritis; such patients were excluded from my study. Second, Eardley *et al* have shown that the correlations CD68 positive cell number with interstitial capillary density and index of chronic damage are robust.

Although immunofluorescence has a distinct advantage over conventional immunohistochemistry where co-localising targets are concerned, it is difficult to gain an appreciation of overall morphology, limiting its utility when quantifying casts and chronic damage. Therefore both these quantifications were carried out using light microscopy. Additionally, the methods used for these two measurements were interlinked.

My investigations confirmed at an early stage, that casts were predominantly present in tubules in areas of chronic damage, suggesting that cast numbers would be correlated positively with the index of chronic damage and macrophage numbers, whilst being inversely correlated with capillary density. This was confirmed by the subsequent statistical analyses performed. In my studies, univariate analyses of the index of chronic damage, capillary density and macrophage numbers were in agreement with the findings of Eardley *et al*, confirming that these data would be suitable for correlation analyses with cast numbers. Univariate analyses also showed that cast numbers were associated with increased interstitial fibrosis, increased interstitial macrophage numbers, and decreased capillary density, indicating that cast formation may be favoured by an ischaemic microenvironment.

In multivariate analyses, the index of chronic damage and macrophage numbers were shown to be independent predictors of each other. This was consistent with the previous findings of Eardley *et al*. The index of chronic damage and the percentage of tubules containing casts also had a similar relationship.

The observation of polyclonal FLC at two specific tissue sites in the kidney in the setting of CKD – the PTEC and the distal nephron – raises the possibility of biological effects exerted by these polyclonal FLCs at these sites, contributing to ongoing interstitial inflammation and progression of fibrosis. Following these detailed *in situ* studies the next chapter will focus on using *in vitro* models to identify potential mechanisms of injury.

7. BIOLOGICAL EFFECTS OF POLYCLONAL FREE LIGHT CHAINS: IN VITRO STUDIES

7.1 Introduction

Results presented in the preceding chapter have demonstrated that in CKD, polyclonal FLCs can be seen co-localising with PTECs *in situ*. In addition, in the distal tubules, proteinaceous precipitates are seen which are composed of uromodulin, and contain polyclonal FLCs. In multiple myeloma, both the proximal tubule and distal tubule are well recognised sites of injury from FLCs, by PTEC activation and cast formation by co-precipitation with uromodulin respectively.(Sanders 2005) The mechanism of PTEC activation is initiated by the generation of H_2O_2 following receptor-mediated endocytosis, which then activates the redox-sensitive tyrosine kinase c-Src, which in turn is integrally involved in downstream signalling resulting in nuclear translocation of NF-κB and transcription, leading to the release of inflammatory cytokines.(Wang and Sanders 2007; Basnayake *et al.* 2010) In the distal tubule, monoclonal FLCs co-precipitate with uromodulin, forming casts, which obstruct tubules and are associated with invasion of the tubules by inflammatory cells, although a direct inflammatory effect of FLC on distal tubular epithelium has not been investigated to date.

Although the presence of polyclonal FLCs at the same sites where monoclonal FLCs cause injury to the kidney has been demonstrated in CKD, a causative link between polyclonal FLCs and the inflammation seen in CKD has not been found to date. In this chapter, results from *in vitro* studies are presented, which test the hypothesis that polyclonal FLCs contribute to the inflammation seen in CKD: (i) contributing to

activation of PTECs and effecting inflammatory cytokine release from these cells, and (ii) by co-precipitation with uromodulin, thus leading to cast formation in tubules and further potentiating inflammation.

7.2 PTEC Culture

HK-2 cells (Ryan *et al.* 1994) were used for *in vitro* experiments investigating the effects of polyclonal FLCs on PTECs. Cells were grown on 6-well plates coated with 5 $\mu g/cm^2$ rat tail collagen. Where measurements of H_2O_2 and MCP-1 were taken, the total quantity present per well was calculated by multiplying by the volume of medium in each well, and expressed as "per day".

7.2.1 Effect of Polyclonal Free Light Chains on Inflammatory Signalling

HK-2 cells were incubated with polyclonal FLCs at 1 mg/ml or 5 mg/ml, or equimolar concentrations of delipidated HSA, or medium alone, for 24 hours (n = 6 per group). Harvested supernatants were promptly assayed for H_2O_2 and MCP-1. The results did not show significant differences in the quantities of H_2O_2 produced (figure 7.1A). In addition, there were no significant differences in the quantities of MCP-1 released from these cells (figure 7.1B). No increases in H_2O_2 or MCP-1 production were seen in wells incubated with HSA, even as high as 15 mg/ml. Positive controls were included using the same monoclonal FLCs used in experiments presented in Chapter 4, which are known to have pro-inflammatory effects on PTECs. These wells showed significantly raised concentrations of H_2O_2 and MCP-1, when compared to wells incubated with polyclonal FLCs or HSA. Given the poor response to HSA as well as polyclonal FLCs,

it may be possible that endocytosis of these proteins was not taking place. Endocytosis has previously been shown to be a key step in inflammatory signalling both in the results presented in Chapter 4 and in studies from the laboratory of Batuman.(Basnayake *et al.* 2010; Li *et al.* 2008a) However, endocytosis of HSA or polyclonal FLCs was not formally demonstrated in the studies presented here. Thus it cannot be conclusively proven in these experiments that polyclonal FLCs do not have pro-inflammatory effects on PTECs.

7.2.2 Cytotoxic Effects of Polyclonal Free Light Chains on Proximal Tubule Epithelial Cells

LDH activity in the supernatant was used as a measure of cytotoxicity of polyclonal FLCs. HK-2 cells were incubated with polyclonal FLCs at 1 mg/ml or 5 mg/ml, or equimolar concentrations of HSA, or medium alone, for 24 hours (n = 6 per group). Supernatants were assayed for LDH activity as described. The LDH activity for each well was expressed as a percentage of maximum LDH release, as assessed by lysis of cells by repeated freeze-thawing in a control plate. There was no significant difference between LDH release from cells treated with polyclonal FLC, HSA, or medium alone (figure 7.2). In positive controls using the same monoclonal FLCs used in Chapter 4, significant increases in supernatant LDH concentrations were detected. As in the previous experiments, these results must be interpreted in the context of endocytosis of HSA and polyclonal FLCs not being formally demonstrated. Thus, as with the previous experiments, it cannot be conclusively proven in these experiments that polyclonal FLCs do not have cytotoxic effects on PTECs.

Figure 7.1. Effect of polyclonal free light chains on inflammatory signalling.

Exposure of HK-2 cells to polyclonal FLCs at 1 mg/ml or 5 mg/ml did not result in an increase in H_2O_2 or MCP-1 release into the supernatant, when compared to HSA or vehicle. In addition, there was no increase in H_2O_2 or MCP-1 release into the supernatant when cells were treated with delipidated HSA, up to 15 mg/ml when compared to vehicle alone. Monoclonal FLCs (κ2 and λ2) known to initiate H_2O_2 and MCP-1 release from HK-2 cells were used as positive controls. Treatment of cells with these positive control proteins showed significant increases in the quantities of H_2O_2 and MCP-1 in the supernatants. ****p <0.0001; n = 6 per group.

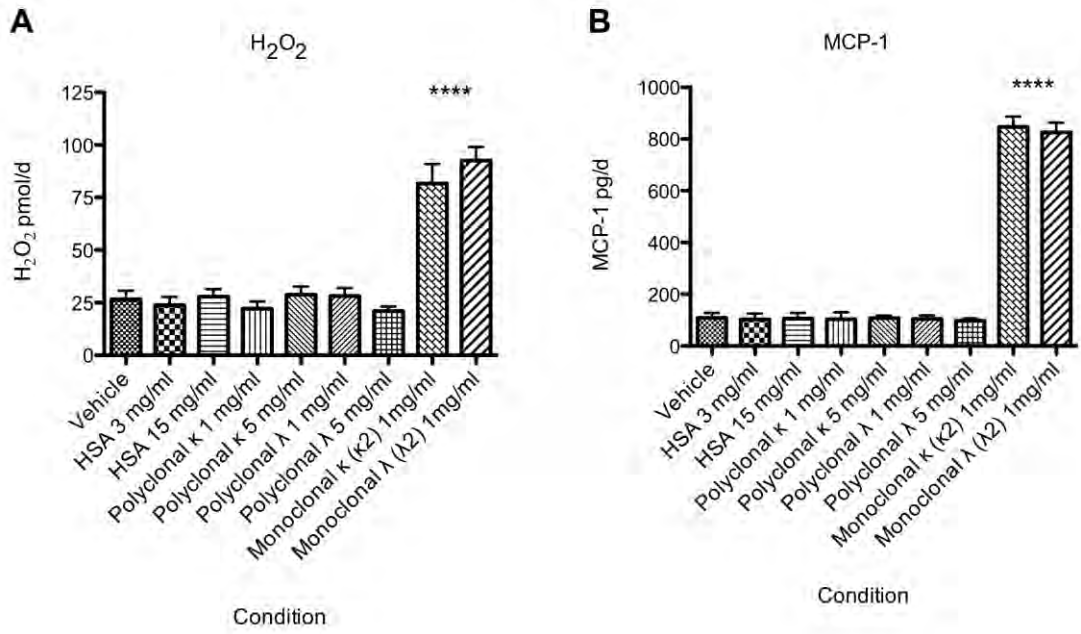

7.3 Uromodulin

7.3.1 Uromodulin is Highly Aggregated in High Salt Solutions

Uromodulin was extracted from pooled urines obtained from healthy volunteers as described. The purified protein was assessed at that stage by SDS-PAGE. Silver staining showed a faint band in the non-reduced lanes, with a broad band above, and

Figure 7.2. Cytotoxic effects of polyclonal free light chains on proximal tubule cells.

Exposure of HK-2 cells to polyclonal FLCs at 1 mg/ml or 5 mg/ml did not result in an increase in LDH release into the supernatant, when compared to HSA or vehicle. In addition, there was no increase in LDH release into the supernatant when cells were treated with delipidated HSA, up to 15 mg/ml, when compared to vehicle alone. Monoclonal FLCs (κ2 and λ2) were used as positive controls. Treatment of cells with these positive control proteins showed significant increases in the quantitiy of LDH in the supernatants. **p <0.01; n = 6 per group.

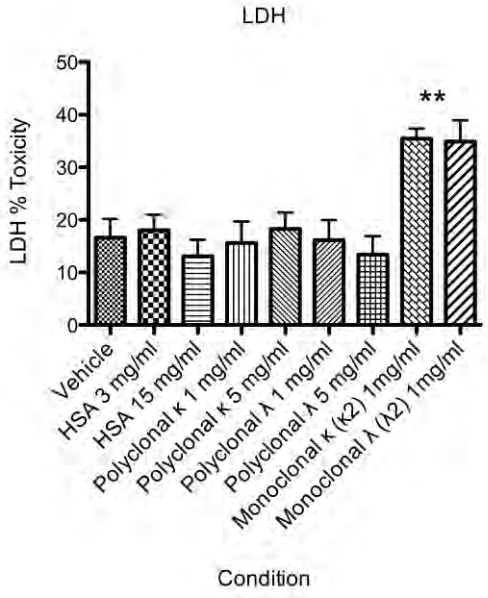

some staining at the bases of the wells (figure 7.3A). This confirms that at high salt concentrations, uromodulin is highly aggregated. Upon reduction, the proteins resolve to a single band between the 102 and 76 kDa standards. Western blotting confirmed that the bands seen on the non-reduced silver stained lanes were in fact uromodulin (figure 7.3B)

7.3.2 Uromodulin Aggregation is Reduced in Water and by Alkaline pH

The uromodulin sample was dialysed into distilled, deionised water for 24 hours. To test the effects of pH manipulation, two 36 µl aliquots were taken, and each mixed with either 4 µl of 0.5 M acetate buffer, pH 4.0, or 0.5 M Tris, pH 8.5 (pH values of 4.0 and 8.5 were confirmed by universal indicator paper testing), and incubated at 4˚C overnight. The next day, samples were separated by SDS-PAGE and visualised by silver staining (Figure 7.4). Uromodulin from a small retained aliquot in PBS (150 mM

Figure 7.3. Uromodulin from healthy volunteer urines prior to dialysis.

Silver staining (A) demonstrates the highly aggregated nature of uromodulin in saline solutions. In non-reduced lanes (5 and 6), a faint band is seen corresponding to monomeric uromodulin, with a broad band above. These resolve when reduced to a single band (lanes 2 and 3). Lanes L-R 1, standard; 2 & 3, uromodulin (reduced); 4, blank; 5 & 6, uromodulin (non-reduced). Western blotting (B) confirms that the bands seen on silver staining are indeed uromodulin, and that uromodulin exists in highly aggregated states in saline solutions. Lanes L-R 1, standard, 2 & 3, uromodulin (non-reduced).

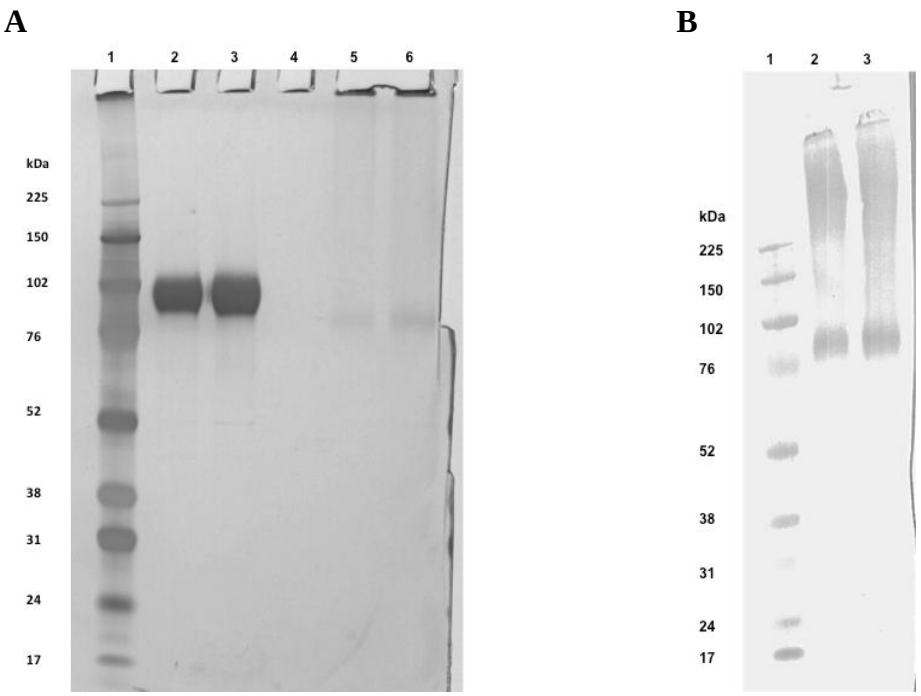

NaCl) was also loaded onto the gel. The results show that when compared to sample in PBS or at acidic pH 4 (lanes 8 and 9, non-reduced), samples dialysed into distilled, deionised water and at alkaline pH 8.5 show intensification of bands (lanes 10 and 11, non-reduced). This indicates that reducing salt concentration in the solution and alkalinisation of pH leads to reduced uromodulin aggregation. A slight upward mobility shift was noted in the lanes representing reduced protein (lanes 2 - 5), a phenomenon that remains unexplained.

Figure 7.4. Uromodulin aggregation is reduced by dialysis into water and by alkaline pH.

Uromodulin aggregation is reduced by dialysis into water and by alkaline pH, as shown by SDS-PAGE with silver staining. When compared to sample in PBS or acid pH (lanes 8 and 9), samples dialysed into water or at alkaline pH (lanes 10 and 11) show intensification of bands, indicating that reducing salt concentration and alkalinisation leads to reduced uromodulin aggregation. Lanes L-R: 1, standard; 2, PBS (reduced); 3, pH 4 (reduced); 4, water only (reduced); 5, pH 8.5 (reduced); 6, blank; 7, standard; 8, PBS (non-reduced); 9, pH 4 (non-reduced); 10, water only (non-reduced); 11, pH 8.5 (non-reduced)

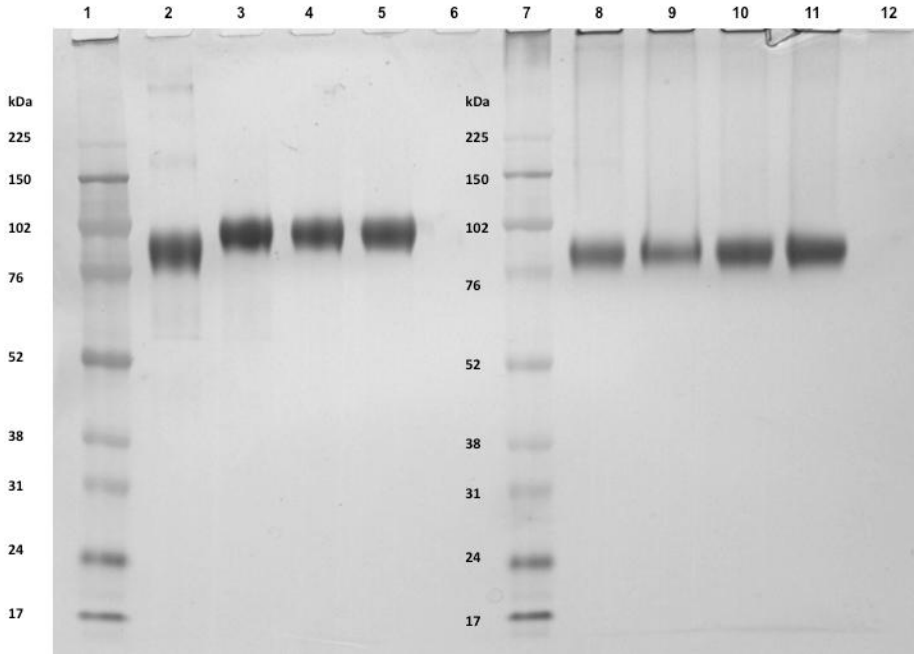

7.4 Polyclonal Free Light Chains Interact with Uromodulin: Dot Blotting

Dot blotting was used in initial experiments to assess the interaction between polyclonal FLCs and uromodulin. In one approach, polyclonal FLCs were spotted at different concentrations onto nitrocellulose membranes and the blots were incubated with either uromodulin diluted to 20 µg/ml in PBS, or PBS alone (figure 7.5). The blots were then probed with HrP conjugated antibodies against either κ or λ FLC, or an anti-uromodulin antibody that was detected by an HrP conjugated secondary antibody. Blots A and B were probed with anti-FLC antibodies, and confirm the presence of FLCs on the blot. Blot C was probed with PBS alone, without uromodulin, and shows that in the absence of uromodulin, there is no cross-reactivity between the polyclonal FLCs and the anti-uromodulin antibody. Blot D shows that uromodulin localises to the polyclonal FLCs spots, showing that there has been binding of uromodulin to polyclonal FLCs. Blot D also shows that the strength of binding is much stronger with polyclonal κ FLCs than with λ FLCs. In this experiment, despite different quantities of polyclonal FLCs being spotted onto the blots, in blot A there was no obvious variation in the intensity of dots, indicating a lack of dose-response to the quantity of polyclonal FLC spotted onto the membrane, such as seen in blot B.

In a second approach, uromodulin and HSA were spotted onto nitrocellulose membranes at varying concentrations and incubated with either polyclonal κ or λ FLCs at 25 µg/ml, or PBS alone (figure 7.6). Blots were then incubated with HrP conjugated anti-κ or anti-λ FLC antibodies. Blot A shows, as in the previous experiment, that there is binding between polyclonal FLCs and uromodulin on the blot. Blot B shows that there appears to be some cross-reactivity between the uromodulin on the membrane and

the anti-κ or anti-λ FLC antibodies. It was possible that this cross-reactivity was a result of contamination of the uromodulin with immunoglobulin in the urine, and this was addressed in the next experiment (see below). Blot C shows that in this experimental approach, no binding could be demonstrated between uromodulin and polyclonal λ FLC, in contrast to the previous experiment. No reactivity was seen between uromodulin and the HSA control spots.

Following the above experiment, a repeat dot blot was performed by spotting polyclonal FLCs onto nitrocellulose membranes at serial dilutions (figure 7.7). Uromodulin was incubated for 15 minutes with immobilised protein G (Prosep G) The blots were then incubated with uromodulin diluted to 20 µg/ml, and probed with HrP conjugated anti-κ or anti-λ FLC antibody, or anti-uromodulin antibody which was detected with a secondary antibody, as indicated in the figure.

Figure 7.5. Dot blot showing binding of polyclonal FLCs to uromodulin (polyclonal FLC dots).

Blots A and B were probed with anti-κ and anti-λ FLC antibodies, to demonstrate the presence of polyclonal FLC on the membranes. Blots C and D were probed with anti-uromodulin antibody. Blot C was incubated with PBS alone, without uromodulin, and shows no signal with anti-uromodulin antibody, confirming that in the absence of uromodulin, there is no cross-reactivity between polyclonal FLCs and this antibody. Blot D was incubated with uromodulin, then probed with anti-uromodulin antibody. This blot shows that uromodulin has localised to the polyclonal FLC spots, indicating binding. Binding of uromodulin to polyclonal κ-FLC appeared stronger than binding to polyclonal λ-FLC. Polyclonal FLCs dotted onto membrane, and incubated with uromodulin (20 µg/ml). Secondary antibodies are indicated on the right. Uro +Ctrl, uromodulin positive control.

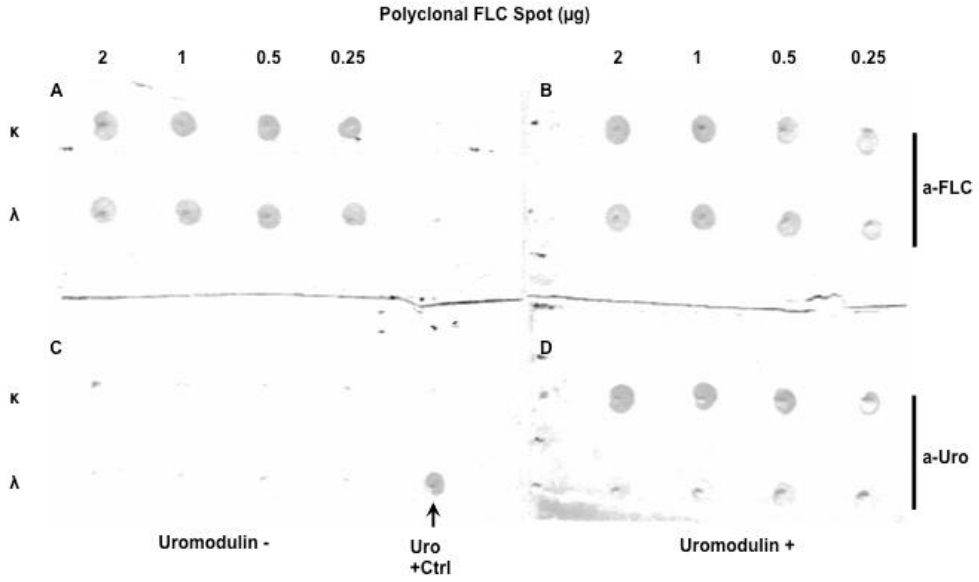

Figure 7.6. Dot blot demonstrating binding of polyclonal FLC to uromodulin (uromodulin dots).

In these blots, uromodulin and HSA have been spotted onto the membranes. Blot A was incubated with polyclonal κ-FLC, then probed with anti-κ FLC antibody. This blot shows that there is binding between uromodulin and polyclonal FLC on the blot. Blot B was incubated with PBS alone, then probed with anti-κ and anti-λ FLC antibodies. This blot shows that there is cross-reactivity between uromodulin and the antibodies. Blot C was incubated with polyclonal λ-FLC before being probed with anti-λ FLC antibody. No signal is This blot shows no signal, in contrast to Figure 7.5. Probes and secondary antibodies are indicated on the right. κ and λ polyclonal FLCs were diluted to 25 µ/ml.

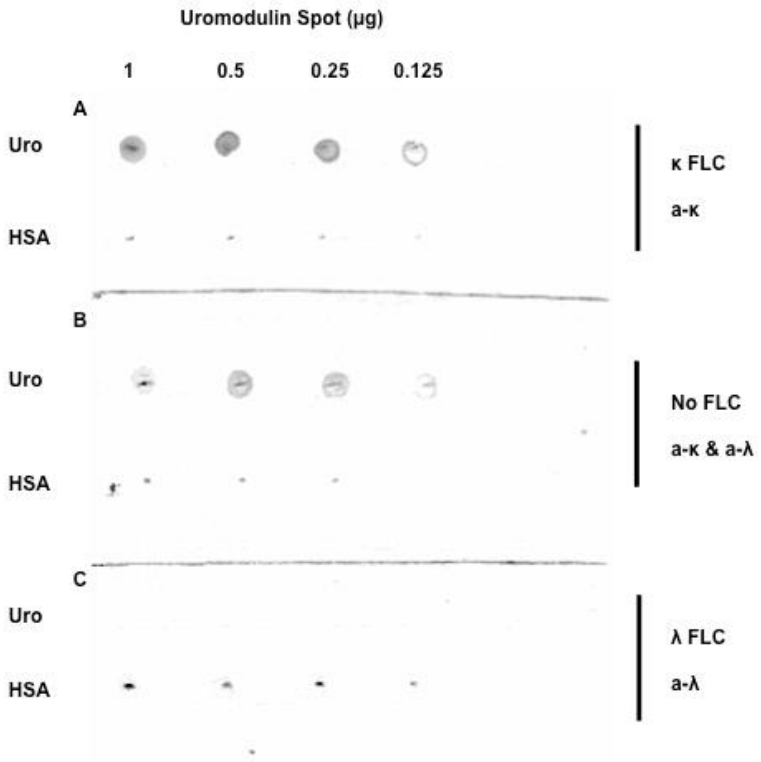

Blot A confirmed the presence of polyclonal FLC on the membrane. Blot B confirmed that there is binding of uromodulin to polyclonal FLC under these experimental conditions. Blot C showed that in the absence of uromodulin, there is no binding of anti-uromodulin antibody to the polyclonal FLCs. In blot D, uromodulin was spotted onto the membrane (1 µg). When probed with anti-κ and anti-λ FLC antibodies, no

signal was seen, confirming that the cross-reactivity seen in the previous experiment was most likely due to contamination with immunoglobulin.

Figure 7.7. Dot blot (repeated) demonstrating binding of polyclonal FLC to uromodulin (FLC dots).

In these blots A-C, polyclonal FLC has been dotted onto the membranes. Uromodulin was incubated with protein G prior to use. Polyclonal κ-FLC has been spotted onto the membranes to the left of the vertical dotted line and polyclonal λ-FLC has been spotted to the right. Blot A has been incubated with uromodulin, then probed with anti-κ FLC antibody on the left and anti-λ FLC antibody on the right. This blot confirms the presence of FLCs on the membranes. Blot B was incubated with uromodulin, then probed with anti-uromodulin antibody. This blot shows uromodulin localising to the FLC spots, indicating that there is binding between these proteins. Blot C was incubated with PBS alone, then probed with anti-uromodulin antibody. No signal is seen, confirming that in the absence of uromodulin, there is no cross-reactivity between polyclonal FLCs and anti-uromodulin antibody. In blot D, uromodulin has been spotted onto the membrane and probed with anti-κ FLC antibody on the left, and anti-λ FLC antibody on the right. No signal is seen, confirming that there is no cross-reactivity between uromodulin and the anti-FLC antibodies. Uromodulin, 20 µg/ml. Where uromodulin spotted onto membrane = 1 µg.

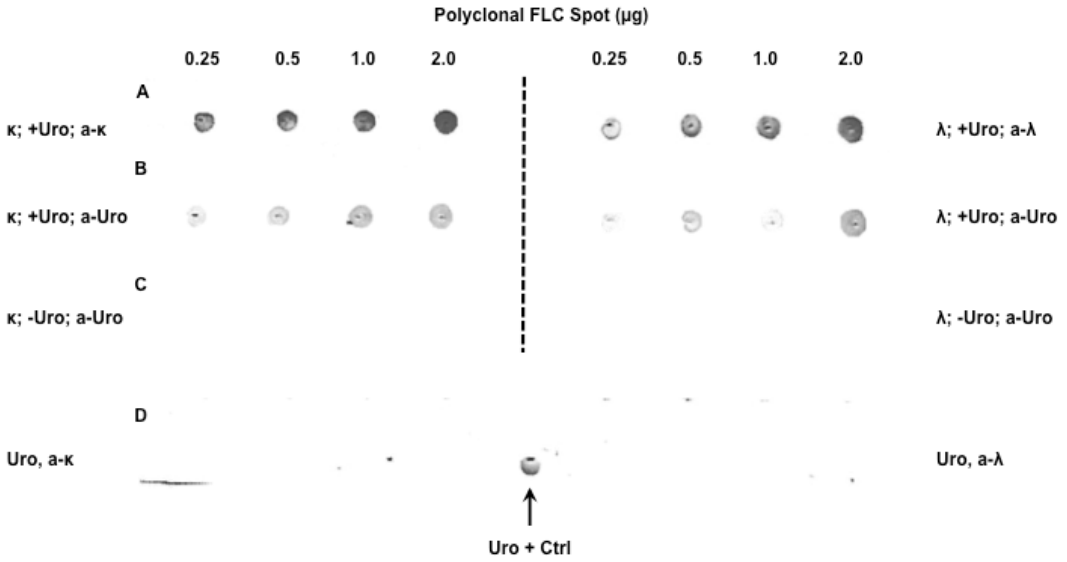

7.5 Polyclonal Free Light Chains Interact with Uromodulin: ELISA

Following the immunoblotting experiments described above, binding of uromodulin to polyclonal FLCs was assessed further by ELISA. Three approaches were used: (i) plate coated with uromodulin, (ii) plate coated with polyclonal FLCs (iii) plate coated with anti-uromodulin antibody and Sandwich type ELISA performed. Wells on each plate were loaded in triplicate, and averages of the absorbance was taken. Each plate experiment was repeated three times.

7.5.1 Plate Coated with Uromodulin

Plates were coated with uromodulin diluted to 1 μg/ml in distilled, deionised water, overnight. The next day, plates were incubated with polyclonal κ and λ FLCs as well as monoclonal κ and λ FLCs (Sigma Aldrich), all serially diluted, starting at 1 mg/ml. Equimolar HSA was also applied, serially diluted, starting from 3 mg/ml. The results are shown in figure 7.8. The results showed that both the monoclonal and polyclonal κ and λ FLCs tested had similar binding patterns to uromodulin on the plates (figure 7.8A and 7.8B). Significant binding of HSA was noted in the ELISAs. At dilutions of 1:8 and higher, there was no significant difference between binding of HSA and both the polyclonal and monoclonal FLCs. At a dilutions of 1:4 and less however, there was significantly more binding detected with both the monoclonal and polyclonal FLCs, compared to HSA. At high concentration (dilution 1:1), there was significantly more binding of polyclonal λ than polyclonal κ.

7.5.2 Plate Coated with Polyclonal Free Light Chains

Plates were coated with monoclonal and polyclonal κ and λ FLCs diluted to 1 µg/ml, or HSA 3 µg/ml, overnight. The next day, serial dilutions of uromodulin were prepared, starting at 1 mg/ml, and ELISA procedure was carried out. The results are shown in figure 7.9. No significant differences were seen between binding of polyclonal or monoclonal FLCs, or with HSA. Moreover, there were considerable variations in the readings. Readings at higher concentrations of uromodulin were not significantly different from those at lower concentrations, suggesting that there was no significant binding occurring in the wells. One other possible explanation for these results is that the coating step failed. However, in these experiments, positive controls for coating, using anti-FLC antibodies, were not included.

Figure 7.8. Assessment of binding of polyclonal FLC to uromodulin by ELISA: Plate coated with uromodulin.

A: Greater binding of polyclonal κ-FLC to uromodulin was seen when compared to HSA, at dilutions of ≤4 (**p <0.01). No difference was seen between polyclonal and monoclonal κ-FLCs. B: Similarly, greater binding of polyclonal λ-FLC to uromodulin as seen when compared to HSA, at dilutions of ≤4 (*p <0.05). No difference was seen between polyclonal and monoclonal λ-FLCs. C: Polyclonal κ-FLC showed greater binding to uromodulin than polyclonal λ-FLC at high concentration (dilution factor 1, ***p <0.001). mFLC, monoclonal FLC; pFLC, polyclonal FLC.

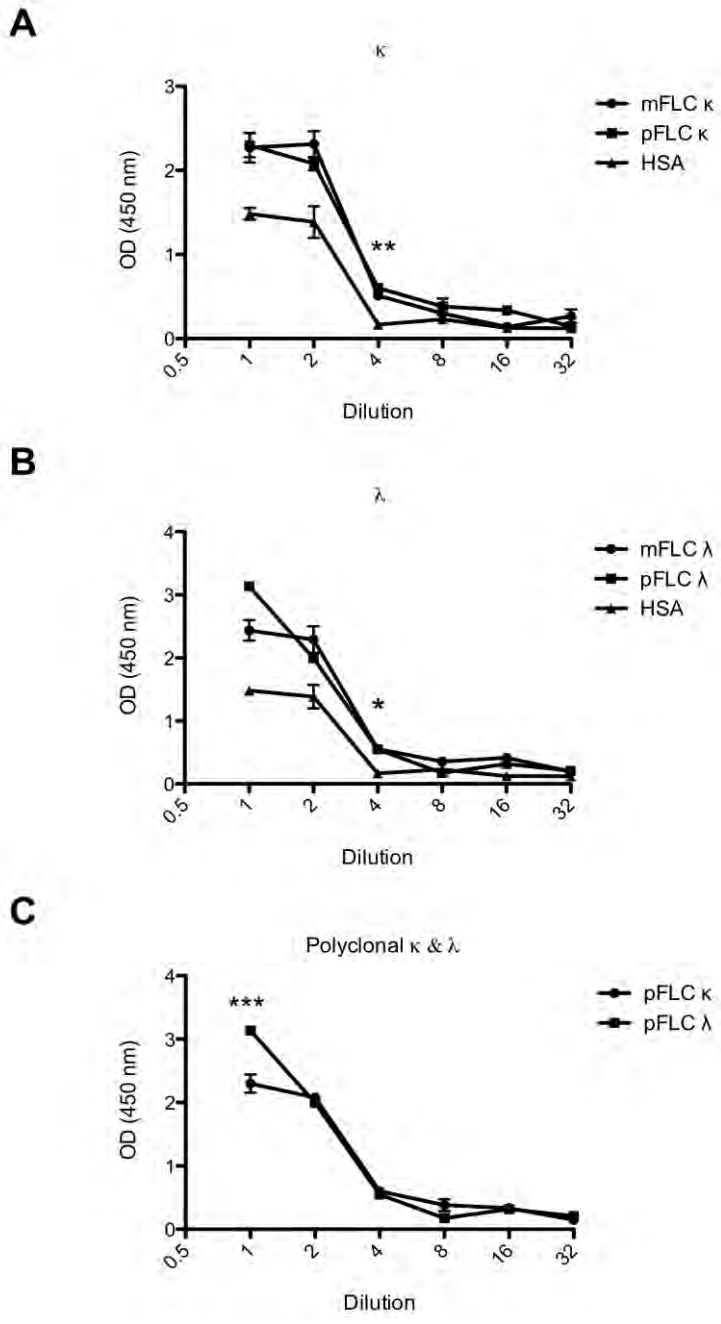

Figure 7.9. Assessment of binding of polyclonal FLC to uromodulin by ELISA: Plate coated with FLC.

ELISA procedure was carried out with the plate coated with monoclonal and polyclonal FLCs, or HSA. Incubation with even high concentrations of uromodulin showed no significant differences between the proteins were seen, and the absorbance values were low, indicating that no binding had taken place using this approach. mFLC, monoclonal FLC; pFLC, polyclonal FLC.

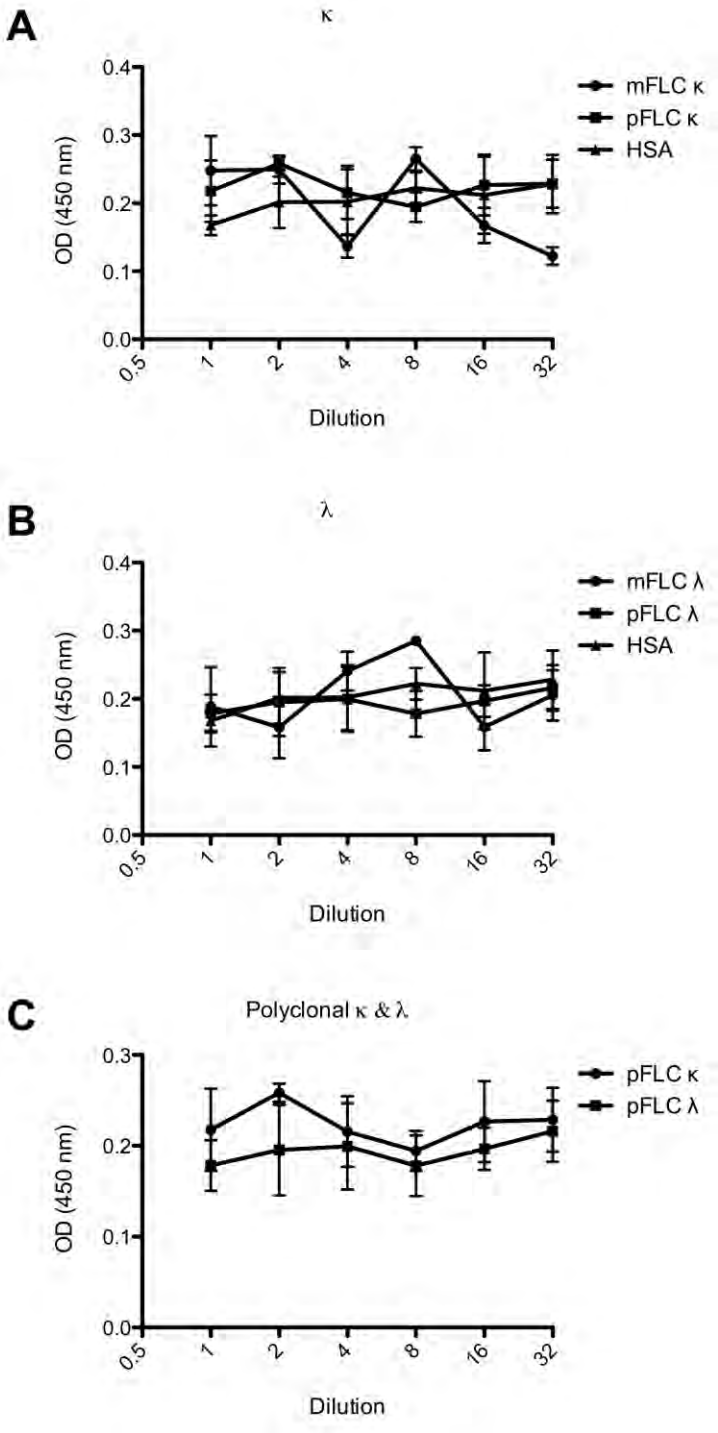

7.5.3 Sandwich ELISA

In order to address the poor binding in the above experiment, and in an attempt to reduce any background so as to improve the specificity of the assay, a sandwich approach was adopted. Anti-uromodulin antibody was diluted to 1/5000 and coated onto the plate. The next day, uromodulin was diluted to 100 µg/ml and applied to the plate, followed by serial dilutions of monoclonal and polyclonal FLCs, starting at 1 mg/ml, as well as HSA, starting at 3 mg/ml (figure 7.10). The results from this experiment were similar to the previous one. There were no significant differences between binding of polyclonal or monoclonal FLCs, or with HSA. Again, considerable variations in readings were seen. There was no dilution-dependent change in readings, suggesting, in this setting as well, that no significant binding had taken place in the wells. As with the previous experiment, one possible explanation for these results was that the coating step failed. However, a positive control, using an anti-sheep antibody, was not included.

7.6 Polyclonal Free Light Chains Interact with Uromodulin: Nephelometry

Following the findings of the ELISAs presented above, the association of polyclonal FLCs and formation of higher MW aggregates with uromodulin was assessed by nephelometry. The binding of uromodulin to proteins, can promote the formation of aggregates with an effective increase in molecular size and diameter. These larger aggregated molecules cause light to be scattered to a greater extent as it passes through the cuvette. The degree of light scatter, and therefore the degree of binding, can be assessed by means of a nephelometer (see Chapter 2).

Uromodulin was diluted to 200 µg/ml and added to equal volumes of solutions of polyclonal and monoclonal κ and λ FLCs at 500µg/ml. In this setting the final concentrations of uromodulin and FLCs were 100 µg/ml and 250 µg/ml, respectively.

The effect of altering salt concentration was assessed by using three strengths of NaCl in the PBS buffer: 50 mM, 100 mM and 150 mM. Each experiment was repeated three times. A significant amount of background scatter was detected, with PBS alone. This background scatter was not constant, and increased with time. One possibility was that gas bubbles were forming as the cuvette sat in the nephelometer for prolonged periods. However, degassing the buffer under suction prior to experiments made no difference to this background scatter (data not shown). This background was subtracted from the results presented below.

Figure 7.10. Assessment of binding of polyclonal FLC to uromodulin by ELISA: Sandwich ELISA.

Plates were coated with anti-uromodulin antibody, and then incubated with uromodulin at 100 µg/ml. Serial dilutions of monoclonal and polyclonal FLCs and HSA were then incubated in the plates. No significant differences between the proteins were seen, and the absorbance values were low, indicating that no binding had taken place using this approach. mFLC, monoclonal FLC; pFLC, polyclonal FLC.

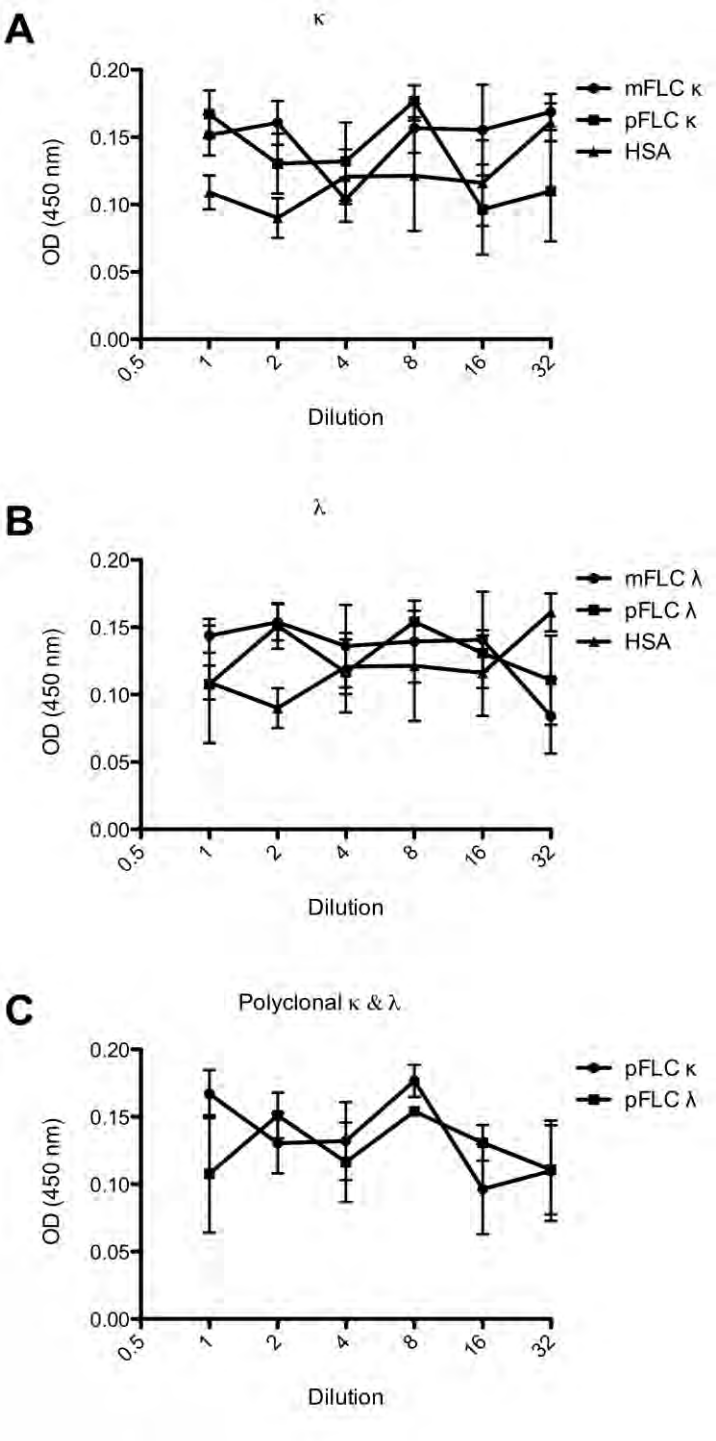

7.6.1 Experiments in Buffer Containing 50 mM NaCl

Experiments were performed with PBS containing 50 mM NaCl. Formation of higher molecular weight aggregates was detected as increases in light scatter. There were no differences between monoclonal and polyclonal κ or λ FLCs (figure 7.11). However, there were significant increases in light scatter in cuvettes containing both κ and λ polyclonal FLCs, compared to uromodulin alone (figure 7.12). No differences were detected between polyclonal FLCs and HSA.

7.6.2 Experiments in Buffer Containing 100 mM NaCl

When the concentration of NaCl was increased to 100 mM, again, there was no difference between the monoclonal and polyclonal FLCs in their binding to uromodulin, as indicated by light scatter (figure 7.13). There were significant increases in light scatter, indicating formation of higher molecular weight aggregates in cuvettes containing polyclonal FLCs with uromodulin, compared to those containing HSA with uromodulin, or uromodulin alone (figure 7.14). Differences were significant at 360 minutes, as indicated in the figure.

Figure 7.11. Nephelometric assessment of the formation of higher molecular weight aggregates with uromodulin; comparison of polyclonal and monoclonal FLCs; 50 mM NaCl.

Assessment of the formation of higher molecular weight aggregates, as determined by increased light scatter, with uromodulin in the presence of monoclonal and polyclonal and κ FLC (A) and λ FLC (B), at 50 mM NaCl. At this concentration of NaCl, no differences were seen between monoclonal and polyclonal κ-FLCs or between monoclonal and polyclonal λ-FLCs. mFLC, monoclonal FLC; pFLC, polyclonal FLC.

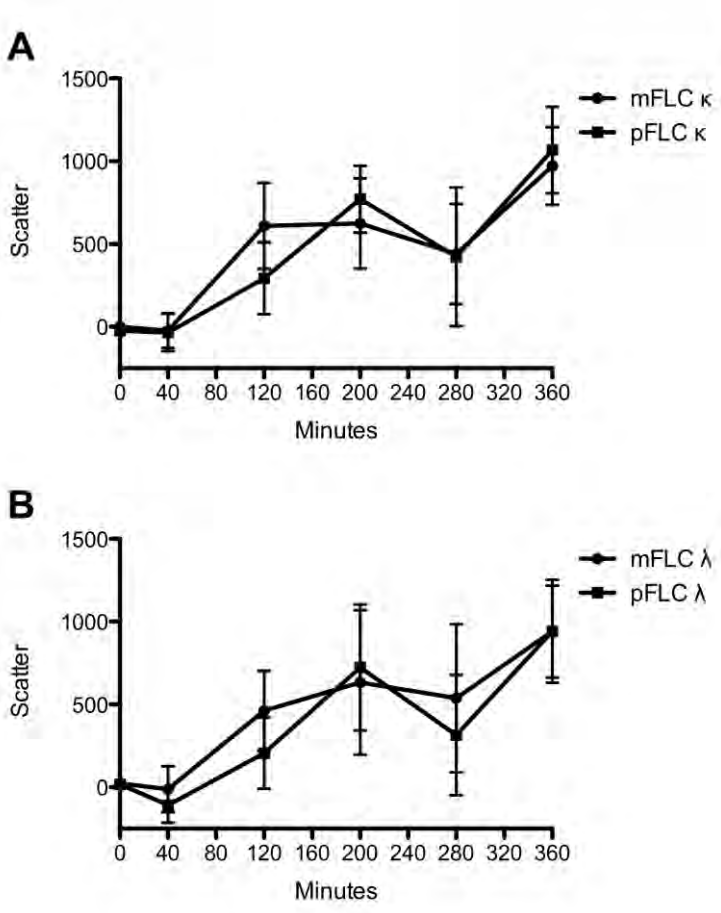

Figure 7.12. Nephelometric assessment of the formation of higher molecular weight aggregates with uromodulin; comparison of polyclonal FLCs with HSA and uromodulin; 50 mM NaCl.

Formation of higher molecular weight aggregates with uromodulin, as determined by increased light scatter, at 50 mM NaCl. Comparison of polyclonal and κ FLC (A) and λ FLC (B) with HSA and uromodulin alone. At 360 minutes, there were significantly increased light scatter readings in cuvettes containing polyclonal κ-FLC with uromodulin, when compared to uromodulin alone (**$p < 0.01$), but no difference when compared to HSA. Similarly, at 360 minutes, there were significantly increased light scatter readings in cuvettes containing polyclonal λ-FLC when compared to uromodulin alone (*$p < 0.05$), but no difference when compared to HSA.

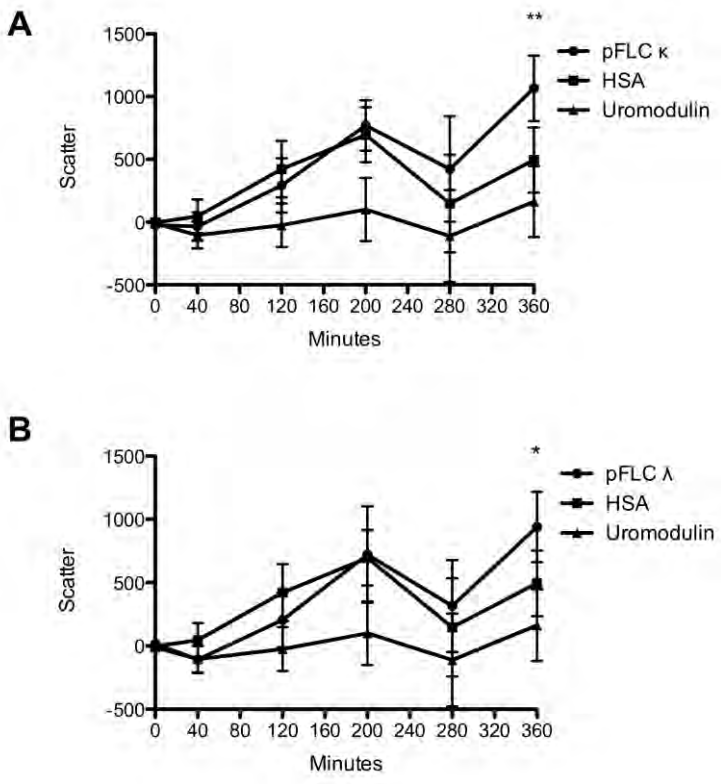

Figure 7.13. Nephelometric assessment of the formation of higher molecular weight aggregates with uromodulin; comparison of monoclonal and polyclonal FLCs; 100 mM NaCl.

Formation of higher molecular weight aggregates with uromodulin, as determined by increased light scatter, in the presence of monoclonal and polyclonal and κ FLC (A) and λ FLC (B), at 100 mM NaCl. At this concentration of NaCl, no differences were seen between polyclonal and monoclonal κ-FLCs or between polyclonal and monoclonal λ-FLCs. mFLC, monoclonal FLC; pFLC, polyclonal FLC.

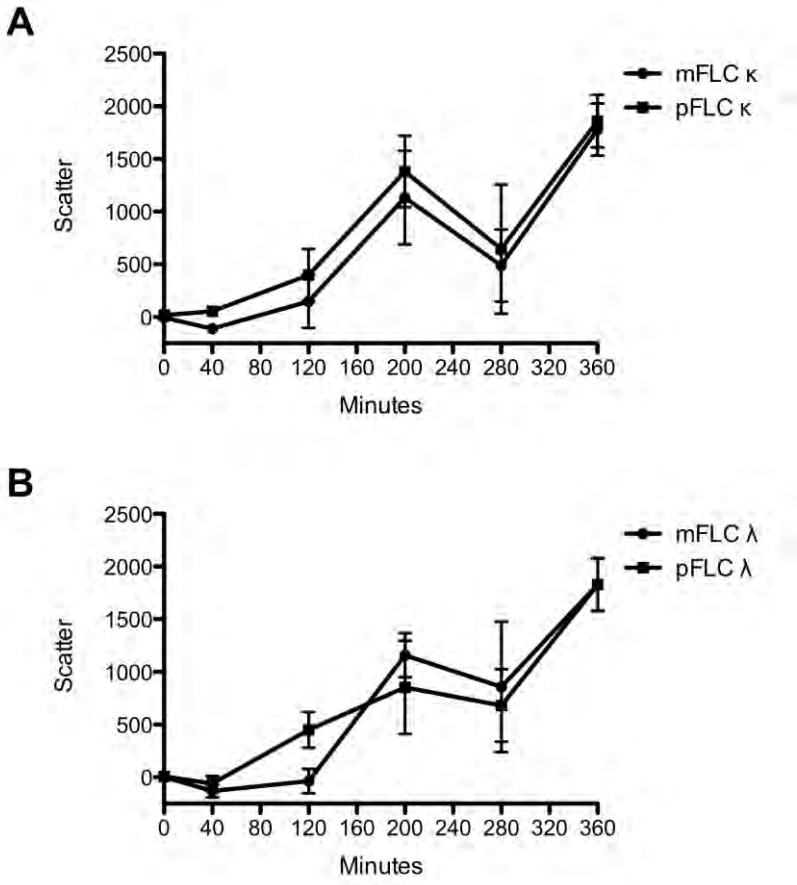

Figure 7.14. Nephelometric assessment of the formation of higher molecular weight aggregates with uromodulin; comparison of polyclonal FLCs with HSA or uromodulin alone; 100 mM NaCl.

Formation of higher molecular weight aggregates with uromodulin, as determined by increased light scatter, at 100 mM NaCl. Comparison of polyclonal and κ FLC (A) and λ FLC (B) with HSA, or uromodulin alone. At 360 minutes, there were significantly higher readings in cuvettes containing polyclonal κ-FLC when compared to compared to HSA (***$p < 0.001$), or uromodulin alone (*$p < 0.05$). pFLC, polyclonal FLC; HSA, human serum albumin.

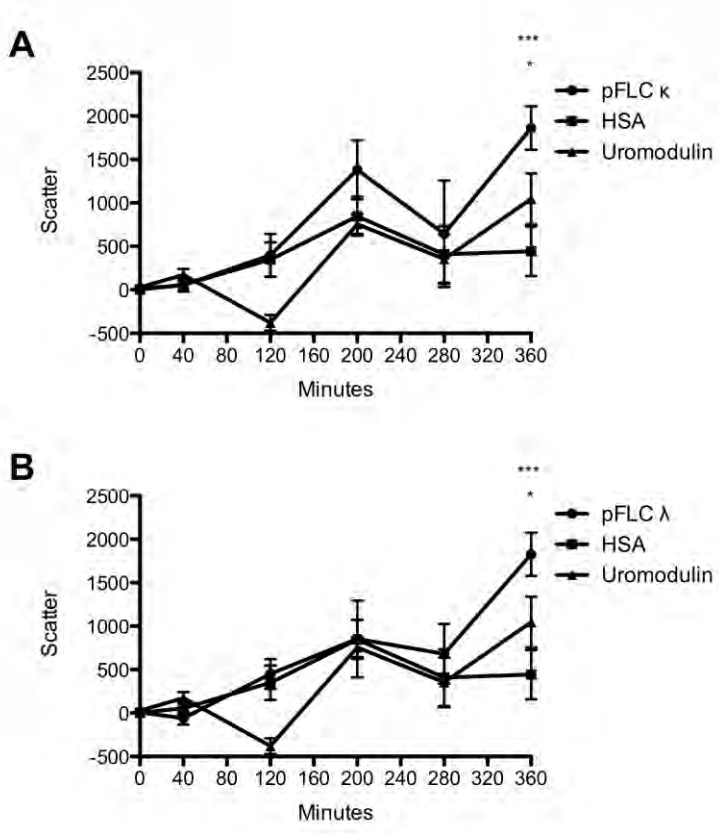

7.6.3 Experiments in Buffer Containing 150 mM NaCl

When the concentration of NaCl was increased further to 150 mM, a significant increase in aggregate formation, as indicated by increase in light scatter, was seen with polyclonal κ FLCs, compared to monoclonal κ FLCs (figure 7.15). The development of light scatter was accelerated with a significant difference seen at 120 minutes There were also significant increases in light scatter in cuvettes containing uromodulin with

both polyclonal κ and polyclonal λ FLCs, compared to those containing uromodulin with HSA, or uromodulin alone (figure 7.16). These differences were significant at an earlier stage in 150 mM NaCl than at 100 mM NaCl.

7.7 Discussion

This chapter presents results from detailed *in vitro* studies investigating the potential biological effects of polyclonal FLCs in the kidney. The results from my experiments have not demonstrated that polyclonal FLCs have a direct pro-inflammatory effect on PTECs. However, there does appear to be an interaction between polyclonal FLCs and uromodulin, which in some experiments was comparable in magnitude to that of monoclonal myeloma FLCs.

Generation of H_2O_2 after receptor mediated endocytosis has been established as the initiating event for pro-inflammatory signalling following exposure of PTECs to monoclonal FLCs.(Wang and Sanders 2007) The result of this signalling is transcription and release of inflammatory cytokines from PTECs, leading to recruitment of inflammatory cells and subsequent fibrosis. Intra-renally produced MCP-1 plays a key role in the development of fibrosis in the kidney.(Grandaliano *et al.* 1996; Prodjosudjadi *et al.* 1995) In the experiments presented here, H_2O_2 and MCP-1 in the supernatants of HK-2 cells was not increased, in contrast to the monoclonal FLCs used as positive controls, as well as demonstrated in Chapter 4.

Previous studies using monoclonal FLCs have demonstrated the cytotoxic potential of these proteins, by detecting increased release of LDH after exposure to these

FLCs.(Pote *et al.* 2000) Experiments performed with polyclonal FLCs in the present study did not show increased LDH release into the cell culture supernatants, when compared to HSA controls.

However, there were a number of limitations in the experimental designs, making a definitive conclusion impossible. In studies investigating the potential of polyclonal FLCs to initiate inflammatory signalling and cytotoxicity in PTECs, no increases in H_2O_2, MCP-1 or LDH levels were detected in supernatants of cells treated with polyclonal FLCs. Similar results were obtained when cells were treated with delipidated HSA, up to 15 mg/ml. These poor responses to HSA raises the possibility that endocytosis of these proteins was not taking place. Endocytosis is a key step in the pathway to the release of inflammatory mediators such as MCP-1; this is demonstrated by the abrogation of these responses when megalin and cubilin expression was silenced with siRNA, in Chapter 4. The presence of megalin and cubilin (demonstrated by Western blotting in Chapter 4) and robust responses to the monoclonal FLCs seen indicate that the endocytic machinery of the HK-2 cells used were functioning normally. Other laboratories have shown that delipidated albumin can induce MCP-1 release from PTECs.(Wang *et al.* 1999) However, independent studies from the laboratories of Batuman as well as Sanders have noted a lack of response from PTEC lines (SV40 transfected PTECs and HK-2 cells respectively) to delipidated HSA, at doses of up to 15 - 30 mg/ml.(Sengul *et al.* 2002; Wang and Sanders 2007) Both these laboratories have performed studies to demonstrate endocytosis of monoclonal FLCs, but have not formally shown endocytosis of HSA. As endocytosis of HSA or polyclonal FLCs was not formally demonstrated in my own studies presented in this chapter, it cannot be

conclusively proven in these experiments that polyclonal FLCs do not have pro-inflammatory effects on PTECs.

The *in vitro* studies presented in this chapter utilised type 1 collagen from rat tail tendons for thin-coating of containers, to facilitate HK-2 cell anchorage and proliferation. This type of collagen was chosen for consistency, as it has previously been used for the same purpose at independent laboratories.(Pote *et al.* 2000; Wang and Sanders 2007) However, type 4 collagen is a more physiological thin-coating agent for epithelial cells, being more abundant in basement membranes, while type 1 collagen is more abundant in the interstitium. A recent study has also indicated that type 1 collagen may promote EMT in epithelial cells, including HK-2 cells, thus raising the possibility that some of the inflammatory effects seen were attributable to the choice of thin-coating agent.(Medici and Nawshad 2010) However, low levels of H_2O_2, MCP-1 and LDH seen when cells were treated with vehicle alone indicate that the pro-inflammatory effects of the thin-coating agent were minimal.

Figure 7.15. Nephelometric assessment of the formation of higher molecular weight aggregates with uromodulin; comparison of monolconal and polyclonal FLCs; 150 mM NaCl.

Formation of higher molecular weight aggregates with uromodulin, as determined by increased light scatter, in the presence of monoclonal and polyclonal κ FLC (A) and λ FLC (B), at 150 mM NaCl. At this concentration of NaCl, a dramatic increase in light scatter was seen with polyclonal κ FLC, compared to monoclonal κ-FLC, which was evident at 40 minutes, and was significant by 120 minutes (***p < 0.001). No differences were seen between polyclonal and monoclonal λ-FLCs. mFLC, monoclonal FLC; pFLC, polyclonal FLC.

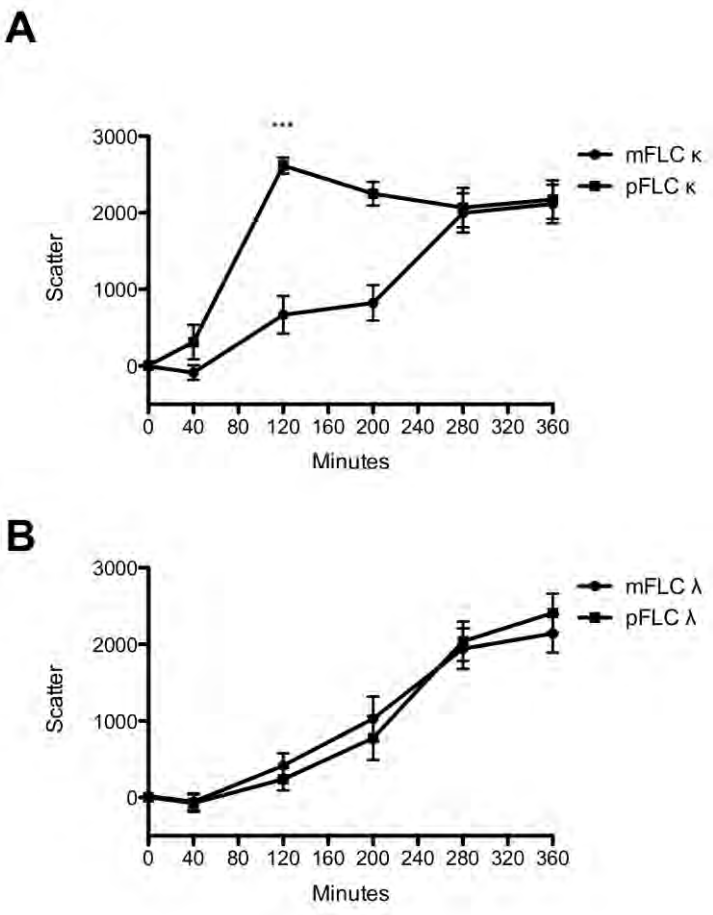

Monoclonal FLCs which are associated with inflammatory potential exert these effects by activating specific post-receptor signalling pathways.(Sengul *et al.* 2009) In successive studies, the inflammatory potential both *in vitro* and *in vivo* has been shown

Figure 7.16. Nephelometric assessment of the formation of higher molecular weight aggregates with uromodulin; comparison of polyclonal FLCs with HSA or uromodulin alone; 150 mM NaCl.

Formation of higher molecular weight aggregates with uromodulin, as determined by light scatter, at 150 mM NaCl. Comparison of polyclonal and κ FLC (A) and λ FLC (B) with HSA, or uromodulin alone. At 120 mintues, significantly increased light scatter was noted with polyclonal κ-FLC, compared with HSA (***$p < 0.001$), or with uromodulin alone (***$p < 0.001$). Significant increases in light scatter were noted with polyclonal λ-FLC, compared with HSA (***$p < 0.001$), or uromodulin alone (***$p < 0.001$) at 280 minutes. pFLC, polyclonal FLC; HSA, human serum albumin.

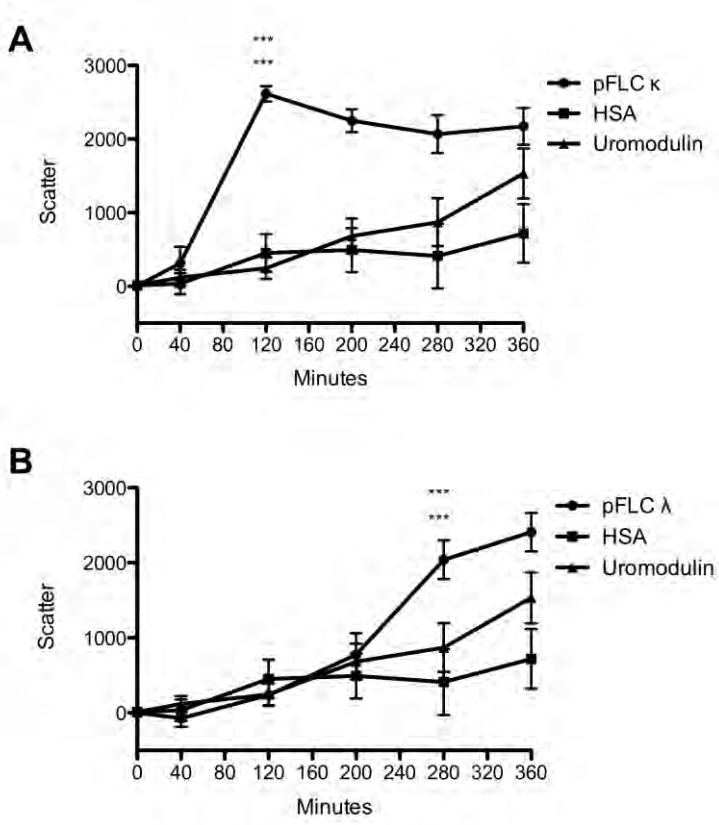

to vary from one FLC species to another.(Pote *et al.* 2000; Sengul *et al.* 2002; Sanders *et al.* 1988a; Wang and Sanders 2007) An explanation for this phenomenon may lie in the fact that due to the extreme primary structure heterogeneity of FLCs, no two FLCs are physicochemically identical.(Sanders 2005) In addition, mutations leading to

abnormal FLC primary structure are well described in plasma cell dyscrasias,(Stevens 2000) although precise associations between the physicochemical properties of the proteins and patterns of PTEC injury in myeloma cast nephropathy have not been established. However, a link between primary structure and pathology is also supported by the observation that some patients with multiple myeloma develop progressive renal failure, while there are others who excrete large quantities of urinary FLCs with little or no disturbance in renal function.(DeFronzo *et al.* 1978)

Uromodulin is a glycoprotein secreted apically by cells of the thick ascending limb of the Loop of Henle. It is initially GPI-anchored, but once this is cleaved, free uromodulin passed down the nephron, and in health, is the most abundant urinary protein.(Kumar and Muchmore 1990) Increasing the ambient NaCl or calcium ion concentrations as well as acidic pH is associated with aggregation of uromodulin molecules, and the enhanced binding of uromodulin to many low MW proteins.(Porter and Tamm 1955; Sanders *et al.* 1990; Kobayashi and Fukuoka 2001) The results presented in this chapter, of the initial analyses of uromodulin purified from healthy volunteers are in agreement with past studies, showing that aggregation of uromodulin was reduced by dialysing the protein into water, and by alkalinisation of the solution. It was therefore decided to store uromodulin in water, but mix with buffers to form physiological solutions immediately prior to use in experiments.

The binding of polyclonal FLCs to uromodulin was initially confirmed by the dot-blotting experiments. In these experiments, it appeared that the binding of polyclonal κ FLC was stronger than that of λ FLC. This was a phenomenon which had not been

described in previous studies investigating the interactions between monoclonal FLCs and uromodulin, although the numbers of proteins studied in these situations were small.(Sanders *et al.* 1990) In the initial dot-blotting experiment, one of the control blots (Figure 7.5, Blot A) failed to demonstrate a dose-response with the quantity of polyclonal κ or λ FLC dotted onto the membrane. This blot was not probed with uromodulin, therefore the result is not a reflection of interaction between uromodulin and polyclonal FLCs. The observed result was most likely explained by a method error, such as excessive exposure to HrP substrate during the development step, because subsequent blots showed that there were dose-responses.

In order to apply a more quantitative approach to these findings, ELISA was employed. The results from these experiments confirmed a dose-dependent binding relationship between polyclonal FLCs and uromodulin, when the plate was coated with uromodulin. When polyclonal FLCs were immobilised on plates, or the sandwich method was used, these experiments produced no significant results. One explanation for this might have been the fact that uromodulin in the assays was prepared in a salt-containing buffer (standard PBS with 150 mM NaCl), which might have caused significant aggregation between uromodulin molecules, a phenomenon which is known to interfere with assays where uromodulin is in the liquid phase, often necessitating treatment of the protein with strong denaturing agents prior to an ELISA-type assay.(Kjellsson *et al.* 1987; Reinhart *et al.* 1989; Kobayashi and Fukuoka 2001) One approach would have been to lower the NaCl concentration of the buffer; however, this was not performed, as a hypo-osmolar solution was likely to result in sub-optimal binding. In my own experiments, the degree of binding between polyclonal κ and polyclonal λ FLCs did not differ,

except at high concentration (1 mg/ml). Also of note was the observation that there was no difference between polyclonal and monoclonal FLCs in their binding to uromodulin in this assay.

An alternative explanation for the latter two ELISA methods (plate coated with polyclonal FLC and the sandwich method) not showing significant results was that the coating step had failed. Whilst this question was not addressed formally in my experiments, future studies should include a positive control step, using anti-FLC antibodies and anti-sheep antibodies respectively, to prove that polyclonal FLCs and the sheep-anti-human uromodulin antibody had been successfully coated onto the microplates.

Nephelometric assays were performed for two reasons: (i) to assess binding of polyclonal FLCs with uromodulin in the free liquid phase, where neither protein is tethered to a membrane or a plate; (ii) to assess the formation of higher MW aggregates. The concentrations of polyclonal FLCs used in the nephelometric experiments were within the range that would be expected in patients with CKD.(Hutchison *et al.* 2008a) The results indicate that there is indeed aggregation of uromodulin in the presence of polyclonal FLCs. This was enhanced by increasing the concentration of NaCl, and this finding was consistent with past studies.(Sanders *et al.* 1990) There was considerable background light scatter in these experiments from buffer alone, which was not constant for the duration of the experiment, and indeed increased significantly. In previous studies with monoclonal FLCs, significant light scatter due to higher MW aggregates was detectable within minutes of starting the reactions.(Sanders *et al.* 1990) In my

experiments, however, no significant differences in light scatter were detectable for up to 3 hours. This may have been a result of the different methods used, including different preparation methods of proteins, and different instrument. In addition, the proteins used in the study by Sanders *et al* were myeloma proteins, extracted from patients known to have myeloma related kidney failure. In some experiments, the scatter values were very high, approaching the upper detection limit of the nephelometer, thus explaining the flattening of curves at these values, and the minimal variation between individual results in this range.

In the proximal tubule, toxicity appears to be related to the physicochemical property of each FLC clone. In a large pool of polyclonal FLCs such as that used in the experiments described here, the importance of the toxicity of an individual FLC may be diminished. In the distal nephron however, the presence of uromodulin and ambient conditions such as NaCl and calcium concentrations, as well as pH, may play a more important role. In conclusion, in my studies, the results indicate that in the distal tubule the interaction of polyclonal FLCs might contribute to the formation of casts. Further studies would need to be undertaken to dissect out these effects in more detail. Further detailed studies are also required to assess whether polyclonal FLCs and delipidated HSA are endocytosed by HK-2 cells.

8. GENERAL DISCUSSION, IMPLICATIONS FOR FUTURE RESEARCH AND THERAPEUTIC STRATEGIES

8.1 Introduction

The experiments reported in this thesis were designed to provide further data on the pathogenic potential of monoclonal FLCs (derived from patients in myeloma) and to perform a comprehensive evaluation of the biological effects of polyclonal FLCs in the kidney and, specifically, to evaluate their potential role in the development and progression of fibrosis in the setting of CKD. The findings of these investigations further elucidated the signalling pathways that are activated by monoclonal FLCs and showed that in the distal tubule, there appears to be a detectable interaction between polyclonal FLCs and uromodulin, a ubiquitous protein, which has been shown to have potentially far-reaching biological effects.(Weichhart *et al.* 2005)

8.2 Histological Examination in Cast Nephropathy

In Chapter 3, results were presented from *in situ* measurements that were made by examining renal biopsy tissue from patients with multiple myeloma and AKI due to cast nephropathy. Historically, studies that included patients with multiple myeloma and kidney injury have not utilised histological examination of kidney tissue as a matter of routine. Indeed, there has traditionally been a reluctance to perform percutaneous biopsies in these patients. There are perhaps two reasons for this. First, the procedure of percutaneous renal biopsy, although generally considered safe in the absence of a bleeding diathesis, still carries a not inconsiderable risk of serious haemorrhage.(Parrish

1992) This risk is theoretically increased in patients with multiple myeloma.(Magee 2006; Clark *et al.* 2005) However, a recent retrospective study of 1993 patients has been reported, which showed that renal biopsy posed no excess risk in patients who had multiple myeloma.(Fish *et al.* 2010) This observation may well be explained at least in part by improved techniques, equipment, the use of ultrasound in real time, and improved after care of patients.

Second, to date there is no direct therapy to target the renal injury component of multiple myeloma, specifically cast nephropathy. Thus some physicians argue that a renal biopsy is only of academic interest and does not provide any useful additional information for diagnosis and/or treatment modification. However, as our knowledge of renal diseases associated with PCDs expands and as novel therapies become established, histological diagnosis is likely to carry increasing importance in the consideration of treatment selection and modification, as well as in stratifying risk and prognosis. For example, specific targeted therapies for cast nephropathy would require a confirmed diagnosis, in order to balance the benefit of treatment against its potential risks. One such example is the ongoing EuLITE trial, where a renal biopsy diagnosis is part of the inclusion criteria.(Hutchison *et al.* 2008b) Therefore, renal biopsies are likely to be performed with increasing frequency in this setting. Indeed, patients with cast nephropathy receiving targeted therapy may well undergo an initial diagnostic renal biopsy, with one or more subsequent biopsies performed to monitor response to treatment, direct future treatment, and determine renal prognosis.

8.3 Histological Markers of Renal Outcome in Cast Nephropathy

Two previous published studies have indicated that in the setting of myeloma cast nephropathy and acute kidney injury, the degree of chronic damage on the renal biopsy, and cast numbers are adverse determinants of renal prognosis.(Pasquali *et al.* 1987; Pozzi *et al.* 1987)

In my own investigations, a patient with persistently elevated cast numbers in a repeat biopsy did not become independent of dialysis. In the study by Pozzi *et al*, renal tissue was assessed from 24 patients, but only 16 were reported has having "myeloma kidney". In this series, fewer casts in the biopsy were associated with a more favourable renal outcome.

However, no study has so far dissected out in detail, the relationships between cast numbers, chronic damage, renal outcomes, and other predictors of progression of renal fibrosis, such as interstitial capillary density and interstitial macrophages. The degree of chronic damage seen on the biopsy has been well established as a rigorous predictor of renal prognosis and is relatively straightforward to perform and reproduce.(Howie *et al.* 2001). Such a study performed in a series of patients at might demonstrate whether or not cast numbers are a good measure of treatment efficacy and a predictor of prognosis. In my own studies, the measurement of cast numbers was shown to be relatively straightforward, and reproducible. However, it is a time consuming task. One possible alternative, not assessed in this thesis, would be to use automated or semi-automated image analysis, performed on uncounterstained sections with the intensity of staining measured as described. An appropriate choice of antibody target for staining would be

uromodulin, as this would be present in all casts. There is likely to be adequate archived tissue held within many centres, for such a study to be undertaken. The emergence of future therapies and an increased number of biopsies might permit a more robust, prospective analysis, where tissue from repeat biopsies might also be available and could be incorporated into the study.

8.4 Proximal Tubular Damage in Cast Nephropathy

In the setting of multiple myeloma and cast nephropathy, the mechanisms of proximal tubular injury have already been elucidated in some detail. In PTECs, endocytosis of monoclonal FLCs occurs through a receptor-mediated process. FLCs are delivered to the proximal tubule, where they bind to the tandem receptors megalin and cubilin.(Batuman *et al.* 1998; Klassen *et al.* 2005) Following endocytosis, the FLCs, like many other proteins, are processed within the lysosomal system, where proteolytic degradation takes place.(Batuman and Guan 1997) In the case of monoclonal FLCs which are toxic to the proximal tubule, a study from the laboratory of Sanders showed that an early event following endocytosis is the generation of H_2O_2 and intracellular oxidative stress, and that generation of this H_2O_2 was linked integrally to the downstream activation of NF-κB, transcription and release of MCP-1 from cells.(Wang and Sanders 2007) This property was not shared with non-immunoglobulin derived proteins such as albumin, which has been implicated in proximal tubule activation in other settings.(Wang *et al.* 1997; Burton *et al.* 1999)

8.4.1 The Role of c-Src in Signal Transduction

The tyrosine kinase c-Src, the 60 kDa product of the *c-src* gene is a redox sensitive enzyme, the activity of which is under tight redox control. It is a central hub in intracellular signalling networks, linking receptors to intracellular signalling cascades.(Parsons and Parsons 2004; Kim *et al.* 2009) It is involved in regulation of crucial cellular processes, such as growth, shape, differentiation, migration and survival. Interest in the involvement of c-Src in proximal tubule inflammation caused by monoclonal FLCs arose from these observations. Results from my own experiments performed at the laboratory of Sanders, using the same monoclonal FLCs, showed that the single initiating event for signal transduction was the activation of c-Src, and that this activation was dependent upon receptor-mediated endocytosis, as detailed in Chapter 4.(Basnayake *et al.* 2010)

How the activation of c-Src by H_2O_2 is linked to downstream activation of NF-κB is not yet known. The activation of NF-κB takes place through complex processes, and several pathways to activation of NF-κB have been described.(Sanz *et al.* 2010) Currently, there are over 800 compounds, both naturally occurring and synthetic, which exert their effects through activation of NF-κB.(Gilmore and Herscovitch 2006) In the canonical pathway, activating stimuli result in engagement and phosphorylation of the inhibitor complex of κB kinase (IKK). This complex phosphorylates the inhibitor subunit of κB (IκB), resulting in its ubiquitination, targeting it for degradation by proteasomes. This permits nuclear translocation of NF-κB subunits, resulting in transcription. This is a rapid and transient response. In what is referred to as the atypical pathway, tyrosine phosphorylation of IκBα can also activate NF-κB, without

involvement of the IKK complex.(Imbert *et al.* 1996) Therefore the potential implications for exposure of PTECs to monoclonal FLCs resulting in the increased activity of an intracellular tyrosine kinase such as c-Src could be far-reaching. The activation of NF-κB by multiple pathways would go some way towards explaining the excessive pro-inflammatory effects on PTECs of H_2O_2 generating monoclonal FLCs, compared to non-immunoglobulin derived proteins such as albumin. There are also potential roles for other ROS other than H_2O_2 which have yet to be explored in the setting of cast nephropathy.

8.5 Distal Tubular Damage in Cast Nephropathy

Studies from the laboratory of Sanders have also elucidated the process of cast formation in distal tubules by the co-precipitation of monoclonal FLCs with uromodulin. Cast formation has been shown to be favoured by reducing extracellular fluid volume, increasing calcium ion and sodium chloride concentrations and acidic pH; in addition, modification of the carbohydrate moiety of uromodulin by reducing the number of sialic acid residues, was shown to reduce aggregation uromodulin, but without affecting the actual binding of FLCs to uromodulin.(Sanders *et al.* 1990; Sanders and Booker 1992; Huang *et al.* 1993) Subsequently, it was shown that the CDR3 region of cast-forming monoclonal FLCs bound to a common peptide segment on uromodulin.(Ying and Sanders 2001)

8.6 Potential Therapeutic Approaches to Cast Nephropathy

8.6.1 Reduction of FLC Load Delivered to Nephrons

Work done to date has identified several potential therapeutic approaches to patients in whom multiple myeloma is complicated by kidney injury due to cast nephropathy. The quantity of monoclonal FLCs delivered to each nephron could be reduced. Two practical approaches to this exist: reduction of tumour load by chemotherapy and extracorporeal removal. If there is significant kidney injury, even if FLC production is reduced, considerable delay will be seen in the removal of the remaining FLCs from the circulation. This is because FLCs (like other low molecular weight proteins) are widely distributed in the extravascular compartment.(Hutchison *et al.* 2007) Therefore the toxic effects of FLCs may be sustained for several weeks and renal recovery might be further compromised, despite reduced production. The extravascular distribution of FLCs might also explain why clinical outcomes with the use of plasma exchange have been disappointing.(Clark *et al.* 2005) The use of extended, high cut-off haemodialysis is therefore under evaluation, as this allows longer treatment with the subsequent redistribution of FLCs from the extravascular to the intravascular compartments. Results from a pilot study have been encouraging and a multi-centre, randomised, controlled trial is currently under way.(Hutchison *et al.* 2009; Hutchison *et al.* 2008b)

8.6.2 Prevention of PTEC Damage

8.6.2.1 Prevention of Endocytosis

One therapeutic option to reduce damage sustained by PTECs would be to prevent endocytosis. Two approaches are possible here; (i) blocking binding sites on the ligand,

thus preventing it from interacting with the receptor and (ii) blocking binding sites on the receptor, thus preventing it from interacting with the ligand. Blocking the binding of ligand to receptor may be more technically challenging than the opposite, because of ongoing production of monoclonal FLCs, the wide distribution of these FLCs into extravascular compartments, which might not be accessible to a therapeutic agent and the large number of FLC molecules involved might require administration of large quantities of such an agent.

On the other hand, binding of receptor to ligand might be preventable. However, several milestones will need to be achieved before this becomes possible. Both megalin and cubilin have large ligand binding domains, making chemical inhibition potentially difficult.(Christensen and Nielsen 2006) Currently, the inhibitors available for preventing binding to megalin or cubilin are limited to neutralising antibodies. Receptor associated protein (RAP) has a chaperone-like function to megalin, and RAP deficient mice have been shown to have significantly reduced cell surface expression of megalin.(Birn *et al.* 2000) Manipulation of this protein may be another potential approach to preventing endocytosis. Finally, endocytosis might be prevented by the silencing of gene expression and transcription of megalin and cubilin. Because these receptors form part of an essential physiological recovery mechanism, permanent silencing might be deleterious in the medium to long term. In the short term, this may prove to be an effective strategy. The use of siRNA would be an ideal post-transcriptional, temporary approach to silencing of megalin and cubilin expression. Effective gene silencing by this method has been described *in vivo* for oncogenes.(Li *et al.* 2008d) However, as megalin and cubilin are continuously recycled and not rapidly

degraded, gene silencing alone will not be sufficient to prevent endocytosis, especially in the acute phase of treatment.

8.6.2.2 Reduction of Intracellular Oxidative Stress

A second therapeutic approach to protect PTECs may be through reduction of intracellular oxidative stress; as this is a key factor in activation of c-Src, it could be hypothesised that the administration of antioxidants might mitigate activation of c-Src. No *in vitro* or *in vivo* studies have been reported to date that use this approach to myeloma kidney. If such studies were undertaken, the method of delivery of such antioxidants to the cell cytoplasm would require careful consideration. Albumin-bound antioxidants such as ascorbic acid might be successfully administered orally, and enter the cells via megalin and cubilin. DMTU is a highly membrane diffusible scavenger of H_2O_2, as well as other ROS such as peroxynitrite, which has been used safely *in vivo*, and may be another potential means of ameliorating renal damage in cast nephropathy. However, because H_2O_2 is an important intracellular messenger in many cell types in response to many stimuli, careful assessments of safety in humans would be required. One notable drawback may be the interference of anti-oxidants with neutrophil function, in a group of patients already suffering form immunoparesis caused by multiple myeloma.(Jackson *et al.* 1988)

8.6.2.3 c-Src Inhibition

A third potential therapeutic approach, which may have a protective effect on PTECs, is c-Src inhibition. A number of inhibitors of Src family kinases exist, and have been used

safely *in vivo* in the treatment of malignant tumours.(Kim *et al.* 2009) No *in vivo* data have been published to date on their safety and efficacy with myeloma FLCs, however. The *in vitro* results with PP2 in my experiments were encouraging; the excess production of MCP-1 in response to monoclonal FLCs was reduced to baseline when PP2 was used, without any discernible toxicity to the cells. If its efficacy can be demonstrated *in vivo*, human studies could be undertaken. Therapy with siRNA to silence c-Src expression might also prove beneficial.

8.6.2.4 MAPK Inhibition

A further approach is through MAPK inhibition. Batuman and co-workers have shown that p38 MAPK is particularly important in renal inflammation in response to monoclonal FLCs.(Sengul *et al.* 2002) PACAP38 has been shown to inhibit the activation of p38 MAPK and ameliorate the pro-inflammatory effects of monoclonal FLCs on PTECs. This chemical compound, which acts by binding to any of three closely related G-protein coupled receptors on PTECs (PAC1, VPAC1 and VPAC2), is effective even in subnanomolar quantities both *in vitro* and *in vivo*.(Li *et al.* 2008c) mRNA for these receptors have also been detected in malignant plasma cells in multiple myeloma and the bone marrow stromal cells they grow on, while administration of PACAP38 was shown to attenuate myeloma cell growth *in vitro*.(Arimura *et al.* 2006) It was also safely used in one human, without any observed adverse effects.(Li *et al.* 2007) Further studies are now needed to determine if it can be established as an effective therapy not just for cast nephropathy, but also in other settings involving multiple myeloma.

8.6.2.5 Proteasome Inhibition

An additional consideration is proteasome inhibition. This mode of therapy would help prevent inflammatory cytokine release from PTECs by interfering with activation of NF-κB. The proteasome inhibitor bortezomib is already a well established treatment for multiple myeloma and good renal response rates have been reported when renal injury is present.(Ludwig *et al.* 2010) In this study, patients had eGFR measurements of ≤ 50 ml/min at the start of the study. An improvement in renal function was seen in 62% of patients. A good response, defined as a GFR of ≥ 60 ml/min, was achieved in only a minority of this subset (31%), the rest achieving a partial or minor improvement. The use of bortezomib in patients with cast nephropathy may confer an added benefit in mitigating renal fibrosis, although there may be good reasons why a response was not seen in more patients in this study. Firstly, the onset of renal failure is often insidious and in *de novo* patients who are not under surveillance, there may be significant established renal fibrosis by the time a diagnosis is made. Secondly, the inhibition of cytokine release from PTECs by bortezomib might be incomplete, because tyrosine phosphorylation by c-Src might activate NF-κB independently of IKK.

8.6.3 Uromodulin as a Therapeutic Target

In the distal tubule, co-precipitation of monoclonal FLCs with uromodulin as casts is associated with physical damage to the nephron, including obstruction of flow and invasion of the tubule by inflammatory cells.(Weiss *et al.* 1981; Sanders *et al.* 1990) Damage to the tubule may result in spillage of tubular contents into the interstitium. Casts may therefore underlie additional inflammatory processes within the kidney that

contribute to fibrosis. Central to the formation of casts is uromodulin.(Sanders *et al.* 1990) in which two distinct but related processes must be considered. First, the binding of monoclonal FLCs to uromodulin and second, the aggregation of uromodulin molecules, which is influenced by environmental factors. The binding of monoclonal FLC to uromodulin has been shown to be preventable *in vitro* by a peptide with a sequence corresponding to CDR3 of FLC.(Ying and Sanders 2001) No *in vivo* data has been published to date, but it is a potentially attractive strategy for preventing cast formation. The importance of supportive care cannot be overstated here. Aggregation of uromodulin is promoted by slow tubular flow, increased NaCl and calcium ion concentrations, acidic pH, and the presence of drugs such as furosemide.(Sanders and Booker 1992; Huang and Sanders 1995) Many of these factors, which are all reversible, will be present in patients with cast nephropathy at diagnosis. Finally, it has also been shown that colchicine alters the carbohydrate moiety of uromodulin, and reduces aggregation. Administration of colchicine over long periods of time is not practical, especially in the setting of acute kidney injury. However, short-term administration might be another strategy to reduce cast formation, but has yet to be tested in humans.

It is a major undertaking to assess the utility of a new therapy in clinical practice; careful pilot studies are required and followed by well-designed randomised controlled trials. However, all the approaches outlined above may be applicable to improving outcomes in people with myeloma cast nephropathy and even CKD.

8.7 The Inflammatory Role of Filtered Proteins in CKD

In both cast nephropathy and CKD, the release of cytokines from PTECs in response to activating stimuli, may result in the recruitment of inflammatory cells and progressive fibrosis. Whilst cast nephropathy is predominantly caused by monoclonal FLCs, in CKD there are a number of factors including the leakage of low molecular weight proteins (<40 kDa) and some intermediate molecular weight proteins (40–100 kDa) from the glomerulus, which are then presented to PTECs and may be activating these cells.(D'Amico and Bazzi 2003) As CKD progresses, the number of functioning nephrons declines. This appears to lead to compensatory hypertrophy and hyperfiltration occurring in the remaining healthy nephrons.(Kriz and LeHir 2005) This leads to the PTECs in these remaining nephrons being exposed to increased quantities of low molecular weight proteins and intermediate molecular weight proteins also. The most abundant intermediate molecular weight protein is albumin; polyclonal FLCs also constitute a significant proportion of low molecular weight proteins filtered. PTECs endocytose and process these proteins, and this protein overloading leads to intracellular pro-inflammatory signalling, resulting in activation of NF-κB and transcription of cytokines, notably MCP-1. Thus a self-perpetuating vicious circle is established in CKD, which ensures that once nephron loss and fibrosis begins, it is likely to continue.

8.8 The Role of Polyclonal FLCs in CKD

8.8.1 The Effects of Polyclonal FLCs on PTECs

One aim of the experiments presented in this thesis was to determine whether polyclonal FLCs had a similar pro-inflammatory effect to monoclonal FLCs. Whilst

there were no responses to polyclonal FLCs in the experiments, this observation may well be due to failure of the cells to endocytose these proteins. The studies presented in this thesis have shown that the endocytic receptors of HK-2 cells were functioning normally with respect to monoclonal FLCs. However, as the polyclonal FLCs used were demonstrated to be pure proteins, produced without the use of any denaturing processes, it was presumed that these proteins were handled no differently to any other class of protein. In fact the immunofluorescence studies performed on renal biopsies from patients with CKD demonstrated that polyclonal FLCs localised to the cytoplasms of PTECs. The lack of response of HK-2 cells to delipidated HSA was another factor which indicated a problem with endocytosis. While there are studies in the literature which demonstrate definite responses of PTECs to delipidated HSA, my own findings are not inconsistent with those from previous studies reported by Batuman and Sanders. However, it cannot be concluded from my findings that polyclonal FLCs do not have pro-inflammatory potential in PTECs without undertaking an endocytosis study, by fluorochrome-labelling polyclonal FLCs and observing their co-localisation with cells after exposure.

It could be hypothesised that, because the potential toxicity of FLCs varies from one light chain clone to another and is caused by the differential ability to generate H_2O_2, which is most likely related to differences in primary structure, polyclonal FLCs may well not possess the same pro-inflammatory potential as monoclonal FLCs. Indeed, different monoclonal FLCs generated different quantities of H_2O_2 and induced MCP-1 release to different degrees *in vitro*.(Wang and Sanders 2007) It is therefore possible that polyclonal FLCs, despite being found in increased concentrations in sera in CKD,

do not exert an excess biological effect when compared to other filtered proteins because they do not produce H_2O_2 in the same way as some monoclonal FLCs and therefore do not initiate inflammatory signalling.

8.8.2 The Interaction of Uromodulin and Polyclonal FLCs in CKD

My experiments demonstrated a link in the distal tubule between polyclonal FLCs and uromodulin. I observed in CKD, proteinaceous precipitates, similar to casts. The distribution of these casts were largely limited to areas of chronic damage. Immunofluorescence showed that these proteins consisted of uromodulin, and contained polyclonal FLCs. Polyclonal FLCs were shown to bind to uromodulin *in vitro* with more avidity than HSA. The relationship between these casts and markers of progression of CKD were examined in detail. It has previously been shown that the index of chronic damage, interstitial macrophage numbers and peritubular capillary density are interrelated.(Eardley *et al.* 2006; Eardley *et al.* 2008) The findings of my own studies showed that cast numbers were correlated positively with the index of chronic damage and interstitial infiltrating macrophage numbers, and negatively correlated with interstitial peritubular capillary density.

These findings raise two broad hypotheses. First, as chronic damage becomes established and progresses, the loss of capillary density leads to an ischaemic tubular microenvironment. This in turn causes reduced tubular flow and dysregulation of both proximal and distal tubular function. There may also be impairment of resorptive capacity of PTECs, leading to increased delivery of polyclonal FLCs to the distal tubule. Dysregulation of distal tubular function may alter electrolyte content and pH of

tubular fluid, perhaps aided in part by medications such patients will be taking, such as angiotensin converting enzyme inhibitors and loop diuretics. These factors may combine to facilitate cast formation in such tubules. The intra-nephronal obstruction then accelerates nephron loss and may represent an important component of the CKD pathway.

Second, the presence of these casts in CKD have traditionally not been considered to have pathophysiological relevance, and to represent incidental findings in areas of the kidney which have already been scarred to a degree beyond functional recovery. However, the presence of uromodulin in these casts may be important as uromodulin is a molecule which has a complex relationship with the immune system.(Weichhart *et al.* 2005) It is capable of activating macrophages via TLR4.(Saemann *et al.* 2005) and it has also been shown that infiltrating macrophages are concentrated in areas of chronic damage, where casts were also found in the present studies.(Eardley *et al.* 2008) Tubules in areas of chronic damage may have weakened epithelia and basement membranes, permitting the leakage of uromodulin into the interstitium. This might then have an additive chemoattractant and activating effect on macrophages. This is supported by a recent study, which showed that in CKD, diminishing eGFR was associated with increased concentrations of uromodulin in blood and that addition of uromodulin to whole blood led to release of inflammatory cytokines.(Prajczer *et al.* 2010) Uromodulin has also been shown to facilitate transmigration of neutrophils across epithelial membranes.(Schmid *et al.* 2010) Furthermore, Eardley *et al* have indicated that once significant chronic damage is established, factors other than albuminuria alone

may play a part in macrophage recruitment to the kidney.(Eardley *et al.* 2008) It is possible that one such factor is uromodulin.

Additional evidence that uromodulin might be related to development of CKD exists in the form of genomic studies. Kottgen *et al* have shown that single nucleotide polymorphisms (SNP) at the UMOD gene locus, which encodes uromodulin, are associated with an increased incident risk of CKD.(Kottgen *et al.* 2009) They subsequently also showed that urinary uromodulin concentrations were associated with incident risk of CKD.(Kottgen *et al.* 2010)

8.9 Conclusion

Collectively, the results presented in this thesis indicate that polyclonal FLCs in CKD might promote cast formation in the distal tubules, leading to uromodulin interacting with macrophages and thereby promoting fibrosis. This conclusion has considerable implications, because it identifies uromodulin as a potential therapeutic target, with the aim of delaying the progression of CKD. Thus disrupting the interaction of uromodulin with polyclonal FLCs may slow loss of renal function. However, the risks of such an approach might be significant, and must be evaluated carefully. One possible therapy that is already in use in this setting is the administration of oral sodium bicarbonate to patients with CKD who are acidaemic. A recent study showed that bicarbonate supplementation in patients with advanced CKD slowed the decline in renal function.(de Brito-Ashurst *et al.* 2009) Although other mechanistic explanations for this phenomenon may be important, it is also possible to hypothesise that the resultant alkalinisation of urine resulted in fewer casts forming within tubules.

The treatment of progressive CKD, in the absence of identifiable underlying diseases (e.g. ANCA associated vasculitis, SLE, etc) is usually limited to control of blood pressure and diabetes, if either are present, and blockade of the renin-angiotensin system. CKD affects a significant proportion of the adult population and constitutes a major health economic problem. Identification of additional therapeutic targets are therefore crucial. Further studies are now required to elucidate relationships between uromodulin, macrophages and fibrosis in CKD.

9. PUBLICATIONS & ABSTRACTS FROM THIS THESIS

9.1 Papers

9.1.1 Basnayake K, Hutchison C, Kamel D, Sheaff M, Ashman N, Cook M, Oakervee H, Bradwell A, Cockwell P: Resolution of cast nephropathy following free light chain removal by haemodialysis in a patient with multiple myeloma: a case report. *J Med Case Reports* 2**:** 380, 2008.

9.1.2 Basnayake K, Cheung CK, Sheaff M, Fuggle W, Kamel D, Nakoinz N, Hutchison CA, Cook M, Stoves J, Bradwell AR, Cockwell P: Differential progression of renal scarring and determinants of late renal recovery in sustained dialysis dependent acute kidney injury secondary to myeloma kidney. *J Clin Pathol* 63**:** 884-887, 2010.

9.1.3 Basnayake K, Ying WZ, Wang PX, Sanders PW: Immunoglobulin light chains activate tubular epithelial cells through redox signaling. *J Am Soc Nephrol* 21**:** 1165-1173, 2010.

9.1.4 Ying WZ, Wang PX, Aaron KJ, Basnayake K, Sanders PW: Immunoglobulin light chains activate NF-κB in renal epithelial cells through a Src-dependent mechanism. *Blood*: In press.

9.2 Abstracts

9.2.1 Basnayake K, Cheung CK, Hutchison CA, Stringer SJ, Cook M, Rylance P, et al. Differential progression of renal scarring and determinants of late renal recovery in sustained dialysis dependent acute kidney injury secondary to myeloma kidney. . British Renal Society/Renal Association Conference; 2010; Manchester 2010.

9.2.2 Basnayake K, Ying WZ, Wang PX, Cockwell P, Bradwell AR, Hutchison CA, et al. Myeloma Light Chains Activate Tubular Epithelial Cells by a c-Src Mediated Redox Signaling Mechanism. . British Renal Society/Renal Association Conference; 2010; Manchester 2010.

9.2.3 Basnayake K, Ghonemy T, Sanders PW, Hutchison CA, Stringer SJ, Bradwell AR, et al. An assessment of the pathogenicity of polyclonal immunoglobulin free light chains in chronic kidney disease. . British Renal Society/Renal Association Conference; 2010; Manchester2010.

10. APPENDIX

A.1 Antibodies Used for IHC

Target Antigen	Label	Dilution	Species	Vendor/Product No
Albumin (Hu)	-	1:2500	Sh(PC)	/PC032
Calbindin D28K (Hu)	-	1:3000	Mo(MC)	Sigma-Aldrich/C9848
CD34 (Hu)	-	1:25	Mo(MC)	Dako/M7165
CD68 (Hu)	-	1:200	Mo(MC)	Dako/M0814
Cubilin (Y20); (Hu)	-	1:250	Gt(PC)	Santa Cruz
GAPDH (Hu)	-	1:10000	Mo(MC)	Abcam
Gt Ig's	HrP	1:20000	Dk(PC)	Santa Cruz
IgA α chain (Hu)	FITC	1:100	Sh(PC)	/AF010
IgA α chain (Hu)	-	1:2500	Sh(PC)	/AU010
IgG (Mo)	DyLight 549	1:100	Sh(PC)	The Binding Site/AU271
IgG γ chain (Hu)	FITC	1:100	Sh(PC)	/AF004
IgG γ chain (Hu)	-	1:2500	Sh(PC)	/AU004
IgM μ chain (Hu)	FITC	1:100	Sh(PC)	/AF012
IgM μ chain (Hu)	-	1:2500	Sh(PC)	/AU012
Megalin (C19); (Hu)	-	1:250	Gt(PC)	Santa Cruz
Mo Ig's	biotinylated	1:100	Rb(PC)	Dako/E0354
Mo IgG1 isotype	-	1:100	Mo(MC)	Dako/X0931

Target Antigen	Label	Dilution	Species	Vendor/Product No
Phospho-cSrc (Y416); (Hu)	-	1:1000	Rb(PC)	Cell Signalling
Rb Ig's	HrP	1:5000	Sh(PC)	/AP311
Sh Ig's	HrP	1:5000	Dk(PC)	/AP360
Sh IgG isotype	FITC	1:100	Sh(PC)	
Total c-Src (Hu)	-	1:1000	Rb(PC)	Cell Signalling
Transferrin (Hu)	-	1:2500	Sh(PC)	/PC070
Uromodulin (Hu)	DyLight 549	1:100	Sh(PC)	/PC071
κ FLC (Hu)	FITC	1:100	Sh(PC)	/PX016
κ LC (Hu)	-	1:2500	Rb(PC)	Dako/A0191
κ LC (Hu)	HrP	1:2500	Sh(PC)	/AP015
κ LC (Hu)	-	-	Sh(PC)	/AU015
λ FLC (Hu)	DyLight 649	1:50	Sh(PC)	/PX018
λ LC (Hu)	-		Rb(PC)	Dako/A0193
λ LC (Hu)	HrP	1:2500	Sh(PC)	/AP017
λ LC (Hu)	-	-	Sh(PC)	/AU017

Sh, sheep; Hu, human Mo, mouse; MC, monoclonal; PC, polyclonal; Rb, rabbit; Gt, goat; Dk, donkey;

A.2 Buffers and Solutions

Solution or Buffer	Recipe

Solution or Buffer	Recipe
4',6-diamidino-2-phenylindole, dilactate (DAPI)	Stock (10.95 mM): 10 mg lyophilised powder dissolved in 2 ml in ddH2O Working solution (300 nM): Stock diluted 1:36500 in PBS
Acetate buffer for coupling	Sodium acetate 0.1 M Sodium chloride 0.5 M Water pH corrected to 4.0 with acetic acid
Acetic acid 0.02 Normal	1 ml glacial acetic acid (Fisher Scientific) 869 ml cell culture grade water (Invitrogen)
AEC staining solution	AEC stock 0.5 ml Acetate buffer 9.5 ml () Filter Hydrogen peroxide 6 µl.
Avidin and biotin block	0.1% avidin in Tris-HCl, ready-to-use 0.01% biotin in Tris-HCl, ready-to-use (Dako)
Citrate buffer for HIER	Tri-sodium citrate 0.01 M (Sigma-Aldrich) pH corrected to 6.0
Coomassie – destain solution	Ethanol 15% v/v Acetic acid 7.5% v/v
Coomassie – Fixative solution	Ethanol 40 % v/v Acetic acid 10% v/v

Solution or Buffer	Recipe
Coupling buffer for Sepharose	Sodium hydrogen carbonate 0.1 M
	Sodium chloride 0.5 M
	Water
	pH corrected to 8.3
Glycine elution buffer	Glycine 0.1 M (Sigma-Aldrich)
	pH corrected to 3.0
Goat serum block	Wash buffer
	Goat serum 10% v/v (Dako)
HCl for coupling	1000 ml water; remove 83.3 µl
	83.3 µl concentrated (11 M) HCl
HK-2 cell freezing medium	DMSO 7.5% v/v (Sigma-Aldrich)
	K-SFM (Invitrogen)
Hydrogen peroxide block	Methanol (Fisher Scientific)
	Hydrogen peroxide (Sigma-Aldrich) 0.3% v/v
Mouse serum block	Wash buffer
	Mouse serum 10% v/v (Dako)
Neutralisation buffer for elutants	Tris 2 M
	Sodium chloride 1.5 M
	pH corrected to 8.0

Solution or Buffer	Recipe
Phosphate buffered saline (PBS)	Sodium dihydrogen orthophosphate 25 mM (Sigma-Aldrich) Sodium chloride 150 mM (Sigma-Aldrich) pH corrected to 7.2
Variation: PBS-T, Tween-20 added	Tween-20 (Sigma-Aldrich) 0.05% added to some solutions
Phosphate buffered saline for cell culture (PBS)	Ready-to-use (Invitrogen)
Rabbit serum (normal)	Wash buffer Rabbit serum 10% v/v (Dako)
Rabbit serum block	Wash buffer Rabbit serum 10% v/v (Dako)
Rat tail collagen - coating, 5 µg/ml	1 ml Rat tail collagen type 1 (Invitrogen) Dilute 1:1000 in 0.02 Normal acetic acid
Sheep serum block	Wash buffer Sheep serum 10% v/v ()
Silver stain – developer solution	Sodium carbonate 2.5 g Formaldehyde 8 µl Make to 100 ml in ultrapure water

Solution or Buffer	Recipe
Silver stain – sensitisation reagent	Sodium acetate 3.4 g
	Sodium thiosulphate 0.1 g
	Industrial methylated spirit 15 ml
	Glutaraldehyde 0.26 ml
	Make to 50 ml with ultrapure water
Silver stain – silver solution	Silver nitrate 0.05 – 0.06 g
	Formaldehyde 7 µl
	Make to 50 ml in ultrapure water
Silver stain – stop solution	Tris 25 g
	Acetic acid 11 ml
	Make to 500 ml in ultrapure water
Size-exclusion chromatography	Sodium chloride 200 mM
(SEC) buffer	Sodium dihydrogen orthophosphate 25 mM
	pH corrected to 7.2
Sodium borate buffer (antibody	Sodium borate 0.67 M, pH 8.5, ready-to-use
labelling)	(Thermo Scientific Pierce)
Sudan black B (0.1% w/v)	5 ml 70% ethanol (Fisher Scientific) v/v in
	ddH2O
	5 mg Sudan black B (Sigma-Aldrich)
Tris-buffered saline	Tris 50 mM (Sigma-Aldrich)
(TBS)	Sodium chloride 150 mM
	pH corrected to 7.6
Variation: TBS-T, Tween-20 added	Tween-20 0.05% added to some solutions

Solution or Buffer	Recipe
Tris-HCl for coupling	Sodium chloride 0.5 M Tris 0.2 M Water pH corrected to 8.0 Filtered to 0.45 µm
Trypsin for cell detachment	Trypsin 0.05%, EDTA 0.2 g/L, ready-to-use (Invitrogen)
Western blotting blocking solution	Skim milk (Marvel or Bio-Rad) 5% w/v TBS-T

ddH2O, deionised distilled water;

A.3 SDS-PAGE - Gel Recipes and Calculation of Measures

	Stacking Gel		**Resolving Gel**	
	4%	7.5%	12%	X%
40% Acrylamide/Bis	2.5ml	18.8ml	30ml	2.5(X%) = A
0.5M Tris-HCl, pH6.8	6.3ml	-	-	-
1.5M Tris-HCl pH8.8	-	25ml	25ml	25ml
10% SDS	250µl	1ml	1ml	1ml
dH_2O	15.9ml	54.7ml	43.5ml	73.5ml – A
TEMED	25µl	50µl	50µl	50µl
10% APS	125µl	500µl	500µl	500µl
Total Volume	25ml	100ml	100ml	100ml

A.4 Useful Common Protein Extinction Coefficients for A280 Measurements

Protein	Extinction Coefficient
Human albumin	4.5
Human Ig free light chain	11.8
Human IgG	13.8
Sheep IgG	14.5

A.5 BCA Assay Standards, Working Range 20 – 2000 µg/ml

Vial	Diluent Volume (µl)	BSA Volume (µl)	Final BSA Conc (µg/ml)
A	0	300 of stock	2000
B	125	375 of stock	1500
C	325	325 of stock	1000
D	175	175 of vial B	750
E	325	325 of vial C	500
F	325	325 of vial E	250
G	325	325 of vial F	125
H	400	100 of vial G	25
I	400	0	0

A.6 Useful Numbers for Cell Culture

Dish/Plate	Area (mm^2)	Seeding Density	Cells at Confluency	Trypsin Vol (ml)	Medium Vol (ml)
35 mm	962	0.3×10^6	1.2×10^6	1	2
60 mm	2827	0.8×10^6	3.2×10^6	2	3
100 mm	7854	2.2×10^6	8.8×10^6	3	10
150 mm	17671	5.0×10^6	20.0×10^6	8	20
6-well	962	0.3×10^6	1.2×10^6	2	3-5
12-well	401	0.1×10^6	0.4×10^6	1	1-2
24-well	200	0.05×10^6	$0.2x\ 10^6$	0.5	0.5-1.0
T-25	2500	0.7×10^6	2.8×10^6	3	3-5
T-75	7500	2.1×10^6	8.4×10^6	5	8-15
T-160	16000	4.6×10^6	18.4×10^6	10	15-30

Number of cells varies with cell type, these numbers are a rough guide.

A.7 Amino Acids

Amino Acid	Abbreviation	1-Letter	Hydropathy Score
Alanine	Ala	A	1.8
Arginine	Arg	R	-4.5
Asparagine	Asn	N	-3.5
Aspartic Acid	Asp	D	-3.5
Cysteine	Cys	C	2.5
Glutamic Acid	Glu	E	-3.5

Amino Acid	Abbreviation	1-Letter	Hydropathy Score
Glutamine	Gln	Q	-3.5
Glycine	Gly	G	-0.4
Histidine	His	H	-3.2
Isoleucine	Ile	I	4.5
Leucine	Leu	L	3.8
Lysine	Lys	K	-3.9
Methionine	Met	M	1.9
Phenylalanine	Phe	F	2.8
Proline	Pro	P	-1.6
Serine	Ser	S	-0.8
Threonine	Thr	T	-0.7
Tryptophan	Trp	W	-0.9
Tyrosine	Tyr	Y	-1.3
Valine	Val	V	4.2

A.8 E-TOXATE Endotoxin Assay Interpretation of Results

Tube	Interpretation

Tube				Interpretation
A Sample	B Sample (LAL Inhibitor Control)	C Negative Control	D – I Endotoxin Standards	
		Result		
-	+	-	+	Endotoxin at a level below the detection limits of assay.
+	+	-	+	Sample contains endotoxin equal to, or greater than, the amount present in the most dilute Endotoxin Standard giving a positive result.
+	+	+	+	Since negative control shows a hard gel, endotoxin contamination of water, glassware or LAL reagent is present.
-	-	-	+	Absence of hard gel in Tube B and presence of hard gel in Tube D show that sample contains an inhibitor of LAL reagent. Test is not valid.
-/+	-/+	-	-	LAL reagent or endotoxin standard has deteriorated. Sample results are not valid unless Tubes B and D show hard gels.

Tubes D – I contain endotoxin standards at 0.5 – 0.015 EU/ml

A.9 Normal HK-2 Cells

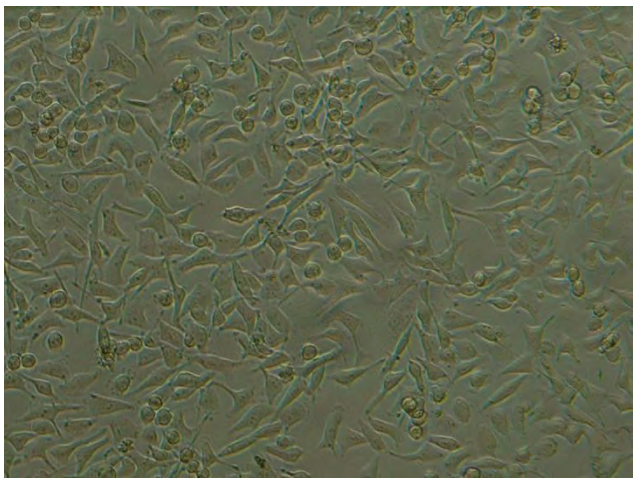

A.10 A Neubauer Haemocytometer

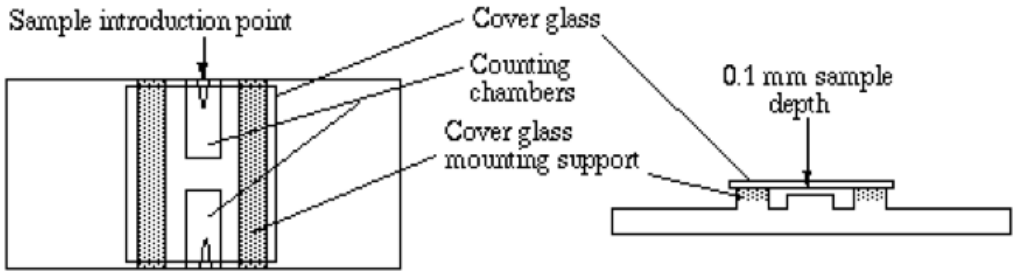

(Courtesy of David Caprette)

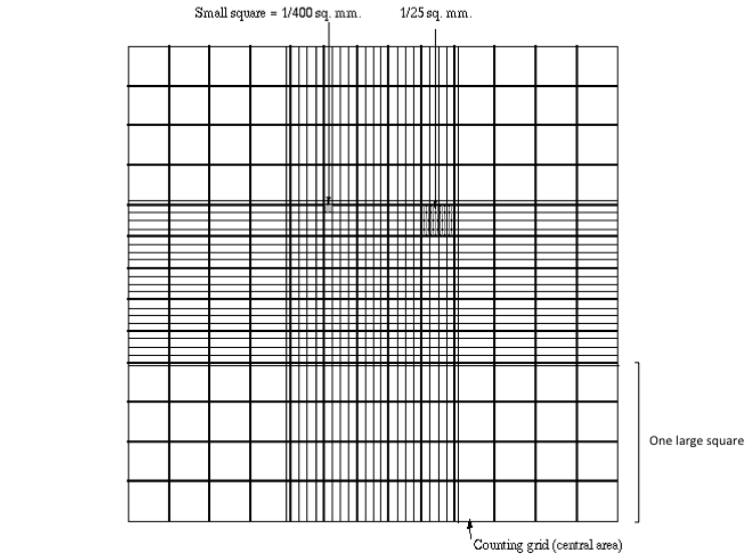

(Courtesy of David Caprette)

A.11 siRNA Mode of Action

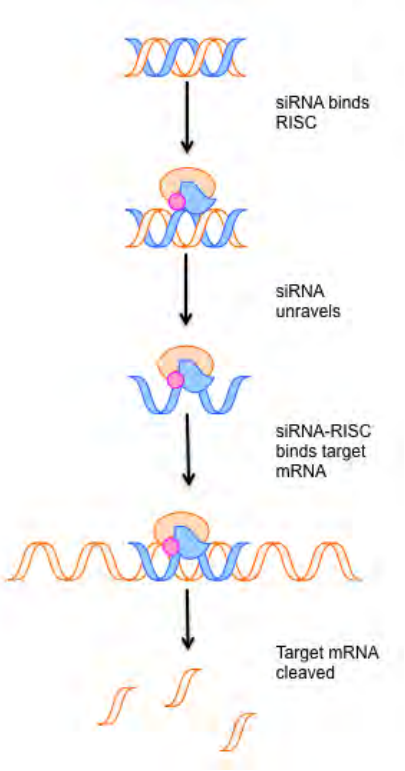

A.12 Chromatography Apparatus

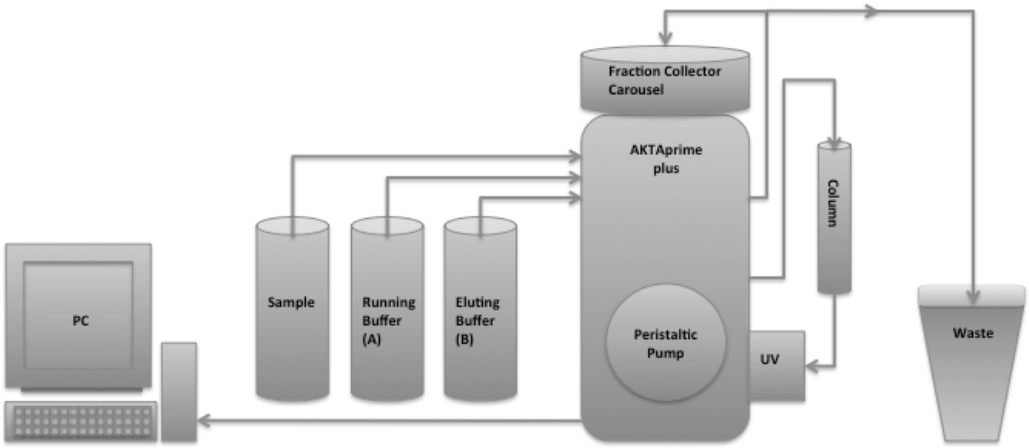

11. REFERENCES

Abbate, M., Zoja, C., Corna, D., *et al.* 1998. In progressive nephropathies, overload of tubular cells with filtered proteins translates glomerular permeability dysfunction into cellular signals of interstitial inflammation. *J Am Soc Nephrol,* 9**,** 1213-24.

Abraham, G. N. & Waterhouse, C. 1974. Evidence for defective immunoglobulin metabolism in severe renal insufficiency. *Am J Med Sci,* 268**,** 227-33.

Abraham, R. S., Geyer, S. M., Price-Troska, T. L., *et al.* 2003. Immunoglobulin light chain variable (V) region genes influence clinical presentation and outcome in light chain-associated amyloidosis (AL). *Blood,* 101**,** 3801-8.

Abuelo, J. G. 2007. Normotensive ischemic acute renal failure. *N Engl J Med,* 357**,** 797-805.

Alpers, C. E., Magil, A. B. & Gown, A. M. 1989. Macrophage origin of the multinucleated cells of myeloma cast nephropathy. *Am J Clin Pathol,* 92**,** 662-5.

Alpers, C. E., Tu, W. H., Hopper, J., Jr., *et al.* 1985. Single light chain subclass (kappa chain) immunoglobulin deposition in glomerulonephritis. *Hum Pathol,* 16**,** 294-304.

Ancsin, J. B. & Kisilevsky, R. 2001. Serum amyloid A peptide interactions with glycosaminoglycans. Evaluation by affinity chromatography. *Methods Mol Biol,* 171**,** 449-456.

Anders, H. J., Banas, B. & Schlondorff, D. 2004. Signaling danger: toll-like receptors and their potential roles in kidney disease. *J Am Soc Nephrol,* 15**,** 854-67.

Arakawa, T. & Timasheff, S. N. 1985. Theory of protein solubility. *Methods Enzymol,* 114**,** 49-77.

Arimura, A., Li, M. & Batuman, V. 2006. Potential protective action of pituitary adenylate cyclase-activating polypeptide (PACAP38) on in vitro and in vivo models of myeloma kidney injury. *Blood,* 107**,** 661-8.

Bang, F. B. 1956. A bacterial disease of Limulus polyphemus. *Bull Johns Hopkins Hosp,* 98**,** 325-51.

Baschong, W., Suetterlin, R. & Laeng, R. H. 2001. Control of autofluorescence of archival formaldehyde-fixed, paraffin-embedded tissue in confocal laser scanning microscopy (CLSM). *J Histochem Cytochem,* 49**,** 1565-72.

Basnayake, K., Ying, W. Z., Wang, P. X., *et al.* 2010. Immunoglobulin light chains activate tubular epithelial cells through redox signaling. *J Am Soc Nephrol,* 21**,** 1165-73.

Bate, K. L., Clouston, D., Packham, D., *et al.* 1998. Lambda light chain induced nephropathy: a rare cause of the Fanconi syndrome and severe osteomalacia. *Am J Kidney Dis,* 32**,** E3.

Bates, J. M., Raffi, H. M., Prasadan, K., *et al.* 2004. Tamm-Horsfall protein knockout mice are more prone to urinary tract infection: rapid communication. *Kidney Int,* 65**,** 791-7.

Batuman, V., Dreisbach, A. W. & Cyran, J. 1990. Light-chain binding sites on renal brush-border membranes. *Am J Physiol,* 258**,** F1259-65.

Batuman, V. & Guan, S. 1997. Receptor-mediated endocytosis of immunoglobulin light chains by renal proximal tubule cells. *Am J Physiol,* 272**,** F521-30.

Batuman, V., Guan, S., O'Donovan, R., *et al.* 1994. Effect of myeloma light chains on phosphate and glucose transport in renal proximal tubule cells. *Ren Physiol Biochem,* 17**,** 294-300.

Batuman, V., Sastrasinh, M. & Sastrasinh, S. 1986. Light chain effects on alanine and glucose uptake by renal brush border membranes. *Kidney Int,* 30**,** 662-5.

Batuman, V., Verroust, P. J., Navar, G. L., *et al.* 1998. Myeloma light chains are ligands for cubilin (gp280). *Am J Physiol,* 275**,** F246-54.

Bellotti, V., Mangione, P. & Merlini, G. 2000. Review: immunoglobulin light chain amyloidosis--the archetype of structural and pathogenic variability. *J Struct Biol,* 130**,** 280-9.

Berggard, I. & Peterson, P. A. 1969. Polymeric forms of free normal kappa and lambda chains of human immunoglobulin. *J Biol Chem,* 244**,** 4299-307.

Bienert, G. P., Moller, A. L., Kristiansen, K. A., *et al.* 2007. Specific aquaporins facilitate the diffusion of hydrogen peroxide across membranes. *J Biol Chem,* 282**,** 1183-92.

Birn, H. & Christensen, E. I. 2006. Renal albumin absorption in physiology and pathology. *Kidney Int,* 69**,** 440-9.

Birn, H., Spiegelstein, O., Christensen, E. I., *et al.* 2005. Renal tubular reabsorption of folate mediated by folate binding protein 1. *J Am Soc Nephrol,* 16**,** 608-15.

Birn, H., Vorum, H., Verroust, P. J., *et al.* 2000. Receptor-associated protein is important for normal processing of megalin in kidney proximal tubules. *J Am Soc Nephrol,* 11**,** 191-202.

Blade, J., Fernandez-Llama, P., Bosch, F., *et al.* 1998. Renal failure in multiple myeloma: presenting features and predictors of outcome in 94 patients from a single institution. *Arch Intern Med,* 158**,** 1889-93.

Bland, J. M. & Altman, D. G. 1986. Statistical methods for assessing agreement between two methods of clinical measurement. *Lancet,* 1**,** 307-10.

Bock, H. A. 1997. Pathogenesis of acute renal failure: new aspects. *Nephron,* 76**,** 130-42.

Bohne, S., Sletten, K., Menard, R., *et al.* 2004. Cleavage of AL amyloid proteins and AL amyloid deposits by cathepsins B, K, and L. *J Pathol,* 203**,** 528-37.

Bonvini, P., Zorzi, E., Basso, G., *et al.* 2007. Bortezomib-mediated 26S proteasome inhibition causes cell-cycle arrest and induces apoptosis in CD-30+ anaplastic large cell lymphoma. *Leukemia,* 21**,** 838-42.

Bradwell, A. R. 2006. *Serum Free Light Chain Analysis,* Birmingham, The Binding Site Ltd.

Bradwell, A. R. 2010. *Serum Free Light Chain Analysis,* Birmingham, The Binding Site Ltd.

Bradwell, A. R., Carr-Smith, H. D., Mead, G. P., *et al.* 2001. Highly sensitive, automated immunoassay for immunoglobulin free light chains in serum and urine. *Clin Chem,* 47**,** 673-80.

Brown, M. T. & Cooper, J. A. 1996. Regulation, substrates and functions of src. *Biochim Biophys Acta,* 1287**,** 121-49.

Bruccoleri, R. E., Haber, E. & Novotny, J. 1988. Structure of antibody hypervariable loops reproduced by a conformational search algorithm. *Nature,* 335**,** 564-8.

Bruneval, P., Foidart, J. M., Nochy, D., *et al.* 1985. Glomerular matrix proteins in nodular glomerulosclerosis in association with light chain deposition disease and diabetes mellitus. *Hum Pathol,* 16**,** 477-84.

Burton, C. J., Combe, C., Walls, J., *et al.* 1999. Secretion of chemokines and cytokines by human tubular epithelial cells in response to proteins. *Nephrol Dial Transplant,* 14**,** 2628-33.
Camargo, M. J., Sumpio, B. E. & Maack, T. 1984. Kinetics of renal catabolism of absorbed proteins: influence of lysosomal pH. *Contrib Nephrol,* 42**,** 19-29.
Catalan, M. P., Subira, D., Reyero, A., *et al.* 2003. Regulation of apoptosis by lethal cytokines in human mesothelial cells. *Kidney Int,* 64**,** 321-30.
Chothia, C. & Lesk, A. M. 1987. Canonical structures for the hypervariable regions of immunoglobulins. *J Mol Biol,* 196**,** 901-17.
Chothia, C., Lesk, A. M., Tramontano, A., *et al.* 1989. Conformations of immunoglobulin hypervariable regions. *Nature,* 342**,** 877-83.
Christensen, E. I. & Birn, H. 2001. Megalin and cubilin: synergistic endocytic receptors in renal proximal tubule. *Am J Physiol Renal Physiol,* 280**,** F562-73.
Christensen, E. I. & Nielsen, R. 2006. Role of megalin and cubilin in renal physiology and
pathophysiology. *Reviews of Physiology, Biochemistry and Pharmacology.* Heidelberg: Springer Berlin Heidelberg.
Cicchetti, D. V. & Feinstein, A. R. 1990. High agreement but low kappa: II. Resolving the paradoxes. *J Clin Epidemiol,* 43**,** 551-558.
Clark, W. F., Stewart, A. K., Rock, G. A., *et al.* 2005. Plasma exchange when myeloma presents as acute renal failure: a randomized, controlled trial.[see comment][summary for patients in Ann Intern Med. 2005 Dec 6;143(11):I20; PMID: 16330784]. *Annals of Internal Medicine,* 143**,** 777-84.
Clyne, D. H., Pesce, A. J. & Thompson, R. E. 1979. Nephrotoxicity of Bence Jones proteins in the rat: importance of protein isoelectric point. *Kidney Int,* 16**,** 345-52.
Clyne, D. H. & Pollak, V. E. 1981. Renal handling and pathophysiology of Bence Jones proteins. *Contrib Nephrol,* 24**,** 78-87.
Cohen, G., Haag-Weber, M., Mai, B., *et al.* 1995. Effect of immunoglobulin light chains from hemodialysis and continuous ambulatory peritoneal dialysis patients on polymorphonuclear leukocyte functions. *J Am Soc Nephrol,* 6**,** 1592-9.
Cohen, G., Rudnicki, M., Deicher, R., *et al.* 2003. Immunoglobulin light chains modulate polymorphonuclear leucocyte apoptosis. *Eur J Clin Invest,* 33**,** 669-76.
Cohen, J. 1960. A coefficient of agreement for nominal scales. *Educ Psychol Meas,* 20**,** 37-46.
Comenzo, R. L., Zhang, Y., Martinez, C., *et al.* 2001. The tropism of organ involvement in primary systemic amyloidosis: contributions of Ig V(L) germ line gene use and clonal plasma cell burden. *Blood,* 98**,** 714-20.
Cooper, J. A. & Howell, B. 1993. The when and how of Src regulation. *Cell,* 73**,** 1051-4.
Cowen, T., Haven, A. J. & Burnstock, G. 1985. Pontamine sky blue: a counterstain for background autofluorescence in fluorescence and immunofluorescence histochemistry. *Histochemistry,* 82**,** 205-8.
D'Amico, G. & Bazzi, C. 2003. Pathophysiology of proteinuria. *Kidney Int,* 63**,** 809-25.
Darby, I., Skalli, O. & Gabbiani, G. 1990. Alpha-smooth muscle actin is transiently expressed by myofibroblasts during experimental wound healing. *Lab Invest,* 63**,** 21-9.

Day, E. D. 1990. The Light Chains of Immunoglobulins. *In:* Day, E. D. (ed.) *Advanced Immunochemistry*. New York: Wiley.

de Brito-Ashurst, I., Varagunam, M., Raftery, M. J., *et al.* 2009. Bicarbonate supplementation slows progression of CKD and improves nutritional status. *J Am Soc Nephrol,* 20**,** 2075-84.

Decourt, C., Bridoux, F., Touchard, G., *et al.* 2003. A monoclonal V kappa l light chain responsible for incomplete proximal tubulopathy. *Am J Kidney Dis,* 41**,** 497-504.

DeFronzo, R. A., Cooke, C. R., Wright, J. R., *et al.* 1978. Renal function in patients with multiple myeloma. *Medicine (Baltimore),* 57**,** 151-66.

Dember, L. M. 2006. Amyloidosis-associated kidney disease. *J Am Soc Nephrol,* 17**,** 3458-71.

Dember, L. M., Sanchorawala, V., Seldin, D. C., *et al.* 2001. Effect of dose-intensive intravenous melphalan and autologous blood stem-cell transplantation on al amyloidosis-associated renal disease. *Ann Intern Med,* 134**,** 746-53.

Denoroy, L., Deret, S. & Aucouturier, P. 1994. Overrepresentation of the V kappa IV subgroup in light chain deposition disease. *Immunol Lett,* 42**,** 63-6.

Deret, S., Chomilier, J., Huang, D. B., *et al.* 1997. Molecular modeling of immunoglobulin light chains implicates hydrophobic residues in non-amyloid light chain deposition disease. *Protein Eng,* 10**,** 1191-7.

Deret, S., Denoroy, L., Lamarine, M., *et al.* 1999. Kappa light chain-associated Fanconi's syndrome: molecular analysis of monoclonal immunoglobulin light chains from patients with and without intracellular crystals. *Protein Eng,* 12**,** 363-9.

DeYulia, G. J., Jr., Carcamo, J. M., Borquez-Ojeda, O., *et al.* 2005. Hydrogen peroxide generated extracellularly by receptor-ligand interaction facilitates cell signaling. *Proc Natl Acad Sci U S A,* 102**,** 5044-9.

Divry, P. & Florkin, M. 1927. Sur les proprietes optiques de l'amyloide. *C R Soc Biol,* 97**,** 1808-1810.

Dominici, S., Valentini, M., Maellaro, E., *et al.* 1999. Redox modulation of cell surface protein thiols in U937 lymphoma cells: the role of gamma-glutamyl transpeptidase-dependent H2O2 production and S-thiolation. *Free Radic Biol Med,* 27**,** 623-35.

Duque, N., Gomez-Guerrero, C. & Egido, J. 1997. Interaction of IgA with Fc alpha receptors of human mesangial cells activates transcription factor nuclear factor-kappa B and induces expression and synthesis of monocyte chemoattractant protein-1, IL-8, and IFN-inducible protein 10. *J Immunol,* 159**,** 3474-82.

Dwulet, F. E., O'Connor, T. P. & Benson, M. D. 1986. Polymorphism in a kappa I primary (AL) amyloid protein (BAN). *Mol Immunol,* 23**,** 73-8.

Eardley, K. S., Kubal, C., Zehnder, D., *et al.* 2008. The role of capillary density, macrophage infiltration and interstitial scarring in the pathogenesis of human chronic kidney disease. *Kidney Int*.

Eardley, K. S., Zehnder, D., Quinkler, M., *et al.* 2006. The relationship between albuminuria, MCP-1/CCL2, and interstitial macrophages in chronic kidney disease. *Kidney Int,* 69**,** 1189-97.

Edelman, G. M., Gall, W. E., Waxdal, M. J., *et al.* 1968. The covalent structure of a human gamma G-immunoglobulin. I. Isolation and characterization of the whole molecule, the polypeptide chains, and the tryptic fragments. *Biochemistry,* 7**,** 1950-8.

Elbashir, S. M., Harborth, J., Lendeckel, W., *et al.* 2001. Duplexes of 21-nucleotide RNAs mediate RNA interference in cultured mammalian cells. *Nature,* 411**,** 494-8.
Enqvist, S., Sletten, K., Stevens, F. J., *et al.* 2007. Germ line origin and somatic mutations determine the target tissues in systemic AL-amyloidosis. *PLoS ONE,* 2**,** e981.
Feinstein, A. R. & Cicchetti, D. V. 1990. High agreement but low kappa: I. The problems of two paradoxes. *J Clin Epidemiol,* 43**,** 543-549.
Fish, R., Pinney, J., Jain, P., *et al.* 2010. The Incidence of Major Hemorrhagic Complications After Renal Biopsies in Patients with Monoclonal Gammopathies. *Clin J Am Soc Nephrol*.
Fletcher, A. P., Neuberger, A. & Ratcliffe, W. A. 1970a. Tamm-Horsfall urinary glycoprotein. The chemical composition. *Biochem J,* 120**,** 417-24.
Fletcher, A. P., Neuberger, A. & Ratcliffe, W. A. 1970b. Tamm-Horsfall urinary glycoprotein. The subunit structure. *Biochem J,* 120**,** 425-32.
Furness, P. N., Rogers-Wheatley, L. & Harris, K. P. 1997. Semiautomatic quantitation of macrophages in human renal biopsy specimens in proteinuric states. *J Clin Pathol,* 50**,** 118-22.
Gallo, G., Picken, M., Frangione, B., *et al.* 1988. Nonamyloidotic monoclonal immunoglobulin deposits lack amyloid P component. *Mod Pathol,* 1**,** 453-6.
Ganeval, D., Noel, L. H., Preud'homme, J. L., *et al.* 1984. Light-chain deposition disease: its relation with AL-type amyloidosis. *Kidney Int,* 26**,** 1-9.
Gertz, M. A. 2005. Managing myeloma kidney.[comment]. *Annals of Internal Medicine,* 143**,** 835-7.
Giannoni, E., Buricchi, F., Raugei, G., *et al.* 2005. Intracellular reactive oxygen species activate Src tyrosine kinase during cell adhesion and anchorage-dependent cell growth. *Mol Cell Biol,* 25**,** 6391-403.
Gilmore, T. D. & Herscovitch, M. 2006. Inhibitors of NF-kappaB signaling: 785 and counting. *Oncogene,* 25**,** 6887-99.
Glockshuber, R., Steipe, B., Huber, R., *et al.* 1990. Crystallization and preliminary X-ray studies of the VL domain of the antibody McPC603 produced in Escherichia coli. *J Mol Biol,* 213**,** 613-5.
Goldfarb, S. & Golper, T. A. 1994. Proinflammatory cytokines and hemofiltration membranes. *J Am Soc Nephrol,* 5**,** 228-32.
Goni, F. & Gallo, G. 2005. Extraction and chemical characterization of tissue-deposited proteins from minute diagnostic biopsy specimens. *Methods Mol Biol,* 299**,** 261-6.
Goranov, S. 1996. Acute renal failure in patients with multiple myeloma. *Folia Med (Plovdiv),* 38**,** 57-63.
Gottenberg, J. E., Aucouturier, F., Goetz, J., *et al.* 2007. Serum immunoglobulin free light chain assessment in rheumatoid arthritis and primary Sjogren's syndrome. *Ann Rheum Dis,* 66**,** 23-7.
Grandaliano, G., Gesualdo, L., Ranieri, E., *et al.* 1996. Monocyte chemotactic peptide-1 expression in acute and chronic human nephritides: a pathogenetic role in interstitial monocytes recruitment. *J Am Soc Nephrol,* 7**,** 906-13.
Guan, S., el-Dahr, S., Dipp, S., *et al.* 1999. Inhibition of Na-K-ATPase activity and gene expression by a myeloma light chain in proximal tubule cells. *J Investig Med,* 47**,** 496-501.

Hanke, J. H., Gardner, J. P., Dow, R. L., *et al.* 1996. Discovery of a novel, potent, and Src family-selective tyrosine kinase inhibitor. Study of Lck- and FynT-dependent T cell activation. *J Biol Chem,* 271**,** 695-701.

Harmar, A. J., Arimura, A., Gozes, I., *et al.* 1998. International Union of Pharmacology. XVIII. Nomenclature of receptors for vasoactive intestinal peptide and pituitary adenylate cyclase-activating polypeptide. *Pharmacol Rev,* 50**,** 265-70.

Hayat, M. A. 2002. *Microscopy, Immunohistochemistry and Antigen Retrieval Methods: For Light and Electron Microscopy,* New York, Kluwer Academic / Plenum Publishers.

Hayden, M. S. & Ghosh, S. 2004. Signaling to NF-kappaB. *Genes Dev,* 18**,** 2195-224.

Heinzelmann, M., Mercer-Jones, M. A. & Passmore, J. C. 1999. Neutrophils and renal failure. *Am J Kidney Dis,* 34**,** 384-99.

Herrera, G. A. 2000. Renal manifestations of plasma cell dyscrasias: an appraisal from the patients' bedside to the research laboratory. *Ann Diagn Pathol,* 4**,** 174-200.

Herrera, G. A., Joseph, L., Gu, X., *et al.* 2004. Renal pathologic spectrum in an autopsy series of patients with plasma cell dyscrasia. *Arch Pathol Lab Med,* 128**,** 875-9.

Herrera, G. A., Russell, W. J. & Cardelli, J. 2001. Phenotypic transformation of mesangial cells precedes and is required for AL-amyloidogenesis in amyloid and amyloidosis. *In:* AA, B. M. (ed.) *The Proceedings of the IXth International Symposium on Amyloidosis.* Budapest: David Apathy.

Herrera, G. A., Russell, W. J., Isaac, J., *et al.* 1999. Glomerulopathic light chain-mesangial cell interactions modulate in vitro extracellular matrix remodeling and reproduce mesangiopathic findings documented in vivo. *Ultrastruct Pathol,* 23**,** 107-26.

Herrera, G. A., Shultz, J. J., Soong, S. J., *et al.* 1994. Growth factors in monoclonal light-chain--related renal diseases. *Hum Pathol,* 25**,** 883-92.

Hoffman, U., Opperman, M., Kuchler, S., *et al.* 2003. Free immunoglobulin light chains in patients with rheumatic diseases. . *Z Rheumatol,* 62**,** 1051.

Holland, M. D., Galla, J. H., Sanders, P. W., *et al.* 1985. Effect of urinary pH and diatrizoate on Bence Jones protein nephrotoxicity in the rat. *Kidney Int,* 27**,** 46-50.

Howie, A. J., Ferreira, M. A. & Adu, D. 2001. Prognostic value of simple measurement of chronic damage in renal biopsy specimens. *Nephrol Dial Transplant,* 16**,** 1163-9.

Hoyer, J. R. & Seiler, M. W. 1979. Pathophysiology of Tamm-Horsfall protein. *Kidney Int,* 16**,** 279-89.

Huang, Z. Q., Kirk, K. A., Connelly, K. G., *et al.* 1993. Bence Jones proteins bind to a common peptide segment of Tamm-Horsfall glycoprotein to promote heterotypic aggregation. *J Clin Invest,* 92**,** 2975-83.

Huang, Z. Q. & Sanders, P. W. 1995. Biochemical interaction between Tamm-Horsfall glycoprotein and Ig light chains in the pathogenesis of cast nephropathy. *Lab Invest,* 73**,** 810-7.

Huang, Z. Q. & Sanders, P. W. 1997. Localization of a single binding site for immunoglobulin light chains on human Tamm-Horsfall glycoprotein. *J Clin Invest,* 99**,** 732-6.

Hutchison, C. A., Bradwell, A. R., Cook, M., *et al.* 2009. Treatment of acute renal failure secondary to multiple myeloma with chemotherapy and extended high cut-off hemodialysis. *Clin J Am Soc Nephrol,* 4**,** 745-54.

Hutchison, C. A., Cockwell, P., Harding, S., *et al.* 2008a. Quantitative assessment of serum and urinary polyclonal free light chains in patients with type II diabetes: an early marker of diabetic kidney disease? *Expert Opin Ther Targets,* 12**,** 667-76.

Hutchison, C. A., Cockwell, P., Reid, S., *et al.* 2007. Efficient removal of immunoglobulin free light chains by hemodialysis for multiple myeloma: in vitro and in vivo studies. *J Am Soc Nephrol,* 18**,** 886-95.

Hutchison, C. A., Cook, M., Heyne, N., *et al.* 2008b. European trial of free light chain removal by extended haemodialysis in cast nephropathy (EuLITE): A randomised control trial. *Trials,* 9**,** 55.

Hutchison, C. A., Harding, S., Hewins, P., *et al.* 2008c. Quantitative assessment of serum and urinary polyclonal free light chains in patients with chronic kidney disease. *Clin J Am Soc Nephrol,* 3**,** 1684-90.

Imai, K., Kusakabe, M., Sakakura, T., *et al.* 1994. Susceptibility of tenascin to degradation by matrix metalloproteinases and serine proteinases. *FEBS Lett,* 352**,** 216-8.

Imbert, V., Rupec, R. A., Livolsi, A., *et al.* 1996. Tyrosine phosphorylation of I kappa B-alpha activates NF-kappa B without proteolytic degradation of I kappa B-alpha. *Cell,* 86**,** 787-98.

Issekutz, A. C. 1983. Removal of gram-negative endotoxin from solutions by affinity chromatography. *J Immunol Methods,* 61**,** 275-81.

Ivanyi, B. 1989. Renal complications in multiple myeloma. *Acta Morphol Hung,* 37**,** 235-43.

Jackson, J. H., Berger, E. M. & Repine, J. E. 1988. Thiourea and dimethylthiourea decrease human neutrophil bactericidal function in vitro. *Inflammation,* 12**,** 515-24.

Jackson, P. 2007. Quality assurance in immunochemistry. *In:* Renshaw, S. (ed.) *Immunohistochemistry.* 1 ed. Bloxham: Scion Publishing Limited.

Johns, E. A., Turner, R., Cooper, E. H., *et al.* 1986. Isoelectric points of urinary light chains in myelomatosis: analysis in relation to nephrotoxicity. *J Clin Pathol,* 39**,** 833-7.

Johnson, R. J. 1994. The glomerular response to injury: progression or resolution? *Kidney Int,* 45**,** 1769-82.

Kapadia, S. B. 1980. Multiple myeloma: a clinicopathologic study of 62 consecutively autopsied cases. *Medicine (Baltimore),* 59**,** 380-92.

Karimi, M., Sletten, K. & Westermark, P. 2003. Biclonal systemic AL-amyloidosis with one glycosylated and one nonglycosylated AL-protein. *Scand J Immunol,* 57**,** 319-23.

Katzmann, J. A., Clark, R. J., Abraham, R. S., *et al.* 2002. Serum reference intervals and diagnostic ranges for free kappa and free lambda immunoglobulin light chains: relative sensitivity for detection of monoclonal light chains. *Clin Chem,* 48**,** 1437-44.

Kawasaki, K., Minoshima, S., Schooler, K., *et al.* 1995. The organization of the human immunoglobulin lambda gene locus. *Genome Res,* 5**,** 125-35.

Keeling, J. & Herrera, G. A. 2005a. matrix composition alters matrix metalloproteinase expression in mesangial cells incubated with glomerulopathic light chains. . *Lab Invest,* 85**,** 267A.

Keeling, J. & Herrera, G. A. 2005b. Matrix metalloproteinases and mesangial remodeling in light chain-related glomerular damage. *Kidney Int,* 68**,** 1590-603.
Keeling, J. & Herrera, G. A. 2005c. MMP-7 expression and the accumulation of tenascin in light chain deposition disease mesangial nodules. *J Am Soc Nephrol,* 16**,** 663A
Keeling, J. & Herrera, G. A. 2009. An in vitro model of light chain deposition disease. *Kidney Int,* 75**,** 634-45.
Keeling, J., Teng, J., Herrera, G. A., *et al.* 2004. AL-amyloidosis and light-chain deposition disease light chains induce divergent phenotypic transformations of human mesangial cells. *Laboratory Investigation,* 84**,** 1322-38.
Kim, J. R., Yoon, H. W., Kwon, K. S., *et al.* 2000. Identification of proteins containing cysteine residues that are sensitive to oxidation by hydrogen peroxide at neutral pH. *Anal Biochem,* 283**,** 214-21.
Kim, L. C., Song, L. & Haura, E. B. 2009. Src kinases as therapeutic targets for cancer. *Nat Rev Clin Oncol,* 6**,** 587-95.
Kjellsson, B., Soderstrom, T. & Hanson, L. A. 1987. An ELISA method for quantification of Tamm-Horsfall protein using monoclonal antibodies. *J Immunol Methods,* 98**,** 105-11.
Klassen, R. B., Allen, P. L., Batuman, V., *et al.* 2005. Light chains are a ligand for megalin. *J Appl Physiol,* 98**,** 257-63.
Knudsen, L. M., Hjorth, M. & Hippe, E. 2000. Renal failure in multiple myeloma: reversibility and impact on the prognosis. Nordic Myeloma Study Group. *European Journal of Haematology,* 65**,** 175-81.
Kobayashi, K. & Fukuoka, S. 2001. Conditions for solubilization of Tamm-Horsfall protein/uromodulin in human urine and establishment of a sensitive and accurate enzyme-linked immunosorbent assay (ELISA) method. *Arch Biochem Biophys,* 388**,** 113-20.
Koss, M. N., Pirani, C. L. & Osserman, E. F. 1976. Experimental Bence Jones cast nephropathy. *Lab Invest,* 34**,** 579-91.
Kottgen, A., Glazer, N. L., Dehghan, A., *et al.* 2009. Multiple loci associated with indices of renal function and chronic kidney disease. *Nat Genet*.
Kottgen, A., Hwang, S. J., Larson, M. G., *et al.* 2010. Uromodulin levels associate with a common UMOD variant and risk for incident CKD. *J Am Soc Nephrol,* 21**,** 337-44.
Kozyraki, R., Fyfe, J., Verroust, P. J., *et al.* 2001. Megalin-dependent cubilin-mediated endocytosis is a major pathway for the apical uptake of transferrin in polarized epithelia. *Proc Natl Acad Sci U S A,* 98**,** 12491-6.
Kreft, B., Jabs, W. J., Laskay, T., *et al.* 2002. Polarized expression of Tamm-Horsfall protein by renal tubular epithelial cells activates human granulocytes. *Infect Immun,* 70**,** 2650-6.
Kriz, W. & LeHir, M. 2005. Pathways to nephron loss starting from glomerular diseases-insights from animal models. *Kidney Int,* 67**,** 404-19.
Kumar, G. L. & Rudbeck, L. 2009. *Immunohistochemical Staining Methods,* Carpinteria, Dako.
Kumar, R., Schaefer, J., Grande, J. P., *et al.* 1994. Immunolocalization of calcitriol receptor, 24-hydroxylase cytochrome P-450, and calbindin D28k in human kidney. *Am J Physiol,* 266**,** F477-85.

Kumar, S. & Muchmore, A. 1990. Tamm-Horsfall protein--uromodulin (1950-1990). *Kidney Int,* 37**,** 1395-401.
Kyle, R. A. 1975. Multiple myeloma: review of 869 cases. *Mayo Clin Proc,* 50**,** 29-40.
Kyle, R. A., Gertz, M. A., Witzig, T. E., *et al.* 2003. Review of 1027 patients with newly diagnosed multiple myeloma. *Mayo Clin Proc,* 78**,** 21-33.
Kyle, R. A. & Rajkumar, S. V. 2004. Multiple myeloma. *N Engl J Med,* 351**,** 1860-73.
Kyle, R. A., Therneau, T. M., Rajkumar, S. V., *et al.* 2006. Prevalence of monoclonal gammopathy of undetermined significance. *N Engl J Med,* 354**,** 1362-9.
Kyle, R. A., Wagoner, R. D. & Holley, K. E. 1982. Primary systemic amyloidosis: resolution of the nephrotic syndrome with melphalan and prednisone. *Arch Intern Med,* 142**,** 1445-7.
Lacy, M. Q. & Gertz, M. A. 1999. Acquired Fanconi's syndrome associated with monoclonal gammopathies. *Hematol Oncol Clin North Am,* 13**,** 1273-80.
Lathe, G. H. & Ruthven, C. R. 1956. The separation of substances and estimation of their relative molecular sizes by the use of colums of starch in water. *Biochem J,* 62**,** 665-74.
Leung, N., Dispenzieri, A., Fervenza, F. C., *et al.* 2005. Renal response after high-dose melphalan and stem cell transplantation is a favorable marker in patients with primary systemic amyloidosis. *Am J Kidney Dis,* 46**,** 270-7.
Li, M., Balamuthusamy, S., Simon, E. E., *et al.* 2008a. Silencing megalin and cubilin genes inhibits myeloma light chain endocytosis and ameliorates toxicity in human renal proximal tubule epithelial cells. *Am J Physiol Renal Physiol,* 295**,** F82-90.
Li, M., Cortez, S., Nakamachi, T., *et al.* 2006. Pituitary adenylate cyclase-activating polypeptide is a potent inhibitor of the growth of light chain-secreting human multiple myeloma cells. *Cancer Res,* 66**,** 8796-803.
Li, M., Hering-Smith, K. S., Simon, E. E., *et al.* 2008b. Myeloma light chains induce epithelial-mesenchymal transition in human renal proximal tubule epithelial cells. *Nephrol Dial Transplant,* 23**,** 860-70.
Li, M., Maderdrut, J. L., Lertora, J. J., *et al.* 2008c. Renoprotection by pituitary adenylate cyclase-activating polypeptide in multiple myeloma and other kidney diseases. *Regul Pept,* 145**,** 24-32.
Li, M., Maderdrut, J. L., Lertora, J. J., *et al.* 2007. Intravenous infusion of pituitary adenylate cyclase-activating polypeptide (PACAP) in a patient with multiple myeloma and myeloma kidney: a case study. *Peptides,* 28**,** 1891-5.
Li, S. D., Chono, S. & Huang, L. 2008d. Efficient oncogene silencing and metastasis inhibition via systemic delivery of siRNA. *Mol Ther,* 16**,** 942-6.
Liu, Y. 2004. Epithelial to mesenchymal transition in renal fibrogenesis: pathologic significance, molecular mechanism, and therapeutic intervention. *J Am Soc Nephrol,* 15**,** 1-12.
Loffing, J., Vallon, V., Loffing-Cueni, D., *et al.* 2004. Altered renal distal tubule structure and renal Na(+) and Ca(2+) handling in a mouse model for Gitelman's syndrome. *J Am Soc Nephrol,* 15**,** 2276-88.
Ludwig, H., Adam, Z., Hajek, R., *et al.* 2010. Light Chain-Induced Acute Renal Failure Can Be Reversed by Bortezomib-Doxorubicin-Dexamethasone in Multiple Myeloma: Results of a Phase II Study. *J Clin Oncol*.

Lundmark, K., Westermark, G. T., Olsen, A., *et al.* 2005. Protein fibrils in nature can enhance amyloid protein A amyloidosis in mice: Cross-seeding as a disease mechanism. *Proc Natl Acad Sci U S A,* 102**,** 6098-102.
Maack, T., Johnson, V., Kau, S. T., *et al.* 1979. Renal filtration, transport, and metabolism of low-molecular-weight proteins: a review. *Kidney Int,* 16**,** 251-70.
Magee, C. C. 2006. Kidney biopsy in myeloma. *Nephrol Dial Transplant,* 21**,** 3601-2; author reply 3602.
Malcolm, S., Barton, P., Murphy, C., *et al.* 1982. Localization of human immunoglobulin kappa light chain variable region genes to the short arm of chromosome 2 by in situ hybridization. *Proc Natl Acad Sci U S A,* 79**,** 4957-61.
Maldonado, J. E., Velosa, J. A., Kyle, R. A., *et al.* 1975. Fanconi syndrome in adults. A manifestation of a latent form of myeloma. *Am J Med,* 58**,** 354-64.
Mallozzi, C., Di Stasi, A. M. & Minetti, M. 1999. Activation of src tyrosine kinases by peroxynitrite. *FEBS Lett,* 456**,** 201-6.
Mardle, S. 2007. The selection of reporter labels. *In:* Renshaw, S. (ed.) *Immunohistochemistry.* 1 ed. Bloxham: Scion Publishing Limited.
Martin, J., Eynstone, L., Davies, M., *et al.* 2001. Induction of metalloproteinases by glomerular mesangial cells stimulated by proteins of the extracellular matrix. *J Am Soc Nephrol,* 12**,** 88-96.
Mason, D. Y., Micklem, K. & Jones, M. 2000. Double immunofluorescence labelling of routinely processed paraffin sections. *J Pathol,* 191**,** 452-61.
Massova, I., Kotra, L. P., Fridman, R., *et al.* 1998. Matrix metalloproteinases: structures, evolution, and diversification. *FASEB J,* 12**,** 1075-95.
McBride, O. W., Hieter, P. A., Hollis, G. F., *et al.* 1982. Chromosomal location of human kappa and lambda immunoglobulin light chain constant region genes. *J Exp Med,* 155**,** 1480-90.
McGiven, A. R., Hunt, J. S., Day, W. A., *et al.* 1978. Tamm-Horsfall protein in the glomerular capsular space. *J Clin Pathol,* 31**,** 620-5.
Medici, D. & Nawshad, A. 2010. Type I collagen promotes epithelial-mesenchymal transition through ILK-dependent activation of NF-kappaB and LEF-1. *Matrix Biol,* 29**,** 161-5.
Merlini, G. & Bellotti, V. 2003. Molecular mechanisms of amyloidosis. *N Engl J Med,* 349**,** 583-96.
Merlini, G. & Westermark, P. 2004. The systemic amyloidoses: clearer understanding of the molecular mechanisms offers hope for more effective therapies. *J Intern Med,* 255**,** 159-78.
Messiaen, T., Deret, S., Mougenot, B., *et al.* 2000. Adult Fanconi syndrome secondary to light chain gammopathy. Clinicopathologic heterogeneity and unusual features in 11 patients. *Medicine (Baltimore),* 79**,** 135-54.
Mian, I. S., Bradwell, A. R. & Olson, A. J. 1991. Structure, function and properties of antibody binding sites. *J Mol Biol,* 217**,** 133-51.
Miettinen, T. A. & Kekki, M. 1967. Effect of impaired hepatic and renal function on Bence Jones protein catabolism in human subjects. *Clin Chim Acta,* 18**,** 395-407.
Misko, T. P., Highkin, M. K., Veenhuizen, A. W., *et al.* 1998. Characterization of the cytoprotective action of peroxynitrite decomposition catalysts. *J Biol Chem,* 273**,** 15646-53.

Mohanty, J. G., Jaffe, J. S., Schulman, E. S., *et al.* 1997. A highly sensitive fluorescent micro-assay of H2O2 release from activated human leukocytes using a dihydroxyphenoxazine derivative. *J Immunol Methods,* 202**,** 133-41.
Morel-Maroger, L., Basch, A., Danon, F., *et al.* 1970. Pathology of the kidney in Waldenstrom's macroglobulinemia. Study of sixteen cases. *N Engl J Med,* 283**,** 123-9.
Morigi, M., Macconi, D., Zoja, C., *et al.* 2002. Protein overload-induced NF-kappaB activation in proximal tubular cells requires H2O2 through a PKC-dependent pathway. *J Am Soc Nephrol,* 13**,** 1179-89.
Morii, T., Fujita, H., Narita, T., *et al.* 2003. Increased urinary excretion of monocyte chemoattractant protein-1 in proteinuric renal diseases. *Ren Fail,* 25**,** 439-44.
Mott, J. D. & Werb, Z. 2004. Regulation of matrix biology by matrix metalloproteinases. *Curr Opin Cell Biol,* 16**,** 558-64.
Murphy, C. L., Eulitz, M., Hrncic, R., *et al.* 2001. Chemical typing of amyloid protein contained in formalin-fixed paraffin-embedded biopsy specimens. *Am J Clin Pathol,* 116**,** 135-42.
Myatt, E. A., Westholm, F. A., Weiss, D. T., *et al.* 1994. Pathogenic potential of human monoclonal immunoglobulin light chains: relationship of in vitro aggregation to in vivo organ deposition. *Proc Natl Acad Sci U S A,* 91**,** 3034-8.
Nasr, S. H., Galgano, S. J., Markowitz, G. S., *et al.* 2006. Immunofluorescence on pronase-digested paraffin sections: a valuable salvage technique for renal biopsies. *Kidney Int,* 70**,** 2148-51.
Nathan, C. 2003. Specificity of a third kind: reactive oxygen and nitrogen intermediates in cell signaling. *J Clin Invest,* 111**,** 769-78.
Negulescu, O., Bognar, I., Lei, J., *et al.* 2002. Estradiol reverses TGF-beta1-induced mesangial cell apoptosis by a casein kinase 2-dependent mechanism. *Kidney Int,* 62**,** 1989-98.
Norden, A. G., Flynn, F. V., Fulcher, L. M., *et al.* 1989. Renal impairment in myeloma: negative association with isoelectric point of excreted Bence-Jones protein. *J Clin Pathol,* 42**,** 59-62.
Nyquist, J., Ramstad, H. M., Sletten, K., *et al.* 1993. Structural Studies of two carbohydrate-containing immunoglobulin-kappa-light chain amyloid fibril-proteins of the variable group 1. *In:* Kisilevsky, R., Benson, M. D., Frangione, B., Gsuldie, J., Muckle, T. J. & Young, I. D. (eds.) *Amyloid and Amyloidosis.* New York: Partenton Pub. .
O'Callaghan, C. A. 2004. Renal manifestations of systemic autoimmune disease: diagnosis and therapy. *Best Pract Res Clin Rheumatol,* 18**,** 411-427.
Omtvedt, L. A., Bailey, D., Renouf, D. V., *et al.* 2000. Glycosylation of immunoglobulin light chains associated with amyloidosis. *Amyloid,* 7**,** 227-44.
Onley, C. 2007. Antibodies for immunochemistry. *In:* Renshaw, S. (ed.) *Immunohistochemistry.* 1 ed. Bloxham: Scion Publishing Limited.
Pak, J., Pu, Y., Zhang, Z. T., *et al.* 2001. Tamm-Horsfall protein binds to type 1 fimbriated Escherichia coli and prevents E. coli from binding to uroplakin Ia and Ib receptors. *J Biol Chem,* 276**,** 9924-30.
Parker, N. B., Berger, E. M., Curtis, W. E., *et al.* 1985. Hydrogen peroxide causes dimethylthiourea consumption while hydroxyl radical causes dimethyl sulfoxide consumption in vitro. *J Free Radic Biol Med,* 1**,** 415-9.

Parks, W. C. 1999. Matrix metalloproteinases in repair. *Wound Repair Regen,* 7**,** 423-32.
Parrish, A. E. 1992. Complications of percutaneous renal biopsy: a review of 37 years' experience. *Clin Nephrol,* 38**,** 135-41.
Parsons, S. J. & Parsons, J. T. 2004. Src family kinases, key regulators of signal transduction. *Oncogene,* 23**,** 7906-9.
Pasquali, S., Zucchelli, P., Casanova, S., *et al.* 1987. Renal histological lesions and clinical syndromes in multiple myeloma. Renal Immunopathology Group. *Clin Nephrol,* 27**,** 222-8.
Patel, R., McKenzie, J. K. & McQueen, E. G. 1964. Tamm-Horsfall Urinary Mucoprotein and Tubular Obstruction by Casts in Acute Renal Failure. *Lancet,* 1**,** 457-61.
Perkins, N. D. 2007. Integrating cell-signalling pathways with NF-kappaB and IKK function. *Nat Rev Mol Cell Biol,* 8**,** 49-62.
Pesce, A. J., Clyne, D. H., Pollak, V. E., *et al.* 1980. Renal tubular interactions of proteins. *Clin Biochem,* 13**,** 209-15.
Picken, M. M., Gallo, G., Buxbaum, J., *et al.* 1986. Characterization of renal amyloid derived from the variable region of the lambda light chain subgroup II. *Am J Pathol,* 124**,** 82-7.
Pirani, C. L., Silva, F., D'Agati, V., *et al.* 1987. Renal lesions in plasma cell dyscrasias: ultrastructural observations. *Am J Kidney Dis,* 10**,** 208-21.
Porter, K. R. & Tamm, I. 1955. Direct visualization of a mucoprotein component of urine. *J Biol Chem,* 212**,** 135-40.
Porter, R. R. 1973. Structural studies of immunoglobulins. *Science,* 180**,** 713-6.
Pote, A., Zwizinski, C., Simon, E. E., *et al.* 2000. Cytotoxicity of myeloma light chains in cultured human kidney proximal tubule cells. *Am J Kidney Dis,* 36**,** 735-44.
Pozzi, C., D'Amico, M., Fogazzi, G. B., *et al.* 2003. Light chain deposition disease with renal involvement: clinical characteristics and prognostic factors. *American Journal of Kidney Diseases,* 42**,** 1154-63.
Pozzi, C., Pasquali, S., Donini, U., *et al.* 1987. Prognostic factors and effectiveness of treatment in acute renal failure due to multiple myeloma: a review of 50 cases. Report of the Italien Renal Immunopathology Group. *Clin Nephrol,* 28**,** 1-9.
Prajczer, S., Heidenreich, U., Pfaller, W., *et al.* 2010. Evidence for a role of uromodulin in chronic kidney disease progression. *Nephrol Dial Transplant,* 25**,** 1896-1903.
Preud'homme, J. L., Aucouturier, P., Touchard, G., *et al.* 1994. Monoclonal immunoglobulin deposition disease (Randall type). Relationship with structural abnormalities of immunoglobulin chains. *Kidney Int,* 46**,** 965-72.
Prodjosudjadi, W., Gerritsma, J. S., van Es, L. A., *et al.* 1995. Monocyte chemoattractant protein-1 in normal and diseased human kidneys: an immunohistochemical analysis. *Clin Nephrol,* 44**,** 148-55.
Raffen, R., Dieckman, L. J., Szpunar, M., *et al.* 1999. Physicochemical consequences of amino acid variations that contribute to fibril formation by immunoglobulin light chains. *Protein Sci,* 8**,** 509-17.
Rastaldi, M. P., Ferrario, F., Giardino, L., *et al.* 2002. Epithelial-mesenchymal transition of tubular epithelial cells in human renal biopsies. *Kidney Int,* 62**,** 137-46.

Reinhart, H. H., Obedeanu, N., Walz, D., *et al.* 1989. A new ELISA method for the rapid quantification of Tamm-Horsfall protein in urine. *Am J Clin Pathol,* 92**,** 199-205.
Remuzzi, G. 1999. Nephropathic nature of proteinuria. *Curr Opin Nephrol Hypertens,* 8**,** 655-63.
Remuzzi, G. & Bertani, T. 1998. Pathophysiology of progressive nephropathies. *N Engl J Med,* 339**,** 1448-56.
Renshaw, S. 2007. Immunochemical staining techniques. *In:* Renshaw, S. (ed.) *Immunohistochemistry.* 1 ed. Bloxham: Scion Publishing Limited.
Rhee, S. G. 2006. Cell signaling. H2O2, a necessary evil for cell signaling. *Science,* 312**,** 1882-3.
Richardson, P. G., Hideshima, T. & Anderson, K. C. 2003. Bortezomib (PS-341): a novel, first-in-class proteasome inhibitor for the treatment of multiple myeloma and other cancers. *Cancer Control,* 10**,** 361-9.
Rindler, M. J., Naik, S. S., Li, N., *et al.* 1990. Uromodulin (Tamm-Horsfall glycoprotein/uromucoid) is a phosphatidylinositol-linked membrane protein. *J Biol Chem,* 265**,** 20784-9.
Rocca, A., Khamlichi, A. A., Aucouturier, P., *et al.* 1993. Primary structure of a variable region of the V kappa I subgroup (ISE) in light chain deposition disease. *Clin Exp Immunol,* 91**,** 506-9.
Rocca, A., Khamlichi, A. A., Touchard, G., *et al.* 1995. Sequences of V kappa I subgroup light chains in Fanconi's syndrome. Light chain V region gene usage restriction and peculiarities in myeloma-associated Fanconi's syndrome. *J Immunol,* 155**,** 3245-52.
Ronco, P. M., Alyanakian, M. A., Mougenot, B., *et al.* 2001. Light chain deposition disease: a model of glomerulosclerosis defined at the molecular level. *J Am Soc Nephrol,* 12**,** 1558-65.
Rose, P. E., McGonigle, R., Michael, J., *et al.* 1987. Renal failure and the histopathological features of myeloma kidney reversed by intensive chemotherapy and peritoneal dialysis. *Br Med J (Clin Res Ed),* 294**,** 411-2.
Rovin, B. H., Dickerson, J. A., Tan, L. C., *et al.* 1995. Activation of nuclear factor-kappa B correlates with MCP-1 expression by human mesangial cells. *Kidney Int,* 48**,** 1263-71.
Russell, W. J., Cardelli, J., Harris, E., *et al.* 2001. Monoclonal light chain--mesangial cell interactions: early signaling events and subsequent pathologic effects. *Lab Invest,* 81**,** 689-703.
Ryan, M. J., Johnson, G., Kirk, J., *et al.* 1994. HK-2: an immortalized proximal tubule epithelial cell line from normal adult human kidney. *Kidney Int,* 45**,** 48-57.
Saemann, M. D., Weichhart, T., Zeyda, M., *et al.* 2005. Tamm-Horsfall glycoprotein links innate immune cell activation with adaptive immunity via a Toll-like receptor-4-dependent mechanism. *J Clin Invest,* 115**,** 468-75.
Saito, K., Shimizu, F., Sato, T., *et al.* 1993. Modulation of human mesangial cell behaviour by extracellular matrix components--the possible role of interstitial type III collagen. *Clin Exp Immunol,* 91**,** 510-5.
Sanders, P. W. 2005. Management of paraproteinemic renal disease. *Curr Opin Nephrol Hypertens,* 14**,** 97-103.
Sanders, P. W. & Booker, B. B. 1992. Pathobiology of cast nephropathy from human Bence Jones proteins. *J Clin Invest,* 89**,** 630-9.

Sanders, P. W., Booker, B. B., Bishop, J. B., *et al.* 1990. Mechanisms of intranephronal proteinaceous cast formation by low molecular weight proteins. *J Clin Invest,* 85**,** 570-6.
Sanders, P. W., Herrera, G. A., Chen, A., *et al.* 1988a. Differential nephrotoxicity of low molecular weight proteins including Bence Jones proteins in the perfused rat nephron in vivo. *J Clin Invest,* 82**,** 2086-96.
Sanders, P. W., Herrera, G. A. & Galla, J. H. 1987. Human Bence Jones protein toxicity in rat proximal tubule epithelium in vivo. *Kidney Int,* 32**,** 851-61.
Sanders, P. W., Herrera, G. A., Kirk, K. A., *et al.* 1991. Spectrum of glomerular and tubulointerstitial renal lesions associated with monotypical immunoglobulin light chain deposition. *Lab Invest,* 64**,** 527-37.
Sanders, P. W., Herrera, G. A., Lott, R. L., *et al.* 1988b. Morphologic alterations of the proximal tubules in light chain-related renal disease. *Kidney Int,* 33**,** 881-9.
Sanz, A. B., Sanchez-Nino, M. D., Ramos, A. M., *et al.* 2010. NF-{kappa}B in Renal Inflammation. *J Am Soc Nephrol,* 21**,** 1254-62.
Savill, J., Wyllie, A. H., Henson, J. E., *et al.* 1989. Macrophage phagocytosis of ageing neutrophils in inflammation. Programmed cell death in the neutrophil leads to its recognition by macrophages. *J Clin Invest,* 83**,** 865-875.
Schlondorff, D. 1996. Roles of the mesangium in glomerular function. *Kidney Int,* 49**,** 1583-5.
Schmid, M., Prajczer, S., Gruber, L. N., *et al.* 2010. Uromodulin Facilitates Neutrophil Migration Across Renal Epithelial Monolayers. *Cell Physiol Biochem,* 26**,** 311-318.
Schnaper, H. W., Kopp, J. B., Poncelet, A. C., *et al.* 1996. Increased expression of extracellular matrix proteins and decreased expression of matrix proteases after serial passage of glomerular mesangial cells. *J Cell Sci,* 109 (Pt 10)**,** 2521-8.
Scholefield, Z., Yates, E. A., Wayne, G., *et al.* 2003. Heparan sulfate regulates amyloid precursor protein processing by BACE1, the Alzheimer's beta-secretase. *J Cell Biol,* 163**,** 97-107.
Scopes, R. K. 1994. *Protein Purification: Principles and Practice,* New York, Springer.
Segerer, S., Heller, F., Lindenmeyer, M. T., *et al.* 2008. Compartment specific expression of dendritic cell markers in human glomerulonephritis. *Kidney Int,* 74**,** 37-46.
Sengul, S., Li, M. & Batuman, V. 2009. Myeloma kidney: toward its prevention--with new insights from in vitro and in vivo models of renal injury. *J Nephrol,* 22**,** 17-28.
Sengul, S., Zwizinski, C. & Batuman, V. 2003. Role of MAPK pathways in light chain-induced cytokine production in human proximal tubule cells. *Am J Physiol Renal Physiol,* 284**,** F1245-54.
Sengul, S., Zwizinski, C., Simon, E. E., *et al.* 2002. Endocytosis of light chains induces cytokines through activation of NF-kappaB in human proximal tubule cells. *Kidney Int,* 62**,** 1977-88.
Serafini-Cessi, F., Malagolini, N. & Cavallone, D. 2003. Tamm-Horsfall glycoprotein: biology and clinical relevance. *Am J Kidney Dis,* 42**,** 658-76.
Shirahama, T. & Cohen, A. S. 1973. An analysis of the close relationship of lysosomes to early deposits of amyloid. Ultrastructural evidence in experimental mouse amyloidosis. *Am J Pathol,* 73**,** 97-114.

Shirahama, T. & Cohen, A. S. 1975. Intralysosomal formation of amyloid fibrils. *Am J Pathol,* 81**,** 101-16.
Simerville, J. A., Maxted, W. C. & Pahira, J. J. 2005. Urinalysis: a comprehensive review. *Am Fam Physician,* 71**,** 1153-62.
Simmonds, P. D., Cottrell, B. J., Mead, G. M., *et al.* 1997. Lymphadenopathy due to amyloid deposition in non-Hodgkin's lymphoma. *Ann Oncol,* 8**,** 267-70.
Smith, P. K., Krohn, R. I., Hermanson, G. T., *et al.* 1985. Measurement of protein using bicinchoninic acid. *Anal Biochem,* 150**,** 76-85.
Smithline, N., Kassirer, J. P. & Cohen, J. J. 1976. Light-chain nephropathy. Renal tubular dysfunction associated with light-chain proteinuria. *N Engl J Med,* 294**,** 71-4.
Smolens, P. & Miller, V. 1987. Renal tubular uptake of light chains (LC) of different isoelectric points (pI). *Clin Res,* 35**,** 33A.
Smolens, P., Venkatachalam, M. & Stein, J. H. 1983. Myeloma kidney cast nephropathy in a rat model of multiple myeloma. *Kidney Int,* 24**,** 192-204.
Solling, K., Solling, J. & Romer, F. K. 1981. Free light chains of immunoglobulins in serum from patients with rheumatoid arthritis, sarcoidosis, chronic infections and pulmonary cancer. *Acta Med Scand,* 209**,** 473-7.
Solomon, A. 1985. Light Chains of Human Immunoglobulins. *Meth Enzymol,* 116**,** 101-121.
Solomon, A. 1986. Light chains of immunoglobulins: structural-genetic correlates. *Blood,* 68**,** 603-10.
Solomon, A., Frangione, B. & Franklin, E. C. 1982. Bence Jones proteins and light chains of immunoglobulins. Preferential association of the V lambda VI subgroup of human light chains with amyloidosis AL (lambda). *J Clin Invest,* 70**,** 453-60.
Solomon, A., Waldmann, T. A., Fahey, J. L., *et al.* 1964. Metabolism of Bence Jones Proteins. *J Clin Invest,* 43**,** 103-17.
Solomon, A., Weiss, D. T. & Kattine, A. A. 1991. Nephrotoxic potential of Bence Jones proteins. *N Engl J Med,* 324**,** 1845-51.
Solomon, A., Weiss, D. T. & Pepys, M. B. 1992. Induction in mice of human light-chain-associated amyloidosis. *Am J Pathol,* 140**,** 629-37.
Stanford, B. L. & Zondor, S. D. 2003. Bortezomib treatment for multiple myeloma. *Ann Pharmacother,* 37**,** 1825-30.
Start, D. A., Silva, F. G., Davis, L. D., *et al.* 1988. Myeloma cast nephropathy: immunohistochemical and lectin studies. *Mod Pathol,* 1**,** 336-47.
Steffensen, B., Hakkinen, L. & Larjava, H. 2001. Proteolytic events of wound-healing--coordinated interactions among matrix metalloproteinases (MMPs), integrins, and extracellular matrix molecules. *Crit Rev Oral Biol Med,* 12**,** 373-98.
Stevens, F. J. 2000. Four structural risk factors identify most fibril-forming kappa light chains. *Amyloid,* 7**,** 200-11.
Stevens, F. J. & Kisilevsky, R. 2000. Immunoglobulin light chains, glycosaminoglycans, and amyloid. *Cell Mol Life Sci,* 57**,** 441-9.
Stevens, F. J., Myatt, E. A., Chang, C. H., *et al.* 1995. A molecular model for self-assembly of amyloid fibrils: immunoglobulin light chains. *Biochemistry,* 34**,** 10697-702.

Stevenson, F. K., Cleave, A. J. & Kent, P. W. 1971. The effect of ions on the viscometric and ultracentrifugal behaviour of Tamm-Horsfall glycoprotein. *Biochim Biophys Acta,* 236**,** 59-66.

Striker, L. J., Doi, T., Elliot, S., *et al.* 1989. The contribution of glomerular mesangial cells to progressive glomerulosclerosis. *Semin Nephrol,* 9**,** 318-28.

Su, S. J., Chang, K. L., Lin, T. M., *et al.* 1997. Uromodulin and Tamm-Horsfall protein induce human monocytes to secrete TNF and express tissue factor. *J Immunol,* 158**,** 3449-56.

Sugiyama, H., Kashihara, N., Makino, H., *et al.* 1996. Apoptosis in glomerular sclerosis. *Kidney Int,* 49**,** 103-11.

Tagouri, Y. M., Sanders, P. W., Picken, M. M., *et al.* 1996. In vitro AL-amyloid formation by rat and human mesangial cells. *Lab Invest,* 74**,** 290-302.

Tagouri, Y. M., Sanders, P. W., Zhu, L., *et al.* 1995. Glomerulopathic monoclonal light chains potentiate mesangial cell apoptosis in vitro (abstract). *Lab Invest, Mod Pathol,* 8**,** 161A.

Tamm, I. & Horsfall, F. L., Jr. 1952. A mucoprotein derived from human urine which reacts with influenza, mumps, and Newcastle disease viruses. *J Exp Med,* 95**,** 71-97.

Tanner, G. A. & Evan, A. P. 1989. Glomerular and proximal tubular morphology after single nephron obstruction. *Kidney Int,* 36**,** 1050-60.

Tanner, G. A. & Knopp, L. C. 1986. Glomerular blood flow after single nephron obstruction in the rat kidney. *Am J Physiol,* 250**,** F77-85.

Teng, J., Russell, W. J., Gu, X., *et al.* 2004. Different types of glomerulopathic light chains interact with mesangial cells using a common receptor but exhibit different intracellular trafficking patterns.[erratum appears in Lab Invest. 2004 Sep;84(9):1219]. *Lab Invest,* 84**,** 440-51.

Teng, J., Zhang, P. L., Russell, W. J., *et al.* 2003. Insights into mechanisms responsible for mesangial alterations associated with fibrogenic glomerulopathic light chains. *Nephron Physiol,* 94**,** p28-38.

Tennent, G. A., Lovat, L. B. & Pepys, M. B. 1995. Serum amyloid P component prevents proteolysis of the amyloid fibrils of Alzheimer disease and systemic amyloidosis. *Proc Natl Acad Sci U S A,* 92**,** 4299-303.

Tesch, G. H., Schwarting, A., Kinoshita, K., *et al.* 1999. Monocyte chemoattractant protein-1 promotes macrophage-mediated tubular injury, but not glomerular injury, in nephrotoxic serum nephritis. *J Clin Invest,* 103**,** 73-80.

Thomas, M. E., Harris, K. P., Walls, J., *et al.* 2002. Fatty acids exacerbate tubulointerstitial injury in protein-overload proteinuria. *Am J Physiol Renal Physiol,* 283**,** F640-7.

Thorner, P. S., Bedard, Y. C. & Fernandes, B. J. 1983. Lambda-light-chain nephropathy with Fanconi's syndrome. *Arch Pathol Lab Med,* 107**,** 654-7.

Toor, A. A., Ramdane, B. A., Joseph, J., *et al.* 2006. Cardiac nonamyloidotic immunoglobulin deposition disease. *Mod Pathol,* 19**,** 233-7.

Toyoda, M., Kita, S., Furiya, K., *et al.* 1991. Characterization of AL amyloid protein identified by immunoelectron microscopy: a simple method using the protein A-gold technique. *J Histochem Cytochem,* 39**,** 239-42.

Truong, L. D., Pindur, J., Barrios, R., *et al.* 1994. Tenascin is an important component of the glomerular extracellular matrix in normal and pathologic conditions. *Kidney Int,* 45**,** 201-10.

Turbat-Herrera, E. A., Isaac, J., Sanders, P. W., *et al.* 1997. Integrated expression of glomerular extracellular matrix proteins and beta 1 integrins in monoclonal light chain-related renal diseases. *Mod Pathol,* 10**,** 485-95.

Van Wart, H. E. & Birkedal-Hansen, H. 1990. The cysteine switch: a principle of regulation of metalloproteinase activity with potential applicability to the entire matrix metalloproteinase gene family. *Proc Natl Acad Sci U S A,* 87**,** 5578-82.

Veeramachaneni, R., Gu, X. & Herrera, G. A. 2004. Atypical amyloidosis: diagnostic challenges and the role of immunoelectron microscopy in diagnosis. *Ultrastruct Pathol,* 28**,** 75-82.

Verroust, P. J., Birn, H., Nielsen, R., *et al.* 2002. The tandem endocytic receptors megalin and cubilin are important proteins in renal pathology. *Kidney Int,* 62**,** 745-56.

Viedt, C., Dechend, R., Fei, J., *et al.* 2002. MCP-1 induces inflammatory activation of human tubular

Light Chains Stimulate Cellular Redox Signaling 1245 epithelial cells: Involvement of the transcription factors,

nuclear factor-kappaB and activating protein-1. *J Am Soc Nephrol,* 13**,** 1543-1547.

Viegas, M. S., Martins, T. C., Seco, F., *et al.* 2007. An improved and cost-effective methodology for the reduction of autofluorescence in direct immunofluorescence studies on formalin-fixed paraffin-embedded tissues. *Eur J Histochem,* 51**,** 59-66.

Visse, R. & Nagase, H. 2003. Matrix metalloproteinases and tissue inhibitors of metalloproteinases: structure, function, and biochemistry. *Circ Res,* 92**,** 827-39.

von Gise, H., Christ, H. & Bohle, A. 1981. Early glomerular lesions in amyloidosis. Electronmicroscopic findings. *Virchows Arch A Pathol Anat Histol,* 390**,** 259-72.

Vu, T. H. & Werb, Z. 2000. Matrix metalloproteinases: effectors of development and normal physiology. *Genes Dev,* 14**,** 2123-33.

Wada, T., Furuichi, K., Sakai, N., *et al.* 2000. Up-regulation of monocyte chemoattractant protein-1 in tubulointerstitial lesions of human diabetic nephropathy. *Kidney Int,* 58**,** 1492-1499.

Waldmann, T. A., Strober, W. S. & Mogielnicki, R. P. 1972. The Renal Handling of Low Molecular Weight Proteins II. Disorders of Serum Protein Catabolism in Patients with Tubular Proteinuria, the Nephrotic Syndrome or Uraemia. . *J Clin Invest,* 51**,** 2162-2174.

Walker, R. G. 2003. Chronic Interstitial Nephritis. *In:* Johnson, R. J. & Feehally, J. (eds.) *Comprehensive Clinical Nephrology.* 2 ed. London: Mosby.

Wang, P. X. & Sanders, P. W. 2007. Immunoglobulin light chains generate hydrogen peroxide. *J Am Soc Nephrol,* 18**,** 1239-45.

Wang, Y., Chen, J., Chen, L., *et al.* 1997. Induction of monocyte chemoattractant protein-1 in proximal tubule cells by urinary protein. *J Am Soc Nephrol,* 8**,** 1537-45.

Wang, Y., Rangan, G. K., Tay, Y. C., *et al.* 1999. Induction of monocyte chemoattractant protein-1 by albumin is mediated by nuclear factor kappaB in proximal tubule cells. *J Am Soc Nephrol,* 10**,** 1204-13.

Wangsiripaisan, A., Gengaro, P. E., Edelstein, C. L., *et al.* 2001. Role of polymeric Tamm-Horsfall protein in cast formation: oligosaccharide and tubular fluid ions. *Kidney Int,* 59**,** 932-40.

Watanabe, S., Yoshimura, A., Inui, K., *et al.* 2001. Acquisition of the monocyte/macrophage phenotype in human mesangial cells. *J Lab Clin Med,* 138**,** 193-9.
Weichhart, T., Zlabinger, G. J. & Saemann, M. D. 2005. The multiple functions of Tamm-Horsfall protein in human health and disease: a mystery clears up. *Wien Klin Wochenschr,* 117**,** 316-22.
Weiss, J. H., Williams, R. H., Galla, J. H., *et al.* 1981. Pathophysiology of acute Bence-Jones protein nephrotoxicity in the rat. *Kidney Int,* 20**,** 198-210.
Wentworth, A. D., Jones, L. H., Wentworth, P., Jr., *et al.* 2000. Antibodies have the intrinsic capacity to destroy antigens. *Proc Natl Acad Sci U S A,* 97**,** 10930-5.
Wentworth, P., Jr., Jones, L. H., Wentworth, A. D., *et al.* 2001. Antibody catalysis of the oxidation of water. *Science,* 293**,** 1806-11.
Westermark, P. 2005. Aspects on human amyloid forms and their fibril polypeptides. *FEBS J,* 272**,** 5942-9.
Wetzel, R. 1997. Domain stability in immunoglobulin light chain deposition disorders. *Adv Protein Chem,* 50**,** 183-242.
Whiteman, M. & Halliwell, B. 1997. Thiourea and dimethylthiourea inhibit peroxynitrite-dependent damage: nonspecificity as hydroxyl radical scavengers. *Free Radic Biol Med,* 22**,** 1309-12.
Wochner, R. D., Strober, W. & Waldmann, T. A. 1967. The role of the kidney in the catabolism of Bence Jones proteins and immunoglobulin fragments. *J Exp Med,* 126**,** 207-21.
Wong, T. Y., Phillips, A. O., Witowski, J., *et al.* 2003. Glucose-mediated induction of TGF-beta 1 and MCP-1 in mesothelial cells in vitro is osmolality and polyol pathway dependent. *Kidney Int,* 63**,** 1404-16.
Xu, W., Harrison, S. C. & Eck, M. J. 1997. Three-dimensional structure of the tyrosine kinase c-Src. *Nature,* 385**,** 595-602.
Yamaguchi, I., Suda, H., Tsuzuike, N., *et al.* 2003. Glycosaminoglycan and proteoglycan inhibit the depolymerization of beta2-microglobulin amyloid fibrils in vitro. *Kidney Int,* 64**,** 1080-8.
Ying, W. Z. & Sanders, P. W. 2001. Mapping the binding domain of immunoglobulin light chains for Tamm-Horsfall protein. *Am J Pathol,* 158**,** 1859-66.
Zeier, M., Perz, J., Linke, R. P., *et al.* 2003. No regression of renal AL amyloid in monoclonal gammopathy after successful autologous blood stem cell transplantation and significant clinical improvement. *Nephrol Dial Transplant,* 18**,** 2644-7.
Zhou, M., Diwu, Z., Panchuk-Voloshina, N., *et al.* 1997. A stable nonfluorescent derivative of resorufin for the fluorometric determination of trace hydrogen peroxide: applications in detecting the activity of phagocyte NADPH oxidase and other oxidases. *Anal Biochem,* 253**,** 162-8.
Zhu, H., Yu, J. & Kindy, M. S. 2001. Inhibition of amyloidosis using low-molecular-weight heparins. *Mol Med,* 7**,** 517-22.
Zhu, L., Herrera, G. A., Murphy-Ullrich, J. E., *et al.* 1995. Pathogenesis of glomerulosclerosis in light chain deposition disease. Role for transforming growth factor-beta. *Am J Pathol,* 147**,** 375-85.
Zhu, L., Herrera, G. A., White, C. R., *et al.* 1997. Immunoglobulin light chain alters mesangial cell calcium homeostasis. *Am J Physiol,* 272**,** F319-24.

Zoja, C., Benigni, A. & Remuzzi, G. 1999. Protein overload activates proximal tubular cells to release vasoactive and inflammatory mediators. *Exp Nephrol,* 7**,** 420-8.